SKB

TECHNICAL REPORT 88-14

Validation of MUDEC against Colorado school of mines block test data

Nick Barton, Panayiotis Chryssanthakis,
Karstein Monsen, Norges Geotekniske Institutt, Oslo, Norge

April 1988

SVENSK KÄRNBRÄNSLEHANTERING AB
SWEDISH NUCLEAR FUEL AND WASTE MANAGEMENT CO

BOX 5864 S-102 48 STOCKHOLM
TEL 08-665 28 00 TELEX 13108-SKB

VALIDATION OF MUDEC AGAINST COLORADO SCHOOL OF MINES BLOCK TEST DATA

Nick Barton, Panayiotis Chryssanthakis, Karstein Monsen

Norges Geotekniske Institutt, Oslo, Norge

April 1988

A B S T R A C T

The objective of this study was to validate the discrete element codes MUDEC-linear and MUDEC (with the Barton - Bandis joint model) against a well controlled in situ test. The measured results obtained from the CSM block test by Terra Tek Inc., by Richardson and Brown (CSM) and Leijon (LUT) were compared with the numerical results. Equal biaxial, north-south and east-west uniaxial loading were applied to each type of model. The boundary conditions were varied from the simple uniform stress boundaries of the linear joint model to the more realistic fluid pressurized boundaries, simulating the flat-jacks as rectangular slots. In addition, rigid boundaries prevented movement behind the flat-jacks.

Comparison of the numerical results with the stress measurements performed by Leijon and Brown, with Terra Tek's measurements of shear displacement, shear stiffness and conducting aperture, and with Richardson's measurements of displacement vectors and shear displacements showed generally a good agreement.

Excellent agreement was obtained for joint shear displacements and joint conductive apertures.

C O N T E N T S

CONTENTS (cont.)

1. INTRODUCTION

The realistic simulation of the mechanical and hydraulic properties of rock joints has been an important goal of numerical modelling for many years. Even simplified constitutive models demonstrate the extreme importance of joint characteristics. For example, a simple change of friction angle from 40° to 30° may alter not only the magnitudes of deformation, but also the type of deformation experienced by an excavation. When joint modelling is designed to also include different degrees of joint roughness, dilation and joint aperture, it is clear that a realistic predicted response will be dependent on correct constitutive models, which describe the way these parameters interact with changes of stress. Numerical instability may be experienced if input parameters are not mutually compatible.

Potential siting of nuclear waste repositories in jointed media such as granite, basalt, or tuff places added emphasis on the importance of joint properties. It is known from mining and tunelling practice, and from numerical models and physical models, that joint apertures vary in response to stress changes caused by excavation, to thermal loading and to dynamic loading. The potential migration of groundwater across a repository will be strongly influenced by the zones of reduced permeability caused by joint closure, and by the zones of increased permeability caused by shear displacement.

The constitutive model of joint behaviour described in detail in this report and utilized in the modelling is designed to satisfy two imporant goals:

1. Realistic simulation of observed phenomena
2. Inexpensive joint data acquisition

Preliminary modelling of repository response can be based solely on the characterization of joints recovered from

drillcore, together with the estimate of water conducting aperture obtainable from borehole pumping tests. Once access to the site is available, these preliminary joint characterization studies would be extended to obtain their directional variation.

The validation of a discontinuum code is not a trivial task, due to the difficulty of carrying out and interpreting large scale tests on discontinuous bodies of rock. In this project we have utilized one of the best documented in situ tests, performed on 8 m^3 of jointed gneiss. In the next chapter we summarize key aspects of this test and indicate how the input data is utilized in the performance assessment of the discontinuum code MUDEC (Micro Distinct Element Code for Personal Computer use only) which is a version of UDEC (Cundall, 1980). In other studies, the finite element code HNFEMP (Stephansson et al, 1988) is validated against the same block test, in order to compare discontinuum and continuum type models.

A series of MUDEC runs is reported in the Appendix of this report.

2. CSM BLOCK TEST PHILOSOPHY

The block test used in this code validation is located at Idaho Springs, Colorado in an experimental mine operated by the Colorado School of Mines. The block test facility was initially established by Terra Tek Inc, (Hardin, Barton, Lingle, Board and Voegele, 1982) and has since been utilized by a number of research scientists from CSM and also from LUT (Luleå University of Technology), Brown et al. (1986).

This block test was designed to produce coupled stress-temperature-conductivity data for a selected joint crossing the loaded block. It was also designed to produce rock mass deformation data for a variety of loading scenarious (uniaxial,

biaxial, ambient and elevated temperature). The deformation characteristics of individual joints and of the block as a whole were each measured.

The 8 m^3 block incorporated at least thirty discrete blocks. It is the interaction of rock blocks which largely determines the degree of non-linear, size dependent behaviour typical of rock masses. The presence of joints and additional excavation-induced fracturing has obvious implications to the stability of shafts and repository tunnels prior to terminal waste storage and sealing. However, the most critical property of joints is that they probably penetrate the final barrier to radionuclide migration to the biosphere, and their permeability may be enhanced close to the excavations.

The pervasiveness of joints and major discontinuities to several kilometers depth in the geosphere suggests that special attention be given to flow transport times, both in characterization, testing, and in the numerical modelling. Since flow velocities are proportional to the square of the effective joint conducting aperture, this geometrical property is of the utmost importance in site characterization. As an illustration, one of the test joints intersecting the test block showed variations in conducting aperture from 60 µm to 9 µm in response to stress and temperature perturbations of no more than 7 MPa and 60^{o}C. This variation represents a potential 45-fold increase in transport time for an equally stressed and heated region. Opposite effects of much larger magnitude may occur if shear displacements occur along the joint. These effects have to be accounted for in the proposed discontinuum modelling.

3. CSM BLOCK TEST DATA

Figures 1 and 2 provide an overview of the test block location and an idealized 3 D view of the geometry of the block. The slots drilled in the floor of the test drift for the 2 m long flatjacks were drilled to a depth of 2.25 m. The flatjacks were greased prior to cement grouting in the slots. A grout-steel interface friction of about 10^{o} maybe assumed, but this parameter is a source of uncertainty.

3.1 Joint Structure

The summary of the joint structure presented here is relevant specifically to joints observed in the immediate vicinity of the block, since only these joints have relevance to the mechanical behaviour of the block during the loading and unloading cycles.

The Precambrian granitic gneiss was interspersed with lenses of pegmatite, biotite schist and quartz, resulting in local variations in the foliation orientation. The predominant strike and dip of foliation joints at the block was $45^{o}/88^{o}$. Most of these joints appeared to be continuous over at least 1-2 metres and they crossed the block in an E -W direction (see Figure 3). Their average spacing was 60 cm. The major set of mineralized joints crossing the block diagonally had a predominant orientation of $106^{o}/89^{o}$. Most of these joints appeared to be continuous over at least 2-3 metres, and had an average spacing of 75 cm.

A third set termed the longitudinal set since they strike parallel with the axis of the test adit, were predominantly oriented at $134^{o}/85^{o}$, with an average spacing of about 1 metre, and continuity 0.5-1.5 metres.

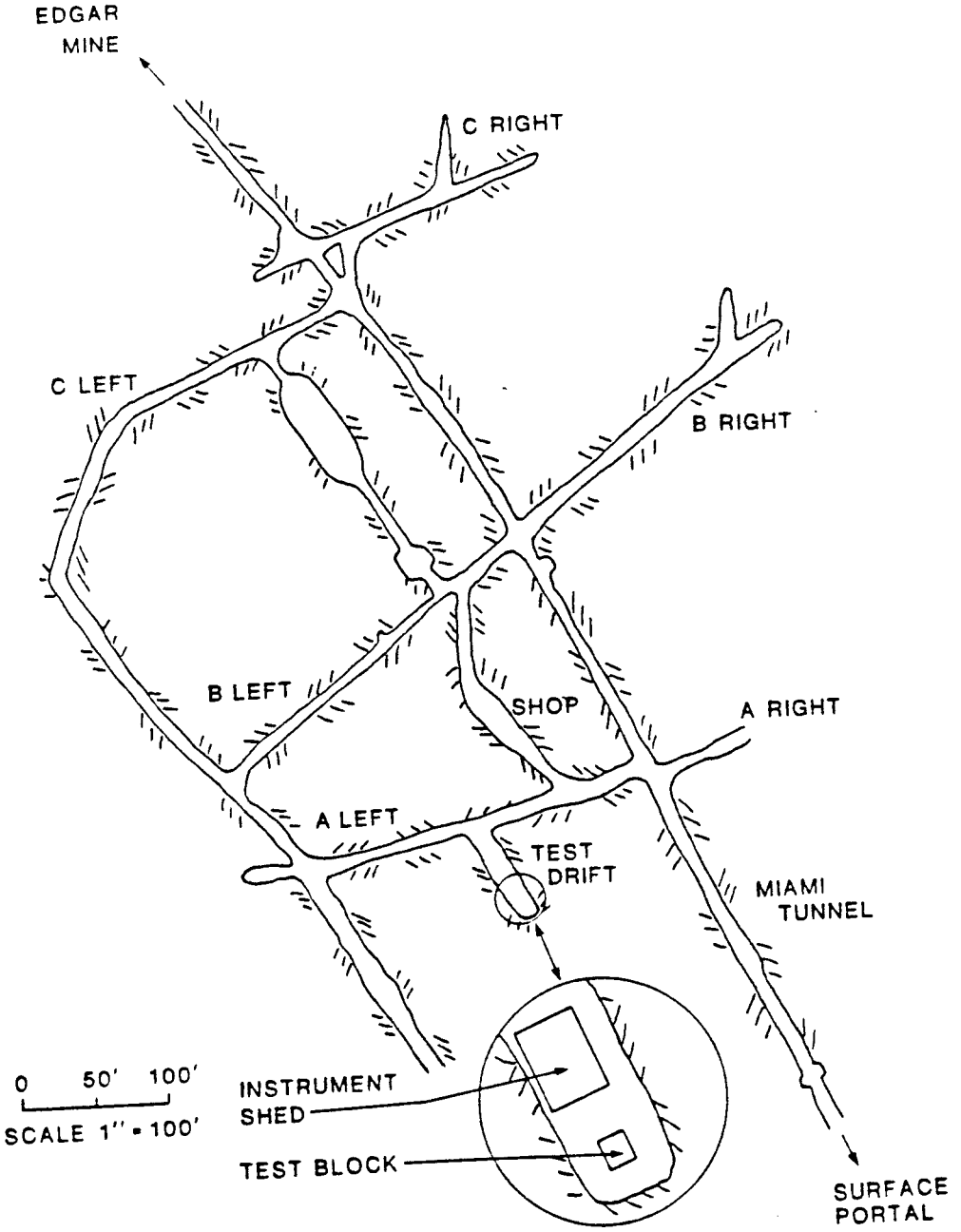

Fig. 1 Plan view of mine layout, showing test block loaction.

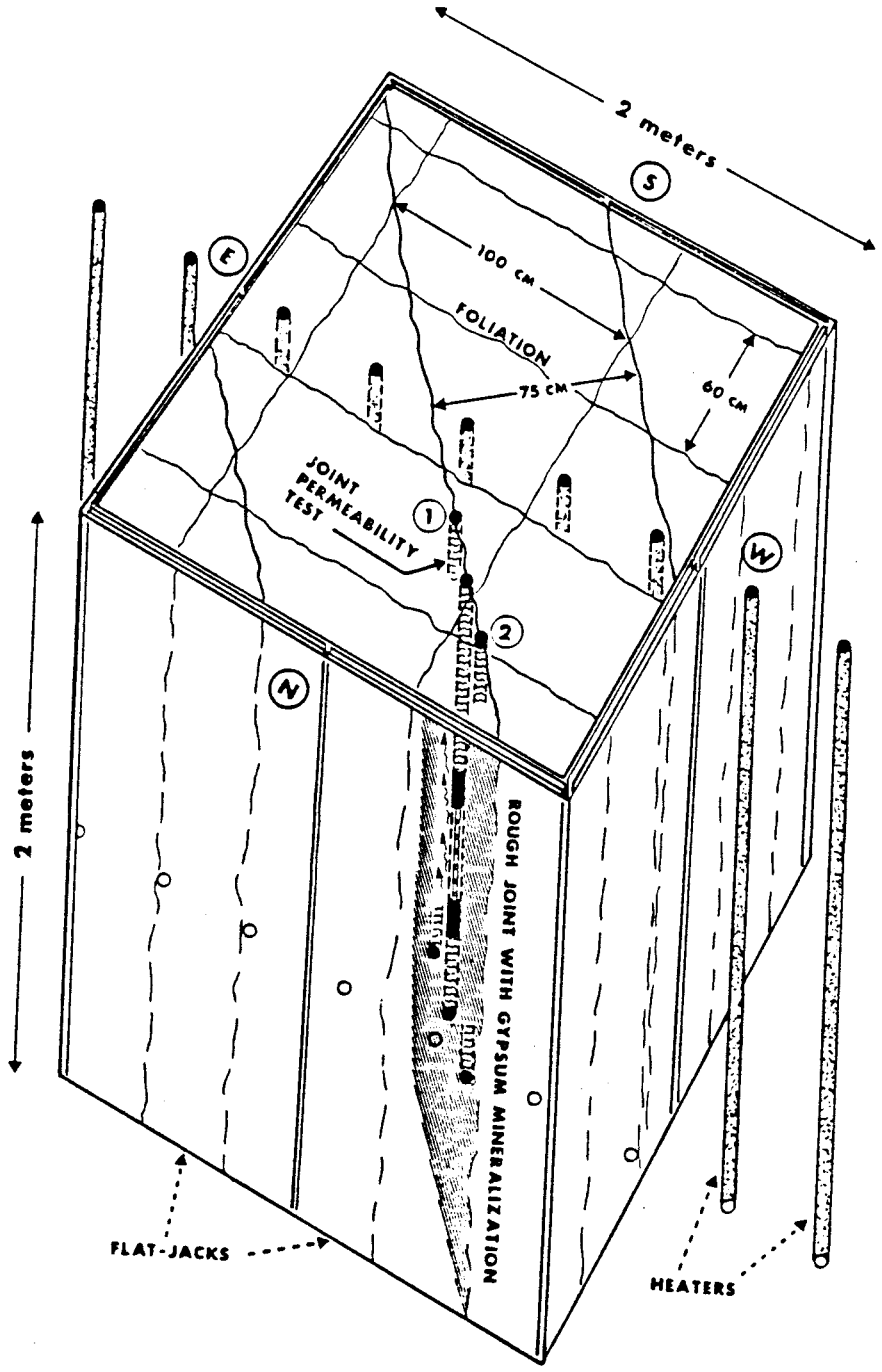

Fig. 2 Schematic diagram showing the relationship of the average joint structure to the flat-jacks used to load the four vertical boundaries of the block.

The stereo-plot of joints observed closed to the block (Figure 4) indicated some minor joints of shallower dip, but their limited continuity of 0.5-1 meter probably made them of less sigificance to block deformability than the three sets depicted in Figures 2 and 3. One of the diagonal joints crossing the block almost from corner to corner (≠1, Fig. 3) was the subject of the permeability measurements described later.

Based on the above observations of significant jointing, the rock block size index (ISRM 1978) is approximately 75 cm, the volumetric joint count approximately 4.8 joints/m^3 (medium size blocks) and the rock quality designation (RQD) is 90-100%. There are a minimum of 30 discrete interlocked blocks within the loaded 8 m^3 test block. Horizontal fracturing due to blast damage may effectively double or triple this number.

3.2 Joint properties

Careful recording of joint roughness profiles, and measurement of the joint wall strengths using a Schmidt hammer allowed estimates to be made of the peak shear strength of the joints (Barton and Choubey, 1977). Bandis (1980) has shown that the two parameters JRC (joint roughness coefficient) and JCS (joint wall compression strength) also control the normal closure of joints. Furthermore, JRC and JCS provide an accurate data base for predicting the dilation path during shearing - which has an enormous influcence on the joint aperture, and hence also on permeability, (Barton, 1981). Due to the powerful predictive properties of these two parameters, and the importance of numerical modelling to the design of geologic waste repositories, considerable attention was paid to the joint characterization during the performance of this block test.

Since the completion of the block test, the parameters JRC and JCS have been incorporated in a comprehensive numerical code capable of coupling the size dependent shear, dilation and conductivity behaviour, and the normal closure and conductivity

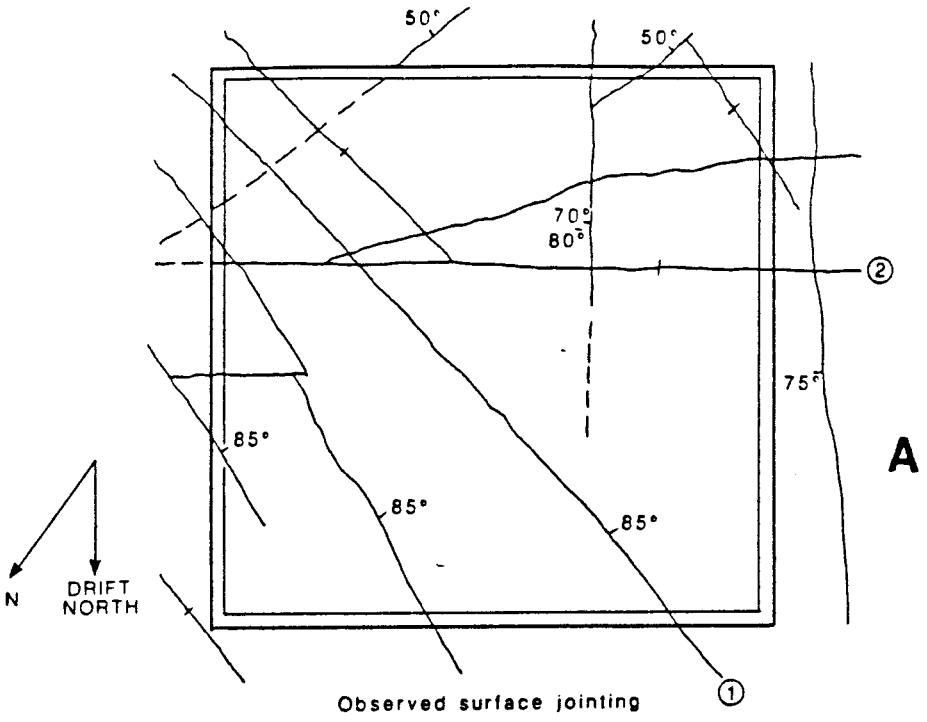

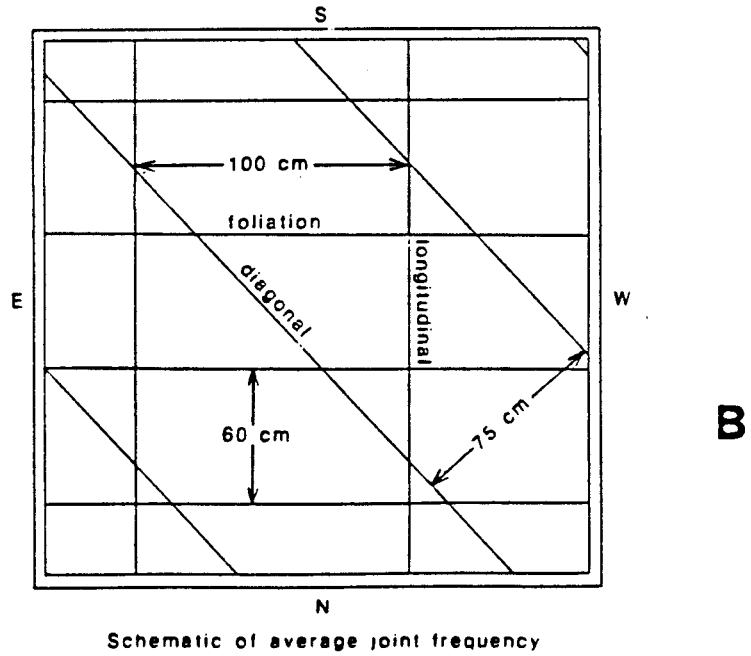

Fig. 3 Three predominantly vertical joint sets intersect the block.

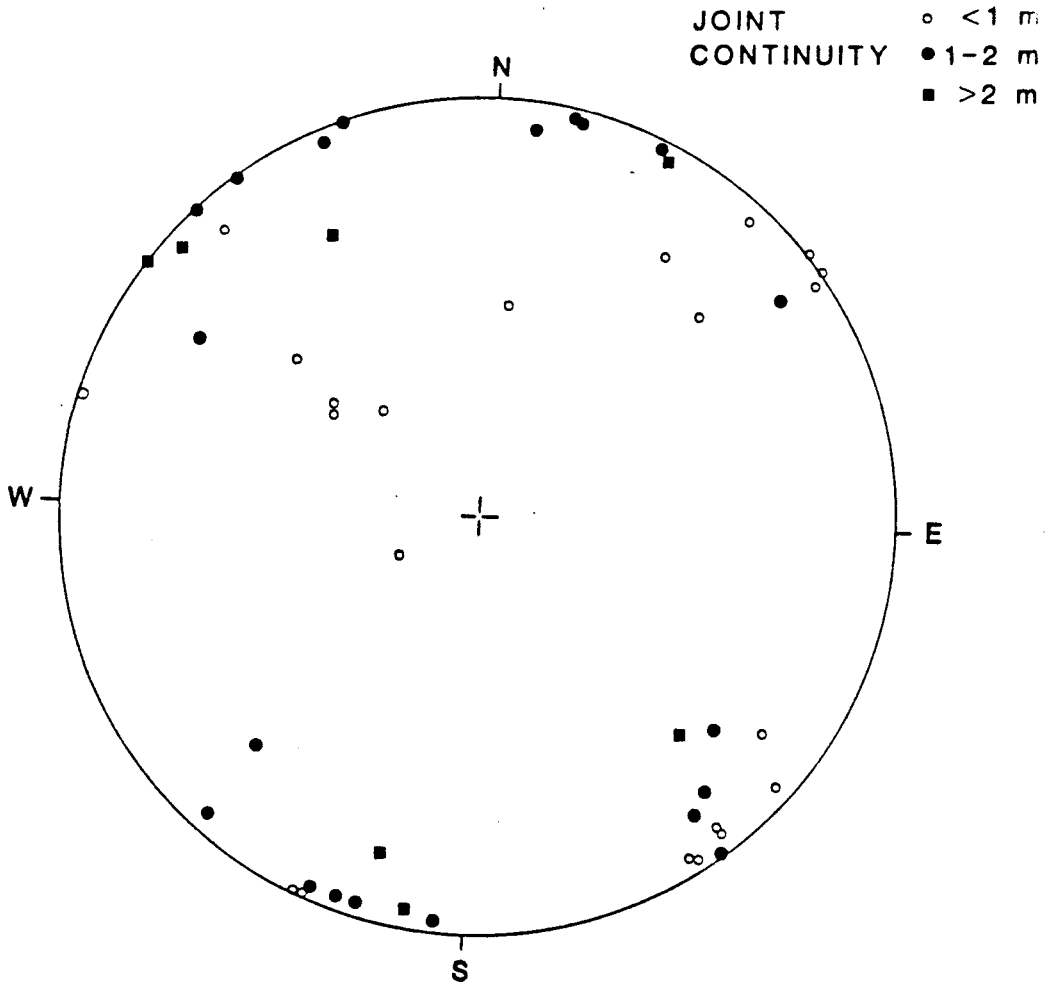

Fig. 4 Stereo plot of fifty joint observations made within 10 metres of the block, indicating the predominance of vertical or steeply dipping significant joints.

(Barton, Bakhtar and Bandis, 1985). The application of this code using block test parameters will be demonstrated in Section 4.

3.2.1 JCS - Joint Wall Compression Strength

Schmidt (L) hammer rebound tests were conducted in large numbers on the weathered, partly mineralized diagnoal joints, which are subject to shear when the N-S or E-W flatjacks are activated separately in the uniaxial loading tests. Rebound tests were also conducted on the generally less weathered foliation joints, and on fresh (blast induced) fracture surfaces in the banded gneiss and quartz lenses. A summary of the results is given in Figure 5. Estimates of JCS and σ_c were made using Miller's (1965) correlation between the rebound number, the rock density (mean 27.8 KN/m^3) and the unconfined compression strength. The extremely high rebound numbers measured in the quartz explain the difficulties experienced during the flatjack slot drilling, Hardin et al., 1982.

On the present report, the subscripts JCS_o and JRC_o indicate the use of laboratory scale parameters for normal closure modelling. Scale effects are assumed to be of only minor consequence to normal closure due to the dominant effect of small scale roughness. However, when shearing occurs scale effects may prove to be of extreme importance since the small scale roughness ceases to be in intimate contact. A value of JCS_o = 90 MPa was determined for the "laboratory scale" value.

The major, mineralized, weathered joint intersect the block diagonally, and also the subject of the permeability test (Figure 2) was assumed to be most closely characterized by the rebound tests on the weathered diagonal joints in the vicinity of the block.

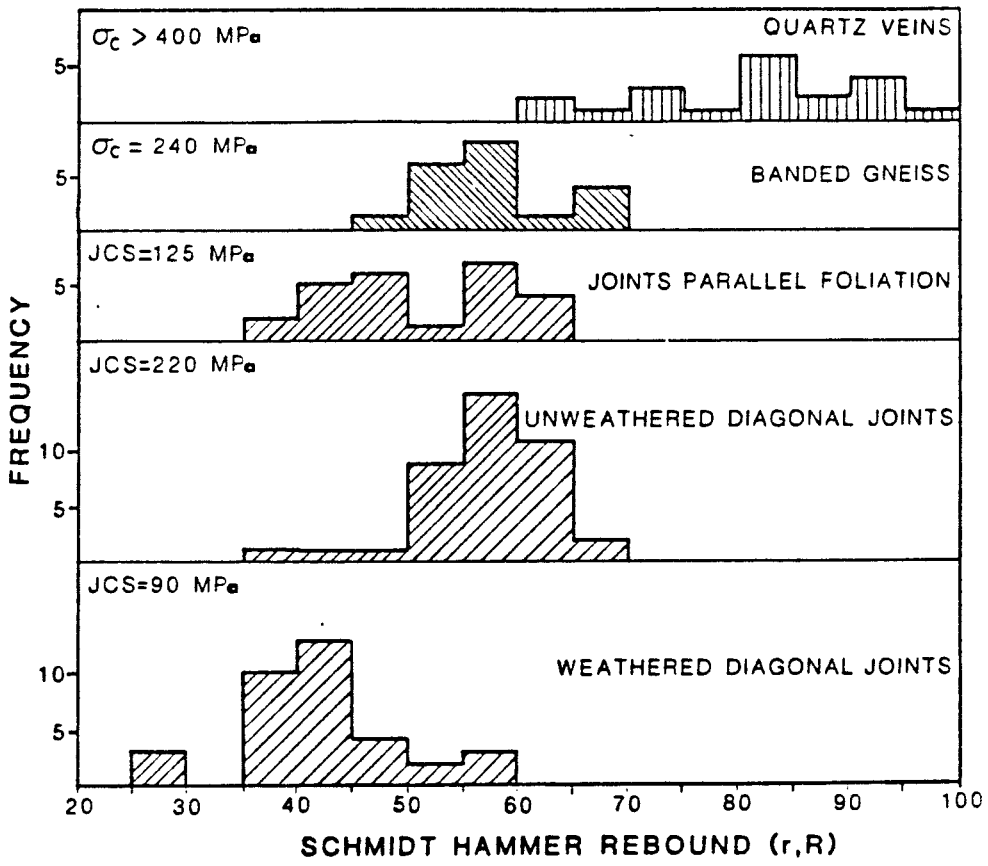

Fig. 5 Estimates of joint wall compression (JCS) and unconfined compression strength (σ_c) obtained from numerous Schmidt Hammer tests.

3.2.2 JRC - Joint Roughness Coefficient

Vertical and horizontal roughness profiles were recorded using a 15 cm long contour gauge. Figures 6 and 7 show that there was a fairly clear distinction between the foliation joints (mean JRC = 10) and the weathered diagonal joints (mean JRC = 13).

Longer profiles were also recorded, in case larger scale waveness proved to be a factor in the mechanical behaviour of the block. The maximum amplitude (a) of the asperities over a 1300 - 1600 mm base length (L) was in the range 31 - 38 mm for the case of the diagonal joints. The various measurements of a/L suggested a fullscale value of JRC of about 10, in comparison with the small scale value of 13.

3.2.3 Tilt Tests of Jointed drillcore

The three vertical boreholes drilled down the plane of the diagonal joint (Figure 2) produced several axially jointed pieces of core. These were profiled (Figure 8) and tilt tested, as shown schematically in Figure 9. Damage to the mineralized joint surfaces during core recovery was probably responsible for the reduced values of JRC (7.9-8.3) back-calculated from these tilt tests (see Barton and Choubey, 1977 for test details).

Methods for correcting JCS and JRC for the observed scale effect on the shear strength of joints were applied to the above results, using the methods developed by Bandis et al. (1981). Significant values for interpreting the block strength and deformability are given below:

	Estimated Full Scale Values		
	JCS_n	JRC_n	ϕ_r
diagonal joints	50-65 MPa	6.7-10.0	25°

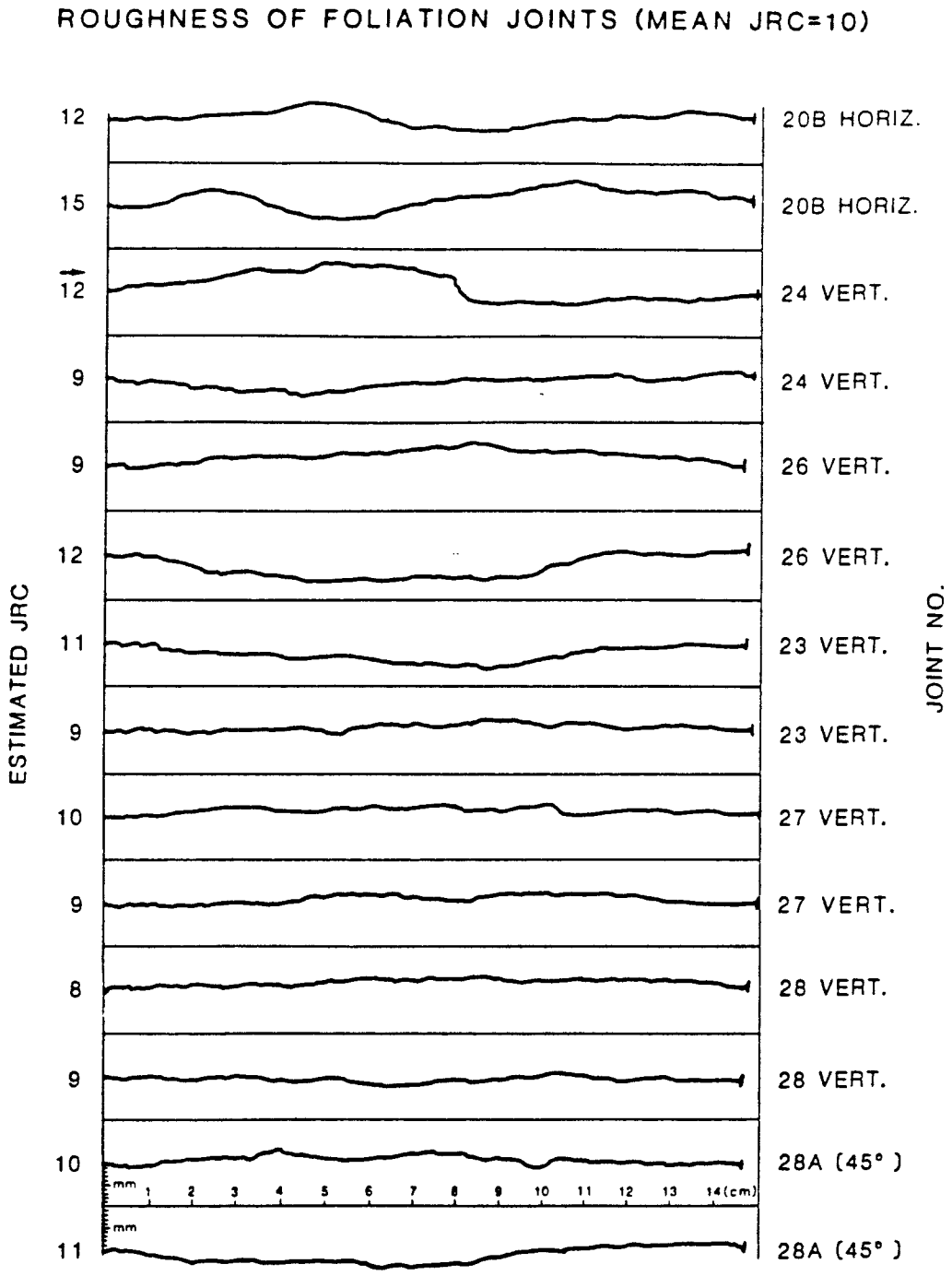

Fig. 6 Roughness profiles measured along the foliation joints.

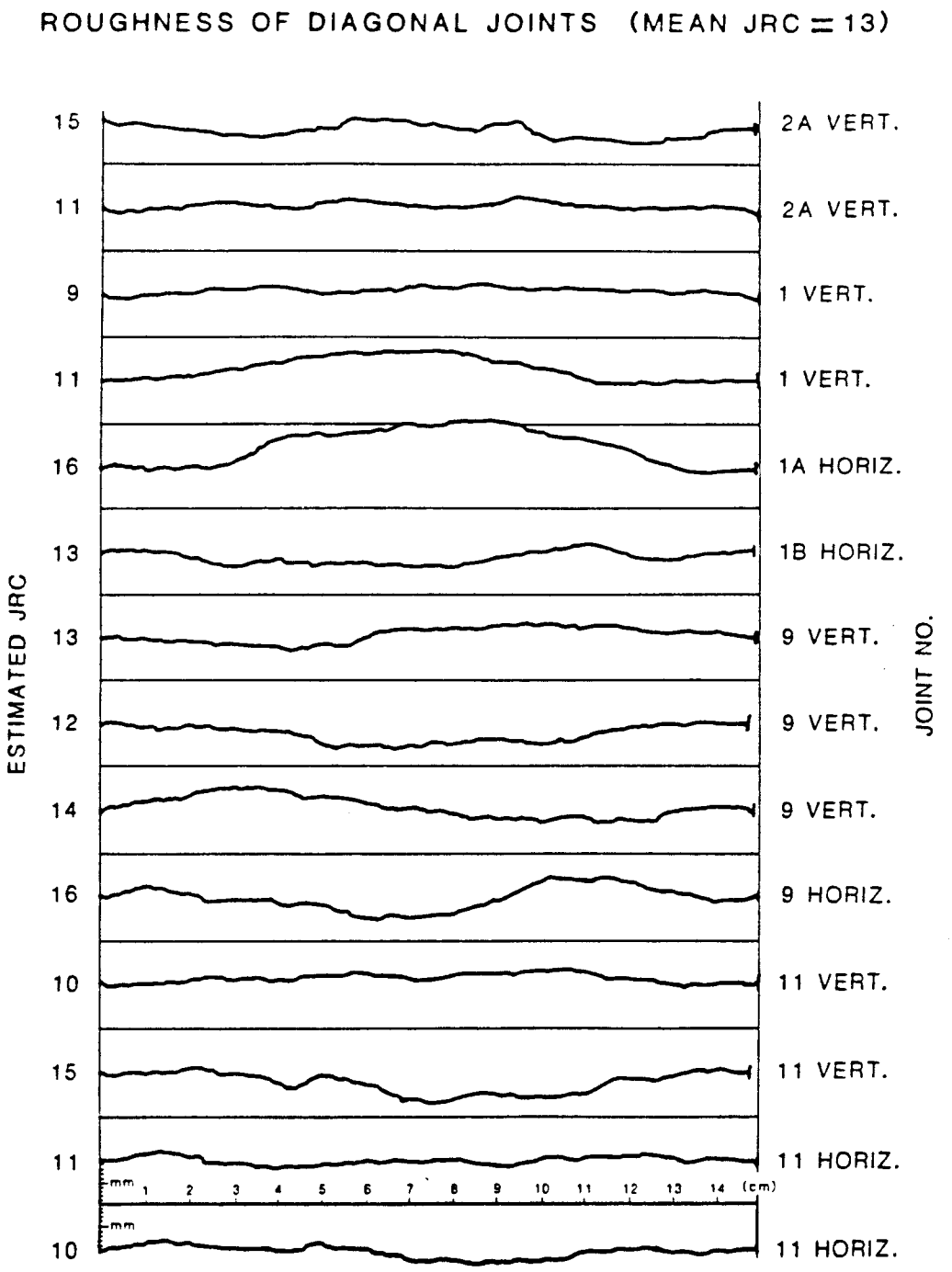

Fig. 7 Roughness profiles measured along the weathered diagonal joints.

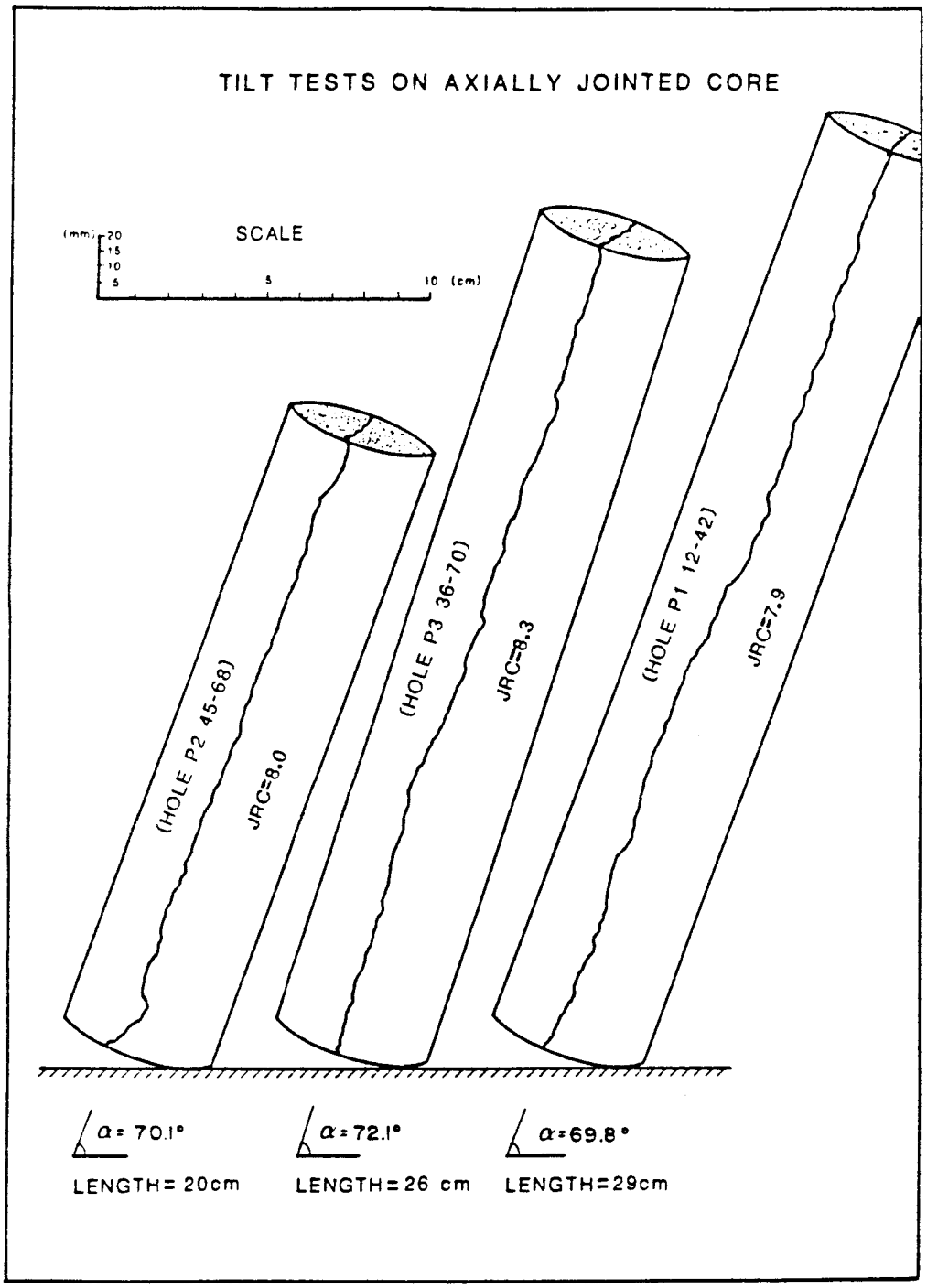

Fig. 8 Measured roughness profiles and tilt angles recorded on three pieces of axially jointed core obtained from the permeability test holes.

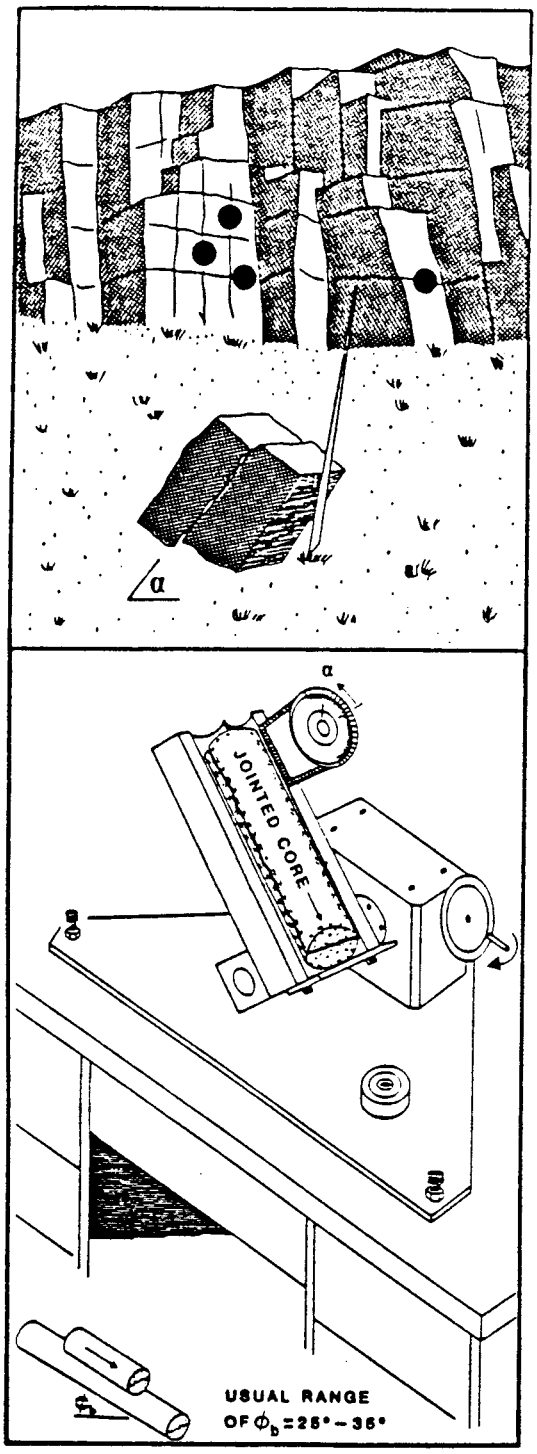

Fig. 9 Tilt test for obtained joint roughness and basic friction parameters.

The peak shear strength (τ) and the peak friction angles (ϕ') for these major joints, which are loaded in shear during the uniaxial tests, are given by the following equations:

$$\tau = \sigma_n' \cdot \tan\phi' \qquad \phi' = JRC \log (JCS/\sigma_n') + \phi_r \qquad (1)$$

where σ_n' = effective normal stress
ϕ_r = residual friction angle

The basic friction angle (ϕ_b) for planar, unweathered surfaces of the rock was obtained by conducting tilt tests on pieces of borecore, as illustrated in Figure 9. Tests run perpendicular to the foliation gave a mean value of $\phi_b = 32.5^o$, and parallel to the foliation: 30.5^o. Since the diagonal joints intersect the foliation at an acute angle, a representative value of $\phi_b = 31°$ was assumed.

The value of the residual friction angle of the weathered joints ($\phi_r = 25^o$) was estimated from the results of Schmidt hammer tests on the weathered joint wall (mean rebound r = 39), and on unweathered surfaces of the gneiss (mean rebound R = 55), using the empirical relationship (Barton and Choubey, 1977):

$$\phi_r = (\phi_b - 20^o) + 20\ (r/R) \qquad (2)$$

4. NUMERICAL MODELLING OF JOINT BEHAVIOUR - BACKGROUND

The method we have developed for obtaining realistic joint behaviour for input into discontinuum codes and the smeared out approach in the non-linear finite element code is based on the parameters:

JCS_o	= lab.scale joint wall compression strength	(MPa)
JRC_o	= lab.scale joint roughness coefficient	(-)
ϕ_r	= residual friction angle	(degrees)
E	= physical joint aperture	(mm)
e	= conducting aperture	(mm)

4.1 Shear and Dilation Behaviour

The peak shear strength given by equation 1 can be generalized to represent full-scale, displacement-dependent shear strength by the following equation:

$$\Phi_{mob} = JRC_n \text{ (mob) } \log (JCS_n/\sigma_n') + \phi_r \qquad (3)$$

where the subscript (n) denotes full scale parameters (based on natural block size) and the subscript (mob) represents the roughness and friction mobilized after a specific displacement. The dilation angle mobilized at any given displacement is given by the following approximation:

$$d_n \text{ (mob)} = 1/2 \; JRC_n\text{(mob)} \log (JCS_n/\sigma_n') \qquad (4)$$

The method of estimating JRC_n and JCS_n from the lab.scale values JRC_o and JCS_o is given in equation 5 and 6:

$$JRC_n = JRC_o \left(\frac{L_n}{L_o} \right)^{-0.02 \; JRC_o} \qquad (5)$$

$$JCS_n = JCS_o \left(\frac{L_n}{L_o} \right)^{-0.03 \; JRC_o} \qquad (6)$$

The concept of JRC (mob) is explained graphically in Fig. 10.

The above model for developing shear strength-displacement and dilation-displacement behaviour is explained more fully by Barton, (1981) and the logic for numerical modelling by Barton and Bakhtar (1984). Examples of its application to individual foliation and diagonal joints in the block test will be given later in this chapter.

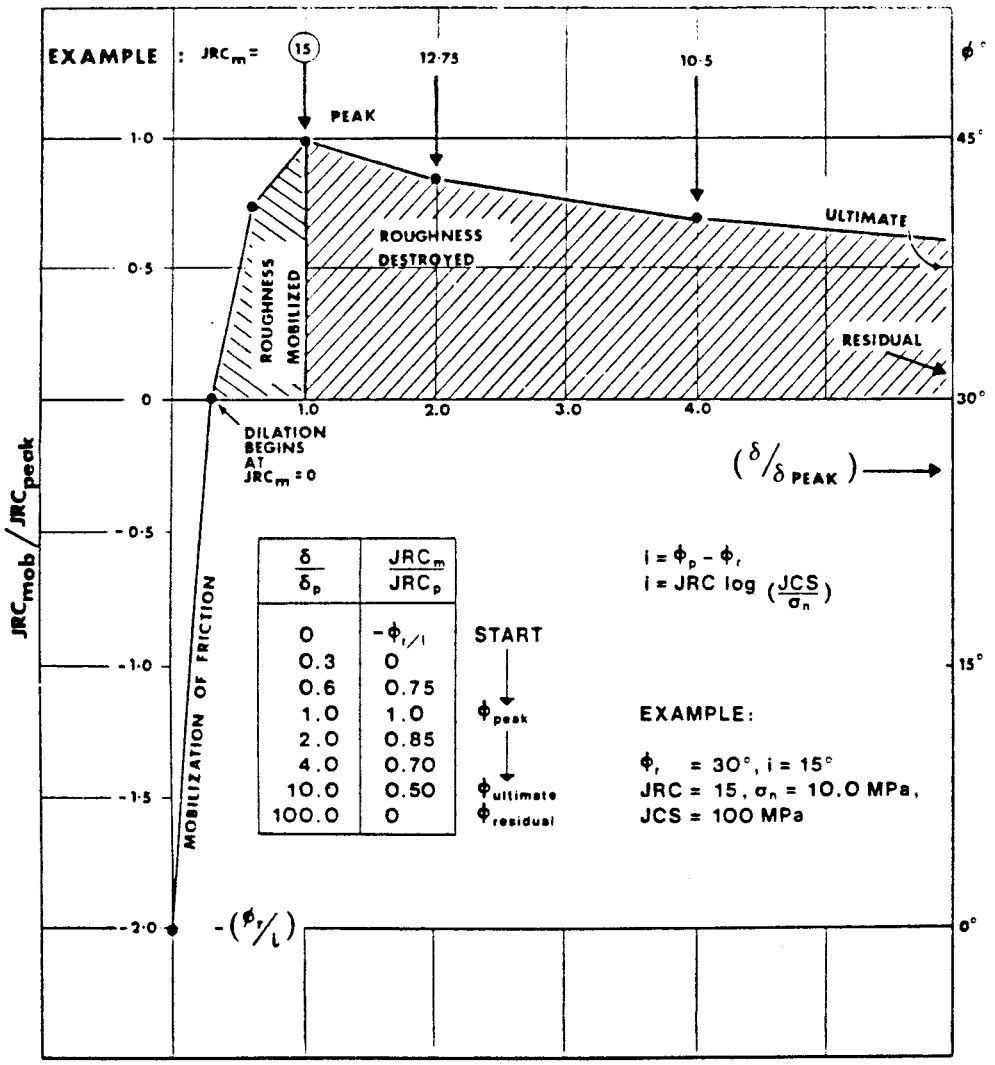

$\frac{\delta}{\delta_p}$	$\frac{JRC_m}{JRC_p}$
0	$-\phi_{r/i}$
0.3	0
0.6	0.75
1.0	1.0
2.0	0.85
4.0	0.70
10.0	0.50
100.0	0

Fig. 10 Dimensionless model for shear stress-displacement modelling, after Barton (1981). In this example $\phi_r/i = 2$.

4.2 Normal Closure Behaviour

The normal stress-closure behaviour of the joints that is modelled in the block test validation is based on the Bandis (1980) hyperbolic function. The equation he developed gave an excellent fit to numerous experimental data, both for fresh and weathered surfaces:

$$\frac{\Delta V_j}{\sigma_n} = a - b\,\Delta V_j \qquad (7)$$

where ΔV_j = joint closure
σ_n' = effective normal stress
a, b = constants

The asymptote to the hyperbole (a/b) is equal to the maximum joint closure (V_m), and the constant (a) is equal to the reciprocal of the initial normal stiffness (K_{ni}).

Expressions for K_{ni} and V_m are based on the following empirical relationships derived by Bandis (1980), see Bandis et al.(1983)

$$V_m = A + B\,(JRC_o) + C\,\left(\frac{JCS_o}{E_o}\right)^D \qquad (8)$$

where A, B, C and D are constants (varying with loading cycle)

E_o = initial physical aperture

The initial normal stiffness (at low stress) is given by:

$$K_{ni} = 0.02\,\left(\frac{JCS_o}{E_o}\right) + 2JRC_o - 10 \qquad (9)$$

(units MPa/mm, GPa/m)

An illustration of the typical shape of loading-unloading curves from Bandis (1980) is given in Figure 11. Modified (reduced) normal stiffness values for increasingly mismatched (sheared) joints are incorporated in our model of joint beha-

viour. Further details of normal closure behaviour are summarized in Fig. 12.

4.3 Joint conductivity

The ultimate barrier to radionuclide migration from a geologic repository is the rock mass. The fact that the rockmass is permeable due to the presence of joints and major discontinutities adds emphasis to the importance of joint characterization. Probably the single most important parameter to be characterized is the effective water conducting apertures of the joints that are intersected by the repository. It is therefore important to consider this parameter in some detail.

During surface borehole studies, estimates of the variation in aperture (e) for the different joint sets may be back-calculated from flow tests, using closely spaced double-packers coupled with a method for accurately locating the packer across joints. The estimates of (e) obtained from these tests could also be based on the statistical method proposed by Snow (1968), which provides a useful estimate of not only the conducting aperure (e), but also the mean spacing of the water conducting joints (S), assuming the rock mass can be idealized by a cubic network of joints.

In each case the estimated apertures will reflect the effective normal stress levels operating across the joints at the various test levels. Care would need to be taken to inject water at very low excess pressures, so as not to significantly reduce the effective normal stress level and cause opening of the joints, close to the borehole walls.

The consequence of shear displacement on repository stability and on joint permeability is also important. If the relevant joints are rough, with high wall strength, stability will not necessarily be reduced by the excavation or thermally-induced

shearing process, since roughness-induced dilation will lock the joints in some finite displaced position. The only serious consequence of this process is the joint "aperture strain". Permeability may be enhanced around the repository tunnels and shafts.

Ambient temperature tests of joint permeability as a function of normal stress or aperture have been widely reported. There appears to be considerable discrepancy in the interpretation of results. Some authors (e.g. Witherspoon et al., 1979a) initially suggested that the cubic law relating aperture and flow rate is valid even for rough fractures in intimate contact. Other authors (e.g. Kranz et al., 1979 and Walsh, 1981) have explained the measured flow reductions caused by tortuosity and roughness, by a modification to the law of effective stress.

The possibility of a scale effect on joint permeability has been suggested by Witherspoon et al. (1979b). At present, the data base is too limited and diverse to make definite conclusions. It is often unreasonable to try to compare the permeabilities of rough, fresh artificial fractures (a typical test configuration) with weathered natural joints of different roughness, since the degree of aperture closure under a given stress level will vary in each case. Barton (1981) suggested that scale dependent joint permeability will probably not be a significant factor under conditions of pure normal closure, but will be observed when shearing occurs. This is due to the scale-dependent dilation that occurs when joints of different length are sheared, as shown in a major test program reported by Bandis (1980), and Bandis et al. (1981).

An attempt to collect together the limited data on joint conductivity under a variety of stress levels is usualy thwarted by insufficient information of the joint characteristics, and lack of deformation measurements. Figure 13 shows a compilation of available data at different stress levels where approximate

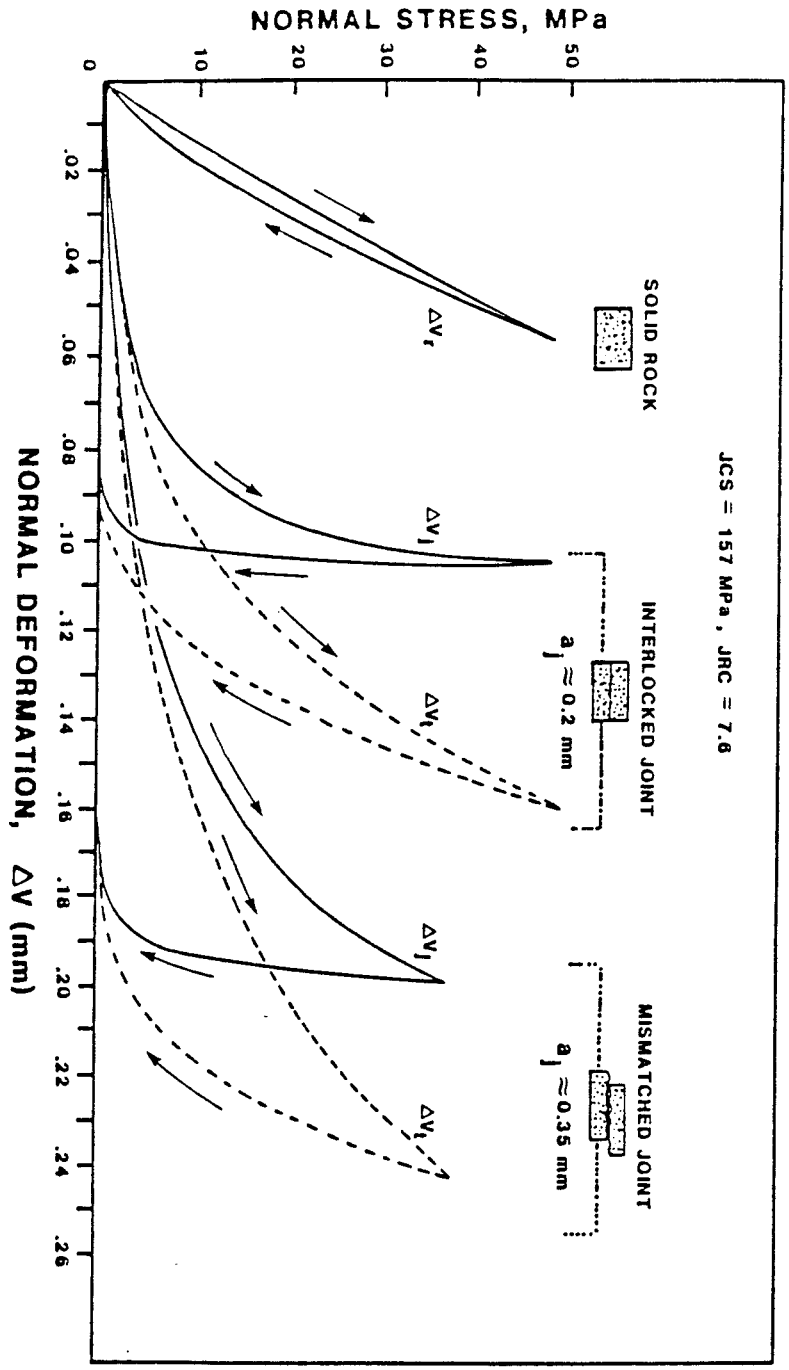

Fig. 11 Stress-closure behviour typical for a medium rough joint (JRC_o = 7.6) in a strong unweathered rock (JCS_o = 157 MPa), after Bandis (1980). Note aj = in text.)

NORMAL CLOSURE OF JOINTS

(HYPERBOLIC FUNCTION) Bandis, 1980

$$\frac{\Delta v_j}{\sigma_n} = a - b\Delta v_j \qquad (1)$$

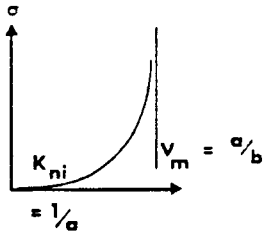

$$v_m \simeq A + B[JRC_o] + C\left[\frac{JCS_o}{a_j}\right]^D \qquad (2)$$

$$K_{ni} \simeq 0{\cdot}02\left[\frac{JCS_o}{a_j}\right] + 2\,JRC_o - 10 \qquad (3)$$

NORMAL STIFFNESS OF JOINTS

(derivative of hyperbolic function)

$$K_n = K_{ni}\left[1 - \frac{\sigma_n}{v_m K_{ni} + \sigma_n}\right]^{-2}$$

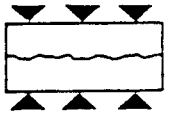

I. INTERLOCKING JOINTS

i.e. K_n is not proportional to σ_n

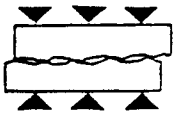

II. MISMATCHED JOINTS

K_n is proportional to σ_n

Fig. 12 Summary of key aspects of joint closure behaviour.

JRC_o values are known. The bars marked NS, EW, B refer to the block test. B refers to equal biaxial loading, with no shear component on the diagonal joint used for conductivity monitoring (Figure 2). Subsequent tests with the NS flatjacks alone, (or the EW flatjacks alone) caused slight shear and perhaps some debris development. Increasing values of $\Delta E/\Delta e$ are expected if contacting areas are fully sealed by debris, leaving only the tortuous channels between as conducting routes.

An attempt to synthesise the data in Figure 13 into a form suitable for numerical simulation is illustrated in Figure 14.

The empirical equation is used to convert physical or real aperture changes (ΔE) to conducting or theoretical aperture changes (Δe). These may be caused by normal stress changes, by dilation, or by pore pressure changes. Conductivity is given by

$$k = e^2/12 \qquad (10)$$

4.4 Modelling Coupled Behaviour

A straightforward application of the joint model to coupled behaviour is illustrated in Figure 15. The input data was obtained from characterization at a second block test site, the welded tuff in G-Tunnel, Nevada Test Site. The values of (E) and (e) shown at three different stress levels for fourth cycle loading demonstrate the manner in which the Figure 14 model keeps track of physical apertures and converts them to conducting apertures.

Figure 16 demonstrates how equations 3, 4, 5 and 6 and Figure 10, (together with Figure 14 and equation 10) are each coupled to provide the predictions of shear strength-displacement, dilation-displacement, and conductivity-displacement. The effects of varying normal stress from 10 to 30 MPa, and of varying block size from 100 to 250 mm are clearly demonstrated.

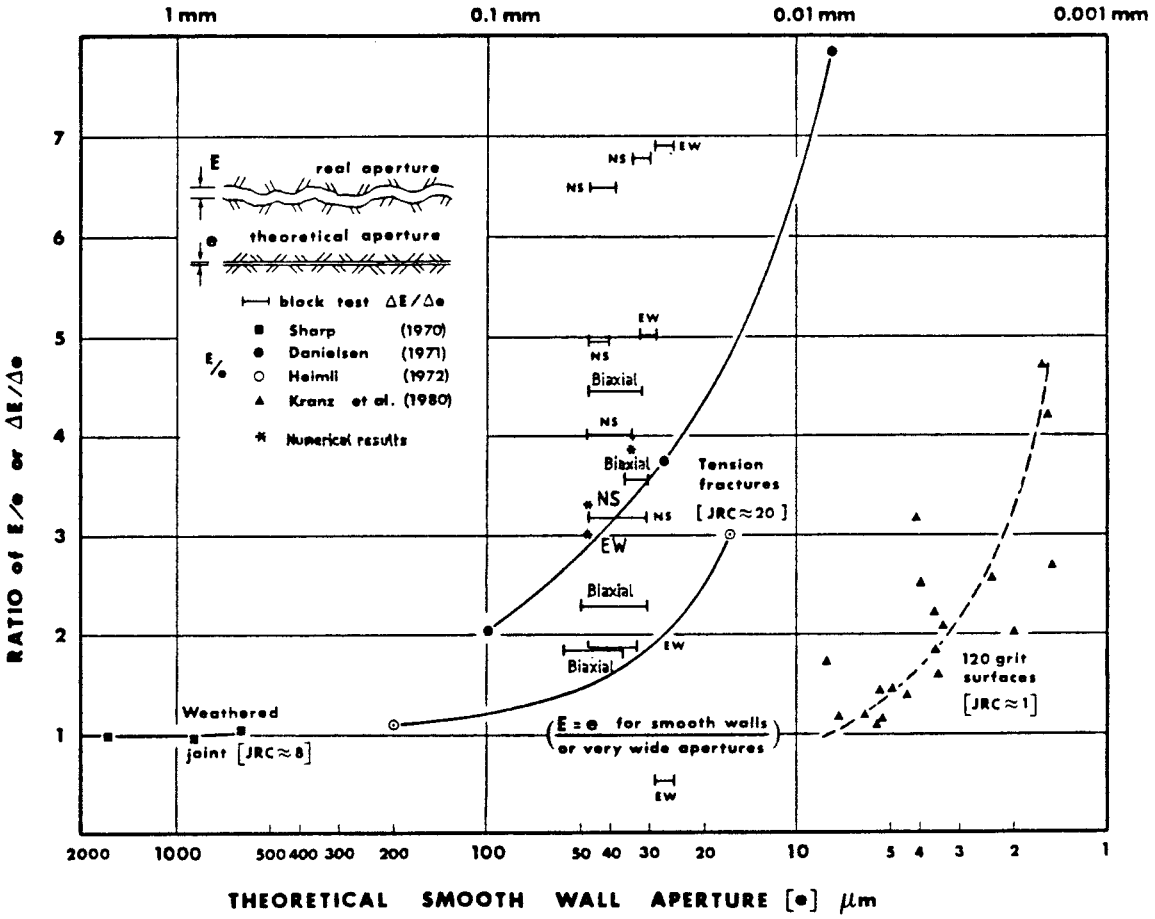

Fig. 13 Ratio of E/e which is expressing losses in tortuosity and roughness. The results obtained from the numerical simulation are marked with an asterisk.

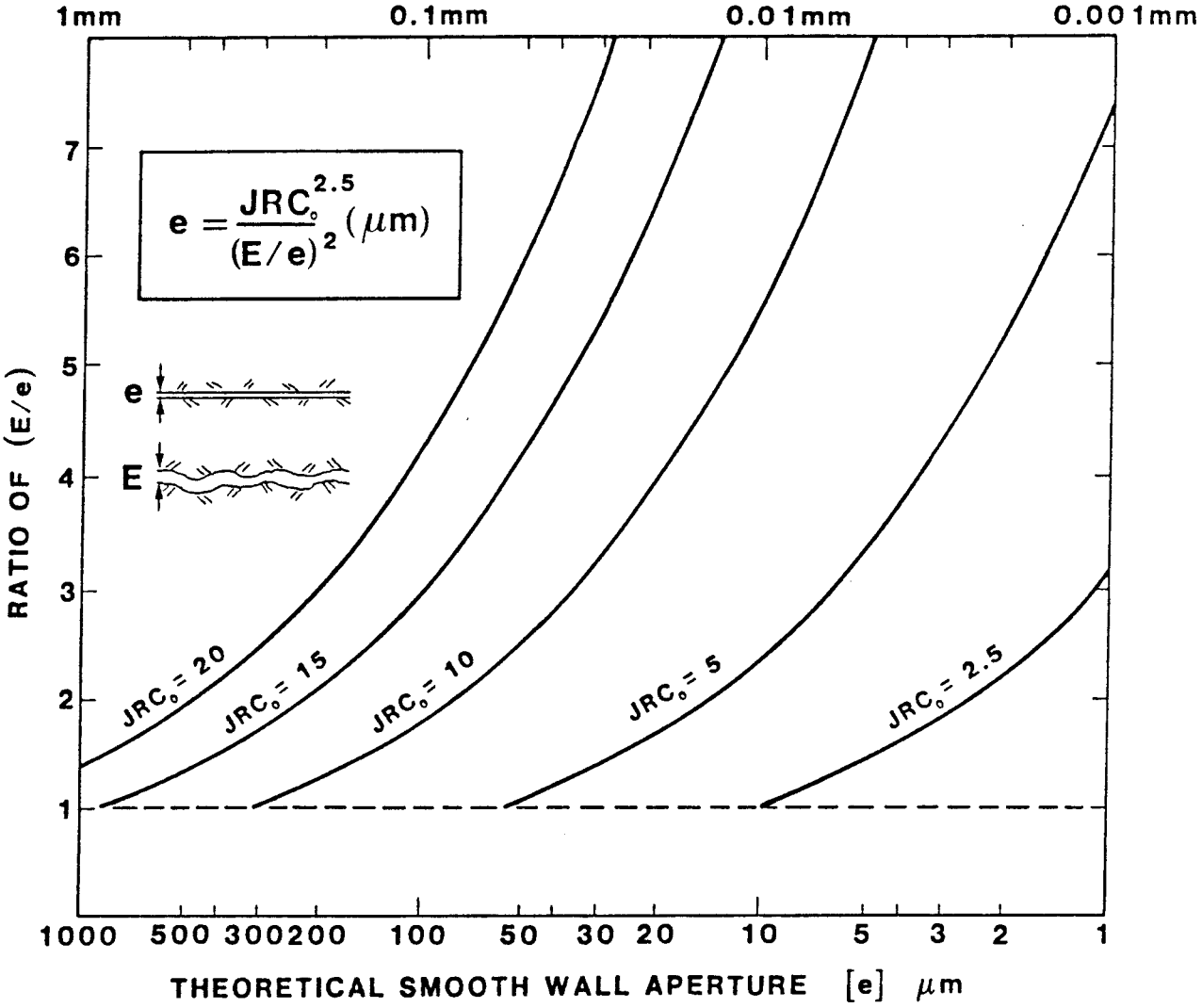

Fig. 14 Empirical approximation to the mismatch of physical (E) and conducting (e) apertures, based on lab. scale roughness, JRC_o.

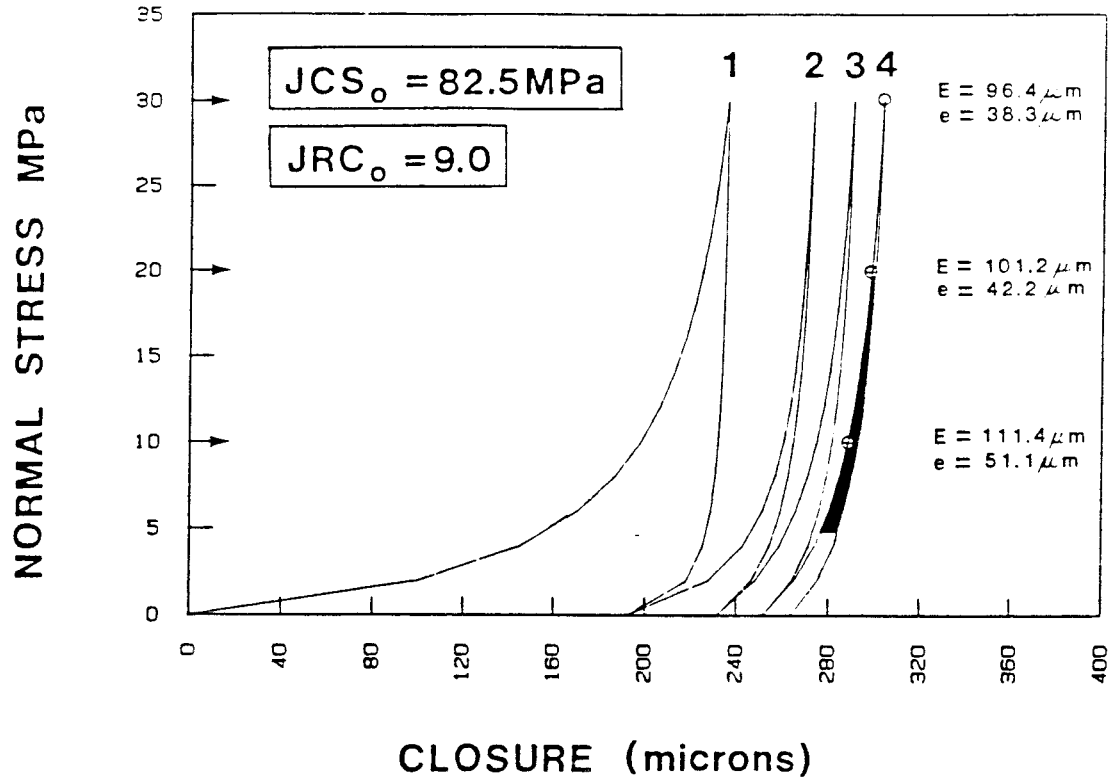

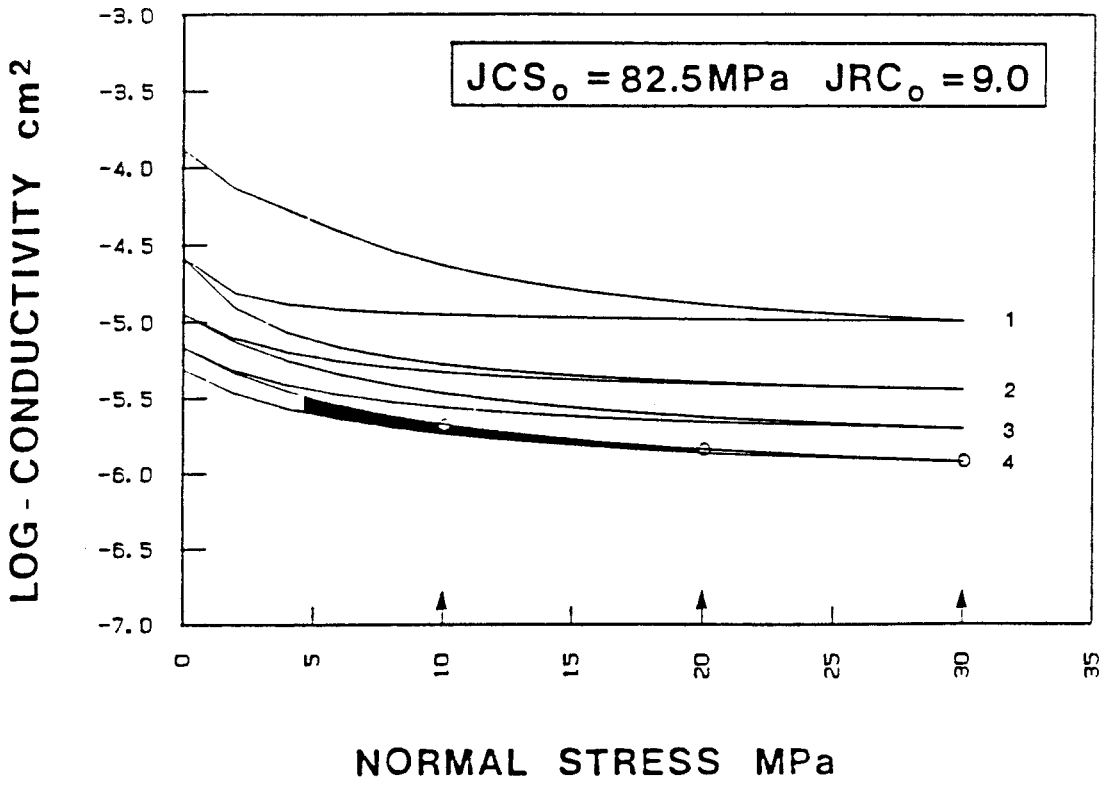

Fig. 15 Example of stress-closures and stress-conductivity modelling, after Barton et al. (1985).

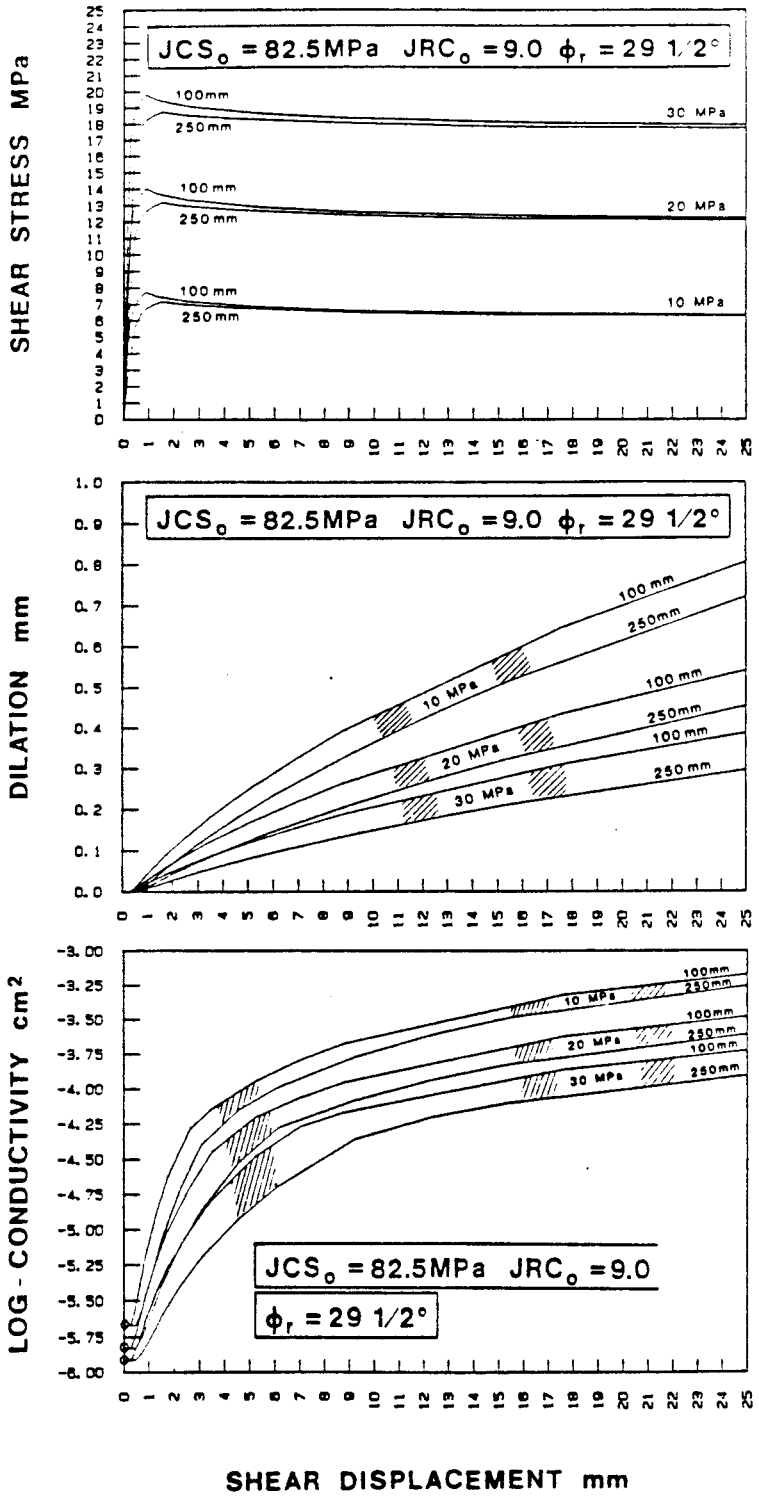

Fig. 16 Modelling the effect of potential events for joints in welded tuff, following the normal closure modelling shown in Fig. 15.

5. BLOCK TEST JOINT MODELLING FOR CODE VALIDATION

The examples of hydro-mechanical coupled joint behaviour illustrated in Figures 15 and 16 were produced by an HP 41CV programmable calculator and peripherals using the programme developed by Bakhtar (Barton and Bakhtar, 1983). A Fortran version has since been developed by Christianson, M., Bandis S. et al. (1985) for use as a sub-routine in MUDEC, together with a LOTUS spread-sheet version to assist in selecting the most realistic input parameters for MUDEC modelling. The latter has been used in developing the input data reported on the following pages.

5.1 Diagonal Joint Set

Based on the joint parameters described in the preceeding paragraphs, we are now in a position to predict the behaviour of individual joints in the block. The input data assumed to best represent the diagonal joints are presented in Tables 1 and 2. Figures 17 and 18 give corresponding sets of stress-deformation-conductivity diagrams, for visualization of the non-linear behaviour.

5.2 Foliation Joint Set

The input data assumed to best represent the foliation joints are presented in Tables 3 and 4. Figures 19 and 20 give corresponding sets of stress-deformation-conductivity diagrams, for visualization of the non-linear behaviour.

5.3 Simplified data for preliminary modelling

Several joint codes were used in the validation phase of this project. A useful starting point, common to each code, is the use of initial linear joint models utilizing single values of c, ϕ, K_n and K_s.

Table 1. Input and output for shear-dilation-conductivity modelling of diagonal joint set, at three normal stress levels (0.5, 3.5 and 7.0 MPa).

DIAGONAL JOINT SET

INPUT PARAMETERS		FULL SCALE PARAMETERS		
JRCo	13.00	JRCn	9.07	
JCSo	90.00 MPa	JCSn	52.41 MPa	
Lo	0.10 M	DPEAK	2.24 mm	
Ln	0.40 M	ROUGH	10.32	
PHIr	25.00 DEG	LFACT	0.04	
SIGNAn	0.50 MPa	PHIr RA	0.44 Rad	
SIGMAC	220.00 MPa	PPEAK	43.32 Degrees	
APERTURE	0.150 mm	ES	0.210 MPa/mm	
		JRC*2.5	609	

DATA									
DISP mm	SRATIO	JRCn	SIGNAn	DILATION ANGLE	INC.	ACCUM.	COND		
*** 0.00	0.00	0.00	0.00	0.00	0.000	0.000	-5.945		9.00
*** 0.00	0.00	-12.37	.00	-12.50	0.000	0.000	-5.945		10.00
*** 0.45	0.20	-3.09	0.17	-3.13	-0.099	0.000	-5.945		11.00
*** 0.67	0.30	0.00	0.23	0.00	-0.012	0.000	-5.945		12.00
*** 1.01	0.45	4.53	0.34	4.58	0.008	0.000	-5.945		13.00
*** 1.34	0.60	6.80	0.40	6.87	0.027	0.027	-5.650		14.00
*** 1.79	0.80	8.16	0.44	8.24	0.054	0.081	-5.195		15.00
*** 2.24	1.00	9.07	0.47	9.16	0.065	0.146	-4.765		16.00
*** 3.36	1.50	8.16	0.44	8.24	0.181	0.326	-3.937		17.00
*** 4.48	2.00	7.66	0.43	7.74	0.162	0.489	-3.469		18.00
*** 6.72	3.00	6.80	0.40	6.87	0.304	0.793	-3.130		19.00
*** 8.96	4.00	6.35	0.39	6.41	0.270	1.063	-2.911		
*** 13.44	6.00	5.44	0.36	5.50	0.504	1.567	-2.618		
*** 17.92	8.00	4.99	0.35	5.04	0.431	1.998	-2.415		
*** 22.41	10.00	4.53	0.34	4.58	0.395	2.393	-2.269		
*** 44.81	20.00	3.63	0.32	3.66	1.795	4.187	-1.805		
*** 89.62	40.00	2.72	0.29	2.75	2.869	7.056	-1.364		
*** 134.43	60.00	1.81	0.27	1.83	2.151	9.207	-1.137		
*** 179.24	80.00	0.91	0.25	0.92	1.433	10.640	-1.013		
*** 224.06	100.00	0.00	0.23	0.00	0.716	11.356	-0.957		

INPUT PARAMETERS		FULL SCALE PARAMETERS		
JRCo	13.00	JRCn	9.07	
JCSo	90.00 MPa	JCSn	52.41 MPa	
Lo	0.10 M	DPEAK	2.24 mm	
Ln	0.40 M	ROUGH	10.66	
PHIr	25.00 DEG	LFACT	0.02	
SIGNAn	3.50 MPa	PHIr RA	0.44 Rad	
SIGMAC	220.00 MPa	PPEAK	25.66 Degrees	
APERTURE	0.135 mm	ES	1.121 MPa/mm	
		JRC*2.5	609	

DATA									
DISP mm	SRATIO	JRCn	SIGNAn	DILATION ANGLE	INC.	ACCUM.	COND		
*** 0.00	0.00	0.00	0.00	0.00	0.000	0.000	-6.128		9.00
*** 0.00	0.00	-21.27	.00	-12.50	0.000	0.000	-6.128		10.00
*** 0.45	0.20	-5.32	1.19	-3.13	-0.099	0.000	-6.128		11.00
*** 0.67	0.30	0.00	1.63	0.00	-0.012	0.000	-6.128		12.00
*** 1.01	0.45	4.53	2.05	2.66	0.000	0.000	-6.128		13.00
*** 1.34	0.60	6.80	2.27	4.00	0.016	0.016	-5.837		14.00
*** 1.79	0.80	8.16	2.41	4.80	0.031	0.047	-5.609		15.00
*** 2.24	1.00	9.07	2.51	5.33	0.030	0.085	-5.283		16.00
*** 3.36	1.50	8.16	2.41	4.80	0.104	0.189	-4.607		17.00
*** 4.48	2.00	7.66	2.36	4.50	0.094	0.283	-4.164		18.00
*** 6.72	3.00	6.80	2.27	4.00	0.176	0.459	-3.553		19.00
*** 8.96	4.00	6.35	2.23	3.73	0.157	0.616	-3.328		
*** 13.44	6.00	5.44	2.14	3.20	0.292	0.908	-3.043		
*** 17.92	8.00	4.99	2.09	2.93	0.250	1.158	-2.856		
*** 22.41	10.00	4.53	2.05	2.66	0.229	1.388	-2.714		
*** 44.81	20.00	3.63	1.96	2.13	1.042	2.430	-2.261		
*** 89.62	40.00	2.72	1.88	1.60	1.668	4.098	-1.826		
*** 134.43	60.00	1.81	1.79	1.07	1.258	5.348	-1.601		
*** 179.24	80.00	0.91	1.71	0.53	0.833	6.182	-1.478		
*** 224.06	100.00	0.00	1.63	0.00	0.417	6.598	-1.423		

INPUT PARAMETERS		FULL SCALE PARAMETERS		
JRCo	13.00	JRCn	9.07	
JCSo	90.00 MPa	JCSn	52.41 MPa	
Lo	0.10 M	DPEAK	2.24 mm	
Ln	0.40 M	ROUGH	7.93	
PHIr	25.00 DEG	LFACT	0.02	
SIGNAn	7.00 MPa	PHIr RA	0.44 Rad	
SIGMAC	220.00 MPa	PPEAK	32.93 Degrees	
APERTURE	0.133 mm	ES	2.023 MPa/mm	
		JRC*2.5	609	

DATA									
DISP mm	SRATIO	JRCn	SIGNAn	DILATION ANGLE	INC.	ACCUM.	COND		
*** 0.00	0.00	0.00	0.00	0.00	0.000	0.000	-6.153		9.00
*** 0.00	0.00	-28.59	.00	-12.50	0.000	0.000	-6.153		10.00
*** 0.45	0.20	-7.15	3.30	-3.13	-0.099	0.000	-6.153		11.00
*** 0.67	0.30	0.00	3.26	0.00	-0.012	0.000	-6.153		12.00
*** 1.01	0.45	4.53	3.07	1.98	0.008	0.000	-6.153		13.00
*** 1.34	0.60	6.80	4.20	2.97	0.012	0.012	-6.008		14.00
*** 1.79	0.80	8.16	4.48	3.57	0.023	0.035	-5.749		15.00
*** 2.24	1.00	9.07	4.53	3.96	0.020	0.063	-5.481		16.00
*** 3.36	1.50	8.16	4.48	3.57	0.078	0.140	-4.901		17.00
*** 4.48	2.00	7.66	4.32	3.35	0.070	0.210	-4.506		18.00
*** 6.72	3.00	6.80	4.20	2.97	0.131	0.341	-3.944		19.00
*** 8.96	4.00	6.35	4.13	2.77	0.116	0.458	-3.563		
*** 13.44	6.00	5.44	4.00	2.38	0.217	0.675	-3.264		
*** 17.92	8.00	4.99	3.94	2.18	0.166	0.841	-3.084		
*** 22.41	10.00	4.53	3.87	1.98	0.171	1.012	-2.947		
*** 44.81	20.00	3.63	3.75	1.59	0.775	1.807	-2.504		
*** 89.62	40.00	2.72	3.63	1.19	1.240	3.047	-2.074		
*** 134.43	60.00	1.81	3.50	0.79	0.930	3.977	-1.851		
*** 179.24	80.00	0.91	3.38	0.40	0.620	4.597	-1.723		
*** 224.06	100.00	0.00	3.26	0.00	0.310	4.907	-1.674		

Table 2. Input and output for normal stress-closure-conductivity modelling of diagonal joint set.

DIAGONAL JOINT SET

Barton Bandis Joint Model NORMAL CLOSURE CALCULATION

INPUT PARAMETERS		SNORM	CYCLE 1	CYCLE 2	CYCLE 3	CYCLE 4	CYCLE 5	
JRC	13	LOAD	54	54	54	7	0	MPa
JCS	90	UNLOAD	0	0	0	0	0	MPa
SIGMAC	220	APERTURE	0.340	0.190	0.172	0.162	0.158	mm
		KNP	4.1E+03	5.2E+04	9.1E+04	2.2E+03	2.6E+01	
CALCULATED PARAMETERS								
	LOAD	KNI	20.28	23.98	24.90	25.44	25.71	MPa/mm
		VMI	-0.203	-0.050	-0.036	-0.033	-0.032	mm
		AJ	0.049	0.042	0.040	0.039	0.039	
		BJ	0.243	0.840	1.103	1.187	1.232	
	UNLOAD	KNI'	23.98	24.90	25.44	25.71	25.71	MPa/mm
		VIRR	-0.150	-0.019	-0.009	-0.004	0.000	mm
		DSM	-0.150	-0.168	-0.178	-0.182	-0.182	
		SIRR	-0.150	-0.168	-0.178	-0.182	-0.150	
		AJ'	0.042	0.040	0.039	0.039	0.039	
		BJ'	1.061	1.329	1.467	1.395	ERR	
		VMI'	-0.039	-0.030	-0.027	-0.028	ERR	

	CONSTANTS			
	CYCLE 1	CYCLE 2	CYCLE 3	CYCLE 4
A	-0.2960	-0.1001	-0.1031	-0.1031
B	-0.0056	-0.0073	-0.0074	-0.0074
C	2.2410	1.0082	1.1350	1.1350
D	-0.2450	-0.2300	-0.2510	-0.2510
C1	84.77	43.37	31.38	20.00
C2	0.02	0.01	0.01	0.01
JRC*2.5	609			

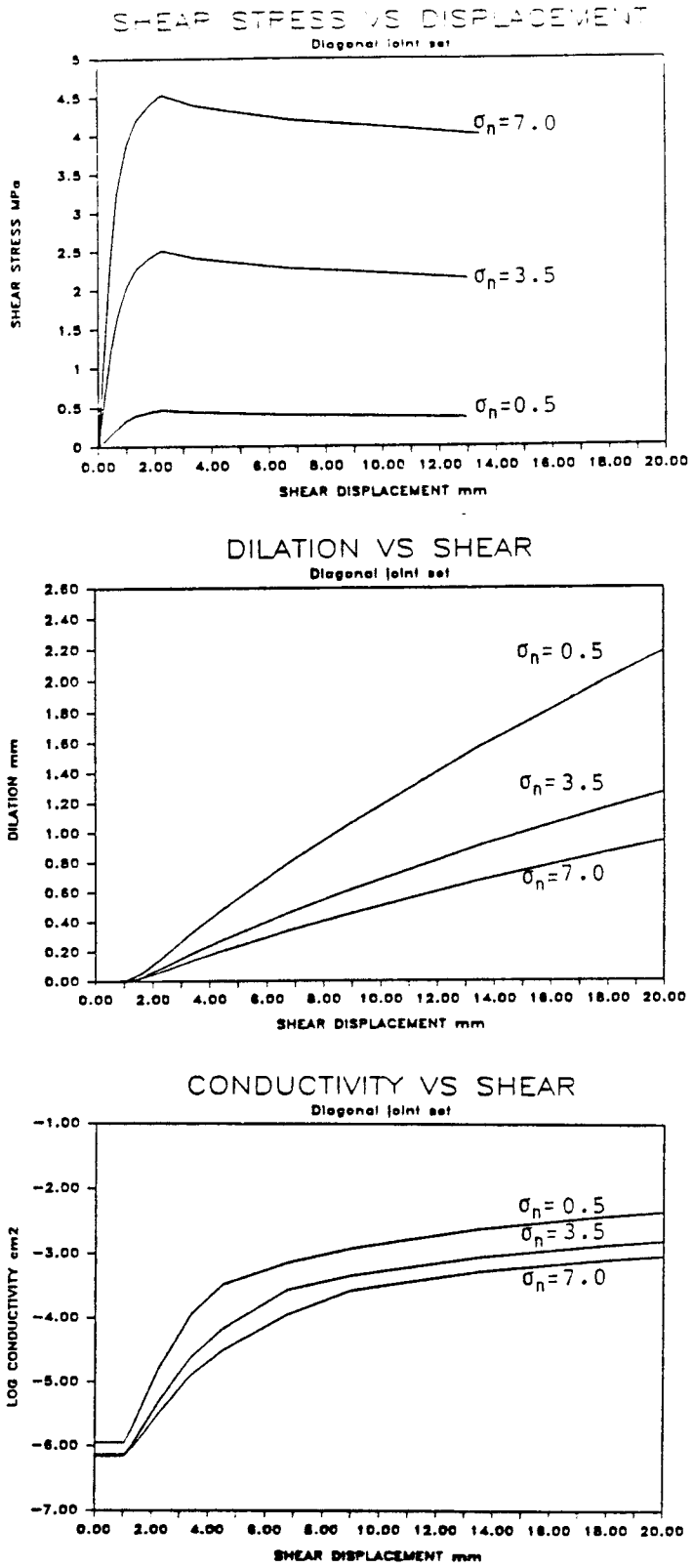

Fig. 17 Shear-dilation-conductivity coupling for diagonal joint set.

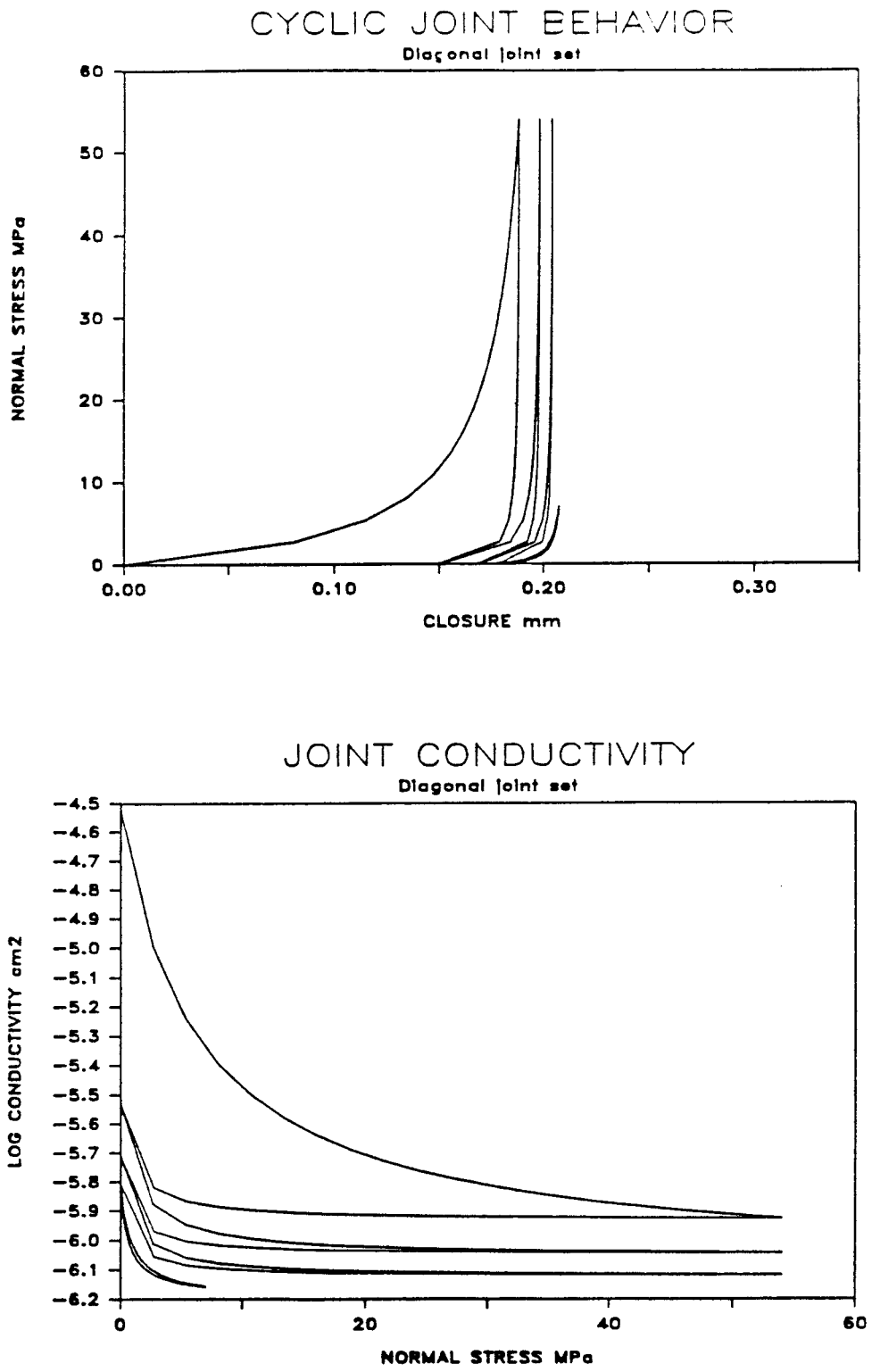

Fig. 18 Stress-closure-conductivity coupling for diagonal joint set. The first three load/unload cycles consolidate the joint to give desired conducting aperture on fourth cycle.

Table 3. Input and output for shear-dilation-conductivity modelling of foliation joint set, at three normal stress levels (0.5, 3.5 and 7.0 MPa).

FOLIATION JOINT SET

INPUT PARAMETERS

JRCo	10.00
JCSo	120.00 MPa
Lo	0.10 M
Ln	0.50 M
PHIr	28.00 DEG
SIGNAn	0.50 MPa
SIGMAC	220.00 MPa
APERTURE	0.116 mm

FULL SCALE PARAMTERS

JRCn	7.25
JCSn	74.04 MPa
DMAX	2.42 mm
ROUGH	15.73
LFACT	0.04
PHIr RA	0.49 Rad
PPEAK	43.73 Degrees
KS	0.190 MPa/mm
JRC*2.5	316

DATA

	DISP mm	SRATIO	JRCn	SIGNAn	DILATION ANGLE	INC.	ACCUM.	COND
***	0.00	0.00	0.00	0.00	ANGLE	INC.	ACCUM.	COND
***	0.00	0.00	-12.90	.00	-14.00	0.000	0.000	-5.821
***	0.48	0.20	-3.23	0.19	-3.50	-0.121	0.000	-5.821
***	0.72	0.30	0.00	0.27	0.00	-0.015	0.000	-5.821
***	1.09	0.45	3.62	0.36	3.93	0.000	0.000	-5.821
***	1.45	0.60	5.44	0.42	5.90	0.025	0.025	-5.483
***	1.93	0.80	6.52	0.45	7.08	0.050	0.075	-4.956
***	2.42	1.00	7.25	0.48	7.87	0.060	0.135	-4.481
***	3.62	1.50	6.52	0.45	7.08	0.167	0.302	-3.837
***	4.83	2.00	6.12	0.44	6.65	0.150	0.452	-3.571
***	7.25	3.00	5.44	0.42	5.90	0.282	0.733	-3.221
***	9.67	4.00	5.07	0.41	5.51	0.250	0.983	-2.997
***	14.50	6.00	4.35	0.38	4.72	0.466	1.449	-2.690
***	19.33	8.00	3.99	0.37	4.33	0.399	1.848	-2.493
***	24.17	10.00	3.62	0.36	3.93	0.366	2.214	-2.345
***	48.33	20.00	2.90	0.34	3.15	1.661	3.875	-1.877
***	96.66	40.00	2.17	0.32	2.36	2.657	6.532	-1.434
***	145.00	60.00	1.45	0.30	1.57	1.992	8.524	-1.206
***	193.33	80.00	0.72	0.28	0.79	1.327	9.851	-1.082
***	241.66	100.00	0.00	0.27	0.00	0.664	10.515	-1.026

INPUT PARAMETERS

JRCo	10.00
JCSo	120.00 MPa
Lo	0.10 M
Ln	0.50 M
PHIr	28.00 DEG
SIGNAn	3.50 MPa
SIGMAC	220.00 MPa
APERTURE	0.104 mm

FULL SCALE PARAMTERS

JRCn	7.25
JCSn	74.04 MPa
DMAX	2.42 mm
ROUGH	9.61
LFACT	0.02
PHIr RA	0.49 Rad
PPEAK	37.61 Degrees
KS	1.116 MPa/mm
JRC*2.5	316

DATA

	DISP mm	SRATIO	JRCn	SIGNAn	DILATION ANGLE	INC.	ACCUM.	COND
***	0.00	0.00	0.00	0.00	ANGLE	INC.	ACCUM.	COND
***	0.00	0.00	-21.13	.00	-14.00	0.000	0.000	-6.011
***	0.48	0.20	-5.28	1.34	-3.50	-0.121	0.000	-6.011
***	0.72	0.30	0.00	1.86	0.00	-0.015	0.000	-6.011
***	1.09	0.45	3.62	2.26	2.48	0.000	0.000	-6.011
***	1.45	0.60	5.44	2.47	3.68	0.015	0.015	-5.774
***	1.93	0.80	6.52	2.60	4.32	0.030	0.046	-5.379
***	2.42	1.00	7.25	2.70	4.80	0.037	0.082	-5.000
***	3.62	1.50	6.52	2.60	4.32	0.102	0.184	-4.243
***	4.83	2.00	6.12	2.55	4.06	0.091	0.275	-3.922
***	7.25	3.00	5.44	2.47	3.60	0.171	0.447	-3.598
***	9.67	4.00	5.07	2.43	3.36	0.152	0.599	-3.386
***	14.50	6.00	4.35	2.34	2.88	0.284	0.883	-3.091
***	19.33	8.00	3.99	2.30	2.64	0.243	1.126	-2.899
***	24.17	10.00	3.62	2.26	2.40	0.223	1.349	-2.755
***	48.33	20.00	2.90	2.17	1.92	1.014	3.362	-2.295
***	96.66	40.00	2.17	2.09	1.44	1.621	2.984	-1.856
***	145.00	60.00	1.45	2.01	0.96	1.216	5.200	-1.630
***	193.33	80.00	0.72	1.94	0.48	0.810	6.010	-1.507
***	241.66	100.00	0.00	1.86	0.00	0.405	6.415	-1.451

INPUT PARAMETERS

JRCo	10.00
JCSo	120.00 MPa
Lo	0.10 M
Ln	0.50 M
PHIr	28.00 DEG
SIGNAn	7.00 MPa
SIGMAC	220.00 MPa
APERTURE	0.099 mm

FULL SCALE PARAMTERS

JRCn	7.25
JCSn	74.04 MPa
DMAX	2.42 mm
ROUGH	7.42
LFACT	0.02
PHIr RA	0.49 Rad
PPEAK	35.42 Degrees
KS	2.068 MPa/mm
JRC*2.5	316

DATA

	DISP mm	SRATIO	JRCn	SIGNAn	DILATION ANGLE	INC.	ACCUM.	COND
***	0.00	0.00	0.00	0.00	ANGLE	INC.	ACCUM.	COND
***	0.00	0.00	-27.33	.00	-14.00	0.000	0.000	-6.097
***	0.48	0.20	-6.83	2.69	-3.50	-0.121	0.000	-6.097
***	0.72	0.30	0.00	3.72	0.00	-0.015	0.000	-6.097
***	1.09	0.45	3.62	4.33	1.86	0.000	0.000	-6.097
***	1.45	0.60	5.44	4.65	2.78	0.012	0.012	-5.902
***	1.93	0.80	6.52	4.84	3.34	0.024	0.035	-5.567
***	2.42	1.00	7.25	4.98	3.71	0.028	0.063	-5.236
***	3.62	1.50	6.52	4.84	3.34	0.078	0.142	-4.552
***	4.83	2.00	6.12	4.77	3.14	0.071	0.212	-4.106
***	7.25	3.00	5.44	4.65	2.78	0.132	0.345	-3.785
***	9.67	4.00	5.07	4.58	2.60	0.118	0.462	-3.581
***	14.50	6.00	4.35	4.45	2.23	0.219	0.682	-3.294
***	19.33	8.00	3.99	4.39	2.04	0.188	0.870	-3.107
***	24.17	10.00	3.62	4.33	1.86	0.172	1.042	-2.965
***	48.33	20.00	2.90	4.20	1.48	0.783	1.825	-2.511
***	96.66	40.00	2.17	4.08	1.11	1.253	3.078	-2.075
***	145.00	60.00	1.45	3.96	0.74	0.940	4.018	-1.858
***	193.33	80.00	0.72	3.84	0.37	0.626	4.644	-1.727
***	241.66	100.00	0.00	3.72	0.00	0.313	4.957	-1.672

Table 4. Input and output for normal stress-closure-conductivity modelling of foliation joint set.

FOLIATION JOINT SET

Barton Bandis Joint Model NORMAL CLOSURE CALCULATION

INPUT PARAMETERS		SNORM	CYCLE 1	CYCLE 2	CYCLE 3	CYCLE 4	CYCLE 5	
JRC	10	LOAD	72	72	72	7	0	MPa
JCS	120	UNLOAD	0	0	0.	0	0	MPa
SIGMAC	220	APERTURE	0.250	0.147	0.132	0.126	0.124	mm
		KNP	1.5E+04	1.2E+05	2.5E+05	3.3E+03	2.8E+01	
CALCULATED PARAMETERS								
	LOAD	KNI	18.87	24.83	26.46	27.26	27.60	MPa/mm
		VMI	-0.142	-0.043	-0.028	-0.026	-0.025	mm
		AJ	0.053	0.040	0.038	0.037	0.036	
		BJ	0.374	0.943	1.333	1.418	1.457	
	UNLOAD	KNI'	24.83	26.46	27.26	27.60	27.60	MPa/mm
		VIRR	-0.103	-0.015	-0.006	-0.002	0.000	mm
		DSM	-0.103	-0.118	-0.124	-0.126	-0.126	
		SIRR	-0.103	-0.118	-0.124	-0.126	-0.103	
		AJ'	0.040	0.038	0.037	0.036	0.036	
		BJ'	1.172	1.372	1.669	1.579	ERR	
		VMI'	-0.034	-0.028	-0.022	-0.023	ERR	

	CONSTANTS			
	CYCLE 1	CYCLE 2	CYCLE 3	CYCLE 4
A	-0.2960	-0.1001	-0.1031	-0.1031
B	-0.0056	-0.0073	-0.0074	-0.0074
C	2.2410	1.0082	1.1350	1.1350
D	-0.2450	-0.2300	-0.2510	-0.2510
C1	84.77	43.37	31.38	20.00
C2	0.02	0.01	0.01	0.01
JRC^2.5	316			

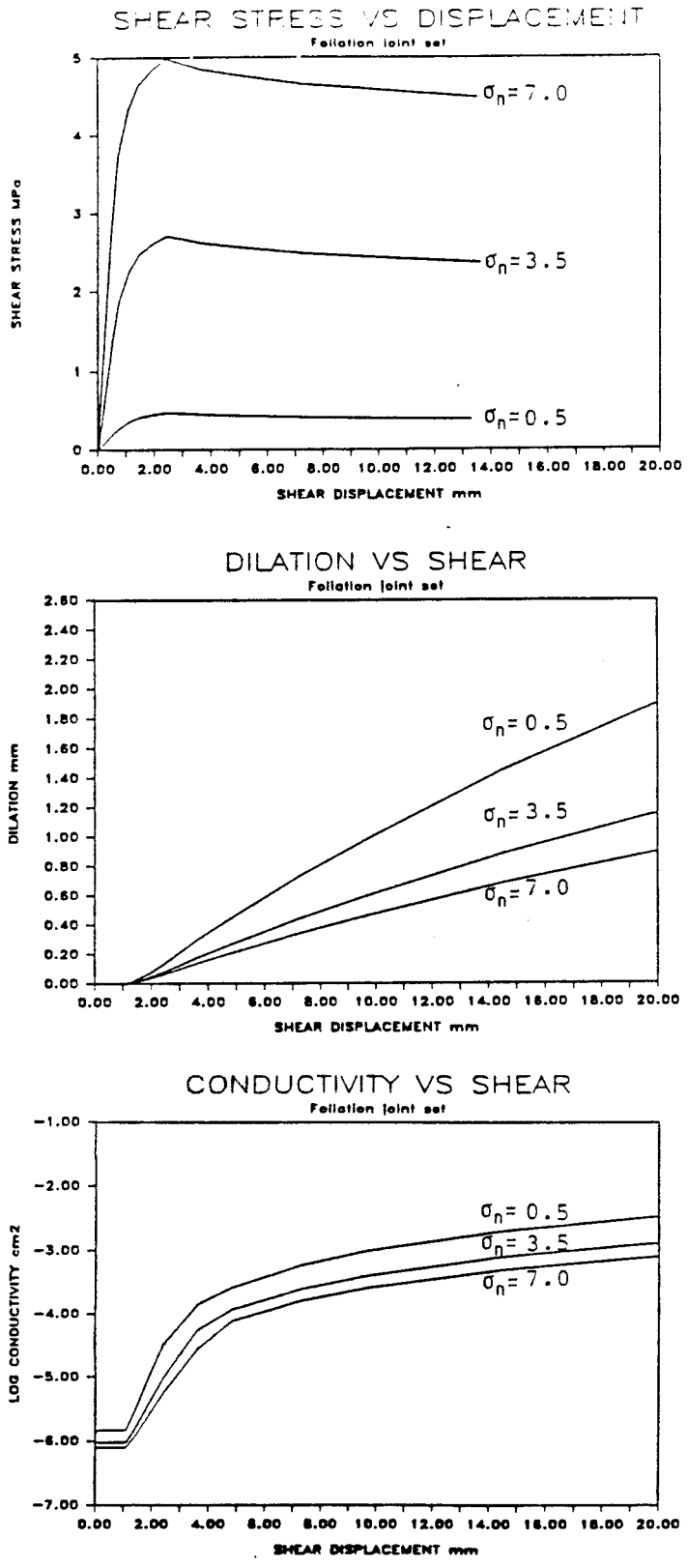

Fig. 19 Shear-dilation-conductivity coupling for foliation joint set.

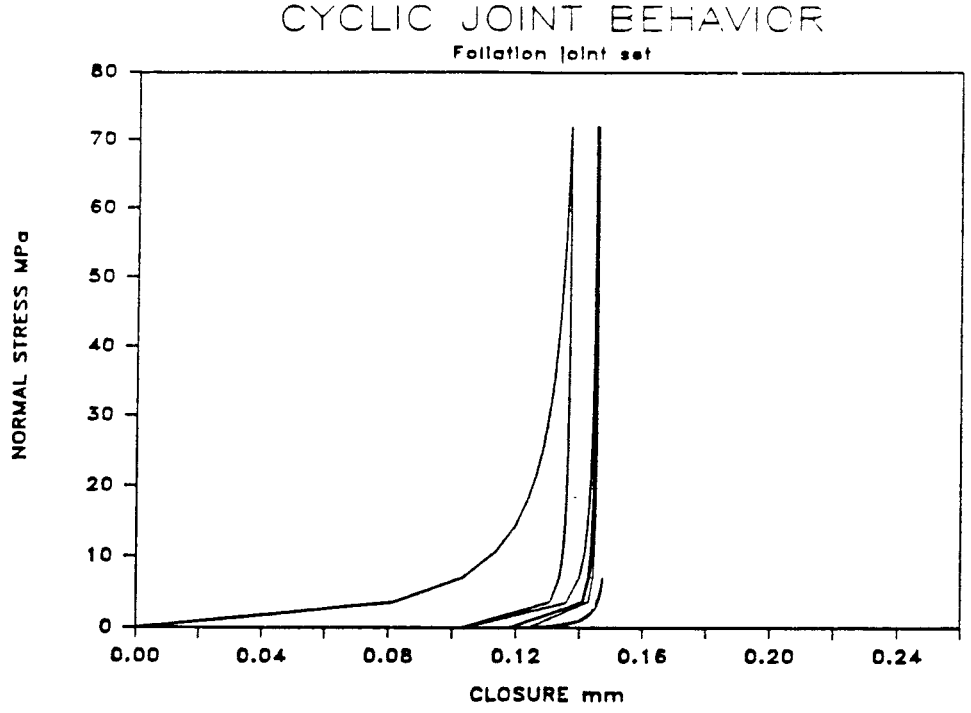

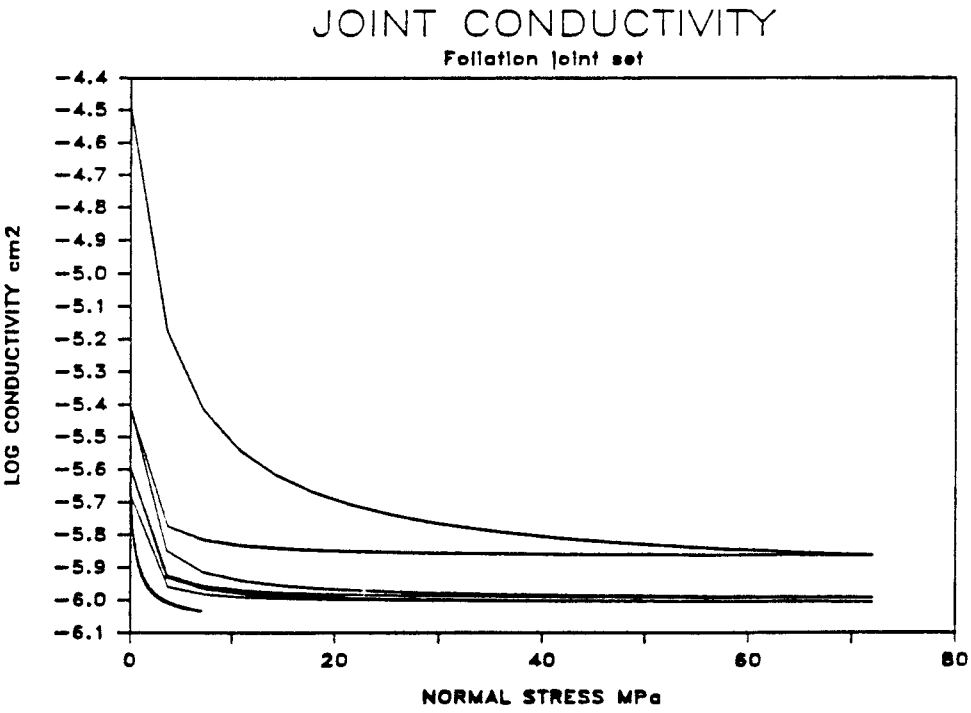

Fig. 20 Stress-closure-conductivity coupling for diagonal joint set. The first three load/unload consolidate the joint to give desired conducting aperture on fourth cycle.

A simplified block geometry based on key block interpretation of the absoute deformation magnitudes was used first, with the above linear joint data. This simplified geometry is shown in Figure 21.

The approach adopted for developing representative linear input data, was to take average values of the input data represented in Tables 1 to 4. Average full scale data were given by the equations 2, 5 and 6.

JRC_n = 9.07, 7.25 mean = 8.2
JCS_n = 52.4, 74.0 MPa mean = 62.2 MPa
ϕ_r = 25.0°, 28.0° mean = 26.5°

The values of L_n = 0.4 m and L_n = 0.5 m for the diagonal and foliation joints on tables 1 and 3 are derived as a statistical mean of the total intersected joint lengths of the two sets.

In MUDEC this is done automatically. This means that we don't need to specify the L_n parameters as input data for the different joint sets.

A non-linear shear strength envelope developed from this mean data (using equation 1) gave the following representative values of cohesion and friction at a representative normal stress level of 3.5 MPa:

c = 0.4 MPa
ϕ = 32°

The dilation curves given in Figures 17 and 19 were used to obtain a single value of the peak dilation angle for use in the linear joint models. The empirical formula giving the peak dilation angles is: (see also equation 4)

$$d_n \text{ (peak)} = \tfrac{1}{2} JRC_n \text{ (peak)} \log \left(\frac{JCS_n}{\sigma_n'}\right) \qquad (11)$$

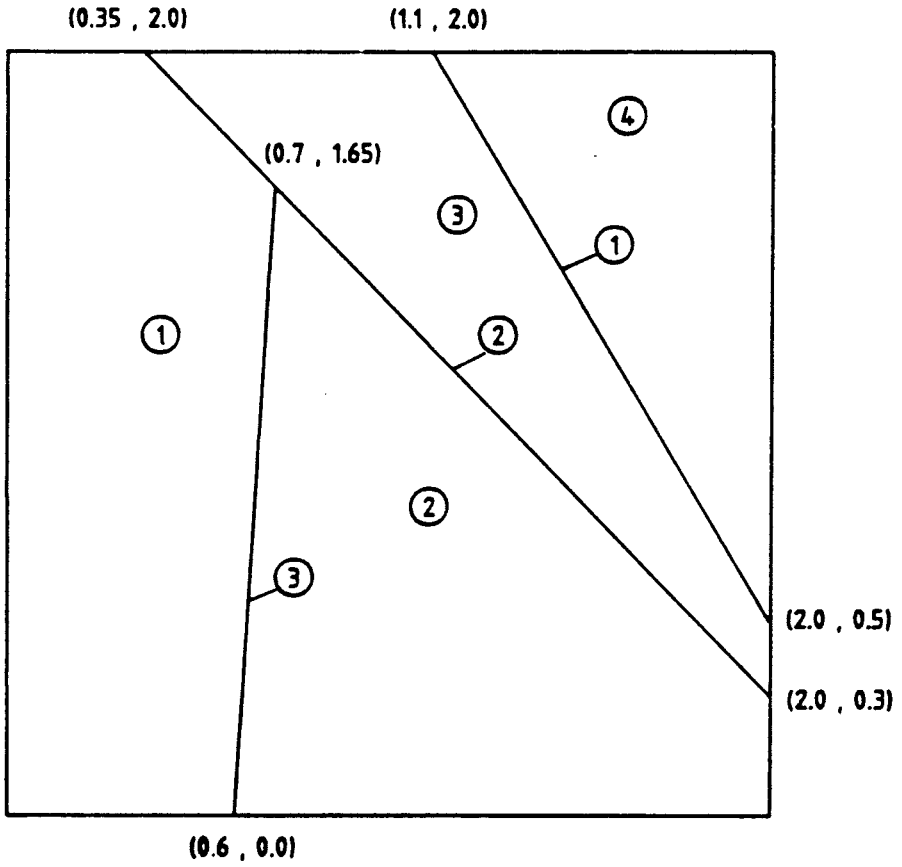

Fig. 21 The block structure modelled is very simple, only the principle fractures are included.

and by using the Tables 1 and 3 for a normal stress range of σ_n' = 0.5 - 3.5 MPa, we obtain a mean $d_n°$ (peak) of 6.7°.

The peak dilation angle $d_n°$= 6.7 is derived as follows:

The equation (11) for JRC_n = 8.2, JCS_n = 62.2 MPA and σ_n = 0.5 and 3.5 MPa gives:
$d_n^{3.5}$ (peak) = 5.12°and $d_n^{0.5}$ (peak) = 8.59
which are giving a mean of d_n = 6.85°.

The Table 1 for σ_n = 0.5 and σ_n = 3.5 MPa is giving peak dilation angles (d_n) of 9.16 and 5.33, respectively. The mean (d_n) for Table 1 is 7.25.

The Table 3 for the same normal stress range is giving peak dilation angle of 7.07° and 4.80°. Mean of Table 2 is 5.93°.

The mean for Tables 1 and 3 is 6.59°. Considering once more the mean values derived from the formula 11 and the mean from Tables 1 and 3, we are concluding in dilation angle 6.7°.

The friction coefficient was derived by using $\tan(\phi_r + d_n)$ = tan 33.2°= 0.654. The stiffness value for the MUDEC linear model was calculated from Tables 1 and 3 for normal stress of 3.5 MPa. Only the linear part of shear stress, shear deformation curve was used.

For the diagonal joint K_s = 1.19/0.45 = 2.64 MPa/mm

For the foliaton joint K_s = 1.34/0.48 = 2.79 MPa/mm

The mean K_s value for foliation and diagonal joint is 2.72 MPa/mm.

The normal stiffness value was derived by considering the tangent in the first cycle when loading the diagonal and foliation joints. Thus:

for the foliation joint K_n = 3.5/0.08 = 43.75

for the diagonal joint $K_n = 9.06/0.15 - 0.05 = 90.60$

which give a mean value of 67.2 MPa/mm.

Figure 22 summarizes input data for the linear joint sub-routine in MUDEC. Figure 23 gives the assumed intact rock data for the preliminary modelling.

The input data for the Barton - Bandis joint are derived from Tables 1, 2, 3 and 4. MUDEC is using the initial aperture value of the diagonal and foliation joint from Tables 2 and 4. The normal stiffness value on the third cycle is used as normal stiffness limit value (KNP = 2.5E8 and 9.1E7 MPa/m for the diagonal and foliation joint sets, respectively).

The input data for the Barton - Bandis joint model was summarized in Figure 24. MUDEC uses laboratory scale input parameters. On the basis of joint lengths, MUDEC computes the full scale joint parameters.

5.4 Description of numerical models

The numerical simulations are performed with two different boundary conditions. The first simulations were run with boundary stress conditions as shown in Figure 25, (Appendix 1.1-3.3 and 4.1 - 6.6). It was also decided to use fixed boundaries with fluid pressure loading when modelling non-linear joint behaviour. (See Chapters 5.4.2. and Appendices 7.1 - 9.6.) Fixed boundaries with fluid pressure loading are described in Chapter 5.4.2.

In all models the flatjacks are represented as blocks parallel to each CSM-block boundary. Both the CSM-block and the flatjacks are modelled as fully-deformable blocks. This means that each block is discretized into constant strain finite difference triangles, and arbitrary deformation of blocks is permitted. The CSM-block is divided into 161 zones for the linear joint model and 652 zones for the non-linear joint model.

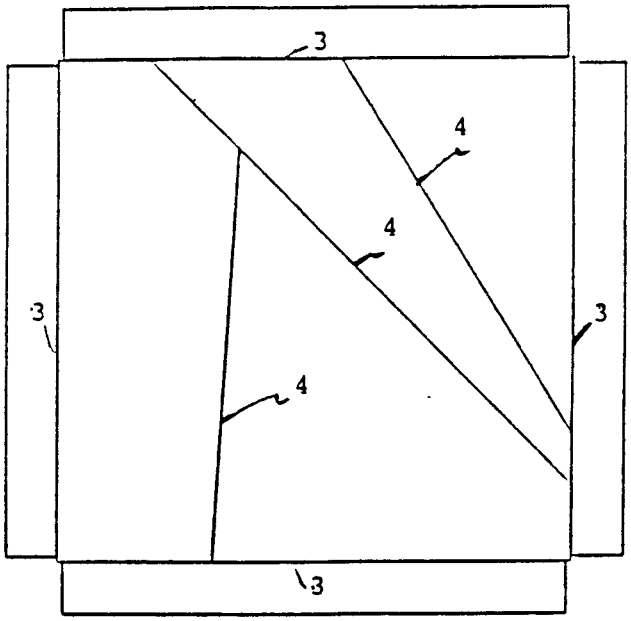

Main joint from CSM-block is called "real joint". Joint between flat-jacks and CSM-block is called "boundary joint".

		MAT = 3 BOUNDARY JOINTS	MAT = 4 REAL JOINTS
Normal stiffness	(MPa/m)	67.18E2	67.18E3
Shear stiffness	(MPa/m)	2.72E2	2.72E3
Cohesion	(MPa/m)	0	0.4
Dilation coefficient	(tangent)	0	0.118
Tensile strength	(MPa)	0	0
Friction coefficient	(tangent)	0.176	0.654

Derivation from: $JRC_n = 8.2$
$JCS_n = 62.2$ MPA, $d_n = 6.7°$
$\phi_r = 26.5°$

Fig. 22 Joint material properties for linear joint model.

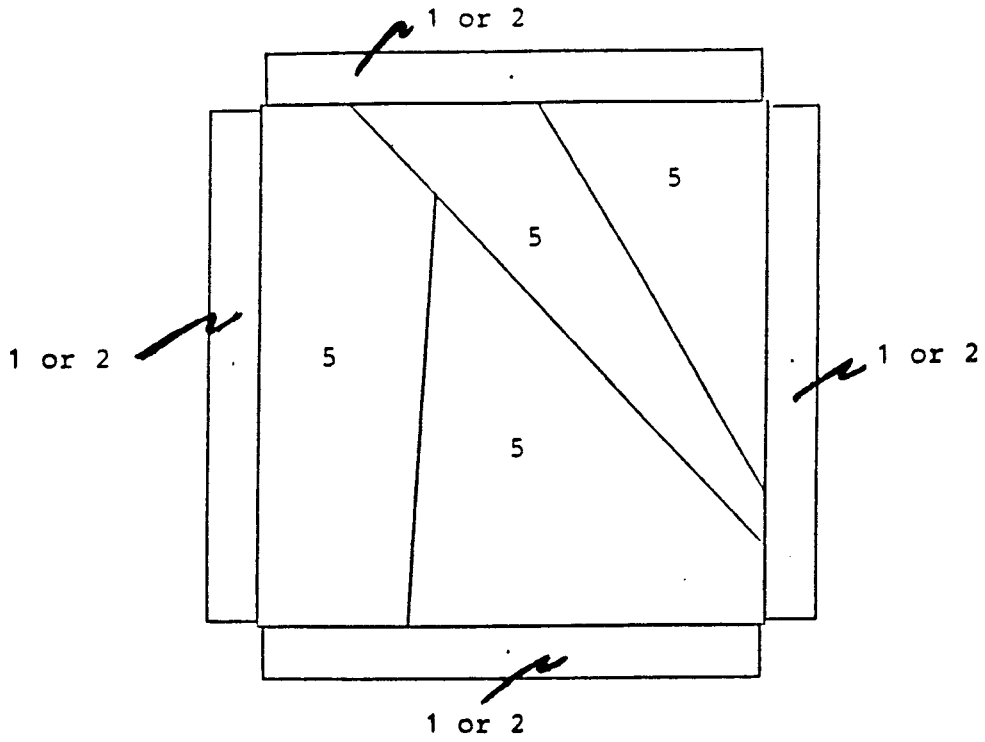

Flat-jacks are modelled as boundary blocks. Their material properties depends on whether they act as active or passive jacks.

	MAT = 1 ACTIVE FLAT-JACKS	MAT = 2 PASSIVE FLAT-JACKS	MAT = 5 CSM-BLOCK
Bulk modulus (MPa)	4.0E3	4.0E2 *	4.0E4
Shear modulus (MPa)	2.4E3	5.0E5	2.4E4
Density (10^6kg/m^3)	2.5E-3	2.5E-3	2.5E-3

$G = E/2(1-\upsilon)$ where $\upsilon = 0.25$
$B = E/3(1-2\upsilon)$ $E = 60$ GPa

* The passive flat-jack properties have been changed during MUDEC runs of the appendices 4 - 9. For the boundary stress model with Barton - Bandis joint model the flat-jacks have the following properties:

	Bulk modulus (MPa)	Shear modulus (MPa)
N - S uniaxial	8.0E4	2.4E7
E - W	4.0E3	2.4E5

For the fluid pressure model with Barton - Bandis joints N-S loading and E-W loading, the passive flat-jacks have bulk modulus = 4.0E4 MPa and shear modulus = 2.4E7 MPa.

Fig. 23 Intact rock material properties

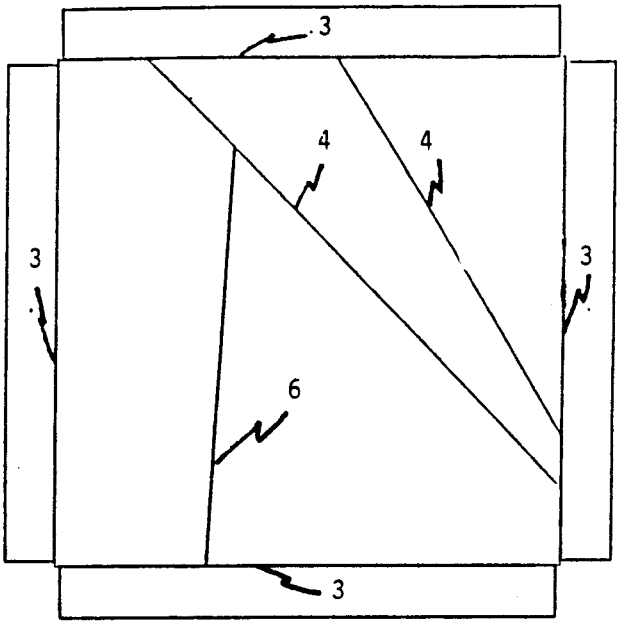

For the Barton - Bandis joint model, the input data are different for the diagonal and the foliation joint sets. Laboratory scale input parameters are used. Data for the boundary joints (3) are given in Fig. 22.

		MAT = 4 DIAGONAL JOINTS	MAT = 6 FOLIATION JOINTS
Joint Roughness Coefficient		13.0	10.0
Joint Compressive Strength	(MPa)	90.0	120.0
Lo	(m)	0.1	0.1
SIGMAC	(MPa)	220.0	220.0
APERTURE INITIAL	(mm)	0.340	0.250
PHIR	(degress)	25.0	28.0
NORMAL STIFFNESS LIMIT	(MPa/m)	9.1E7	2.5E8
SHEAR STIFFNESS LIMIT	(MPa/m)	11.2E5	15.9E5

Fig. 24 Joint material properties for Barton - Bandis joint model.

N-S and E-W displacement (x- and y-directions) histories are computed for 10 and 9 points in the CSM-block. The points have not exactly the same coordinates as the displacement instrumentation stations used in the physical test reported by A. Richardson. This is due to the fact that displacements are only computed in nodal points, and in MUDEC, generation of triangular zones and nodal points are done automatically.

The CSM-block displacement instrumentation stations, nearest nodal points and history number are shown in Figure 26.

The numerical models have peak stress levels of 5.4 MPa for the biaxial runs and 5.14 MPa for the uniaxial runs. These values are chosen because they can be directly comparable with the results reported by A. Richardson. (Ph.D. Thesis 1986.)

5.4.1 Uniform stress boundary model

The load configurations are shown in Figure 25. The applied loads are represented as boundary stresses at the flatjacks. The "flatjack" blocks should behave softer than intact rock. Flatjacks with boundary stress are called active flatjacks and the bulk and shear moduli are 1/10 of the values for the CSM-block intact rock. Flatjacks with fixed outer boundaries are called passive flatjacks and the bulk and shear moduli are different from the values of the CSM-block intact rock, see Figure 23.

For equal biaxial loading the unloaded edges of the flatjacks are fixed in the lateral direction. This is done to achieve a stable numerical model.

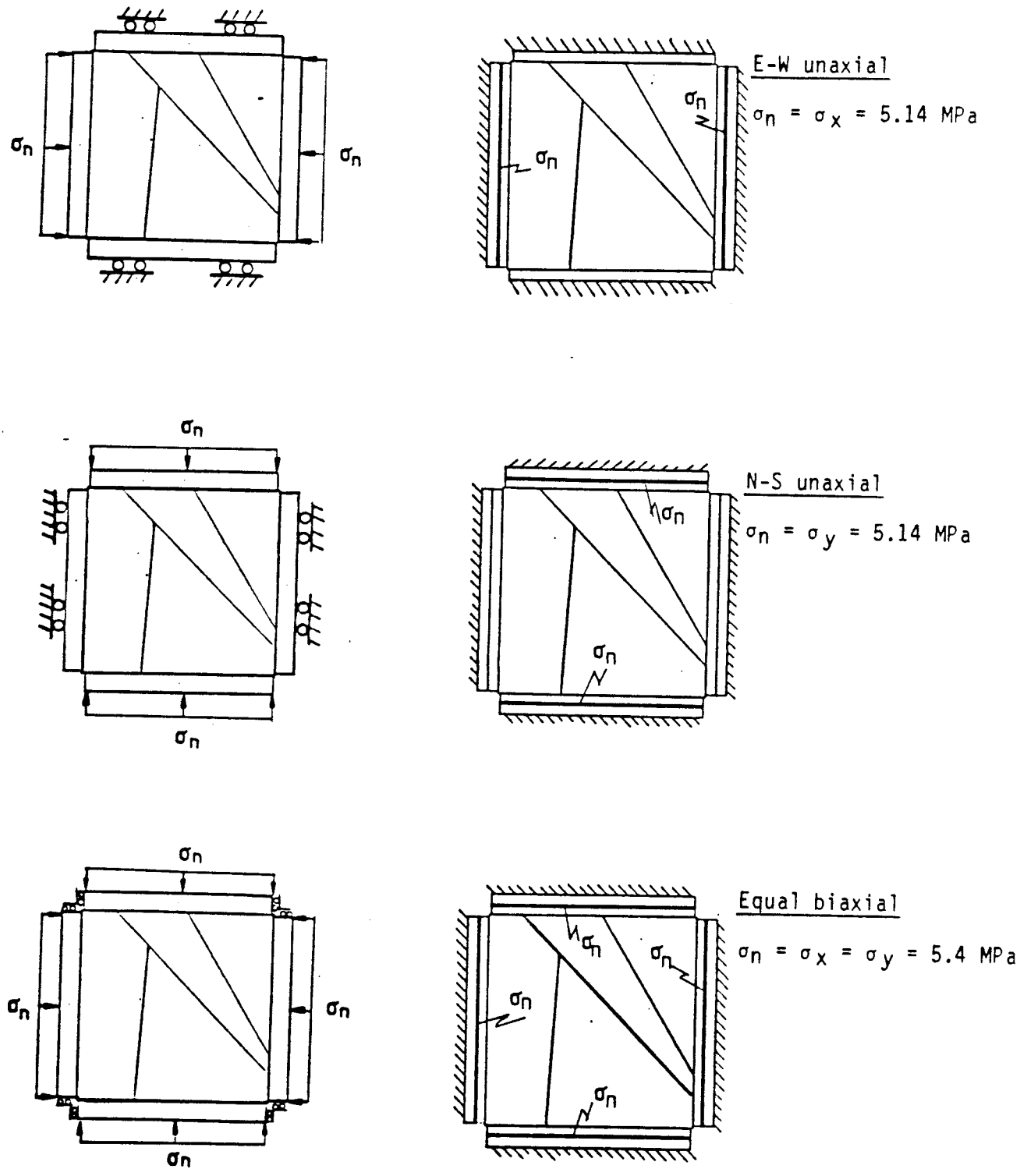

Fig. 25 Load and boundary conditions.

5.4.2 Fluid pressure boundary model

Fixed boundaries are introduced at the outer edges of the flat-jack blocks and the oil pressure is representing internal pressure in slots in the flat-jacks. Fixed foundaries prevent large displacement of the model, which increases the numerical stability. Major rotations of the flat-jack blocks are also prevented. The 4 outer corners of the CSM-block are not allowed to suffer large displacements, which is realistic.

Applying the oil pressure as a pore pressure into the slots permits local bending and rotations of the flatjack blocks; this is also true for a real flatjack. An important, realistic condition is that the model provides a decreasing, active normal stress from the flat-jacks as the ends are approached. By using fluid boundaries we are simulating very closely what happens during a real block test.

The various load configurations are shown in Figure 25. Flat-jacks which have a slot with fluid pressure are called active, with no slot are called passive. The properties of the "flat-jack" blocks are shown in Fig. 23. Different values are used for each type of run in order to achieve better numerical stability.

6. RESULTS FROM NUMERICAL MODELS

Results for a uniform boundary stress model with linear joint behaviour are found in Appendices 1 - 3. Results for the uniform stress boundary model with the Barton - Bandis joint model are shown in Appendices 4 - 6. Finally, results received when using fluid pressure boundaries are presented in Appendices 7-9.

Simulation was performed for the three load configurations (Figure 25) both for the linear joint model and the Barton - Bandis joint model. Results from the 9 runs are presented in the Appendix.

- Richardson, A. (1986)
In situ mechanical characterization of jointed crystalline rock.
Ph.D Thesis. Colorado School of Mines, Department of Mining Engineering.

- Stephansson, O. and Savilahti, T, (1988)
Validation of the rock mechanics HNFEMP against the Colorado School of Mines block test data (Luleå University of Technology).

- Walsh, J.B. (1981)
Effect of pore pressure and confining pressure on fracture permeability", preprint of article accepted for publication in the Journal of Geophysical Research.

- Witherspoon, P.A., J.S.Y. Wang, K. Iwai and J.E. Gale (1979)
Validity of cubic law for fluid flow in a deformable rock fracture.
Lawrence Berkeley Laboratory, LBL-9557, SAC-23, 28 p.

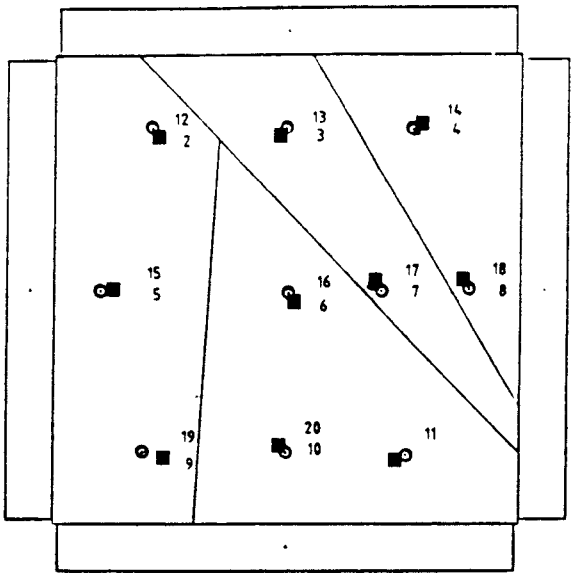

History variables and nearest nodal point for computing

Point History) number	History type	Location		Nearest nodal point for computing	
		Xccoord (m)	Ycoord (m)	Xcoord (m)	Ycoord (m)
1	Damping	factor			
2	XDIS	0.39	1.71	0.44	1.70
3	XDIS	1.00	1.71	0.98	1.70
4	XDIS	1.54	1.71	1.50	1.72
5	XDIS	0.21	1.01	0.25	1.00
6	XDIS	1.00	1.01	1.00	0.99
7	XDIS	1.40	1.01	1.37	1.06
8	DXIS	1.79	1.01	1.78	1.06
9	XDIS	0.39	0.31	0.46	0.33
10	XDIS	1.00	0.31	0.97	0.32
11	XDIS	1.54	0.31	1.50	0.31
12	YDIS	0.39	1.71	0.44	1.70
13	YDIS	1.00	1.71	0.98	1.70
14	YDIS	1.54	1.71	1.50	1.72
15	YDIS	0.21	1.01	0.25	1.00
16	YDIS	1.00	1.01	1.00	0.99
17	YDIS	1.40	1.01	1.37	1.06
18	YDIS	1.79	1.01	1.78	1.06
19	YDIS	0.39	0.31	0.46	0.33
20	YDIS	1.00	0.31	0.97	0.32

Fig. 26 Coordinates for displacements points. Instrumentation stations for measuring and nodal points for computing.

MODEL NAME	APPENDIX NO.	LOADING CONFIGURATION	CSM-BLOCK JOINT BEHAVIOUR	BOUNDARY CONDITIONS
Model A	1	EQUAL BIAXIAL	LINEAR	UNIFORM STRESS
	2	N-S UNIAXIAL	LINEAR	UNIFORM STRESS
	3	E-W UNIAXIAL	LINEAR	UNIFORM STRESS
Model B	4	EQUAL BIAXIAL	BARTON-BANDIS	UNIFORM STRESS
	5	N-S UNIAXIAL	BARTON-BANDIS	UNIFORM STRESS
	6	E-W UNIAXIAL	BARTON-BANDIS	UNIFORM STRESS
Model C	7	EQUAL BIAXIAL	BARTON-BANDIS	FLUID PRESSURE
	8	N-S UNIAXIAL	BARTON-BANDIS	FLUID PRESSURE
	9	E-W UNIAXIAL	BARTON-BANDIS	FLUID PRESSURE

For simplication the MUDEC runs with the linear joint are called MODEL A. The MUDEC runs with stress boundaries are called MODEL B. Finally, the MUDEC runs with fluid pressure boundaries are called MODEL C.

For all tests the following plots are shown:

1 - Displacement vectors and principal stresses.

2 - x-direction and y-direction displacement histories for 10 and 9 points. (Nearest nodal points for displacement computation according to Fig. 26.)

3 - Block or zone rotations for fully deformable blocks.

4 - Shear stresses contours (xy).

5 - Shear displacement on joints.

Additional plots are shown for Appendices 4 - 9.

6 - Mechnical aperture of joints.

7 - Conducting apertures for joints.

Table showing the automatically derived scale for the displacement vectors and principal stresses plots.

The uniform loading creates several point contact areas with subsequent rotation of the block. Model C represents best the actual testing conditions.

6.1 Linear joint behaviour - stress boundary model - MODEL A

6.1.1 Equal biaxial loading

The obtained results for the biaxial loading conditions and the linear joint model are shown in Appendix 1. Figure 1.1 shows the relative movement of the blocks. Note that the lower block is nearly immobile. The maximum recorded displacement is 0.10 mm and the maximum principal stress 11,3 MPa. On the same figure, the zone rotation plot, the maximum rotation is occurring on the edges of the flat jack blocks in opposite directions, an indication that the maximum displacement is taking place in the middle of the flat-jack blocks.

Figure 1.2 shows the shear stress and shear displacement plots. The maximum shear stress concentration is observed at the edges of the block, an indication that the shear displacement will also occur along the boundaries. Figure 1.3 shows the history plots of the nine points (instrumentation stations of Fig. 26).

6.1.2 N-S uniaxial loading

Figure 2.1 shows that mainly the top right block is moving downwards when the system is loaded from the top and the bottom (N-S). The principal stresses developed under this loading are slightly higher than the principal stresses under E-W loading for the same number of cycles. The zone rotation plot on the same figure shows a significant rotation of the upper middle zones probably due to the movement of the top right block. Figure 2.2 shows the shear stresses developed in this block under N-S loading. High shear stress concentration is observed in the upper part of the joints of the central block but most of the shearing is occurring along the boundaries.

Appendix No.	Maximum displacement vectors length in (mm)	Maximum principal stress length in (mm)
1	5.5	5.5
2	5.2	5.5
3	5.2	5.5
4	4.2	5.8
5	5.8	5.8
6	5.8	5.8
7	5.8	5.8
8	5.8	5.8
9	5.8	5.8

The Y-axis of the history plots is referring to displacement values in (m) unless otherwise specified. The horizontal axis is referring to calculation time used by MUDEC (timesteps x cycles). Some of the history plot in the Appendix are exhibiting a fluctuating behaviour (sudden kicks, weavy shape). It is believed that these changes are due to numerical "stick and slip" problems. The maximum values listed on the appendix figures are referring to the obtained values both in the flat-jacks and the CSM block. Table 5 shows the maximum values occurring inside the CSM block only.

Unfortunately, and due ot the colour code used for the creation of the shear stresses iso-figures, it is not possible to reproduce the exact made plot. In principle, concentration of cocentric curves are showing shear stress increase. It must be remembered though, that MUDEC considers positive the shear stresses in anti-clockwise direction. The shear stress plots of Appendices 4 - 9 have been produced with zero countour lines omitted and labelled countours.

From the numerical results it can be seen that Model C with the fluid pressure boundaries gives the most realistic results in terms of pricipal stresses, maximum displacement vectors, shear displacement in joints. The nature of the loading in Model B results in the creation of higher principal stresses inside the CSM block.

(0.13 mm). The mechanical and conducting apertures inside the CSM at a distance of 5 cm from the boundary joints show maximum values of 137 μm and 36.9 μm, respectively. The maximum aperture values are occurring in the upper block flat-jack interface, see Fig. 4.4.

Figures 4.5 and 4.6 show the history plots of ten instrumented points (x-direction) and nine instrumented points (y-direction).

6.2.2 N-S uniaxial loading with Barton - Bandis joint model

Figure 5.1 shows the displacement vectors and the maximum principal stresses occurring inside the CSM block. The maximum displacement vectors are occurring on the top lef sub-block which is suffering most of the displacement (0.75 mm). The recorded on the graph maximum values are referring to maximum values induced on the flat-jack blocks. The maximum recorded principal stress (23.2 MPa) on the intersection of the foliation and diagonal joints is relatively high, probably due to rotation and corner loading of the blocks.

Figure 5.2 show the rotations of the blocks, all in anticlock direction at different angles. The shear stresses and shear displacement plots on Fig. 5.3 show a maximum shearing of 0.30 mm occuring along the main diagonal joint. The single line on the same plots indicates that shearing has exceeded a certain limit on these points.

Figure 5.4 shows the mechanical and conducting aperture plots. Maximum values are 162 μm and 49.9 μm, respectively. E/e ratio is 3.24. The single line on the same figure indicates that the aperture values have exceeded a certain limit.

Figures 5.5 and 5.6 show the history plots for x- and y-direction.

Figure 2.3 shows the history plot of the nine points (ref. Fig.26).

6.1.3 E-W uniaxial loading

The E-W uniaxial loading (Figure 3.1) shows that the displacement occurring under the load is of the same approximate magnitude as in the N-S loading. The principal stresses developed in this block are lower than those developed for the E-W loading. The rotation plot on the same figure shows the tendency of the system to rotate from left to right.

The shear stress concentration shown in Figure 3.2 is resulting in shear displacement occurring mainly along the boundaries of the block and the flat jacks and the upper right subblock.

Figure 3.3 shows the history plot of the nine selected measuring points. (See also Fig. 26.)

6.2 Barton - Bandis joint behaviour model - stress boundary model - MODEL B

6.2.1 Equal biaxial loading

The results obtained with 5.4 biaxial loading using the Barton - Bandis joint model and stress boundaries are shown in figures 4.1 - 4.6. Figure 4.1 shows the displacement vectors and the maximum principal stresses. The maximum displacment vectors developed inside the CSM block is about 0.12 mm and is occurring near the center line between the right and the left flat-jacks. The maximum developed principal stresses inside the CSM block are 8.6 MPa. The higher recorded value of 16.5 MPa is due to tensile stresses near the four corners. Figure 4.2 shows the rotation angles of the four main CSM sub-blocks.

Figure 4.3 shows the shear stresses and shear displacements inside the CSM block. The shearing is occurring mainly along the foliation joint (0.11 mm) and the four boundary joints

The block rotation plot is shown on Figure 7.2. Due to the geometry of the block, all sub-blocks are rotated clockwise. Figure 7.3 shows shear stresses and shear displacement plots. The shear displacement is occurring both along the flat-jack/ block interface and the internal joints. The maximum shear displacement inside the CSM block is 0.13 mm. Figure 4.4 shows plots of the mechanical and conducting apertures along the joints. The maximum recorded mechanical aperture is 136 μm and the maximum conducting aperture is 34.7 μm. E/e ratio is 3.91. Figures 7.5 and 7.6 show the history plots of ten instrumented points (x-direction) and nine instrumented points on the y-direction (see also Fig. 26).

6.3.2 N-S uniaxial loading with Barton - Bandis joint model

Figure 8.1 shows the displacement vectors and principal stresses plot. The maximum recorded displacement inside the CSM block is 0.32 mm and the maximum principal stress is about 21.9 MPa, which is believed to be associated with rotations and corner loading inside the CSM block.

The upper right sub-block seems to suffer most of the displacement, probably due to the closure of the joints on the lower right part. The block rotation plot, Fig. 8.2, shows that all blocks are rotated in an anticlockwise direction at different angles.

Most of the shearing displacement is occurring along the diagonal joints (Fig. 8.3) and partly on the right flat-jack boundary joint with a maximum value of 0.30 mm. Figure 8.4 is showing the maximum mechanical and conducting aperture of 152 μm and 49.6 μm, respectively. E/e ratio is 3.06. It is important to notice the scale describing the joint aperture as line thickness in micrometres (one line corresponds to 5 μm aperture).

Figures 8.5 and 8.6 show the history plots for x-and y-direction, respectively (see also Fig. 26).

6.2.3 E-W uniaxial loading with Barton - Bandis joint model

Figure 6.1 shows the maximum displacement vectors inside the CSM block (0.40 mm) which is mainly occurring on the upper right block. The maximum principal stress is 8.6 MPa, at a distance of 5 cm from the boundary joints inside the CSM block. The high recorded value of 26.3 MPa is tensile stress induced on the upper left corner. The upper right sub-block due to the geometry of the system is rotating most (Fig. 6.2).

Figure 6.3 shows the shear stresses and shear displacement values across the joint of the CSM block. The most shearing is occurring along the main diagonal joint (0.33 mm). Along the boundary joints some shearing is also occurring.

The mechanical and conducting aperture values (Fig. 6.4) inside the CSM block are 160 μm and 49.2 μm, respectively, and they are occurring on the intersection of the diagonal and foliation joint.

Figures 6.5 and 6.6 show the history points for x-direction (ten points) and y-direction (nine points).

6.3 Barton - Bandis joint behaviour model - fluid pressure boundary model - MODEL C

6.3.1 Equal biaxial loading

The results obtained with 5.40 MPa biaxial loading using the Barton - Bandis joint model are shown in Figures 7.1 - 7.6.

Figure 7.1 shows the displacement vectors and the principal stresses. The maximum displacement inside the CSM block is about 0.19 mm. The maximum tensile principal stress is 15.9 MPa and is developed mainly around the four corners near the interface of the flat-jack boundary and the CSM sub-blocks.

following:

- to provide absolute displacement measurements
- to minimize the time required for data acquistion.
- to measure accurately displacements on the block surface

For this reason a unique instrumentation system was designed, fabricated and installed which enabled measurement of the three components of displacement (x, y and z) at ten locations and at three different elevations in the block interior (Figure 27). An external reference frame attached to the mine roof was outside the area influenced by the flat jacks. This rigid frame was used to support the instrumentation system so that displacements in the block were referenced to a global x-y-z axis.

A number of factors affecting block deformation in response to flat jack loading were also investigated by Richardson. The attached block bottom was shown to cause stiffer behaviour with depth. Friction along the flat jack block, caused differential deformation of the sides of the blocks.

This phenomenon was mainly due to the bulging effect of the flat jacks when pressurized with oil. The mix of rock types of the block were found to have little influence on block deformation, the intact rock material contributed little to overall block strains.

The scale effects during the block testing were also evaluated by Richardson (1986). A decrease in strain measurement scatter with increasing measurement length was noted.

7.2 Terra Tek Block Test (Hardin et al., 1982)

The Terra Tek block test was carried out before the Richardson test, in 1980 and 1981. Looking critically on the type of instrumentation used in this block test, we can conclude that

6.3.3 E-W uniaxial loading with Barton - Bandis joint model

The displacement vectors for this run are shown on Fig. 9.1. It is noticeable the slightly higher value (0.37 mm) of displacement vectors inside the CSM block in comparison with the two previous runs. A reasonable explanation can be the fact that most of the joints have a vertical or sub-vertical direction, which is resulting in more deformation, more total joints closure of the model block when loaded from x-direction.

The principal stresses show a maximum value of about 7.9 MPa and some tensile stresses mainly on the top left and right corners.

Figure 9.2 shows all the blocks rotated clockwise at the same approximate angle, except the top right block that rotates in a greater angle.

The shear stress plot is shown in Fig. 9.3. Maximum mechanical and conducting aperture is 158 μm and 48.6 μm, respectively (see Fig. 6.4). The E/e ratio is 3.25.

The history plots of the ten instrumented sections are shown in Fig. 9.5 for the x-direction and in Fig. 9.6 for the y-direction.

7. DESCRIPTION AND COMPARISON OF BLOCK TEST RESULTS

This chapter describes briefly the two previous block test series performed by Terra Tek Richardson and Leijon and coworkers at CSM, in terms of instrumenation and compares some of the results obtained.

7.1 CMS - Block Test (Richardson, 1986)

The block displacement monitoring apparatus presented in Richardson's thesis was designed and developed to satisfy the

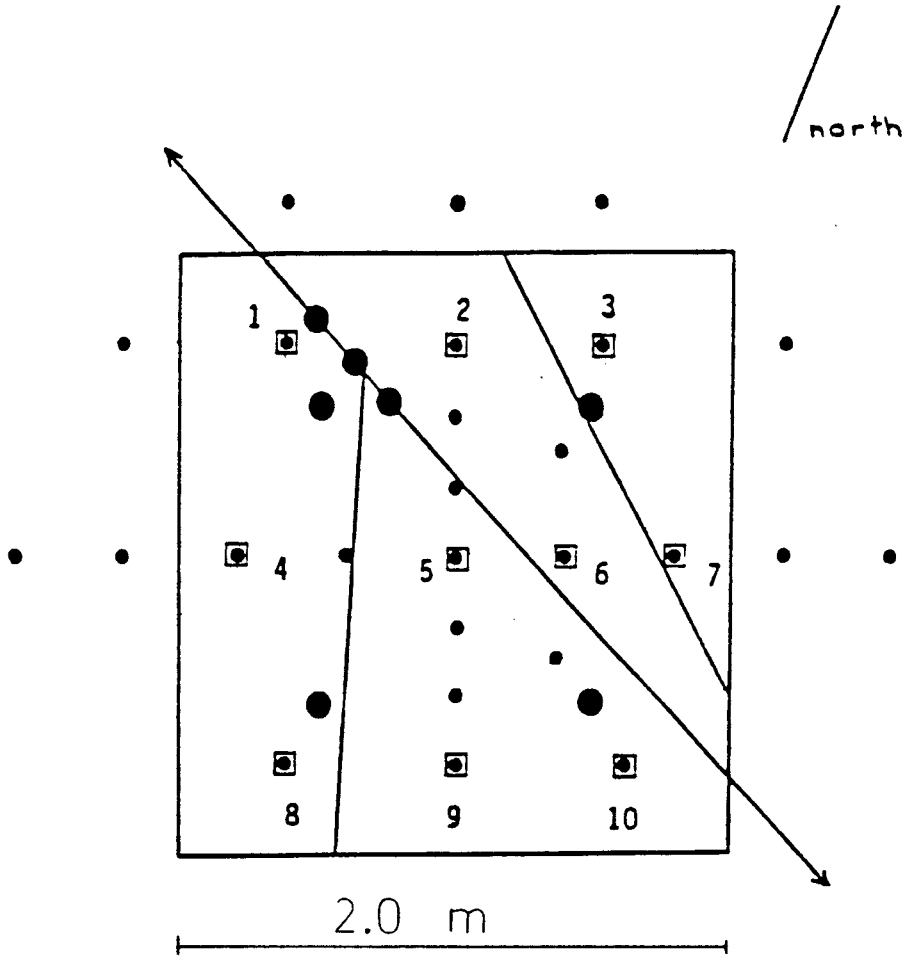

Fig. 27 Richardson's displacement instrumentation stations.

despite the heavily instrumented block with a variety of instrumentation there is a lack of:

- absolute displacement measurements.
- reliable measurements taken on the block surface.

The instrumentation of the block included:

a. Surface Instrumentation

Bonded surface strain gages.
Horizontal Strain Indicators (HSI).
Vibrating Wire Strainmeter (IRAD).
Whittemore Strain gage measurements.

b. Subsurface Instruments

CSIRO Triaxial cells.
Three component Borehole Deformation Gage (USBM).
Vibrating Wire Stress Gages (IRAD).
Multi-position Borehole Extensometers (MPBX).

Suspect results were obtained from the use of bonded resistance strain gauges on the surface of the block which gave elastic modulus from 300 GPa to 3000 GPa. These values were 5 to 50 times higher than the values obtained from the tests in the laboratory. The primary problem for these results appears to be twofold.

a. The block surface may be decoupled from the zone of flat jack loading, or a horizontal fracture had occurred near the block surface.

b. The block surface may have been curved in a convex upward manner.

The most reliable data on overall block deformation in the Terra Tek tests was obtained from extensometers and from simple mechanical Whittemore gages. The latter were used across the whole block surface, and were also used to measure changes in flatjack slot aperture. The gage monitors the relative movement of pairs of pins located approximately 25 cm apart.

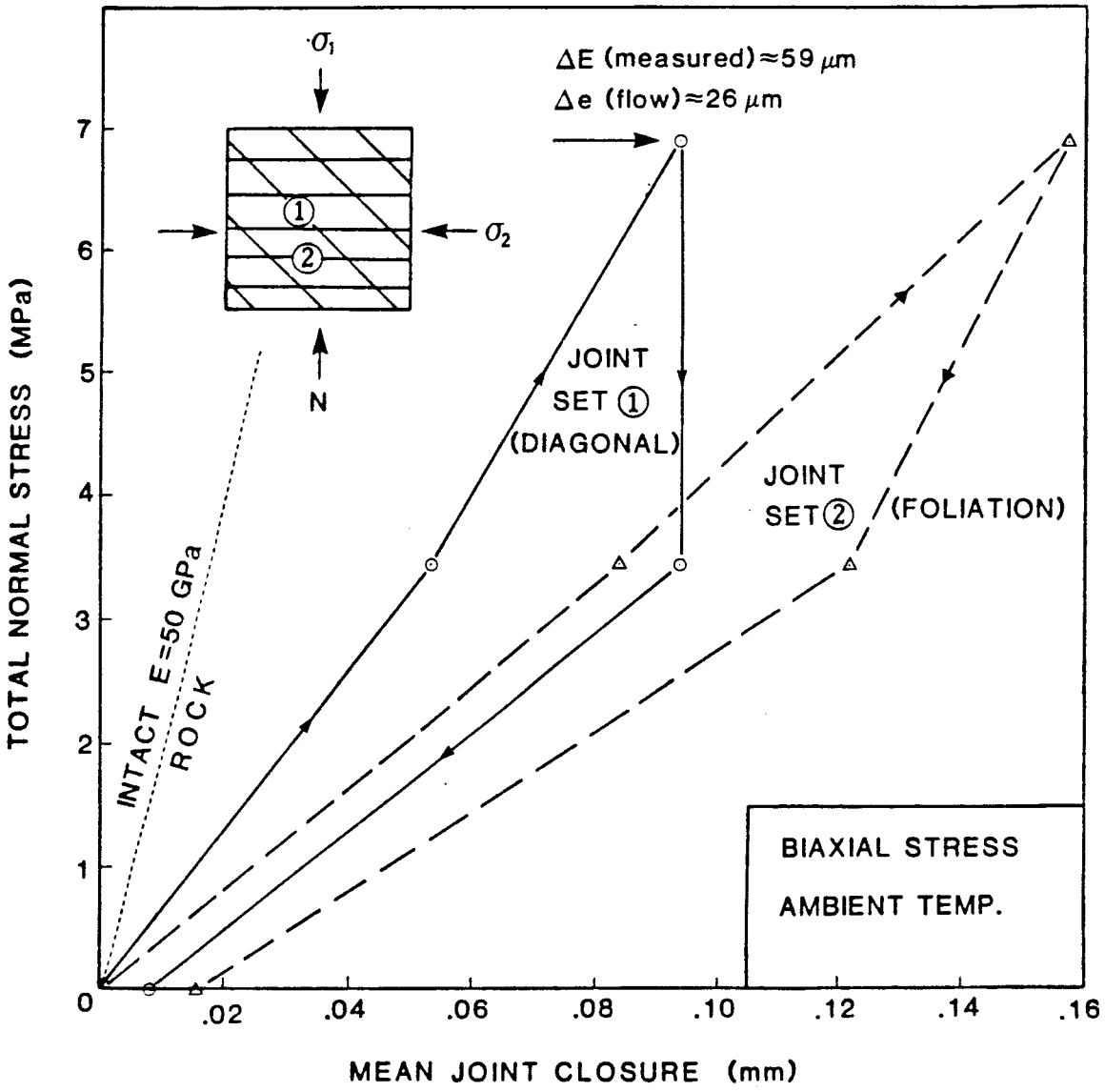

Fig. 28 Terra Tek's measurement of normal stiffness for the diagonal and foliation joints (Whittemore readings). (Net joint deformation is estimated by subtracing the deformation of intact rock.)

The use of relative measurements and limited measuring lengths made it difficult to analyse the block behaviour as a whole in the Terra Tek test series. On the positive side the Terra Tek Whittemore array was more dense and closer to the major joint sets than the sparce 10-position array used by Richardson.

7.3 Comparison of Richardson and Terra Tek Results

7.3.1 Normal and Shear Stiffness

Using pairs of Whittemore pins across major surface joints the Terra Tek researchers obtained average joint normal stiffness values of 117.5 MPa/mm for the diagonal joint set and 57.8 MPA/mm for the foliation joints over a stress range 0 - 6.9 MPa. On Fig. 28 the net joint deformation is estimated by subtracting the deformation of intact rock.

The shear stiffness results for the main diagonal joint obtained from the Terra Tek tests (Figure 29) show a dramatic increase above 1 MPa loading. If the secant value from zero to peak load is used, the shear stiffness is estimated to be 16.7 MPa/mm. The shear stiffness ranges in this case from 4.8 MPa/mm to 84.6 MPa/mm.

Richardson's results concerning the normal stiffness for the two diagonal joints on the upper horizon were about 42.8 MPa/mm and 28.10 MPa/mm which give an average of 35.45 MPa/mm. He also calculated the average value for the shear stiffness (23.9 MPa) for the two diagonal joints on the upper horizon which are ranging between 38.8 MPa/mm and 9.1 MPa/mm.

It is believed that due to the increasing stiffness resulting from the attached bottom of the block, the obtained results are higher than those expected, i.e. from those of an uncoupled block, as modelled.

8. COMPARISON OF NUMERICAL RESULTS WITH EXPERIMENTAL RESULTS

8.1 Comparison of numerical results with Terra Tek's and Richarson Joint aperture changes

The changes of joint apertures measured in the Terra Tek block test for the biaxial loading, was ΔE = 59 μm for the diagonal joint, and the change in conducting aperture was Δe = 26 μm (Fig. 28). For the N-S uniaxial loading and the diagonal joint values of ΔE = 94 μm and Δe = 26 μm were reported. For the E-W uniaxial loading the corresponding values were 63 μm change in the mechanical aperture and 25 μm in the conducting.

Richardson has also reported limited data for the mechanical aperture changes over comparable stress changes, which lie between 7 μm and 11 μm for the diagonal joint and between 2 μm and 15 μm for the foliation joint for the different test conditions. For the main diagonal and foliation joint mechanical apertures of 106 μm and 28 μm are given respectively. Richardson reports no data for conducting aperture.

It should be remembered though when comparing the joint aperture results that Terra Tek's tests were the first test done on the CSM block in 1982, therefore, higher joint apertures are expected. Richardson tests were performed on the same block in 1985 and the rock joints were considerably tighter due to earlier tests.

The rock block is considered as consolidated before the application of load. Therefore the above mentioned joint aperture changes is a result of loading after consolidation.

The numerical results corresponding to the joint aperture changes of the diagonal joint are derived from the LOTUS runs.

Consolidation in LOTUS is achieved after applying a cyclic loading equal to the 60% of the joint compressive strength values The numerical joint aperture changes are therefore the changes

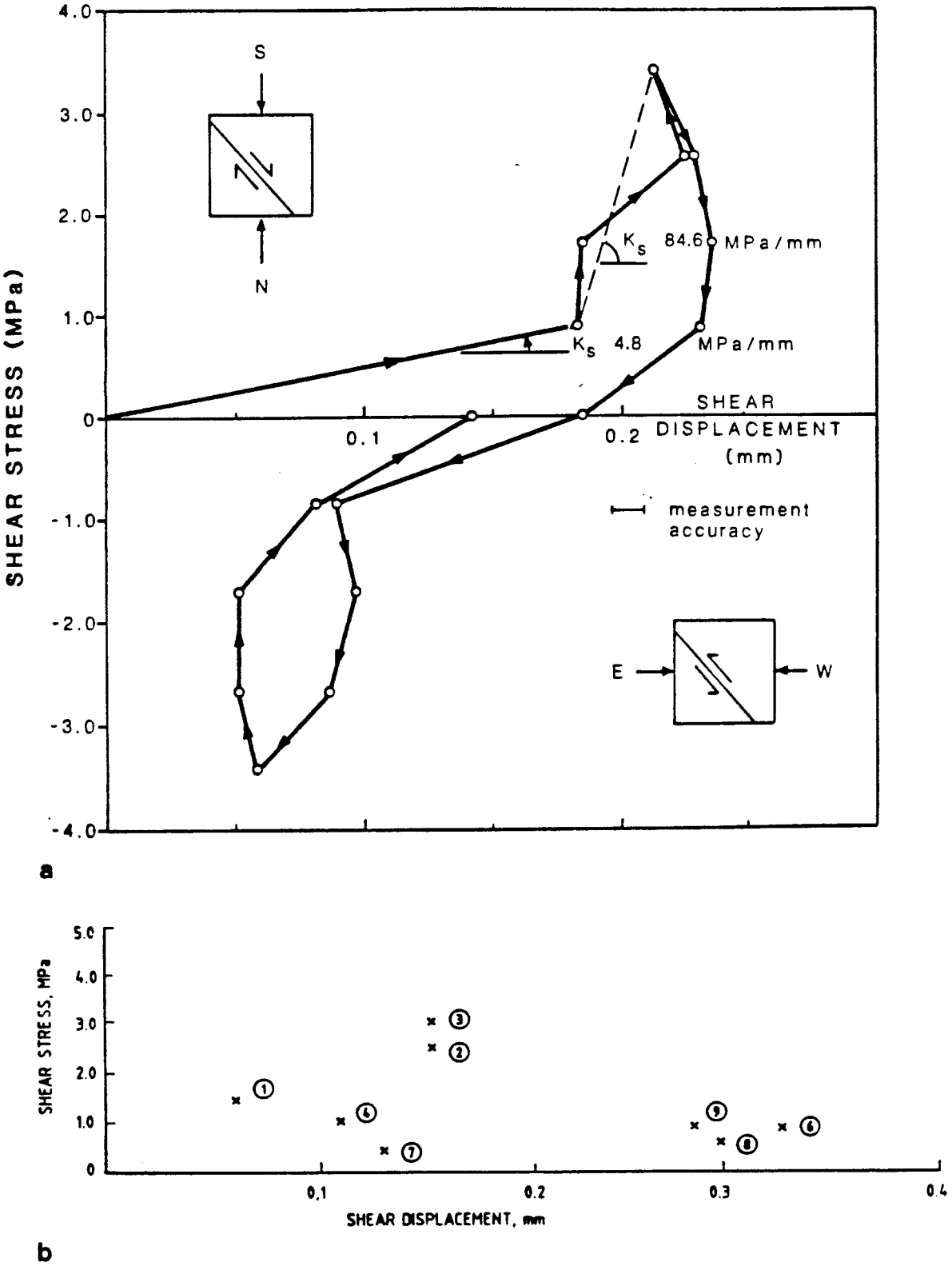

Fig. 29 a) Terra Tek's measurements of shear displacement and shear stiffness along the diagonal joints and during the N-S and E-W uniaxial tests.
b) Numerical results showing shear stress vs shear displacement calculations after equilibrium has been achieved (the numbers in circle represent Appendix Nos).

8.1.2 Comparison of numerical joint apertures with Terra Tek's results

Several sets of data mainly concerning changes in boundary conditions have been run through MUDEC. The joint properties as described in the previous chapters have been unaltered. It is interesting to comment though on the following results:

A biaxial loading of 5.4 MPa resulted in maximum mechanical and conducting apertures of 137 μm and 36.9 μm for Model B, and 136 mm and 34.7 μm for Model C, respectively.

The corresponding values for the N-S uniaxial loading were 162 μm and 49.9 μm for Model B, and 152 μm and 49.6 μm for Model C. It is important to note on the biaxial run of Model C that the maximum aperture values are occurring on the intersection between the boundary joints and the block joints. On the contrary, in the N-S uniaxial run for Model B the maximum values are occurring along the diagonal joints. For ploting reasons the mechanical apertures have been plotted as a single line when a certain value is exceeded (Fig. 5.4). The fact that the diagonal joint gave experimental values of e varying from about 55 μm to 27 μm (at high stress) i.e. slightly larger than those modelled, may be evidence for the stiffening effect of the intact base of the block. Figure 13 shows experimental flow losses due to joint tortuosity and roughness, expressed as the ratio E/e.

The E/e ratio for the numerical results, marked with an asterisk on Fig. 13, is about 3.9 for the biaxial run for Model C. Under the N-S uniaxial loading, the ratio E/e is about 3.1 for Model C. Finally, under E-W uniaxial loading E/e is 3.25 for the same model.

In general the comparison of the numerical results such as shear displacement, displacement vectors and stresses are in good agreement with Terra Tek's results. (See Table 7.)

occurring on the fourth loading cycle. (After consolidation has been achieved.) Using the empirical formula of figure 14 the changes in conducting apertures are calculated

$$e = \frac{E^2}{JRC^{2.5}}$$

A change of 29 μm in the mechanical joint aperture which is corresponding to 14 μm in conducting aperture is reported from the LOTUS runs of the diagonal point during the fourth loading cycle. For the foliation joint, the LOTUS derived values during the fourth loading cycle is 27 μm and 19 μm for the mechanical and conducting aperture change, respectively. Table 6 summarizes the changes of joint apertures.

8.1.1 Terra Tek's joint aperture measurements

Joint conductivity was monitored by the Terra Tek researchers by injecting water along the major diagonal joint. Flow rates were measured in parallel observation holes drilled to each side of the injection hole and at distances of 18.5 cm and 24 cm. The injection pressures used for these tests was 0.14, 0.24 and 0.34 MPa. Figures 30 and 31 summarize the results of the permeability tests. The numbers 1 through 8 indicate the order of testing. The conducting aperture (e) and permeability ($K = e^2/12$) are calculated from the well known equation for linear flow between parallel plates. The relationship between the conducting apertures changes (Δe), and the change of mechanical aperture ΔE measured during the various load cycles is shown in Figures 32 and 33. It is obvious that there is a lack of fit between changes in mechanical (ΔE) and conducting aperture (Δe). In effect the water conducting aperture of a joint according to Terra Tek' conclusions exhibits higher "normal stiffness" than the physical aperture.

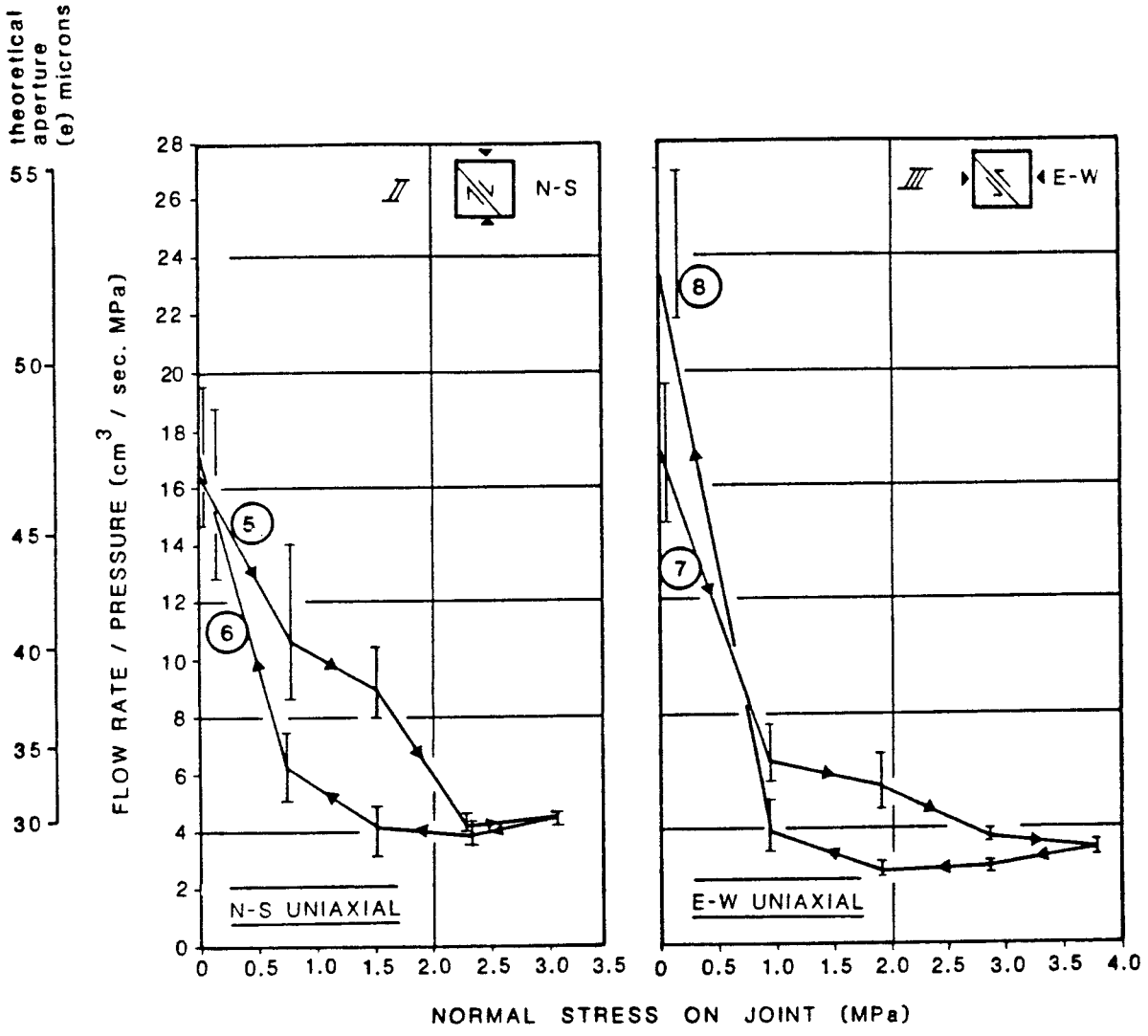

Fig. 31 Terra Tek's graph showing the effect of normal stress on the flow rate and conducting aperture for N-S and E-W uniaxial loading.

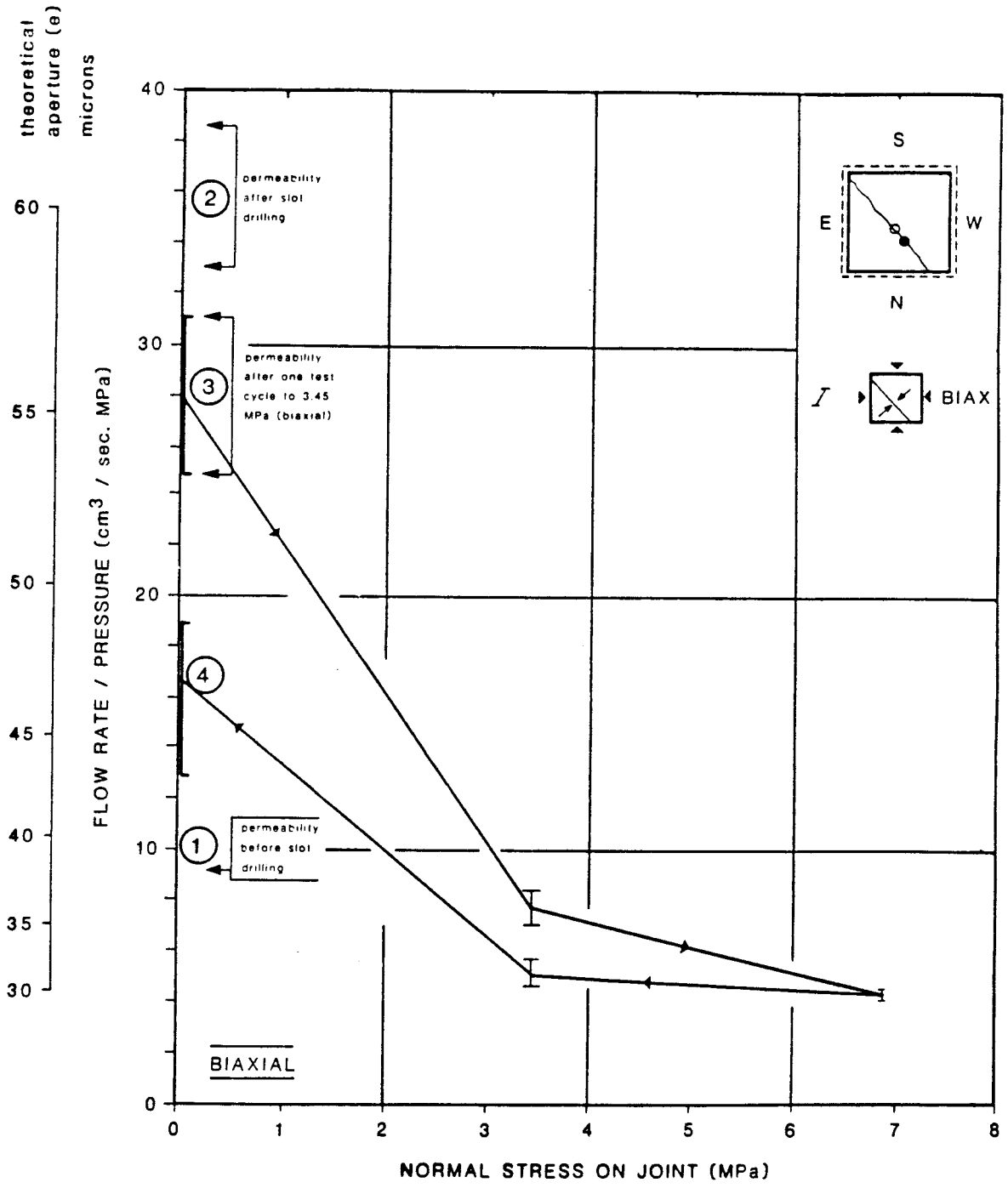

Fig. 30 Terra Tek's graph showing the effect of normal stress on the flow rate and on the conducting aperture (e).

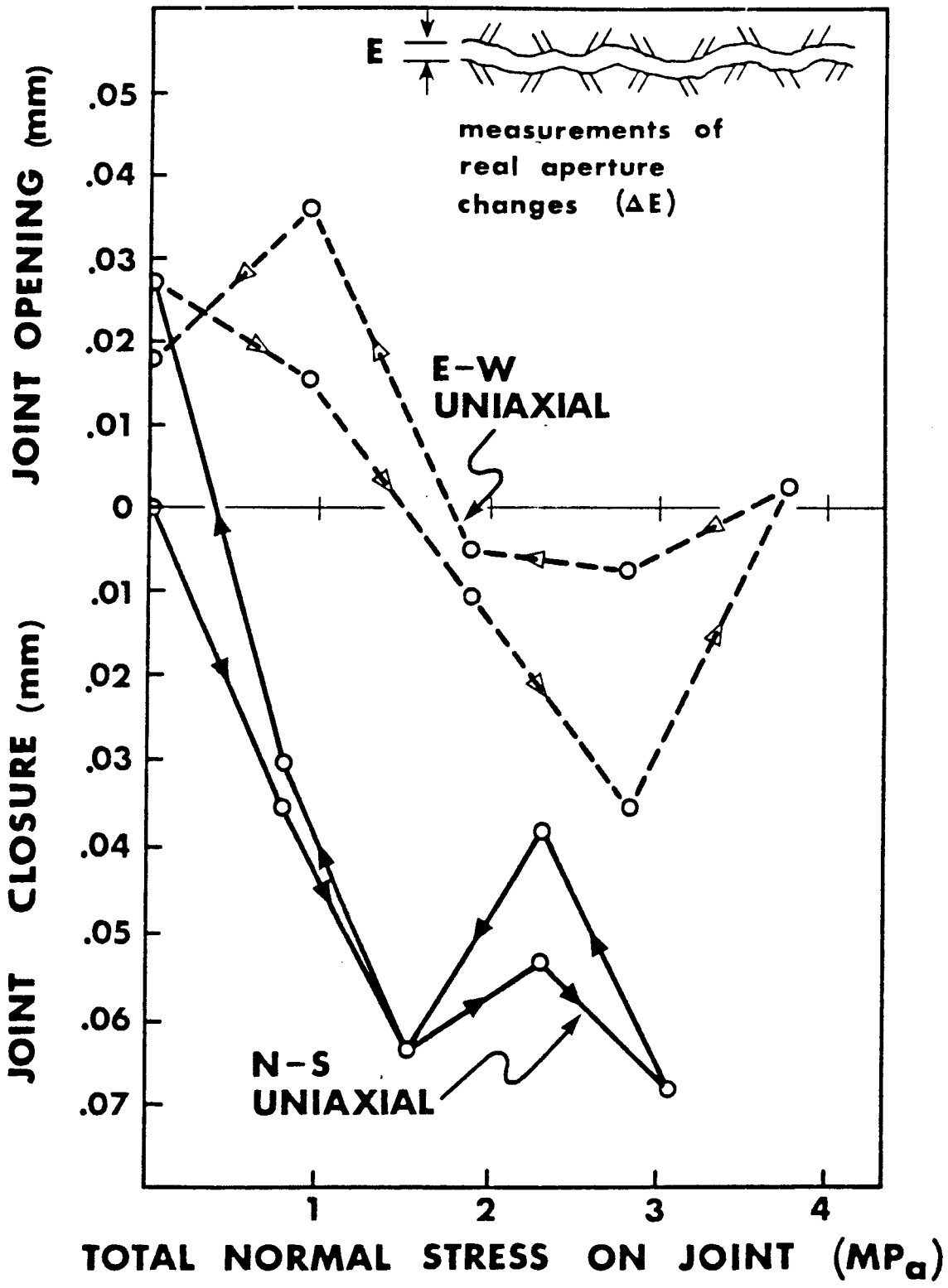

Fig. 33 Terra Tek's calculation of mechanical aperture E measured on the block.

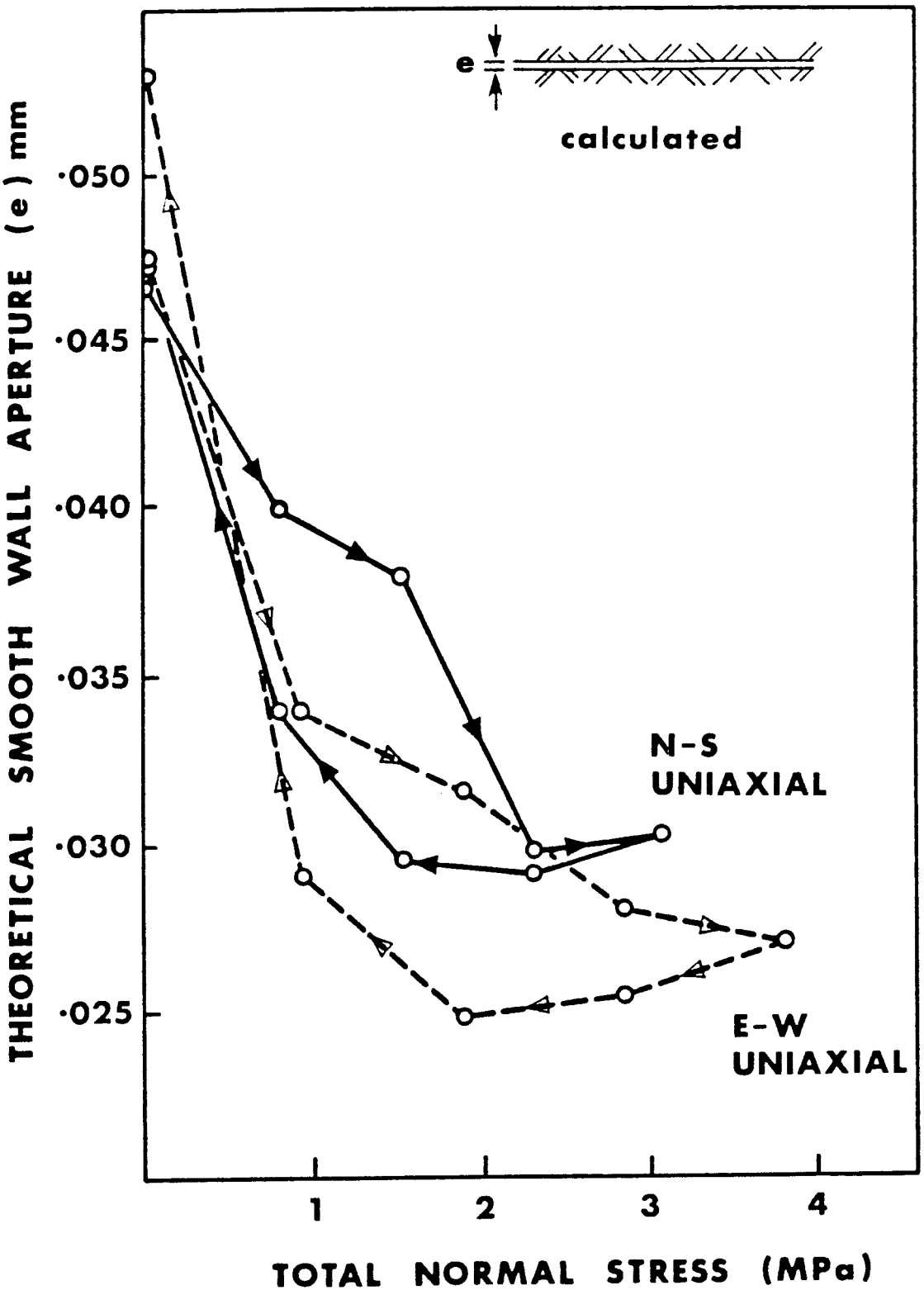

Fig. 32 Terra Tek's calculation of joint aperture changes (Δe) measured from flow tests.

Biaxial Loading

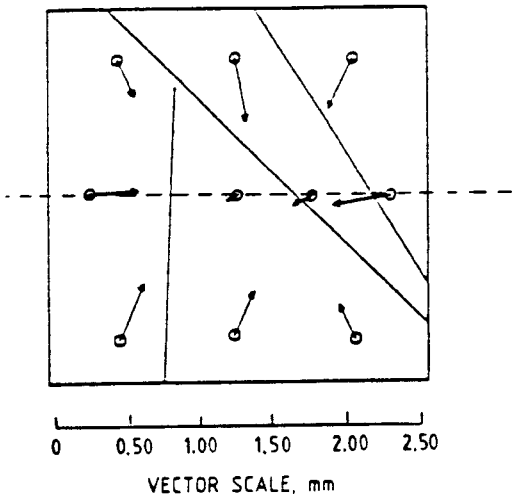

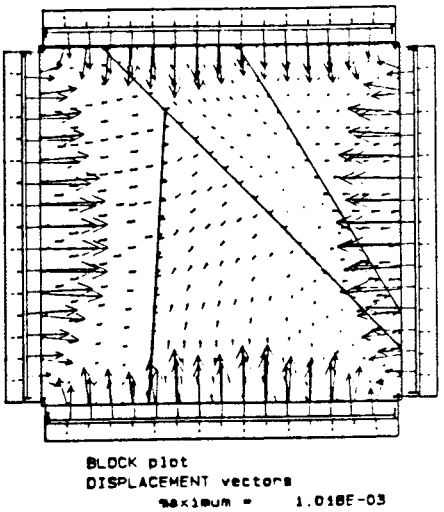

N-S Loading

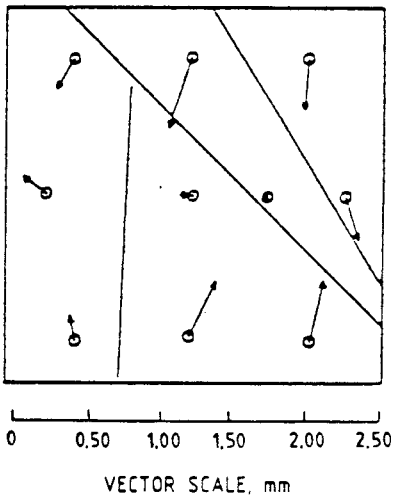

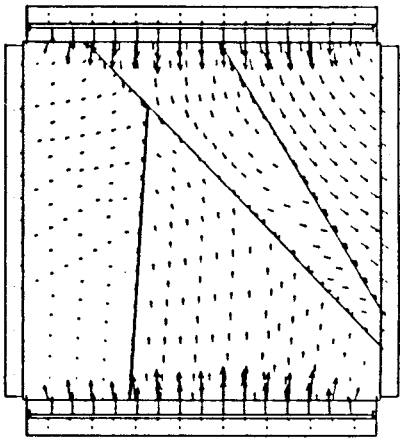

E-W Loading

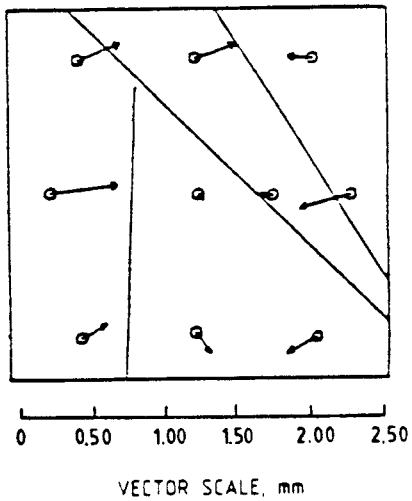

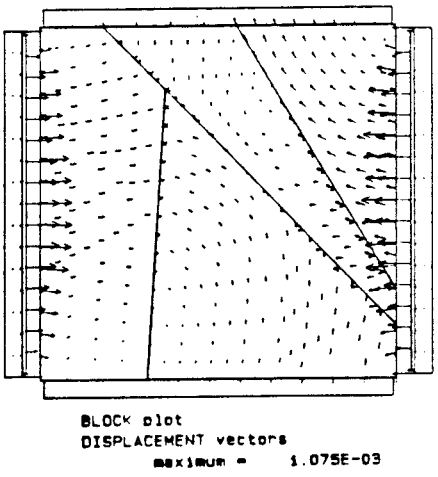

Fig. 34 Comparison of Richardson's graphs showing vector displacement for the upper - horizon tests, with numerical results from Appendix 7 Biaxial run, Appendix 8 N-S Uniaxial loading, Appendix 9 E-W Uniaxial loading.

Parameters such as mechanical joint apertures, and conductive apertures are obviously very sensitive to changes in load and boundary conditions. Therefore it is perhaps not surprising that some small discrepencies occur when the Terra Tek's and numerical results are compared. However, the non-attached nature of the modelled block should be remembered, before expecting exact correlations.

8.2 Comparison of numerical results with Richardson's tests results

A good agreement between the displacement vectors measured by Richardson and the numerical results was achieved for the biaxial loading state. Richardson reports maximum displacement vectors of about 0.5 mm for the upper horizon of the attached block (Fig. 34). The numerical result for the unattached block is about 0.19 mm for Model A, 0.12 mm for Model B, and 0.19 mm for Model C. This difference is reasonable. The corresponding values for the N-S uniaxial loading state are 0.6 mm and between 0.28 mm and 0.53 mm for the numerical simulations. The same order of discrepency is found between the in-situ, 0.6 mm and the numerical results that range between 0.29 and 0.40 mm in E-W loading.

The shear displacement values reported by Richardson, are in very good agreement with the Terra Tek's results. Both researchers are reporting shear displacement values not exceeding 0.25 mm. (see Figures 28 and 29 and Table 7) in the end of the text. The numerical results obtained from Model C, (Appendix 7, 8, 9) are varying between 0.13 and 0.30 mm.

Richardson reports about 0.225 mm and 0.20 mm shear displacement for shear stresses of 2 to 3 MPa (Fig. 35) during uniaxial loading. The corresponding numerical results for the unattached modelled block for Model B are 0.11 mm for the biaxial loading conditions, 0.75 mm for N-S uniaxial loading, and

0.33 mm for E-W uniaxial loading. The obtained results from Model C are: 0.13 mm and 0.30 mm shear displacement for the biaxial and N-S uniaxial loading, and 0.29 mm for E-W loading. These appear very realistic. Once again the fact that the modelled results (for unattached blocks) show larger values of shear than measured on the attached block, is only to be expected.

It is important though to comment on the first set of figures concerning the biaxial loading (Fig. 35). The numerical normal displacement vs normal stress values are derived from the LOTUS run for the diagonal joint set after 3 consolidation cycles reaching a maximum value of 54 MPa (Fig. 18). The measurements Richardson is reporting are including the relaxation of the rock mass after the creation of the access tunnel and the digging of the flat-jack slots around the rock block. Therefore the higher values reported for normal displacement vs normal stress are expected.

8.3 Comparison of Terra Tek deformation measurement and Richardson's displacement vectors with numerical results

Terra Tek's tests on the CSM block were the first tests performed after the creation of the flatjack slots.

The Terra Tek researchers in an attempt to measure the deformation of the CSM block decided to monitor the boundary crack apertures when loading the block. The surrounding rock mass, which acts as a load plate, deforms under the flatjack pressure. As a result formation of boundary cracks in the grout above each flatjack occured. Whittemore pins were used across the boundary cracks so that opening and closures of the cracks could be monitored. The deformation modulus of the block is given by the formula:

$$E_{block} = \frac{\Delta P \cdot 1000}{\delta_b} = \frac{\Delta P \cdot 1920}{(\delta_m + \delta_b)}$$ which is directly derived from

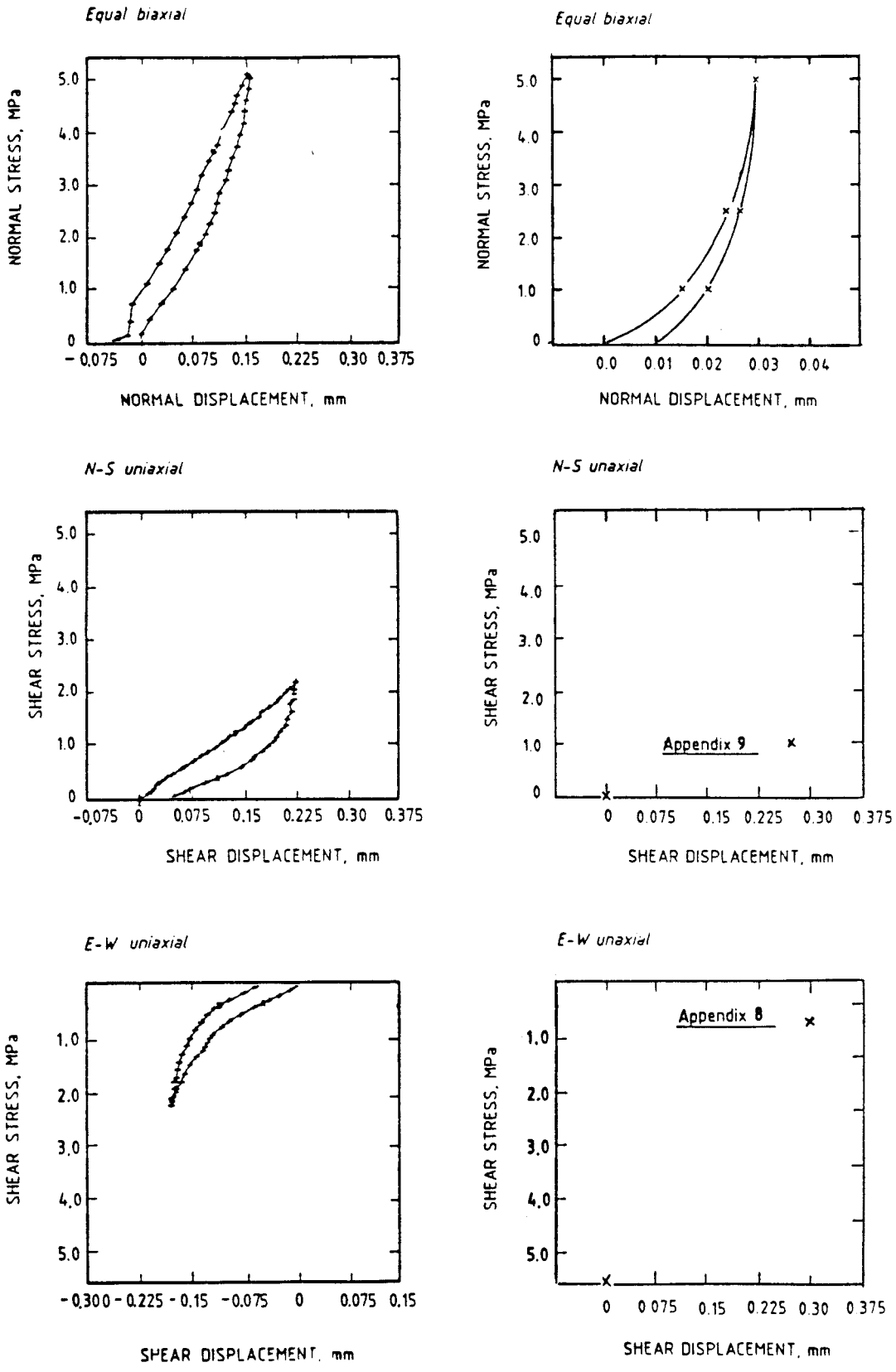

Fig. 35 Comparison of Richardson's displacement curves for the upper diagonal joint with numerical results from the 4th cycle of LOTUS run for the biaxial run. Appendix 8 for N-S uniaxial loading and Appendix 9 for the E-W uniaxial loading.

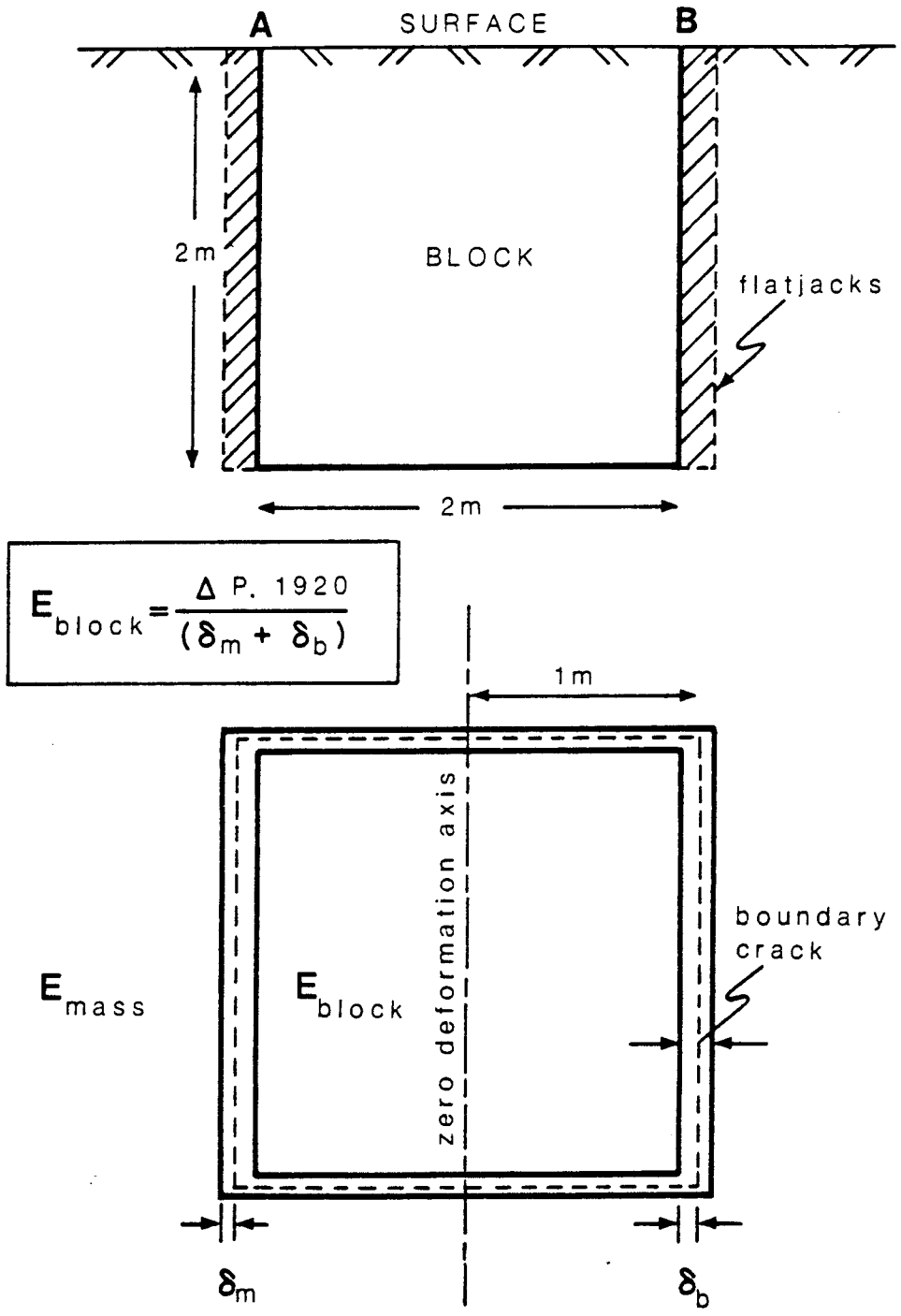

Fig. 36 Deviation of Block Deformation Modulus from the boundary crack aperture changes.

the elastic solution for the deformation of a vertical rectangle subject to uniform horizontal stress by Poulos and Davis (1973).

Where ΔP = horizontal stress increments
and δ_m and δ_b are defined in Figure 36.

The total deformation δ_m and δ_b measured across our two meters square boundary slots is composed of a deformation component for the block and a deformation component for the surrounding rock mass "load platen". At each crack the block deforms a little more than the surrounding rock mass in the ratio 1000/920.

Figure 37 shows block deformation measurements at ambient temperature using the boundary crack monitoring technique. The dotted lines represent the applied horizontal stress of 5 MPa and the mean boundary crack aperture in (mm). The real rock mass deformation for all types of loading is about 0.2 mm.

If we try to compare the measured vectors by Richardson during biaxial run (e.g. a pair of those lying parallel to the dashed lined on the top left of Fig. 34) with the measured displacement values by Terra Tek (see Table 7) and the numerical results, we can consider the modulus of deformation from the displacement measurements at the centre line (Fig. 38) according to the formula

$$\text{"E"} = \frac{\sigma}{\frac{a+b}{L}}$$

where σ = applied load
a,b = deformation vectors
L = block size length

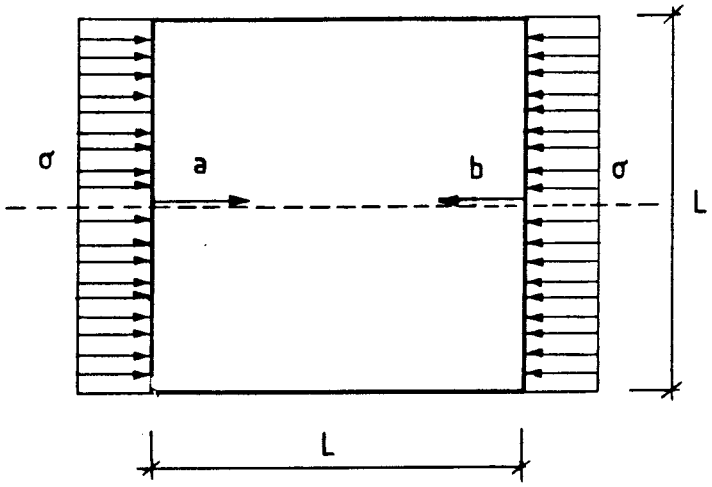

Fig. 38 Schematic representation of a biaxial loading condition and the deformation vectors along the centre line.

Applying the above mentioned deformation formula for the biaxial loading conditions, we get a deformation modulus of 14.9 and 23.5 GPa for Richardson and Terra Tek measurements, respectively, and 27.6 GPa for the numerically derived deformation vectors of Appendix 7.

8.4 Comparison of numerical results with experimental results from Brown et al. (1986)

Brown et al. (1986) has monitored the developed stresses in the jointed block under biaxial and uniaxial boundary loading by using two types of borehole gauges. The USBM Borehole Deformation Gauge (BDG) and the LuT triaxial strain cell. From the displacements and strains recorded as loads were applied, pointwise stresses were calculated assuming both isotropic and anisotropic rock behaviour. The results are characterized by large variations between the stress magnitudes, for both types

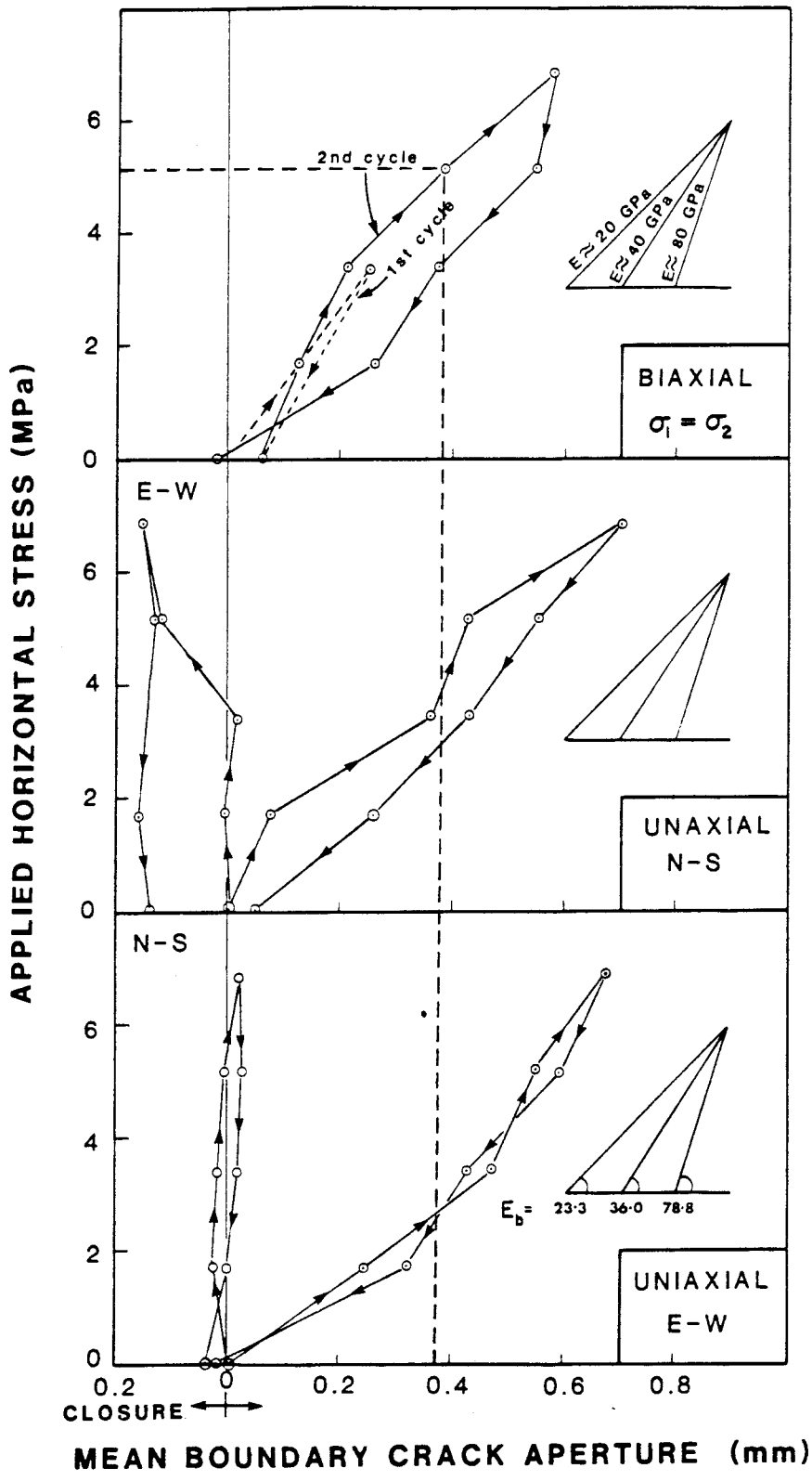

Fig. 37 Block deformation measured from boundary crack monitoring. Ambient temperature.

For better accuracy at each borehole a detailed estimation of the rock deformability proved to be necessary. Dilatometer tests using the CSM-cell were conducted at the block midplane for determination of Young's modulus, E, and the relative stiffness of the zones in the block. The wide variation in the Young's modulus results indicates a high degree of heterogeneity, which is due to the pronounced foliation of the block.

The mean value of modulus E was estimated at 22.9 GPa. The Young's modulus parellel to the foliation plane varied between 9 and 80.3 GPa and perpendicular to the foliation between 6.2 and 54.9 GPa.

The peak load principal stresses obtained by the BDG and LuT gauges are given also in Figure 40a and b, and represent results obtained from the isotropic reduction procedure. (Merill and Pettersen 1962). From the results it can be seen that the stresses measured by BDG gauges are at least 20% higher than those obtained using the LuT-gauge, achieving a maximum value of about 20 MPa for the biaxial loading.

The non-uniform pattern of stress magnitudes can be attributed to:

- Shear forces developing at the block boundaries due to friction between the flatjack arrangement and the block.
- Disturbance from discontinuities on different scales in the block.
- Variation in the modulus of deformation between different parts of the block (zones of varying stiffness.)

of borehole gauges. However, the measured stress directions are in close agreement with the directions of the applied boundary loads. Figure 39 shows the location of the drilled boreholes (EX = 38 mm and NX = 76 mm) for instrumentation purposes.

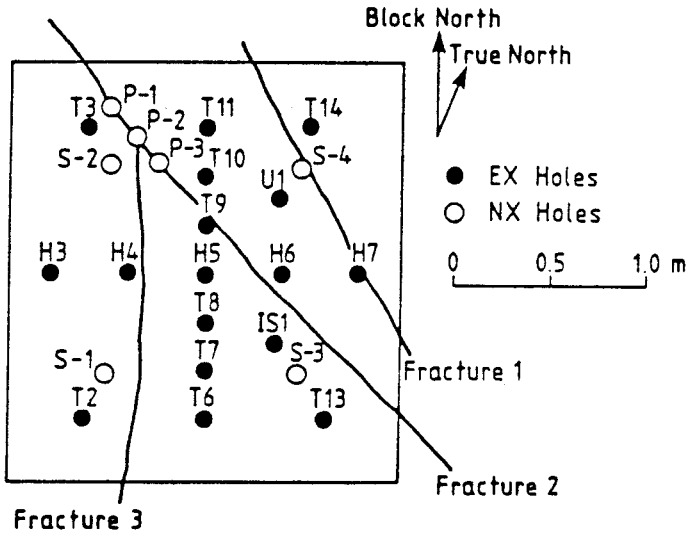

Fig. 39 Surface plan of the tested block showing major discontinuities and vertical borehole locations.

For the numerical simulation in this report the value of Young's modulus was assumed to be 60 GPa and the Poisson's ratio 0.25. The maximum principal stress results derived from the numerical simulation varied between 9.1 and 14.1 MPa, for the linear joint model with stress boundaries between 7.9 MPa and 12.9 MPa for the fluid pressure boundaries model with the Barton - Bandis joint model, and between 8.5 and 23.2 MPa for the stress boundaries model with Barton - Bandis joint model.

For improving numerical stability (block rotation problems) the flatjacks have been fixed on eight points around the block (Appendices 7, 8, 9). When loading the block, some small tensile stresses are developed on the four sides. It is believed that those tensile stresses are not affecting the joint behaviour.

The numerical fluid pressure boundaries represent more accurately the actual testing conditions. In this case the maximum values of the principal stresses lies very near the BDG experimental results and the LUT gauge results (see Fig. 40, Table 7).

It is important to note that the intact rock has been modelled isotropically, the foliaton effect has not been taken in account, the study focusing primarily on the joint behaviour and the conductivity changes. Nevertheless, variations in stress magnitude and direction were also seen in the modelling results resembling in several ways the variation measured in practice.

Table 5 summarizes the obtained results from all MUDEC runs.

Table 6 summarizes the experimental and numerical results for joint aperture changes.

Table 7 shows an overview of numerical and experimental results concerning maximum displacement vectors, total block displacement, shear displacement and maximum principal stresses.

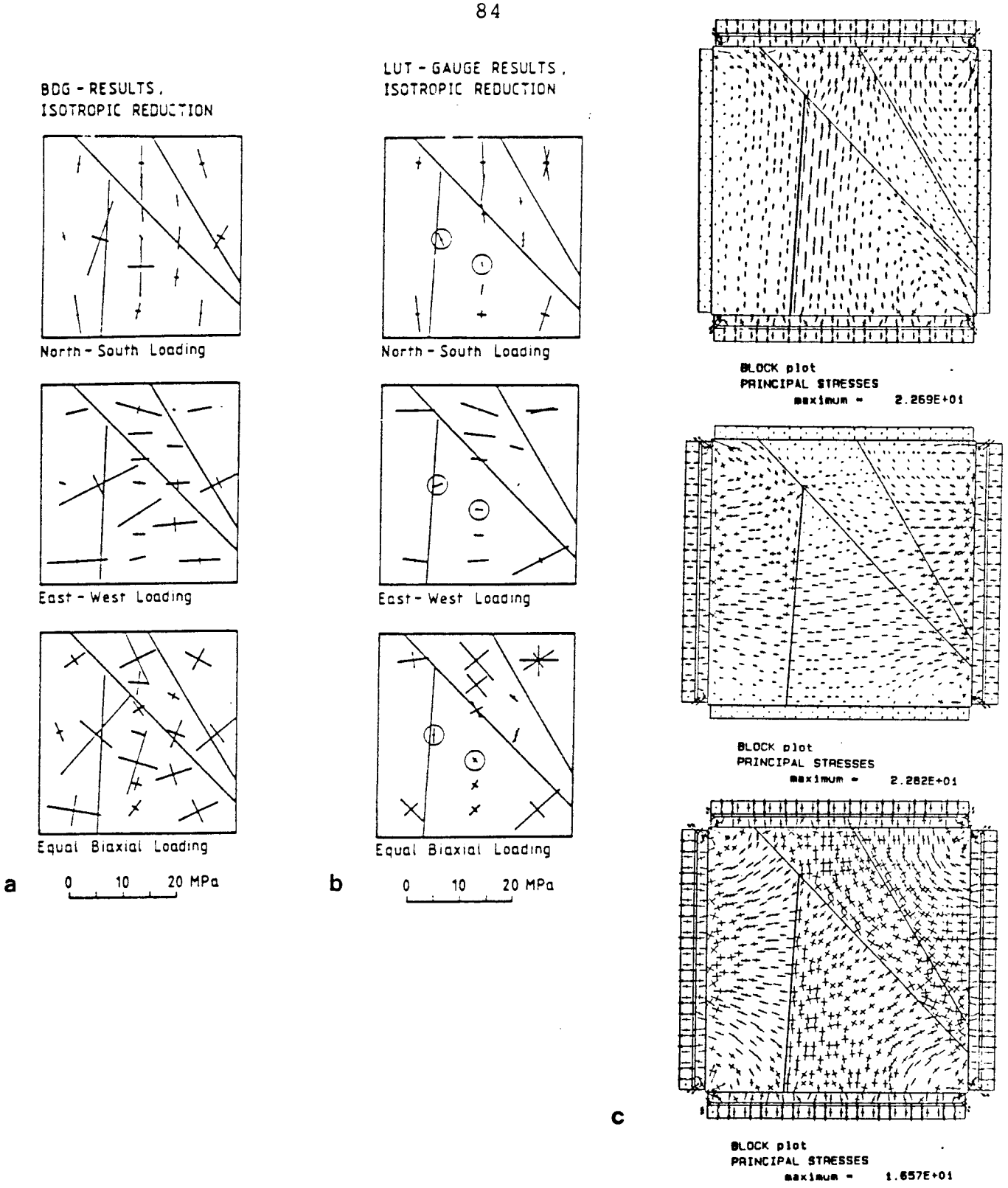

Fig. 40a, b) Peak load principal stresses plot (5.3 MPa applied stress) showing response of the borehole deformation gauge and Luleå University of Technology gauge respectively.

c) Principal stresses plots from numerical simulation (from Appendix 4 Biaxial loading, Appendix 8 N-S uniaxial loading and Appendix 9 E-W uniaxial loading (in MPa)).

Table 6 Summary of the numerical and experimental results from Terra Tek and Richardson tests concerning changes in mechanical and conductive joint apertures.

	Stress range (MPa)	Mechanical joint aperture change (μm)	Conducting joint aperture change (μm)	Mechanical aperture (μm)	Conductive aperture (μm)
Terra Tek's measurements					
Diagonal joint	(0-6.9)	59 BIAX 94 N-S 63 E-W	26 BIAX 17 N-S 26 E-W	- - -	27-55 29-46 28-53
Richardson's measurements					
Diagonal joint	(0-5.2)	7-11 BIAX - -	- - -	106 BIAX - -	- - -
Foliation joint	(0-5.2)	2-15 BIAX - -	- - -	28 BIAX - -	- - -
Numerical results MODELS A, B, C	(0-7)	29 Bia (diag) 27 Bia (fol.)	14 (Bia diag) 19 (Bia fol.)	137-142 Bia 152-162 N-S 160-164 E-W	34.7-36.9 Bia 49.6-49.9 N-S 48.4-49.2 E-W

Table 5 Summary of the numerical results showing the maximum displacement vectors, the maximum shear displacements on joints, maximum principal stresses and mechanical and conducting apertures inside the CSM Block.

TYPE OF MODEL	Appendix No.	Direction of loading	Maximum displacement vectors (mm)	Maximum shear displacment (mm)	Maximum principal stresses (MPa)	Mechanical or real aperture (μm)	Conducting or theoretical aperture (μm)
MODEL A							
Linear joint model	1	BIAX	0.10	0.06	11.3	-	-
	2	N-S	0.28	0.15	14.1	-	-
	3	E-W	0.29	0.15	9.1	-	-
MODEL B							
Stress boundaries model with Barton-Bandis joint model	4	BIAX	0.12	0.11	8.6	137	36.9
	5	N-S	0.53	0.75	23.2	162	49.9
	6	E-W	0.40	0.33	8.5	160	49.2
MODEL C							
Fluid pressure boundaries model with Barton - Bandis joint model	7	BIAX	0.19	0.13	15.9	136	34.7
	8	N-S	0.32	0.30	21.9	152	49.6
	9	E-W	0.37	0.29	7.9	158	48.6

9. SUMMARY AND CONCLUSIONS

1. MUDEC-linear and MUDEC-BB codes have been validated against the measured results obtained from the CSM block test by Terra Tek Inc, and by Richardson (CSM) and Brown et al. For simplicity the block has been modelled with the four principal blocks. Equal biaxial, N-S and E-W uniaxial loading have been applied to each type of model.

2. Boundary condition details have been varied in an attempt to more closely simulate flatjack loading. The linear joint model (MUDEC-linear) was loaded with simple uniform stress boundaries. Runs with the Barton - Bandis non-linear joint subroutine (MUDEC-BB) were also loaded with the simple uniform stress boundaries. (Appendices 4 - 6) More realistic boundary conditions were achieved by applying fluid pressure loading in rectangular slots simulating the flat-jacks, with rigid boundaries resisting movement behind the flat-jack slots. These boundary conditions were only applied to the MUDEC-BB models. (See Appendices 7, 8, 9.)

3. Results have been presented in the form of graphic output for principal stresses, shear stresses, deformation vectors, shear displacements along the joints, and, for the case of MUDEC-BB (non-linear), also plots of joint mechanical apertures and conducting apertures.

4. The principal stress plots indicate similar features to those measured in the CSM block, i.e. rotations from block to block when crossing a joint, particularly when shear has occurred. A representative example can be seen in Fig. 4.1. In general, stress mangitudes were of the order of 4 to 7 MPa compared to the maximum applied boundary stresses of 5.4 MPa. However, due to stress concentrations associated with rotations and corner loading, maximum single

Table 7 Summary of the numerical and experimental results from Terra Tek, Richardson and Leijon tests concerning the maximum displacement vectors, total block displacement, shear displacement and maximum principal stresses.

	Maximum displacement vector (mm)	Total block displacement (mm)	Shear displacement (mm)	Maximum principal stress (MPa) DBG results	LUT results
Richardson measurements	0.5 BIAX 0.6 N-S 0.6 E-W	0.725 BIAX	- BIAX 0.225 (N-S) 0.20 (E-W)		
Terra Tek measurements	* * *	~ 0.23 BIAX ~ 0.23 N-S ~ 0.23 E-W	- BIAX 0.22 (N-S) 0.13 (E-W)		
Leijon et al. Stress measurements				20.0 BIAX 24.7 N-S 16.3 E-W	11.6 BIAX 8.4 N-S 11.8 E-W
Numerical results from Models A, B, C	0.10-0.19 BIAX 0.28-0.53 N-S 0.29-0.40 E-W	0.20-0.38 BIAX - N-S - E-W	0.06-0.13 BIAX 0.15-0.75 N-S 0.15-0.33 E-W	8.6-15.9 BIAX 14.1-23.2 N-S 7.9-9.1 E-W	

* The Terra Tek results concerning maximum displacement vectors were obtained by using the Whittemore strain gauges on the block surface and stress range between 0 and 6.9. They refer to average displacement values and therefore cannot be directly comparable.

tures (E) were only obtained with the MUDEC-BB non-linear models. Maximum values of (e) ranged from 36.9 to 49.9 mm in the uniformly stress loaded models, and from 34.7 to 46.9 μm in the fluid-pressure models. Corresponding ranges of mechanical apertures were 137 to 162 μm and 136 to 158 μm, respectively.

9. Joint aperture, the most sensitive single parameter that can be chosen to describe a rock mass (where water flow rate is proportional to aperture cubed) has modelled very close values ranging from 34.7 to 49.9 μm to the measured values of 27 to 55 mm which were obtained across a small area of the major diagonal joint.

10. ACKNOWLEDGEMENT

Norwegian Geotechnical Institute would like to thank SKB (Svensk Kärnbränslehantering AB) for the financial support of this project. Many thanks are also due to professor Ove Stephansson and Göran Bäckblom for their useful remarks during the preparation of this report.

values of principal stress ranging from 9.1 to 14.3 were recorded in the linear models, and from 7.9 to 23.2 in the non-linear models.

5. Maximum deformation vectors ranged from 0.10 to 0.29 mm in the linear models, from 0.12 to 0.33 mm in the non-linear models (uniform loading), and from 0.19 to 0.37 mm in the non-linear models with fluid pressure boundaries. In general, as expected and measured in practice, the biaxially loaded models gave the minimum deformations. The above ranges of values are very close to ranges measured in practice both by Terra Tek and by Richardson.

6. The total displacement of the block was measured by Terra Tek using the boundary crack analysis method. Richardson measured displacement vectors. The numerically obtained results are ranging between 0.24 and 0.38 mm and they are very close to the values measured by Terra Tek researchers and Richardson (0.2 mm and 0.72 mm, respectively).

7. Shear displacements occurred principally along the diagonal joints, with related shearing along block boundaries and along parallel joints. Maximum shear displacements ranged from 0.06 to 0.15 mm in the linear models, from 0.11 to 0.75 mm in the non-linear models (uniform loading) and from 0.13 to 0.30 mm in the non-linear models with fluid pressure loading. In general, as expected, and measured in practice, the biaxially loaded models showed less joint shear than the uniaxially loaded (N-S or E-W) models. Due to the attached nature of the block base in reality, neither Terra Tek nor Richardson and co-workers obtained more than 0.25 mm of shear along the diagonal joints. In other words the block was stiffer in practice than in our two-dimensional models.

8. Joint apertures expressed as theoretical smooth-wall conducting apertures (e) and mechanical (or physical) aper-

- Barton, N. and Bakhtar, K. (1983)
Rock joint Description and modelling for the hydrothermo-mechanical design of nuclear waste repositories.
Terra Tek Engineering TRE 83-10. Submitted to CANMFT Mining Research Laboratories, Ottawa, 268 p.

- Barton, N., Bakhtar, K. and Bandis, S. (1985)
Strength deformation and conductivity coupling of rock joints.
Int. J. Rock Mech. Min. Sci. Geomechanics Abst., 22 (3): pp. 121-140.

- Cundall, P.A. (1980)
UDEC - a generalized distinct element program for modelling jointed rock.
Report PCAR-1-80, Peter Cundall Associates; Contract DAJA7-79-C-0548, European Research Office, U.S. Army, March 1980.

- Hardin, E.L., Barton, N.R., Lingle, R., Board, M.P. and Voegele, M.D. (1982)
A heated flatjack test to measure the thermomechanical and transport properties of rock masses.
Office of Nuclear Waste Isolation, Columbus, OH, ONWI - 260, p. 1983.

- Kranz, R.L., A.D. Frankel, T. Engelder and C.H. Scholtz (1979)
The permeability of whole and jointed barre granite.
Inter. J. Rock Mech. Min. Science and Geomechanic Abstracts. Vol. 16, pp. 225-234 and Erratum Vol. 17, pp. 237-238.

- Brown, S.M., Leijon, B.A. and Hustrulid, W.A. (1986)
Stress distribution within an artificially loaded jointed block.
Proceeding of the Internat. Symposium on Rock Stress and Rock Stress Measurement, Stockholm.

- Merrill, R and Peterson, J., (1962)
Deformation of a Borehole in Rock.
USBM Report, Investigation No. 5881, Denver, Colorado.

- Miller, R.P. (1965)
Engineering classification and index properties of intact rock.
Ph.D. Thesis. University of Illinois, 322 p.

11. REFERENCES

- Bandis, S. (1980)
  Experimental studies on scale effects on shear strength and deformation of rock joints.
  Ph.D Thesis, The University of Leeds, Department of Earth Sciences.

- Bandis, S., Barton, N. and Christianson, M. (1985)
  Application of a New Numerical Model of Joint Behaviour to Rock Mechanics Problems.
  Intern. Symposium on Fundamentals of Rock Joints, Bjørkliden pp. 345-355.

- Bandis, S., Lumsden, A. and Barton, N., (1983)
  Fundamentals of rock joint deformation.
  Intern. J. Rock Mech. Min. Sci. and Geomech. Abstracts, 20 (6): pp. 249-268.

- Bandis, S., Lumsden, A. and Barton, N.R. (1981)
  Experimental studies of scale effects on the shear behaviour of rock joints.
  International Journal of Rock Mechanics and Mining Engineering, Vol. 18, pp. 1-21.

- Barton, N. (1981)
  Some scale dependent properties of joints and faults.
  Geophysical Research Letters, Vol. 8, No. 7, pp. 667-670.

- Barton, N. (1976)
  The shear strength of rock and rock joints.
  Internat. J. Rock Mech. Min. Sci. and Geomechanics Abstracts 13, pp. 225-279.

- Barton, N. and Choubey, V. (1977)
  The shear strength of rock joints in theory and practice.
  Rock Mech. 10, pp. 1-54.

- Barton, N. (1982)
  Modelling rock joints behaviour from in-situ block tests implications for nuclear waste reposity design.
  ONWI - 308, 96 pp. Office of Nuclear Waste Isolation, Columbus.

A P P E N D I X

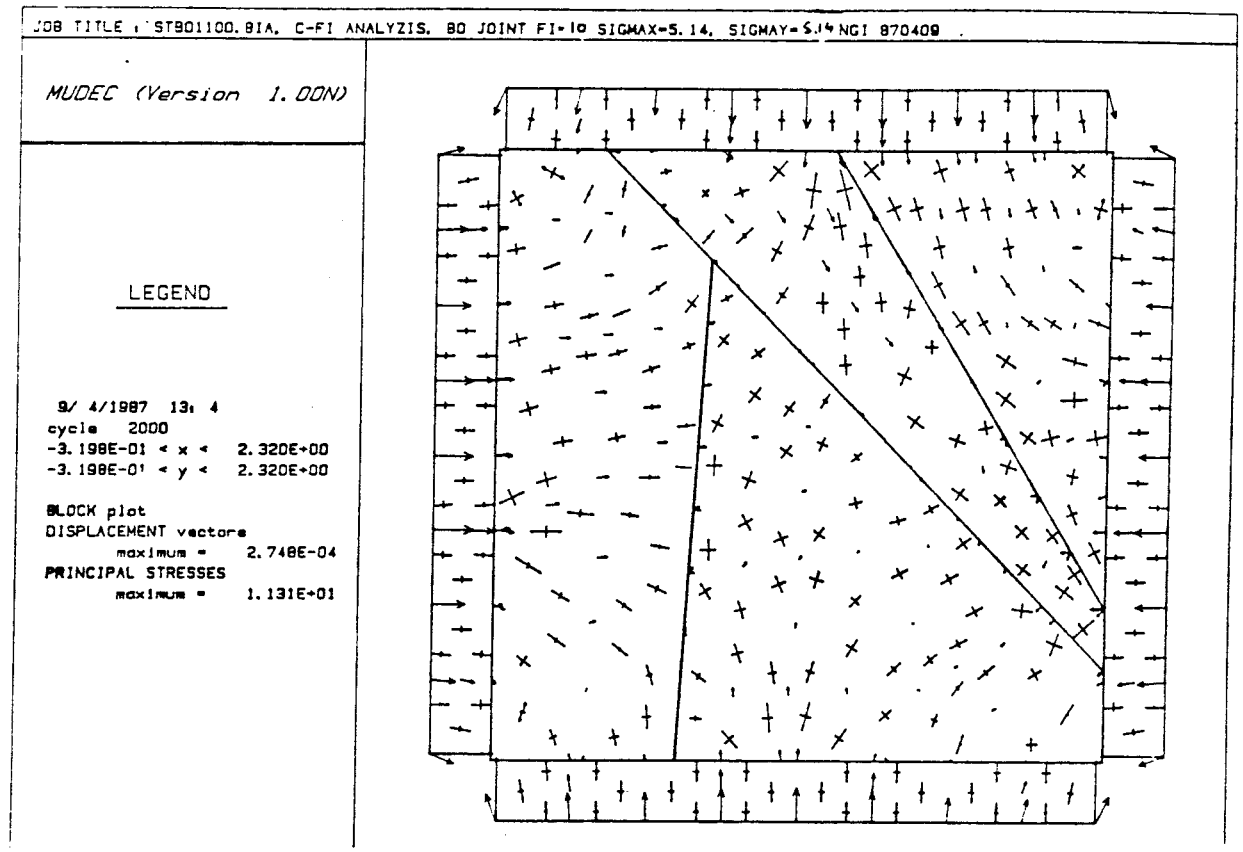

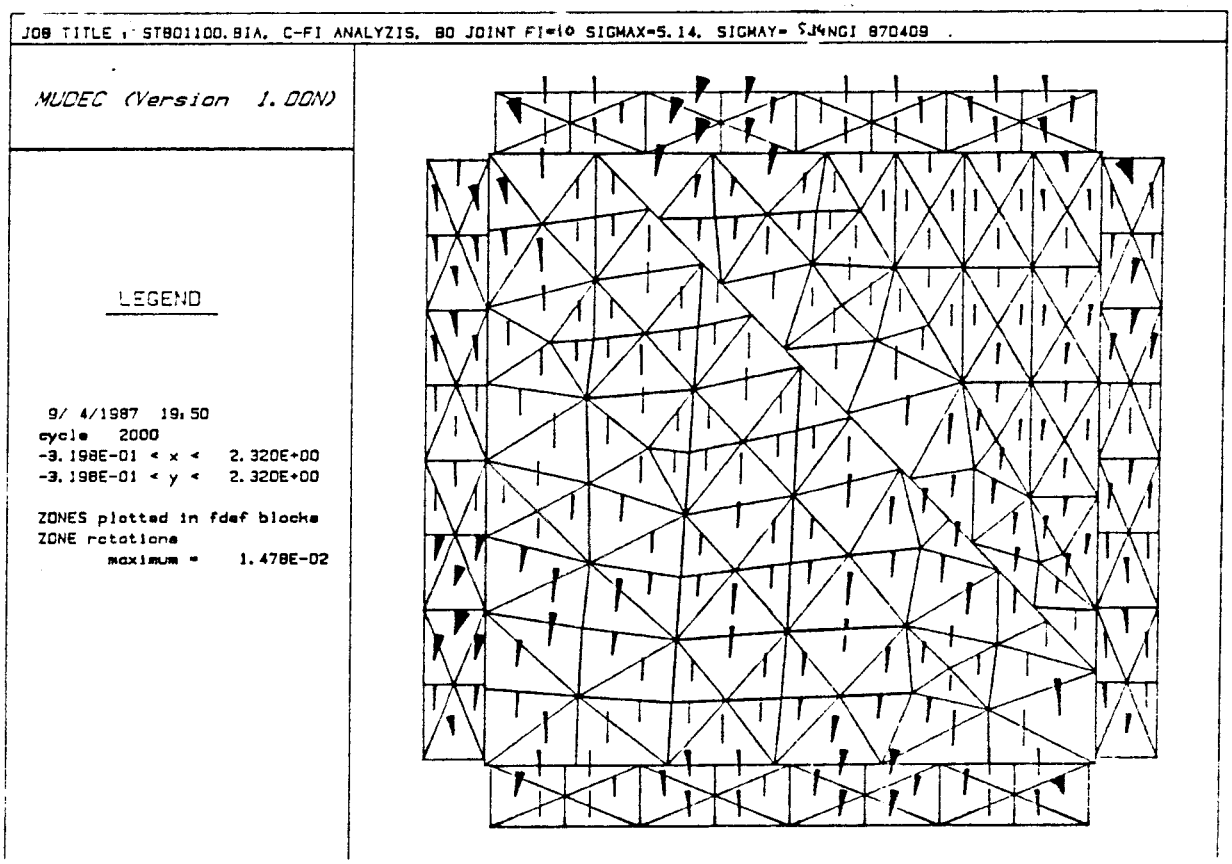

Fig. 1.1 Biaxial loading. Displacement vectors and principal stresses plot. Zone rotation plot.

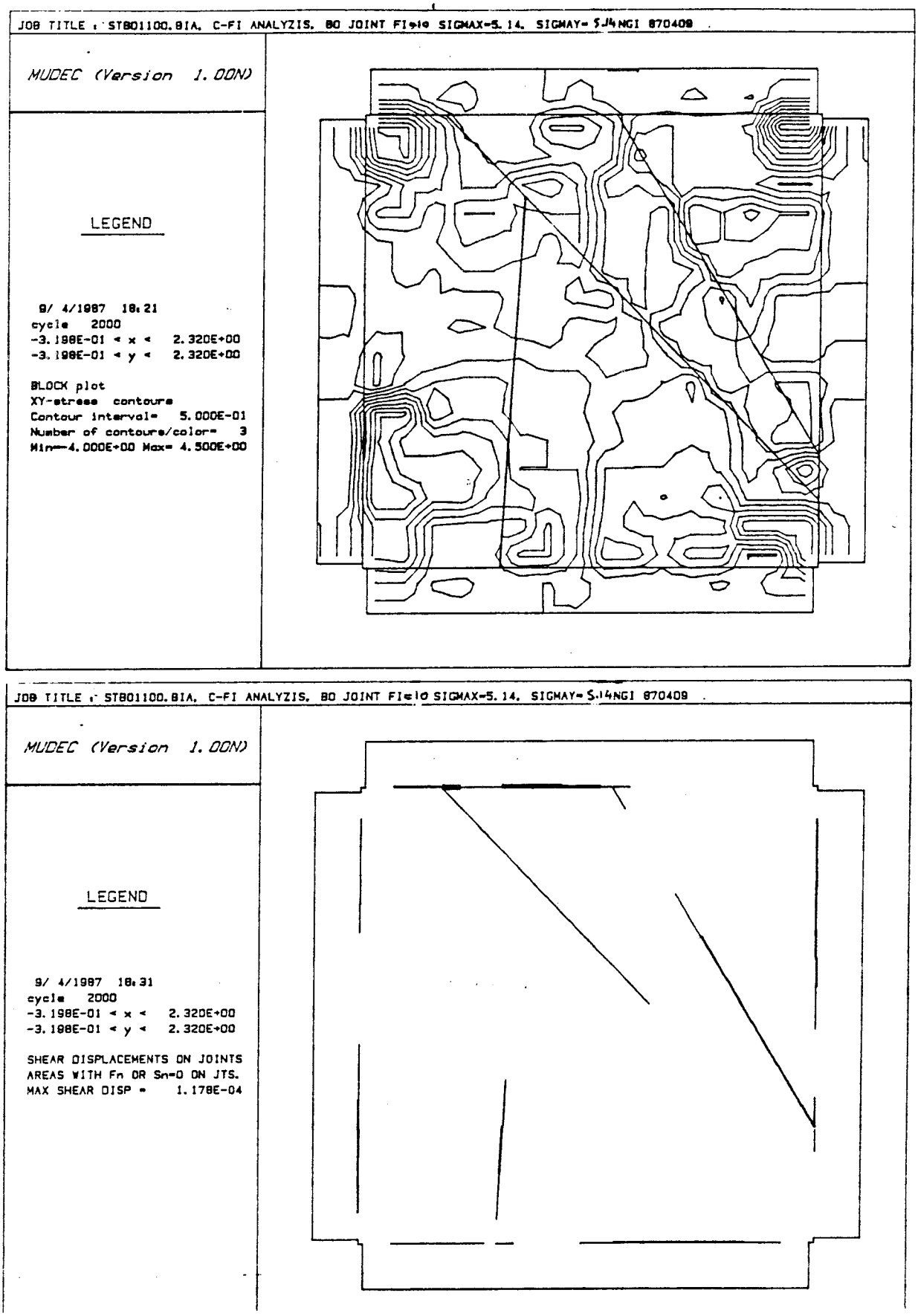

Fig. 1.2 Biaxial loading. Shear stress and shear displacement plots.

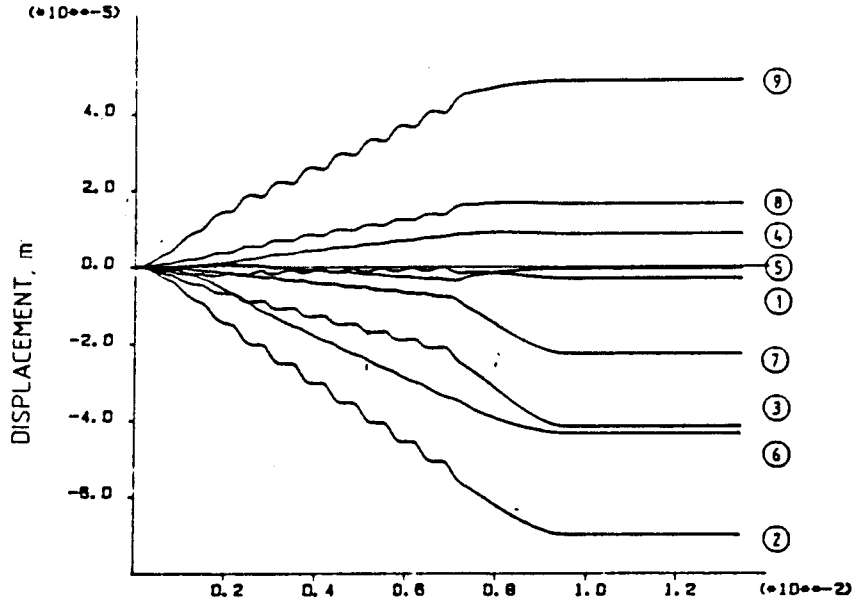

N - S direction displacement

E_{qual} biaxial loading

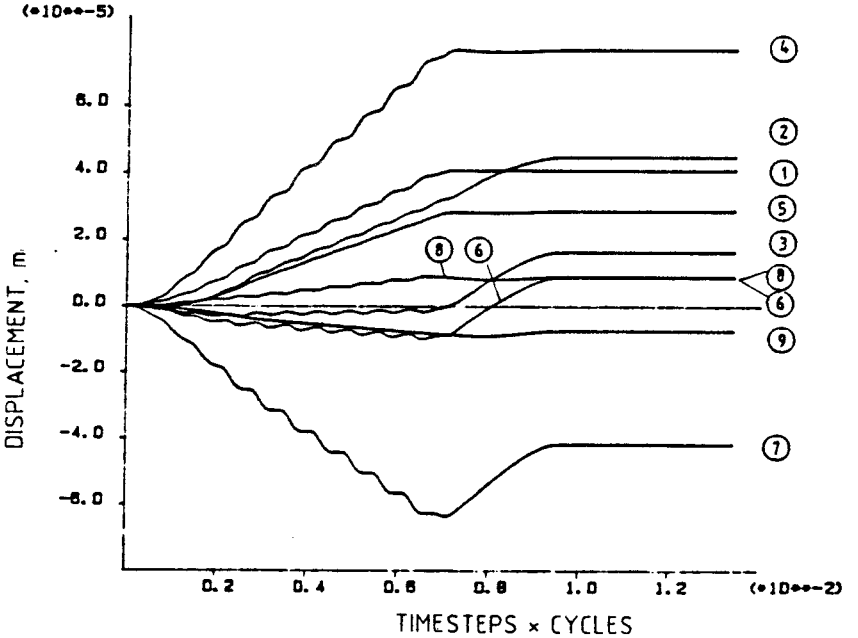

E - W direction displacement

E_{qual} biaxial loading

Fig. 1.3 **Biaxial loading. History plots of nine instrumented points.** (See also fig. 26.)

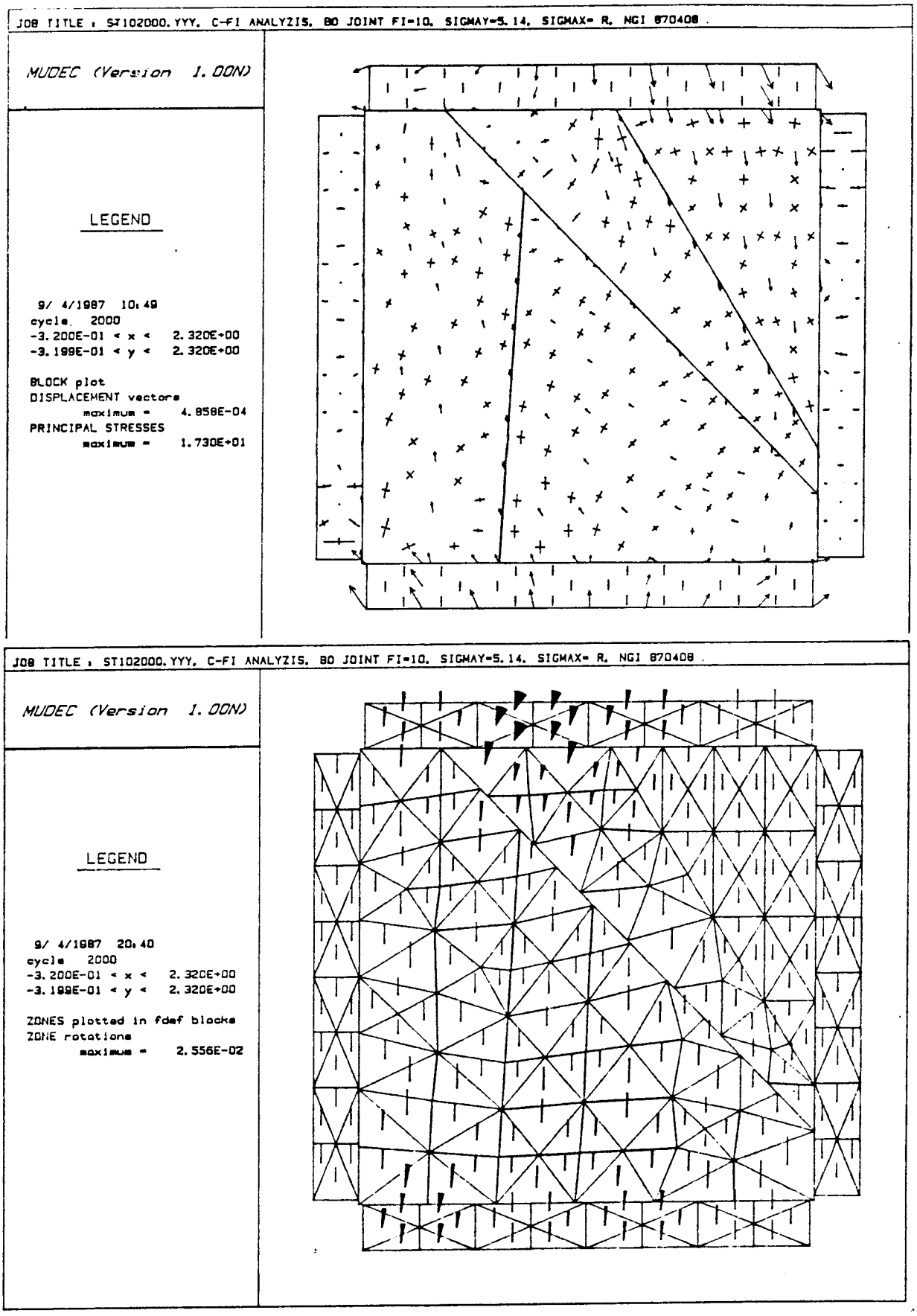

Fig. 2.1 N-S uniaxial loading. Displacement vectors and principal stresses plot. Zone rotation plot.

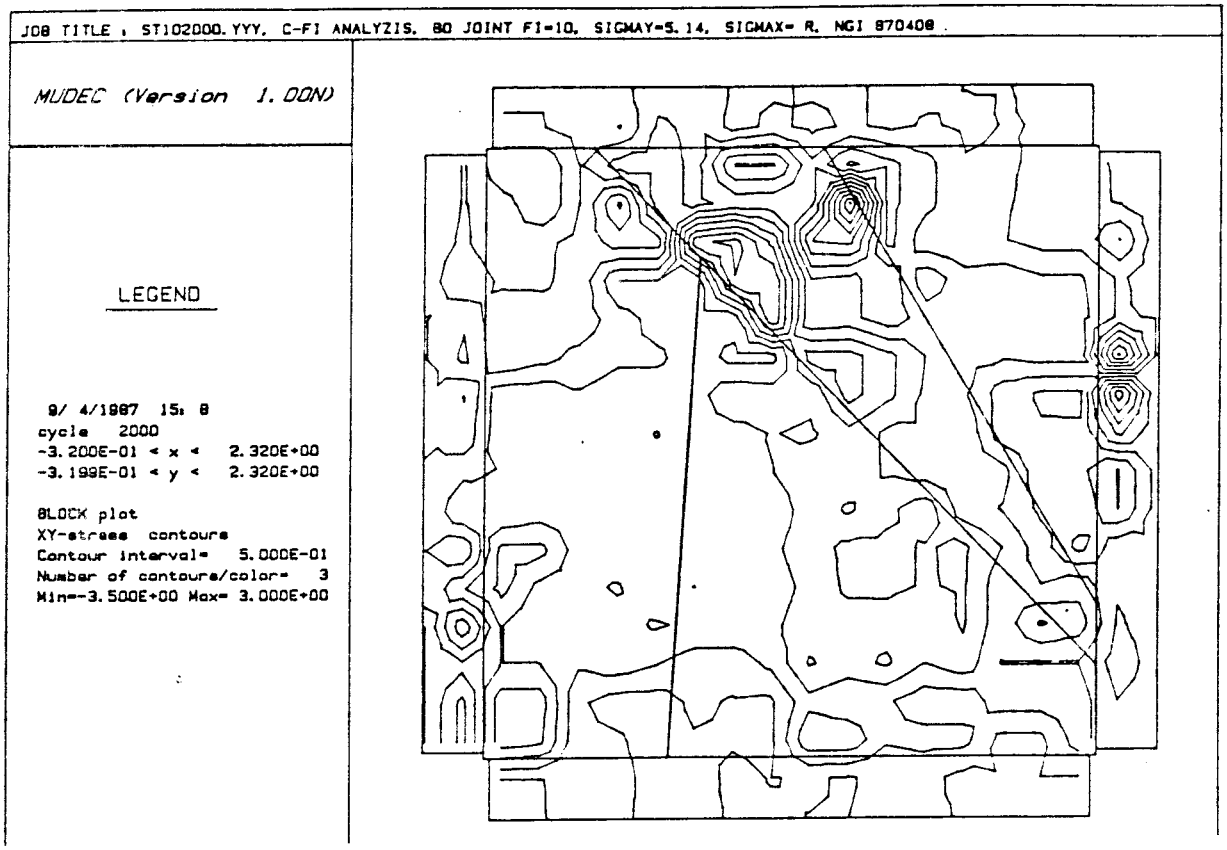

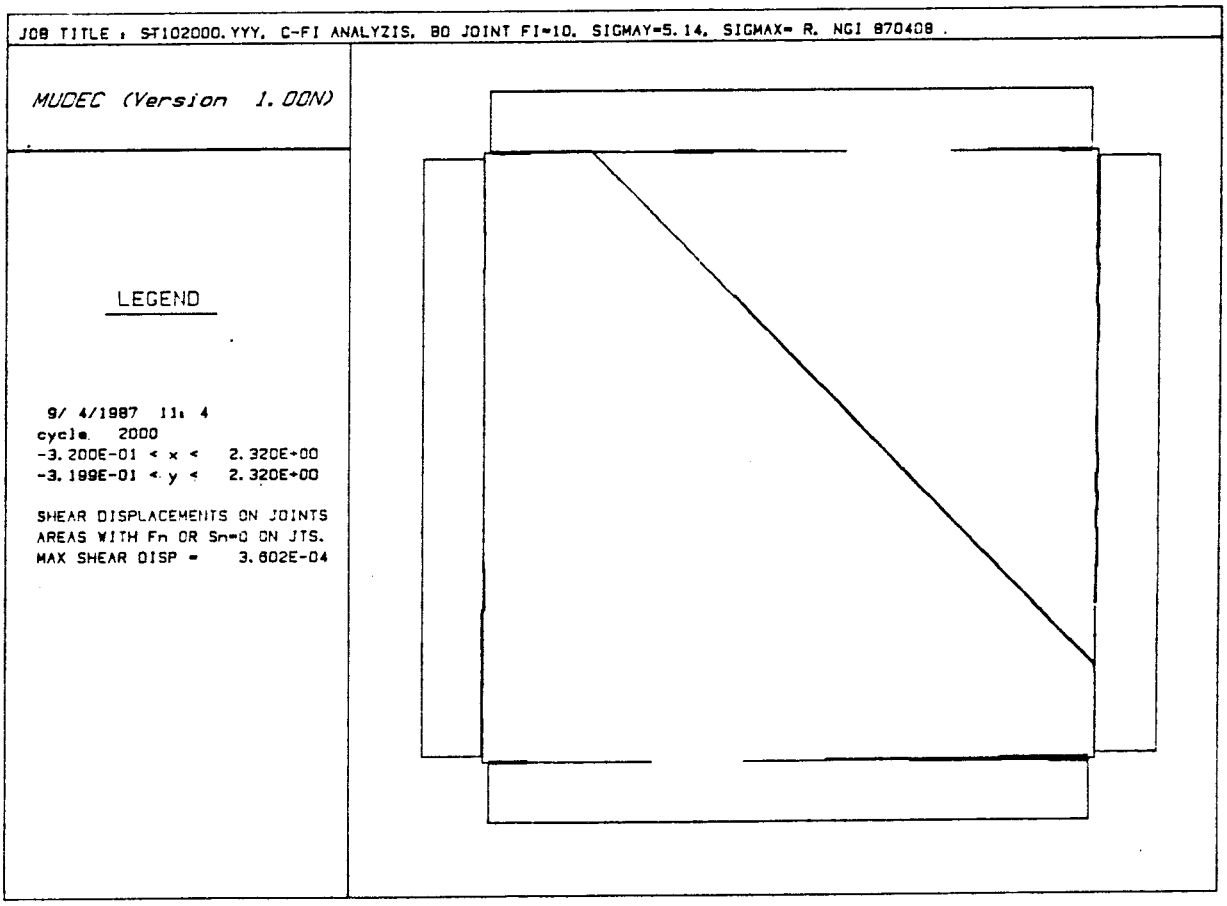

Fig. 2.2 N-S uniaxial loading. Shear stresses and shear displacement plots.

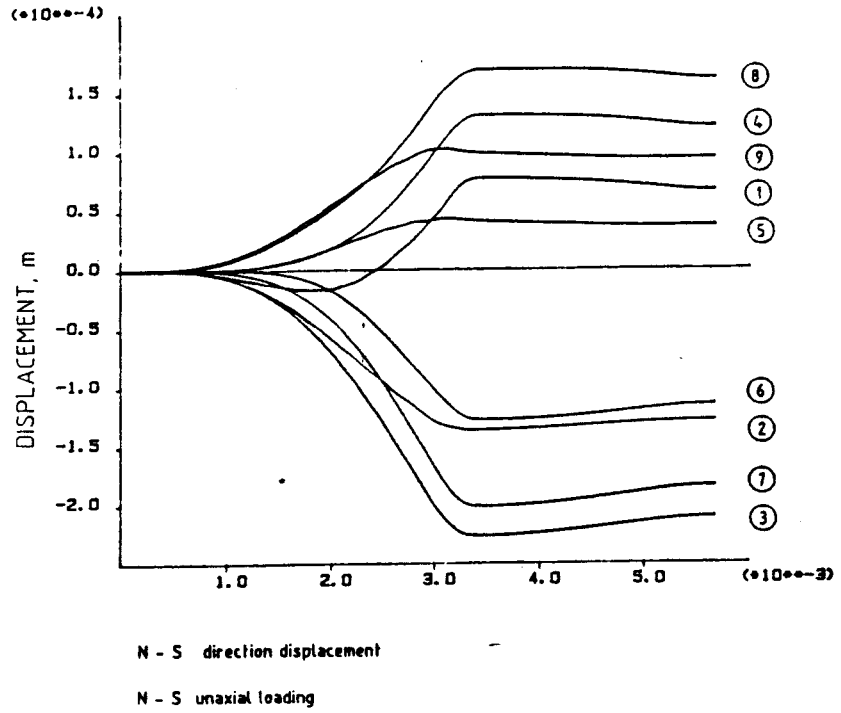

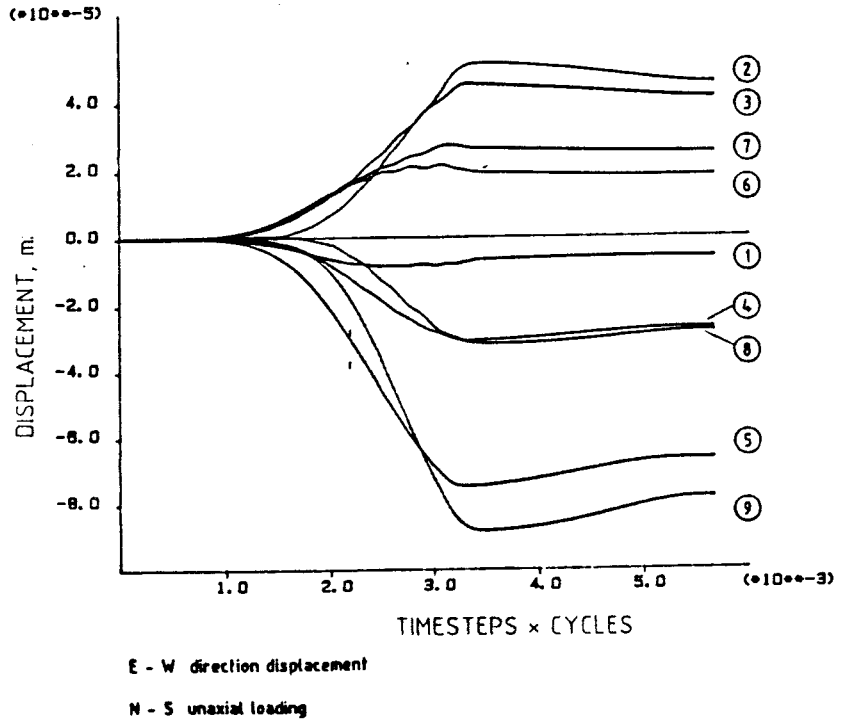

Fig. 2.3 N-S uniaxial loading. History plots of nine instrumented points. (See also Fig. 26.)

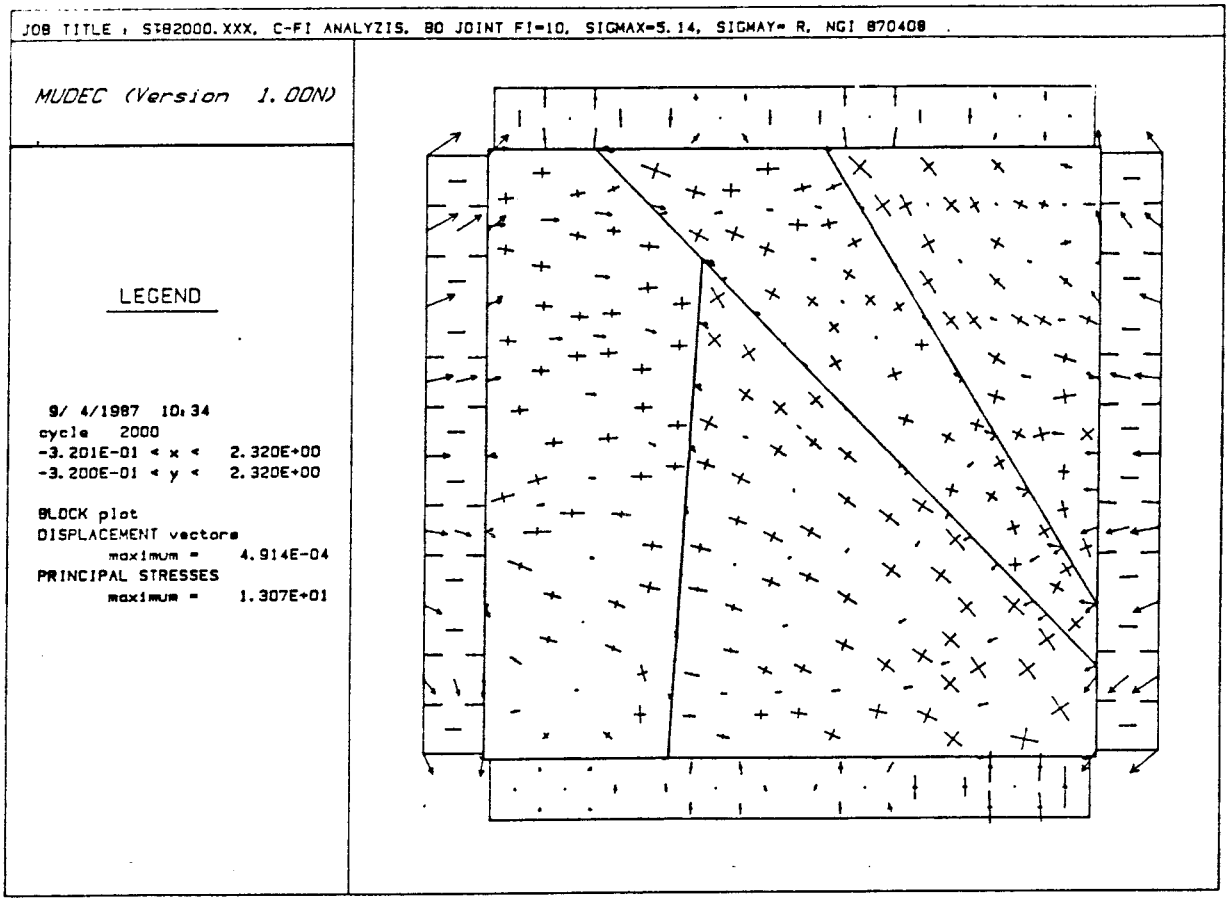

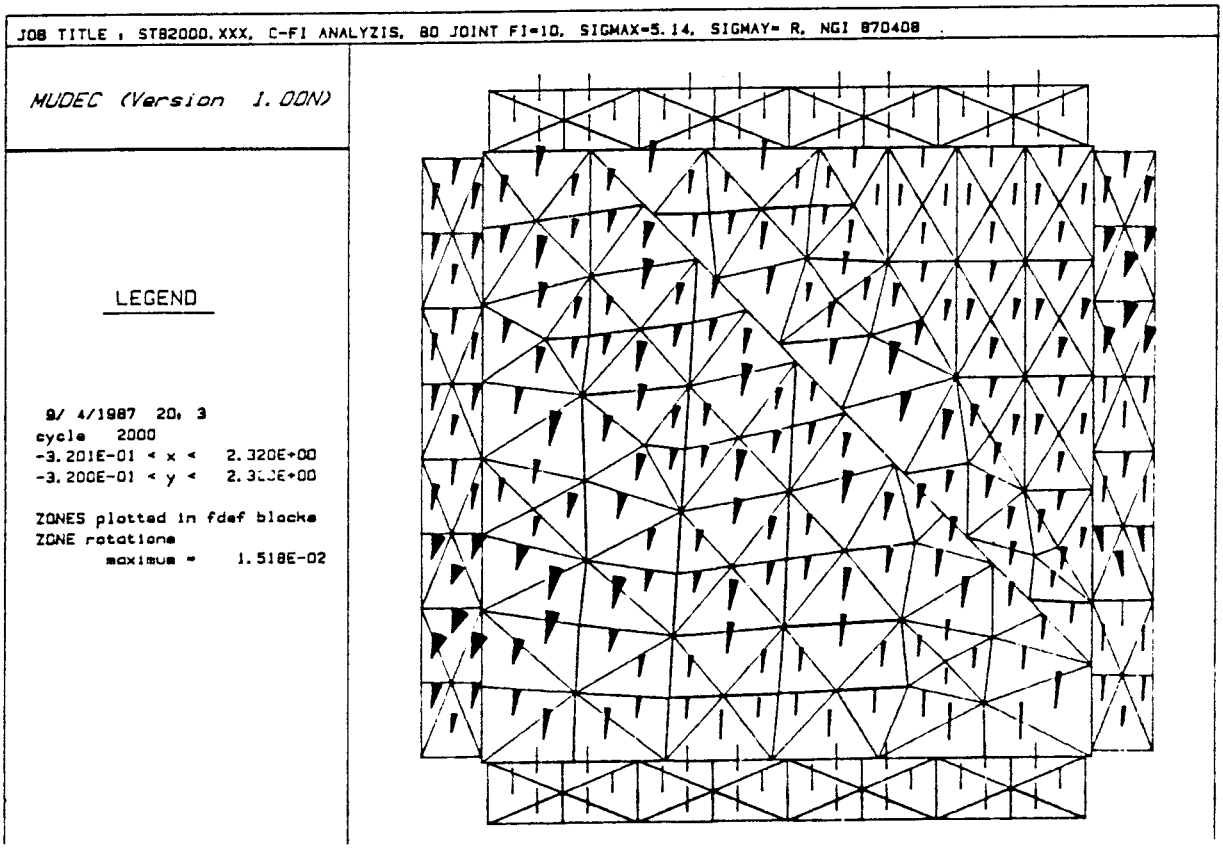

Fig. 3.1 E-W uniaxial loading. Displacement vectors and principal stresses plot. Zone rotation plot.

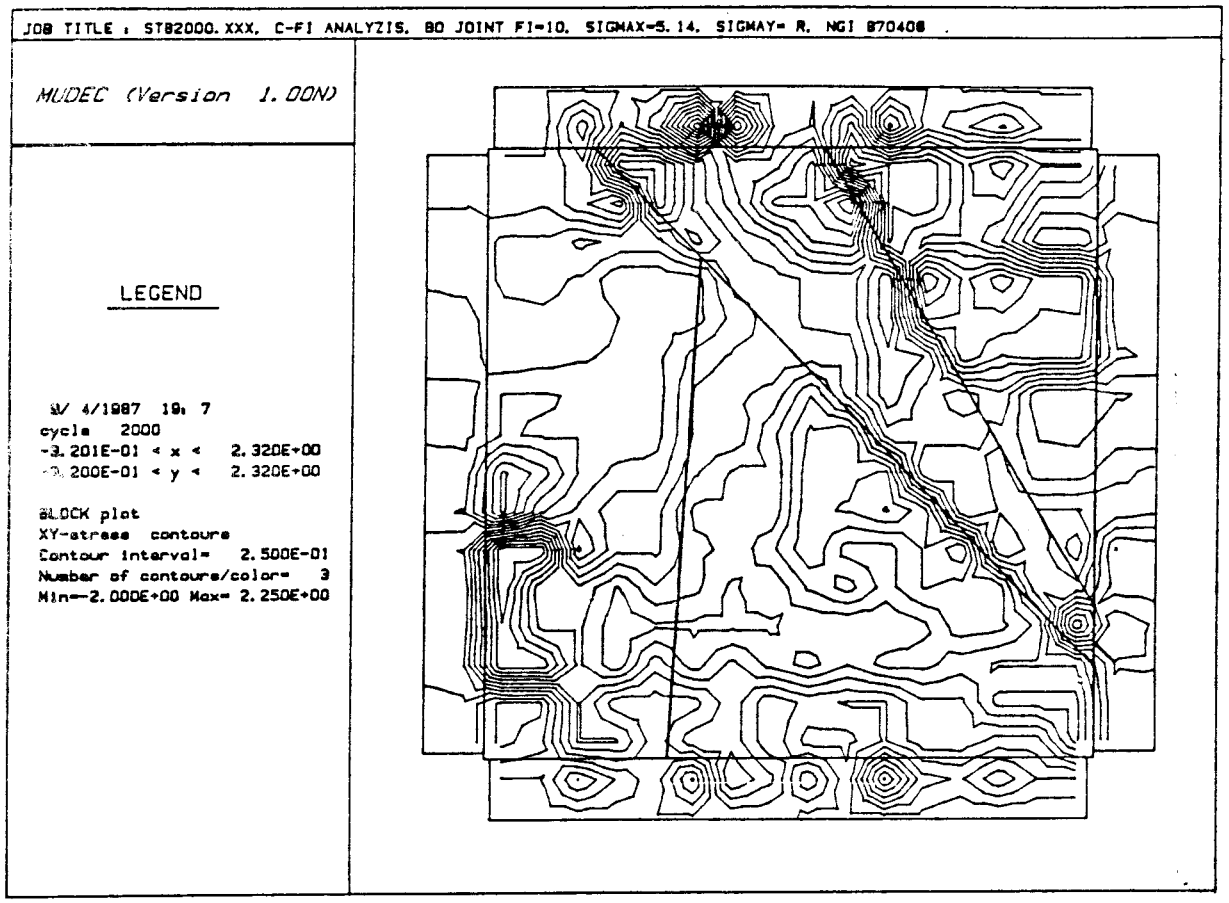

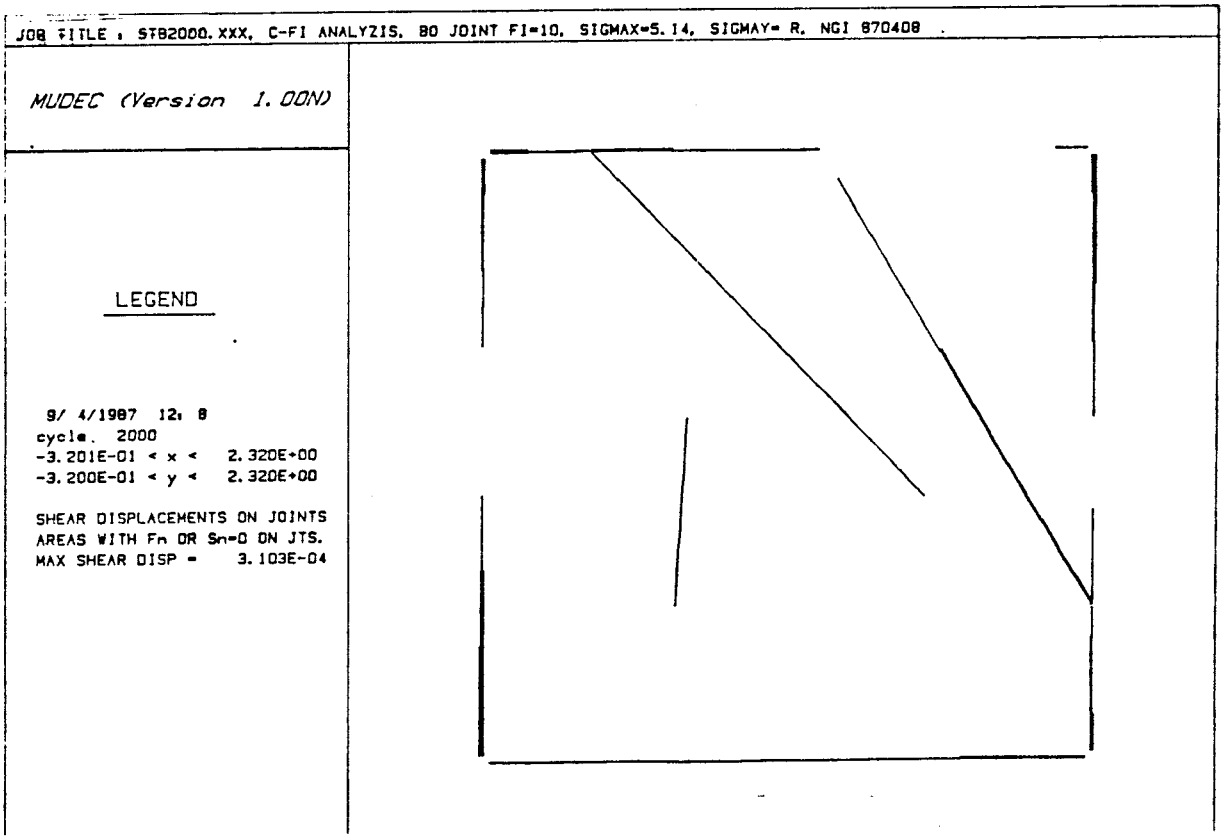

Fig. 3.2 E-W uniaxial loading. Shear stresses and shear displacement plots.

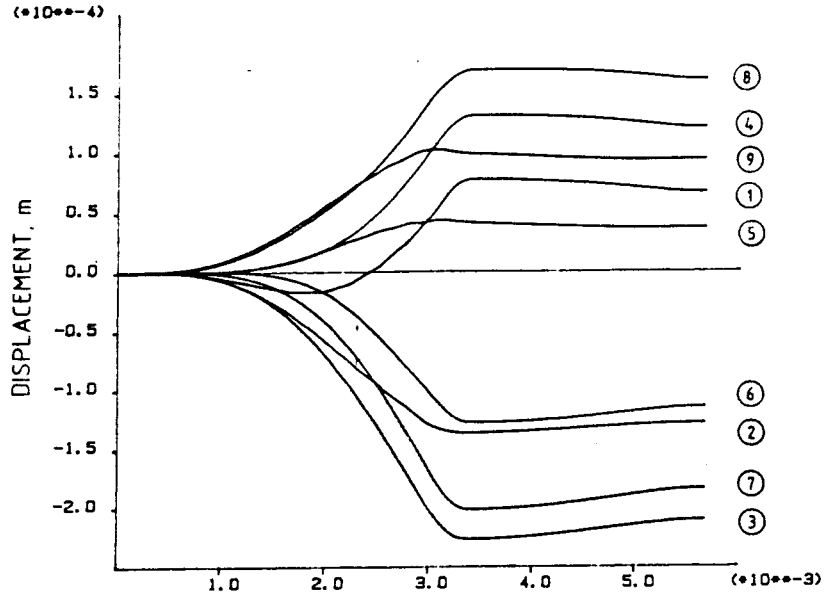

N - S direction displacement

N - S unaxial loading

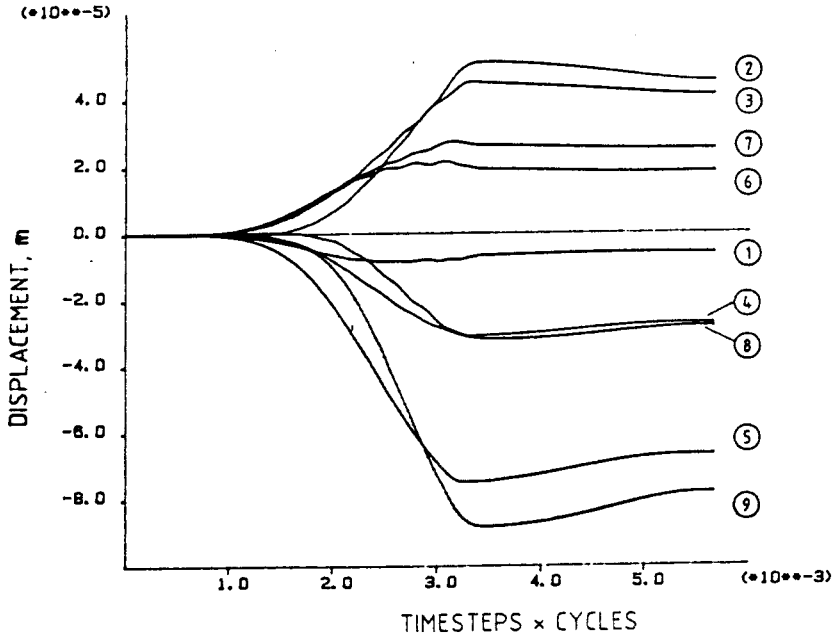

E - W direction displacement

N - S unaxial loading

Fig. 3.3 **E-W uniaxial loading. History plots of nine instrumented points. (See also Fig. 26.)**

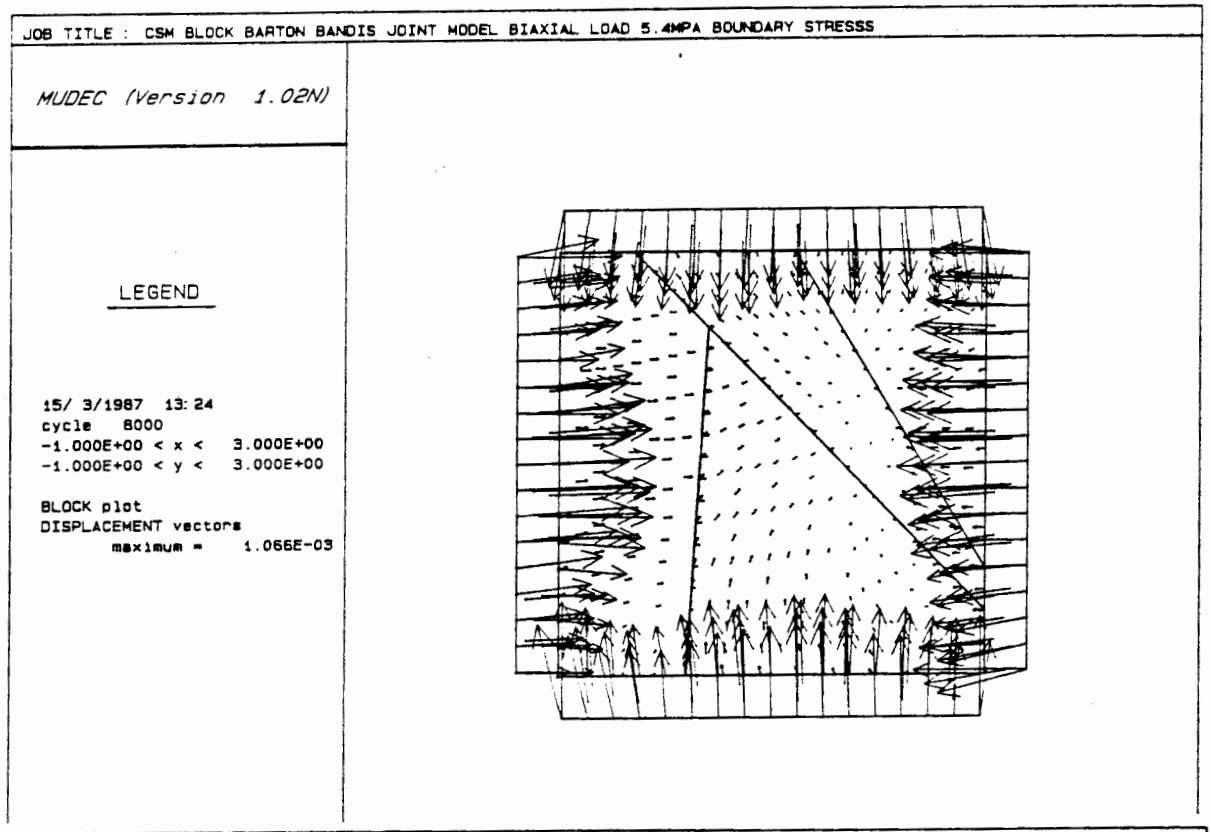

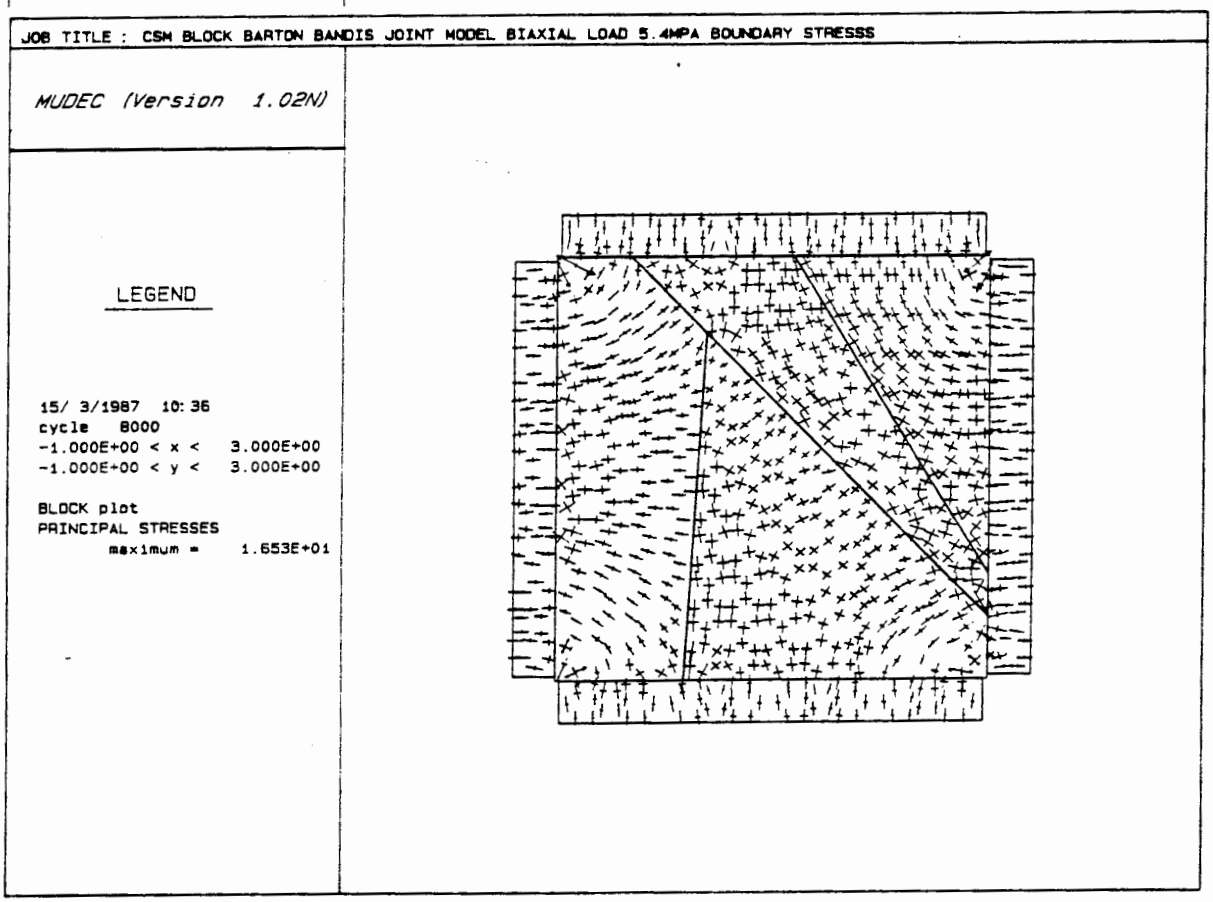

Fig 4.1 Biaxial Loading. Stress boundaries with Barton-Bandis joint model. Displacement vectors and principal stresses plots.

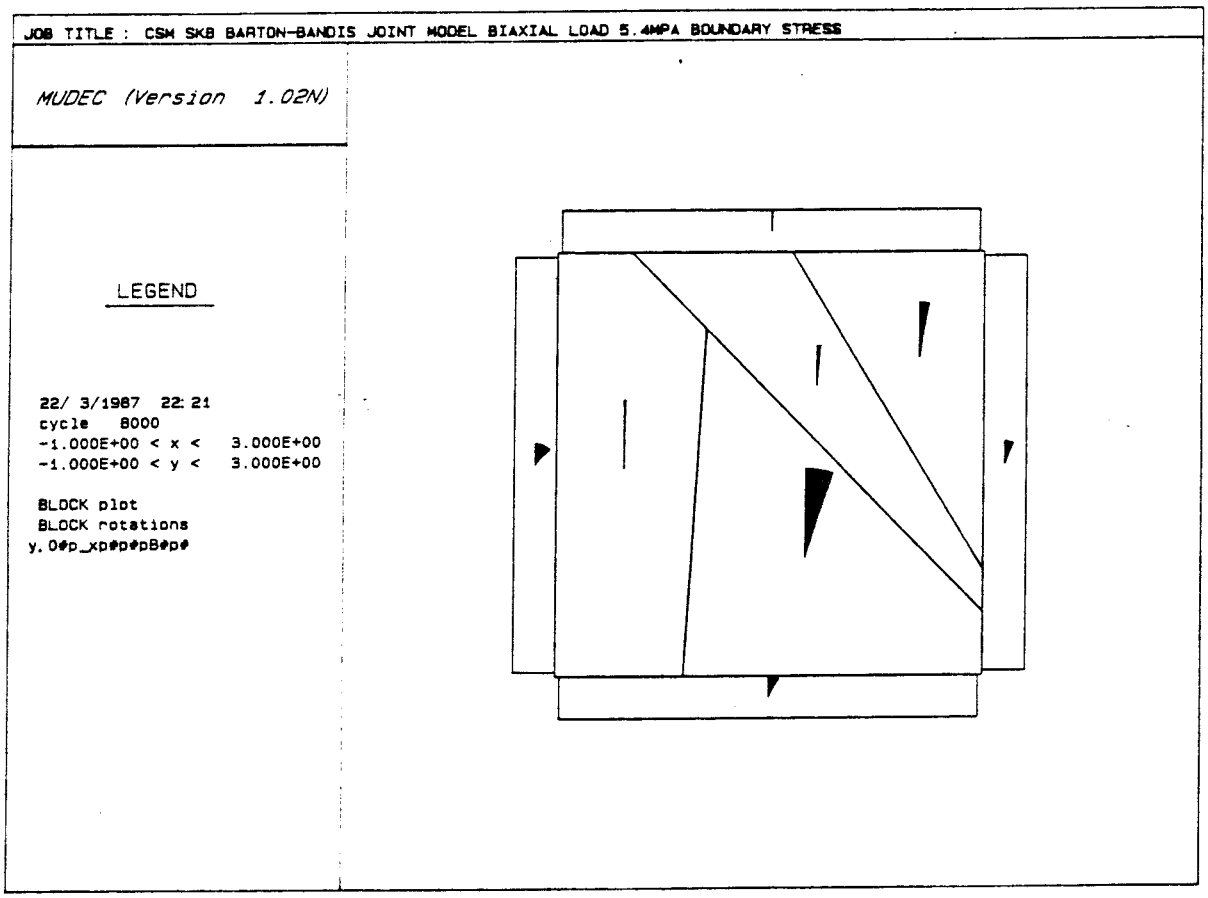

Fig 4.2. Biaxial Loading. Stress boundaries with Barton-Bandis joint model Block rotation plot.

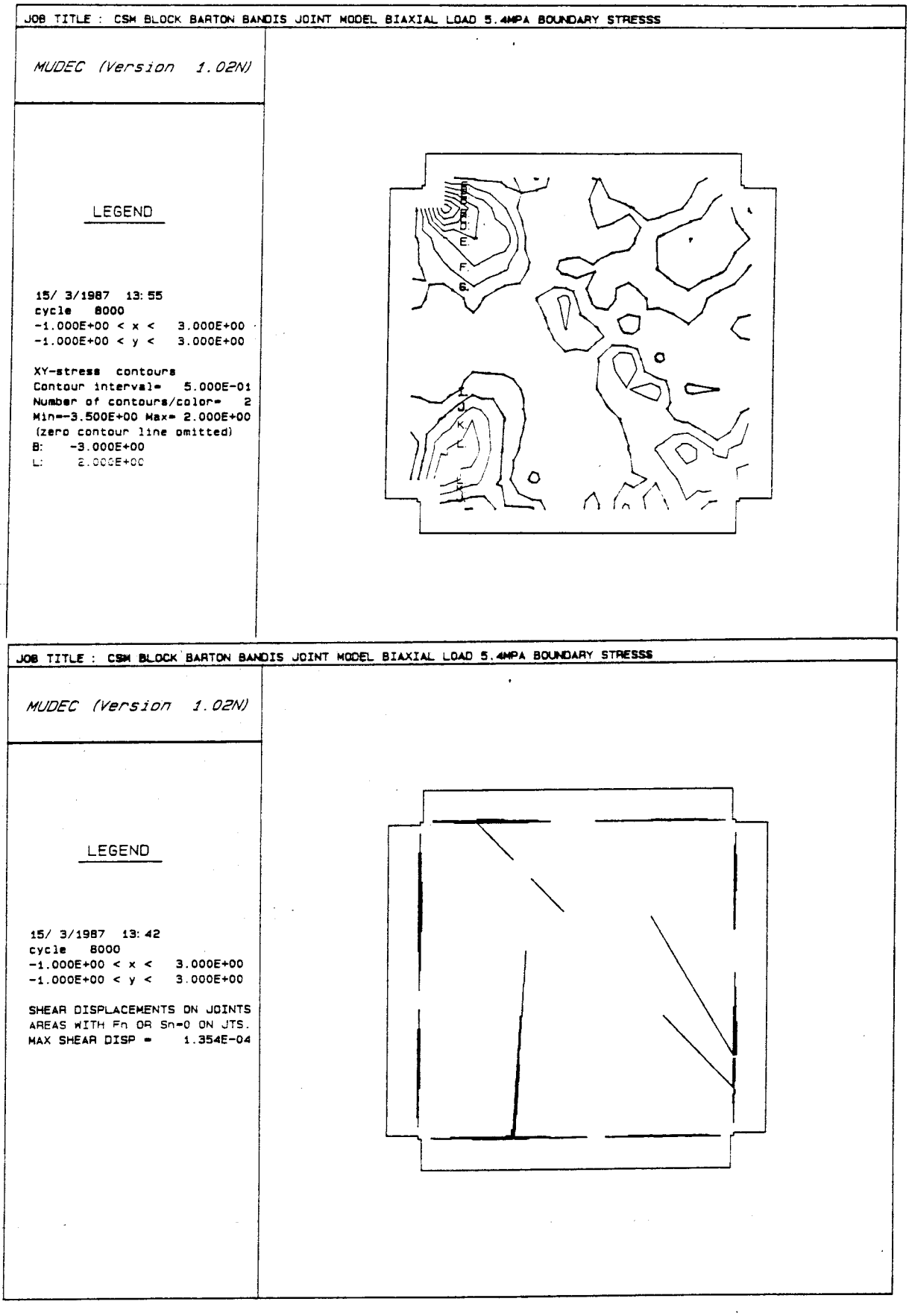

Fig.4.3. Biaxial Loading. Stress boundaries with Barton-Bandin joint model. Shear stresses and shear displacement plots.

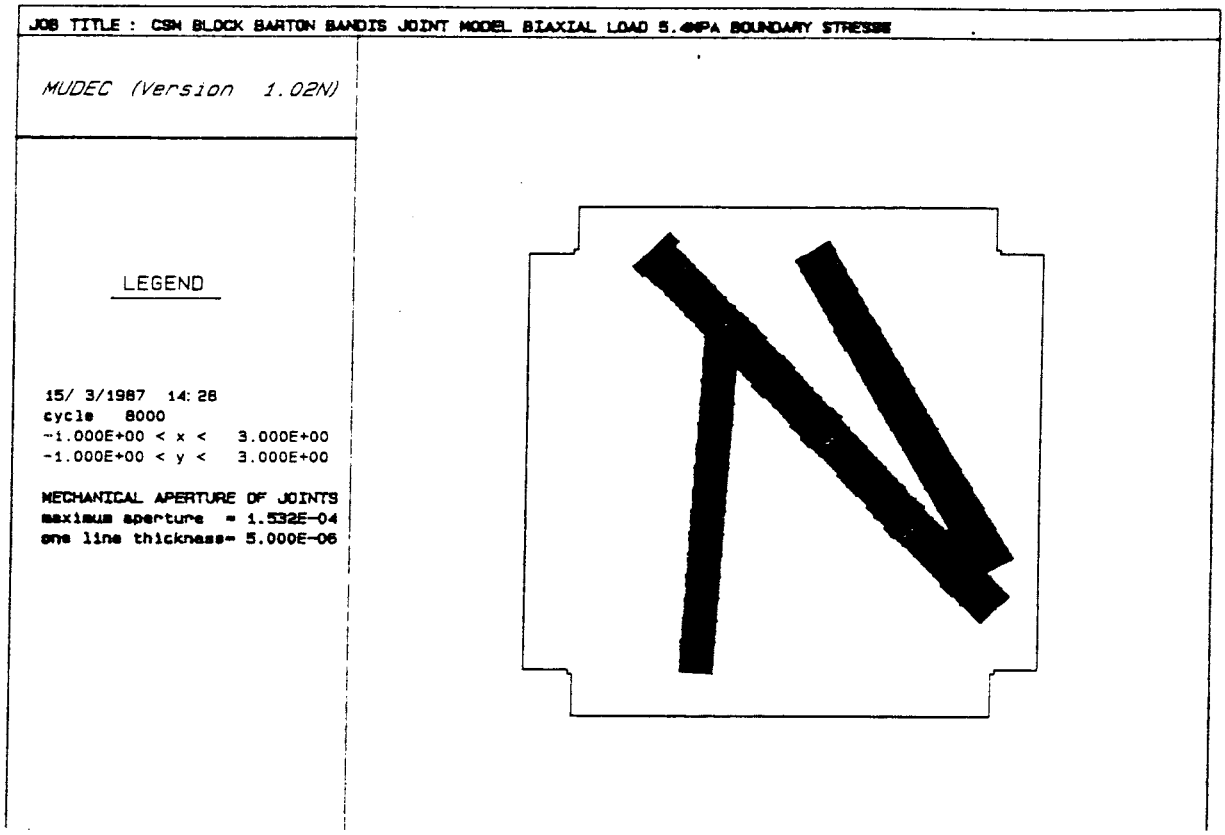

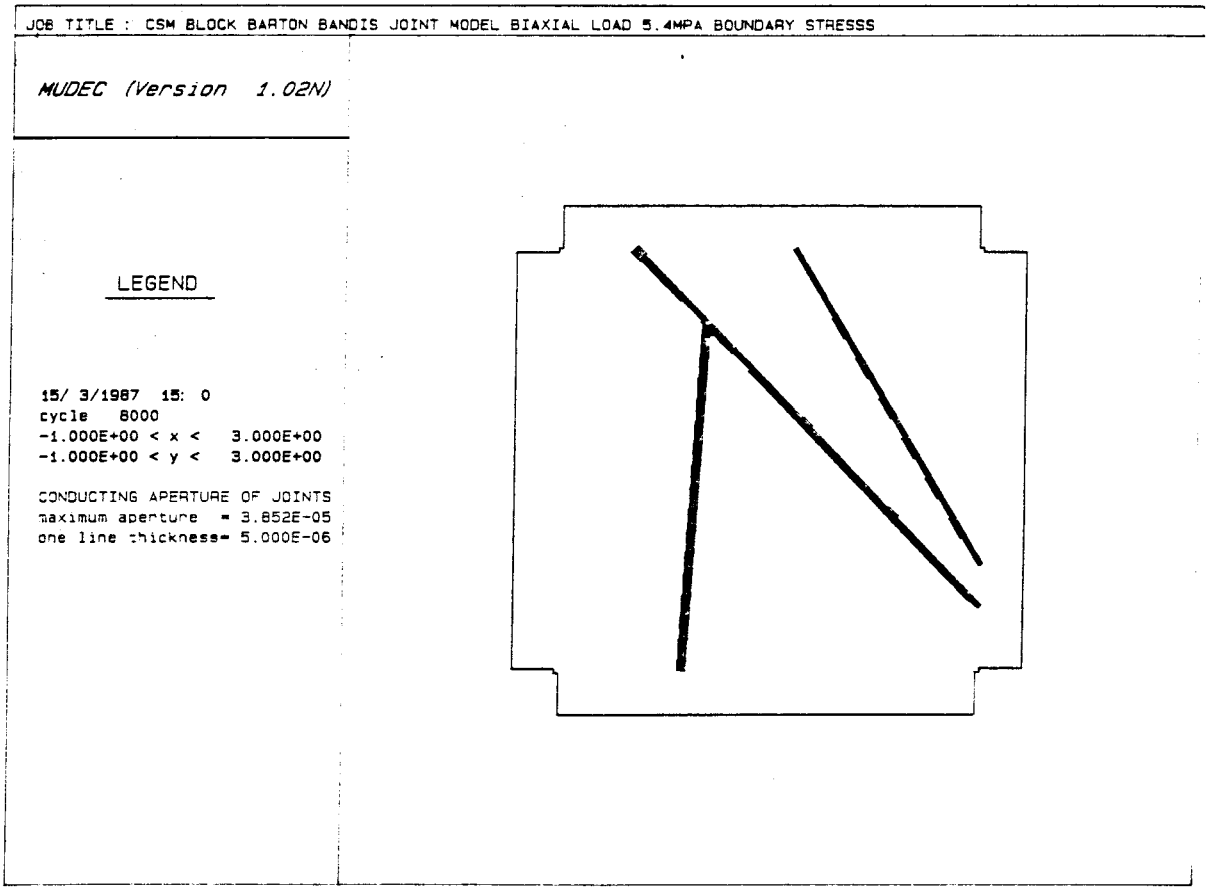

Fig.4.4. Biaxial Loading. Stress boundaries with Barton-Bandin joint model. Mechanical and conducting apertures of joint sets.

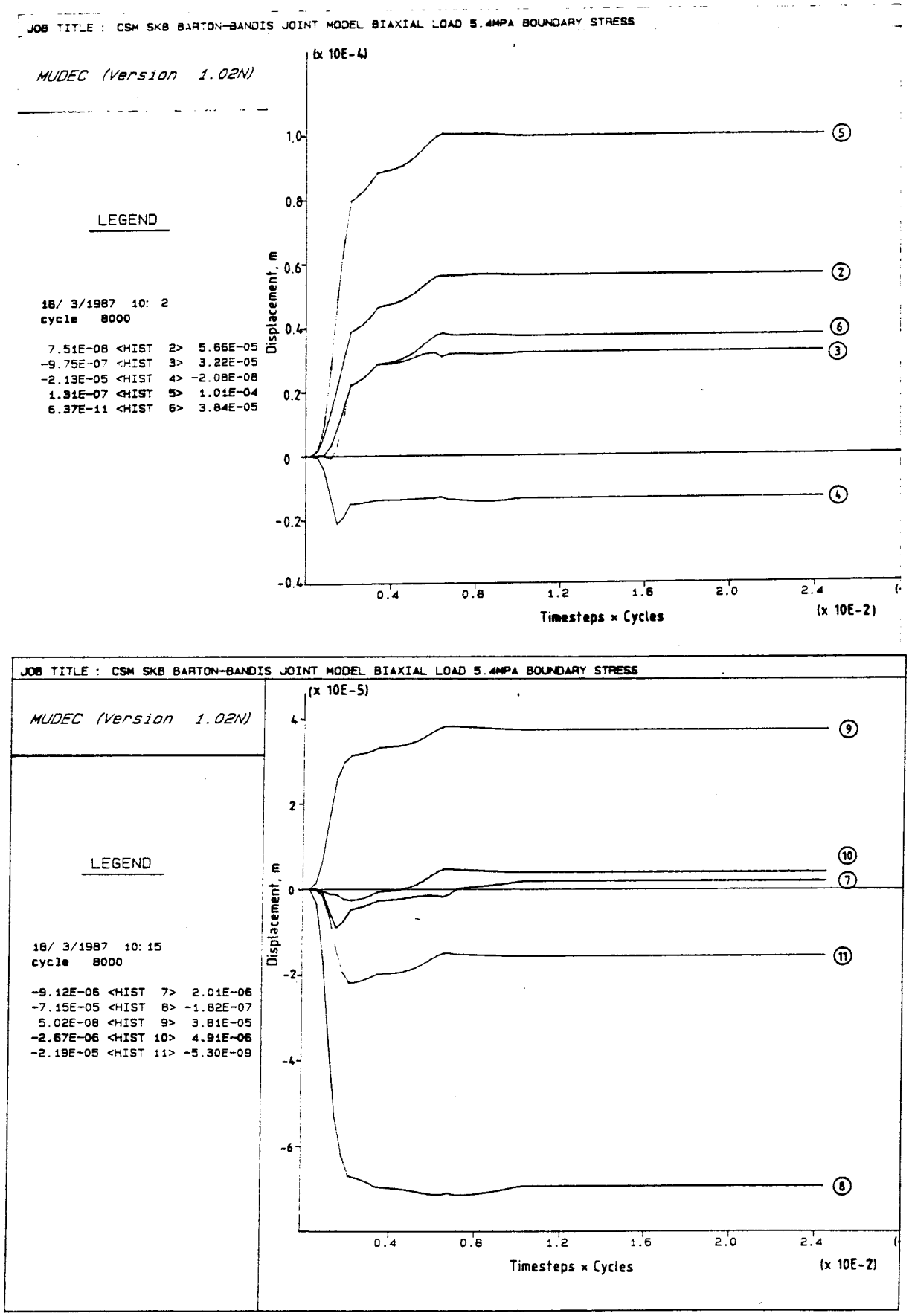

Fig.4.5. Biaxial Loading. Stress boundaries with Barton-Bandis joint model. History plots of ten instruments points (x-direction).

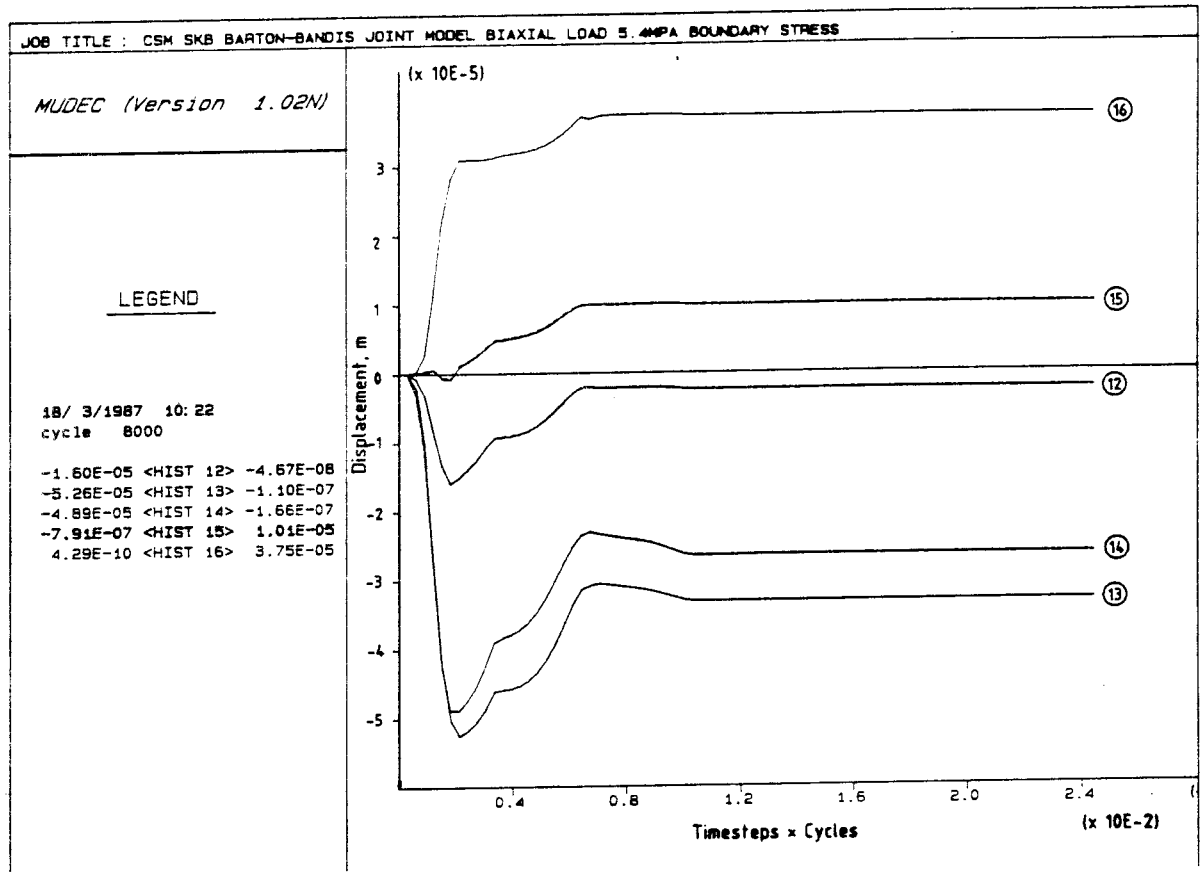

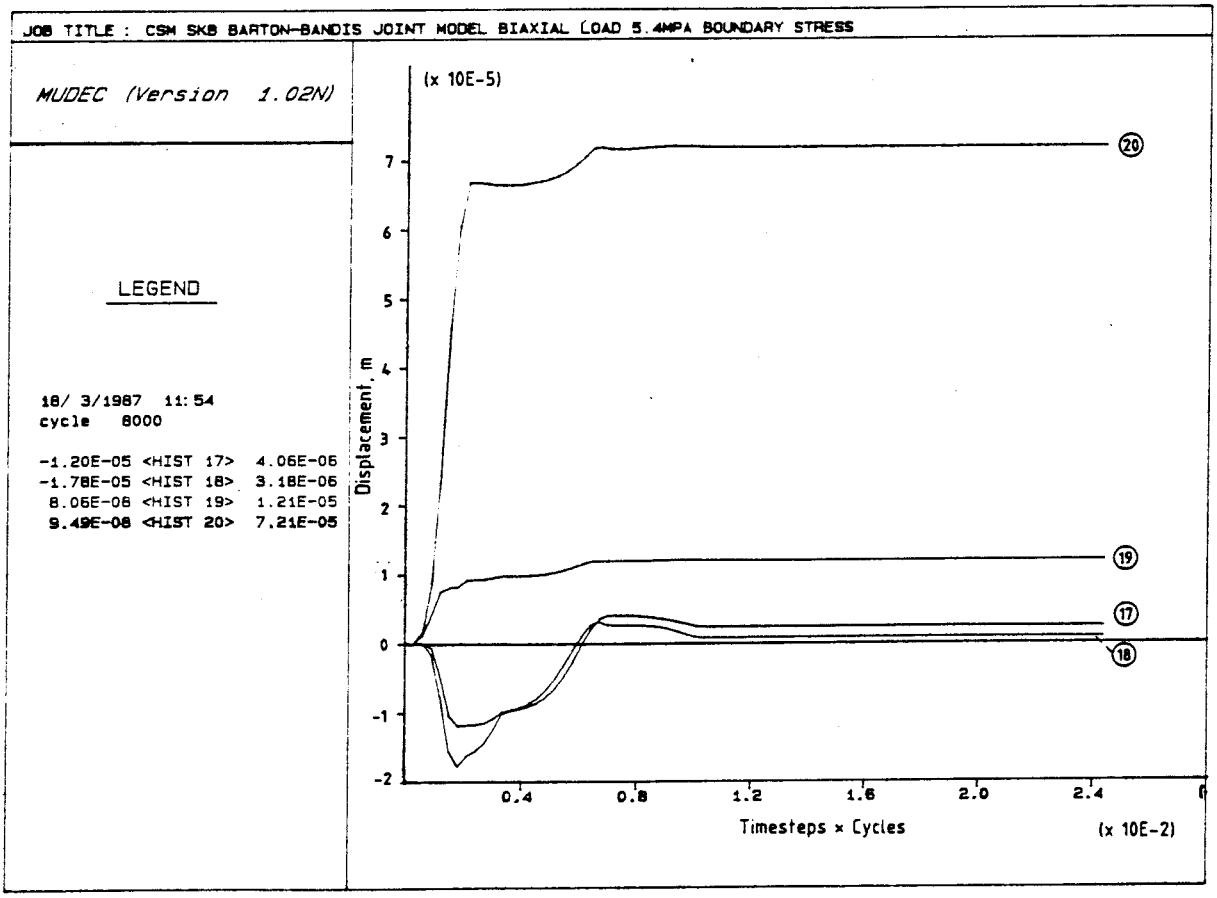

Fig.4.6. Biaxial Loading. Stress boundaries with Barton-Bandis joint model. History plots of nine instruments points (y-direction).

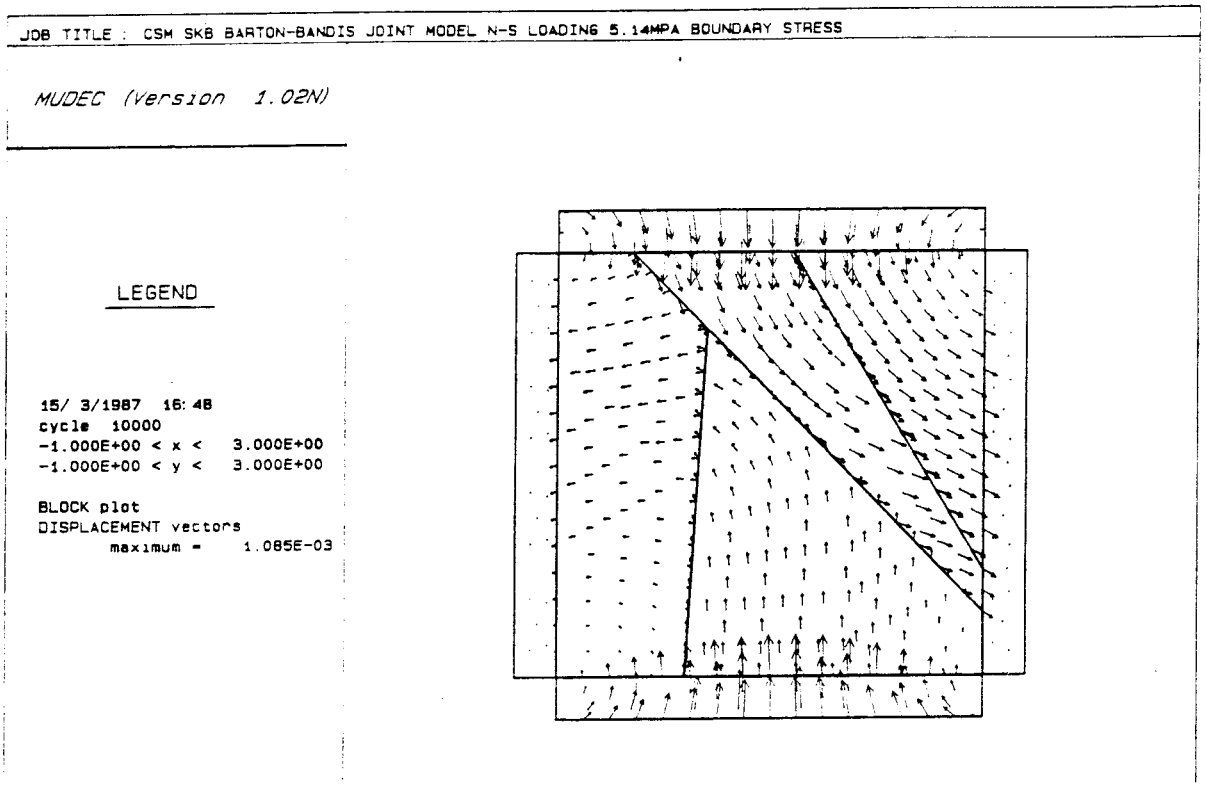

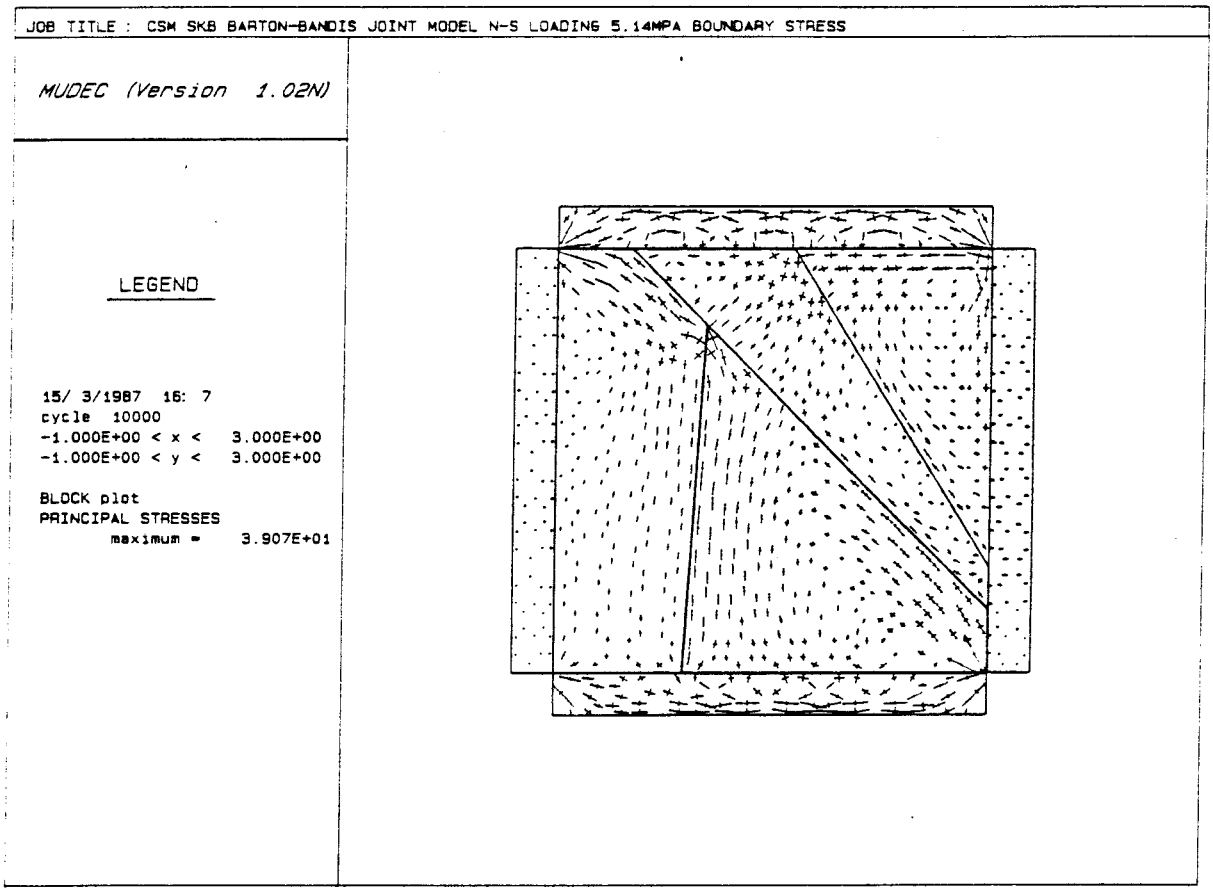

Fig.5.1. N-S Uniaxial Loading. Stress boundaries with Barton-Bandis joint model. Displacement vectors and principal stresses plots.

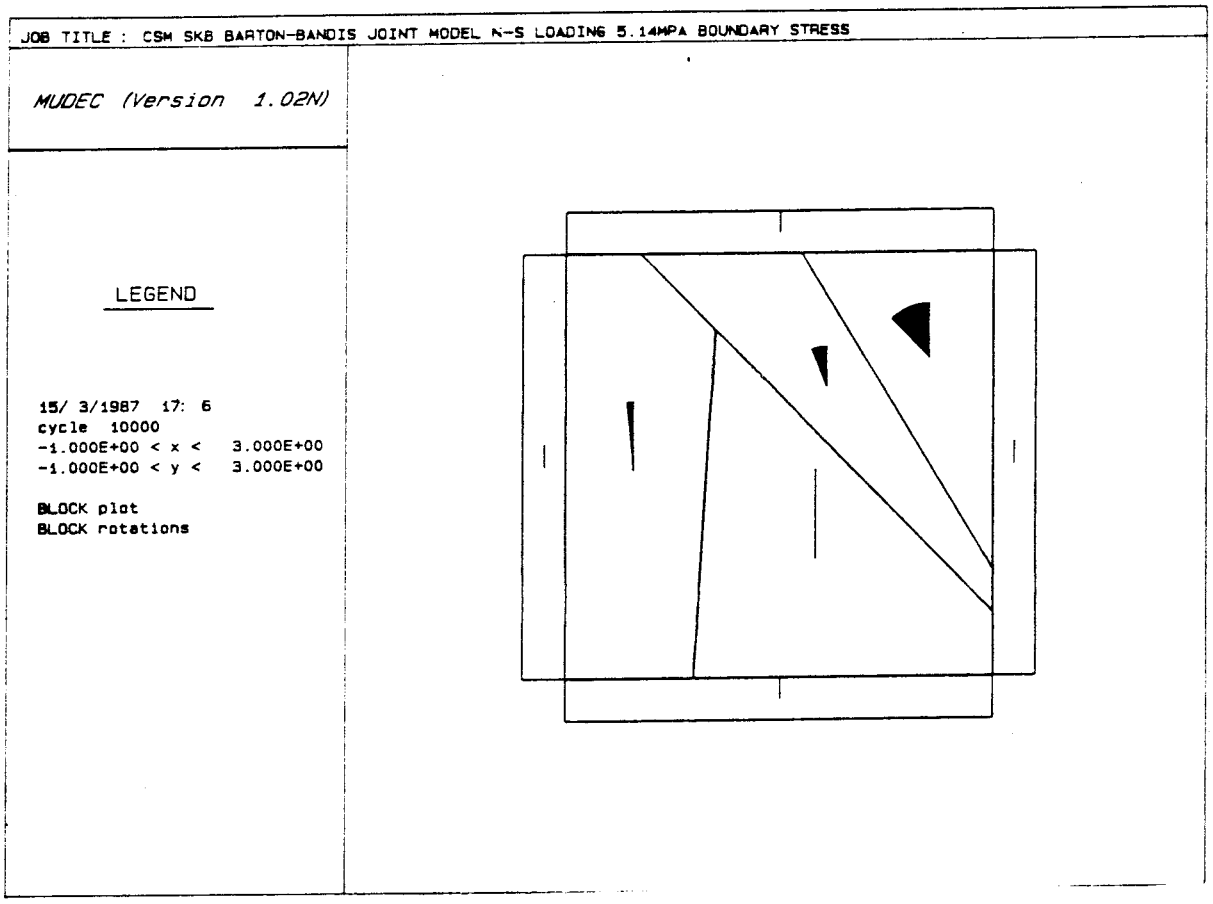

Fig.5.2. N-S Uniaxial Loading. Stress boundaries with Barton-Bandis joint model Block rotation plot.

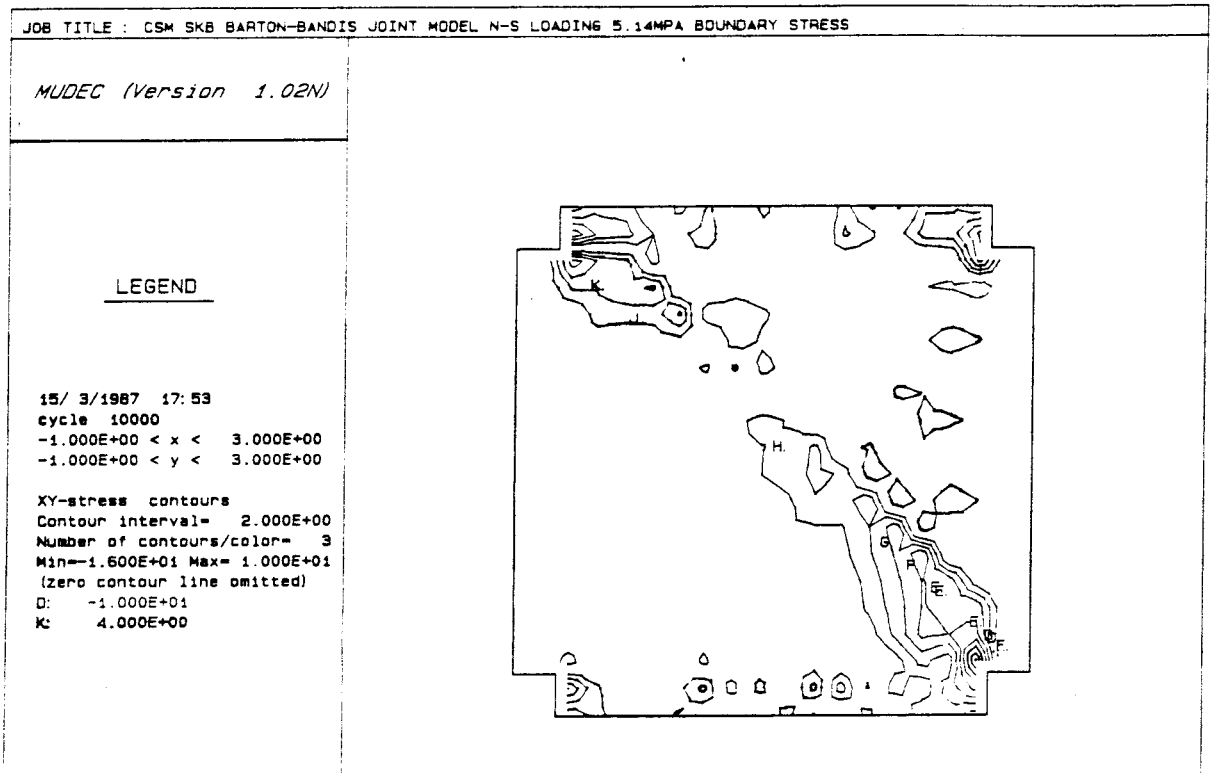

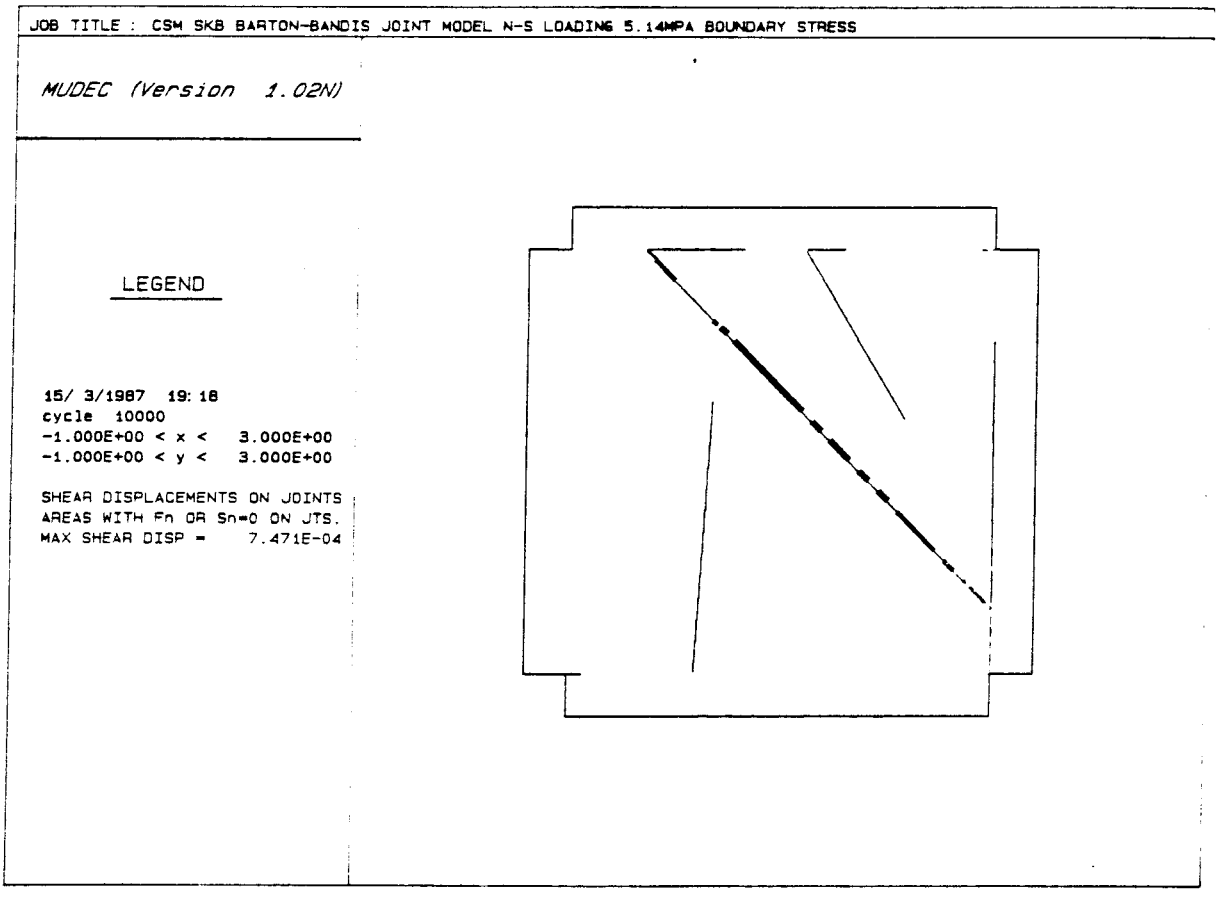

Fig.5.3. N-S Uniaxial Loading. Stress boundaries with Barton-Bandis joint model. Shear stresses and shear displacement plots.

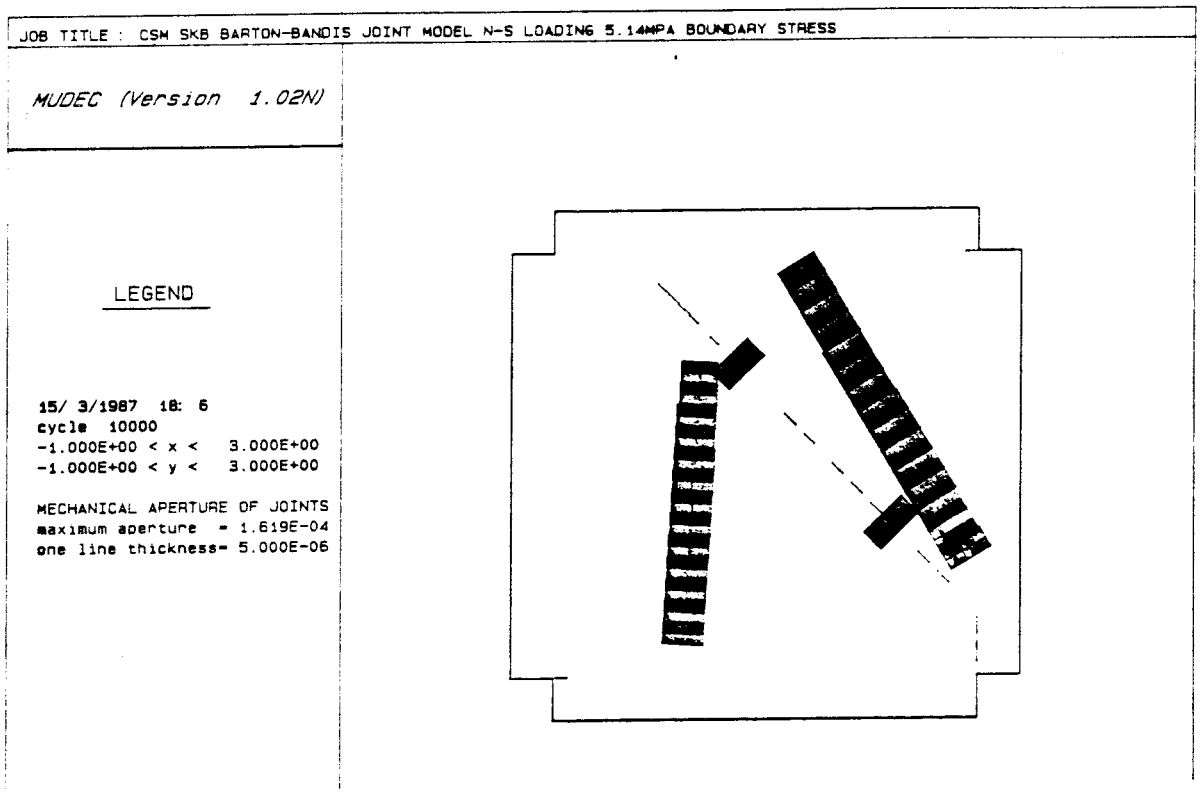

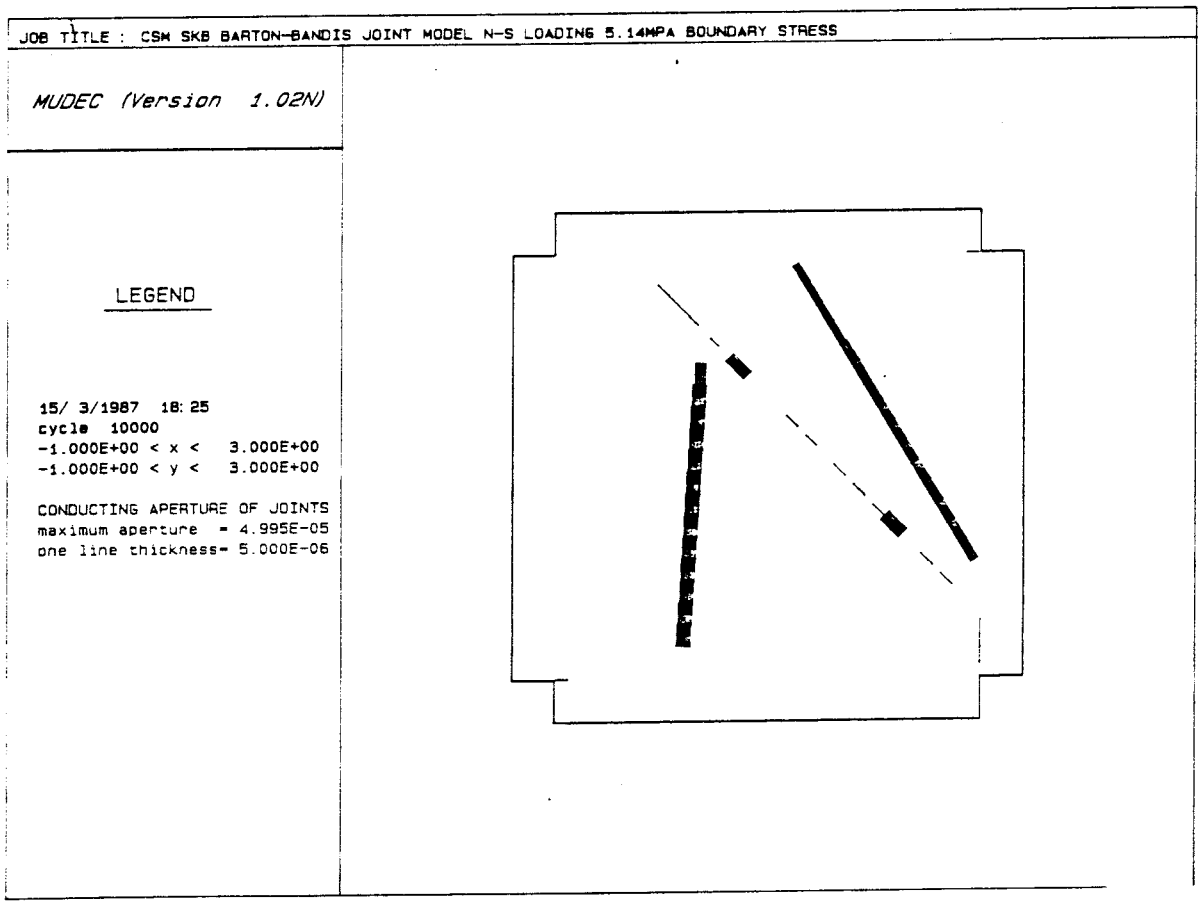

Fig.5.4. N-S Uniaxial Loading. Stress boundaries with Barton-Bandis joint model. Mechanical and conducting aperture of joint sets.

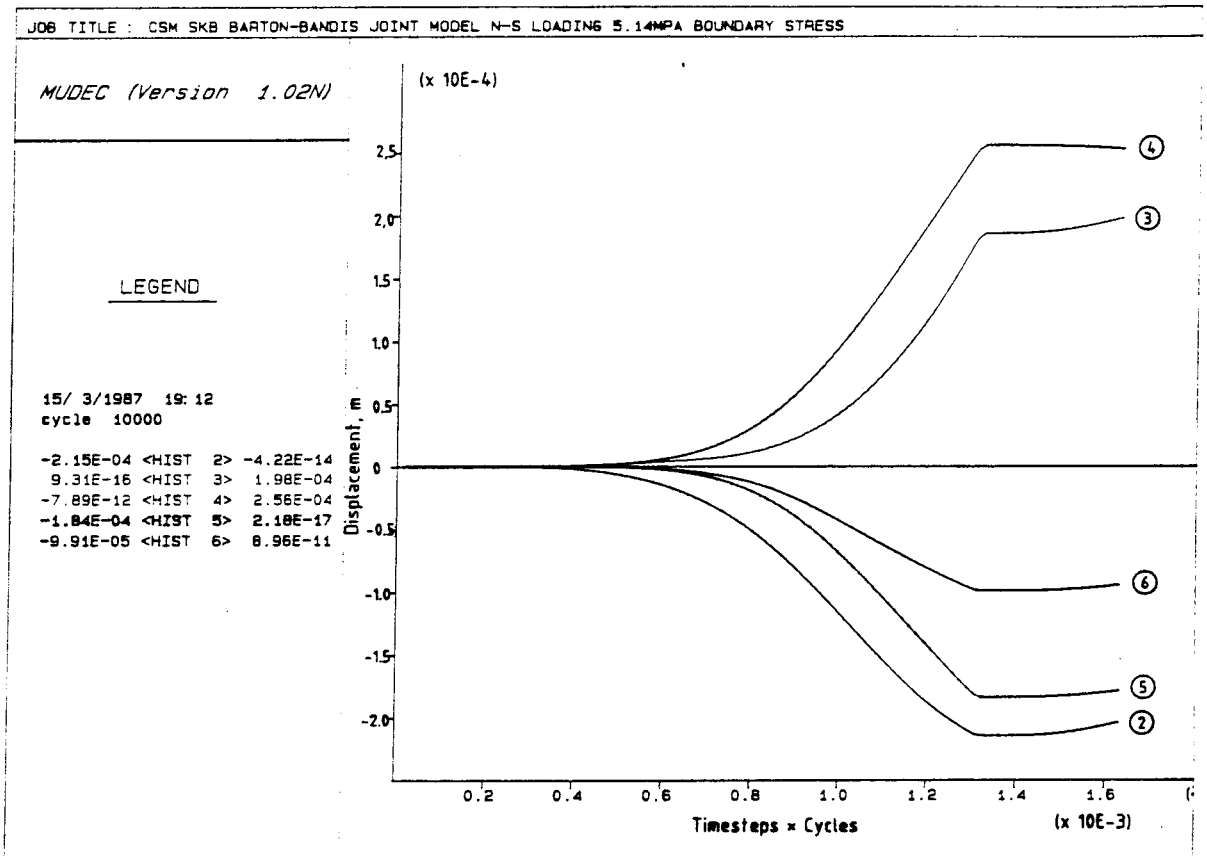

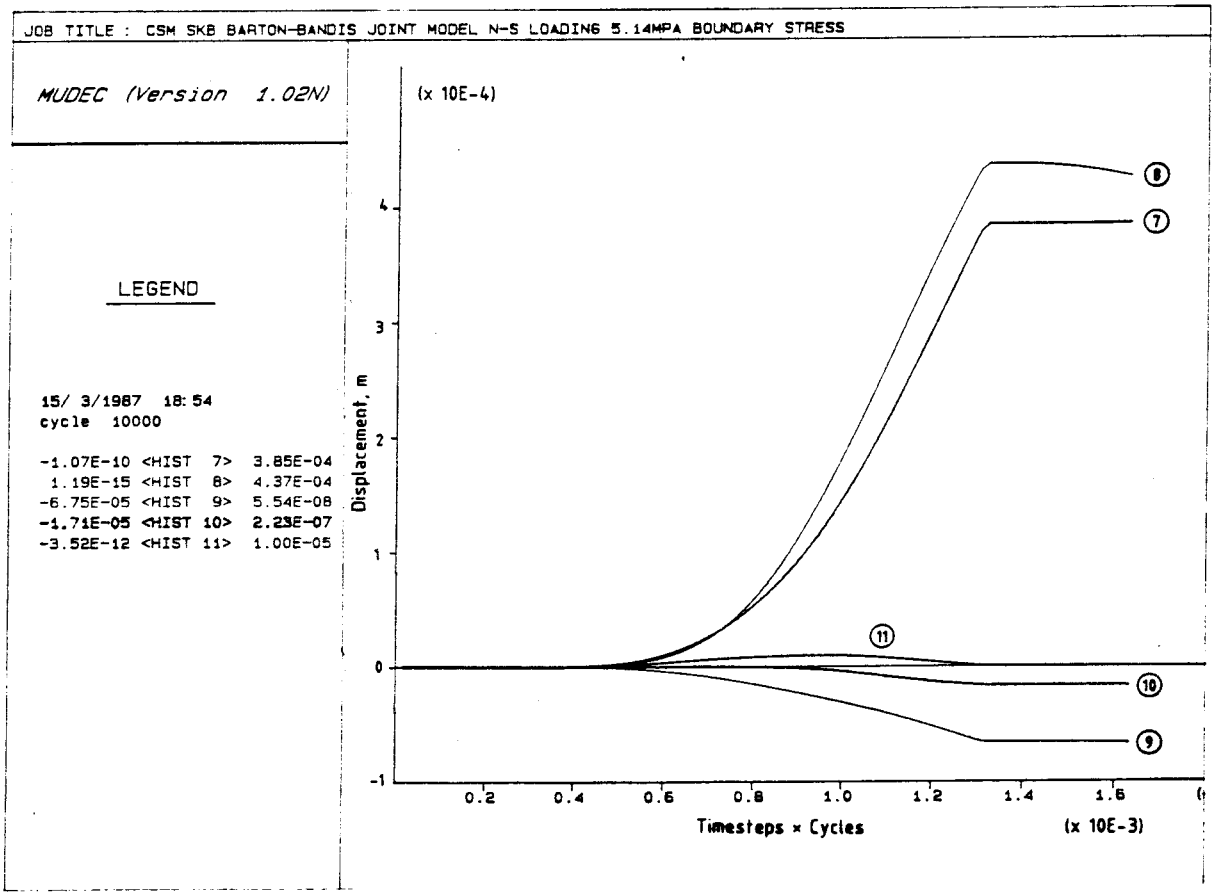

Fig.5.5. N-S Uniaxial Loading. Stress boundaries with Barton-Bandis joint model. History plots of ten instrumented points (x-direction).

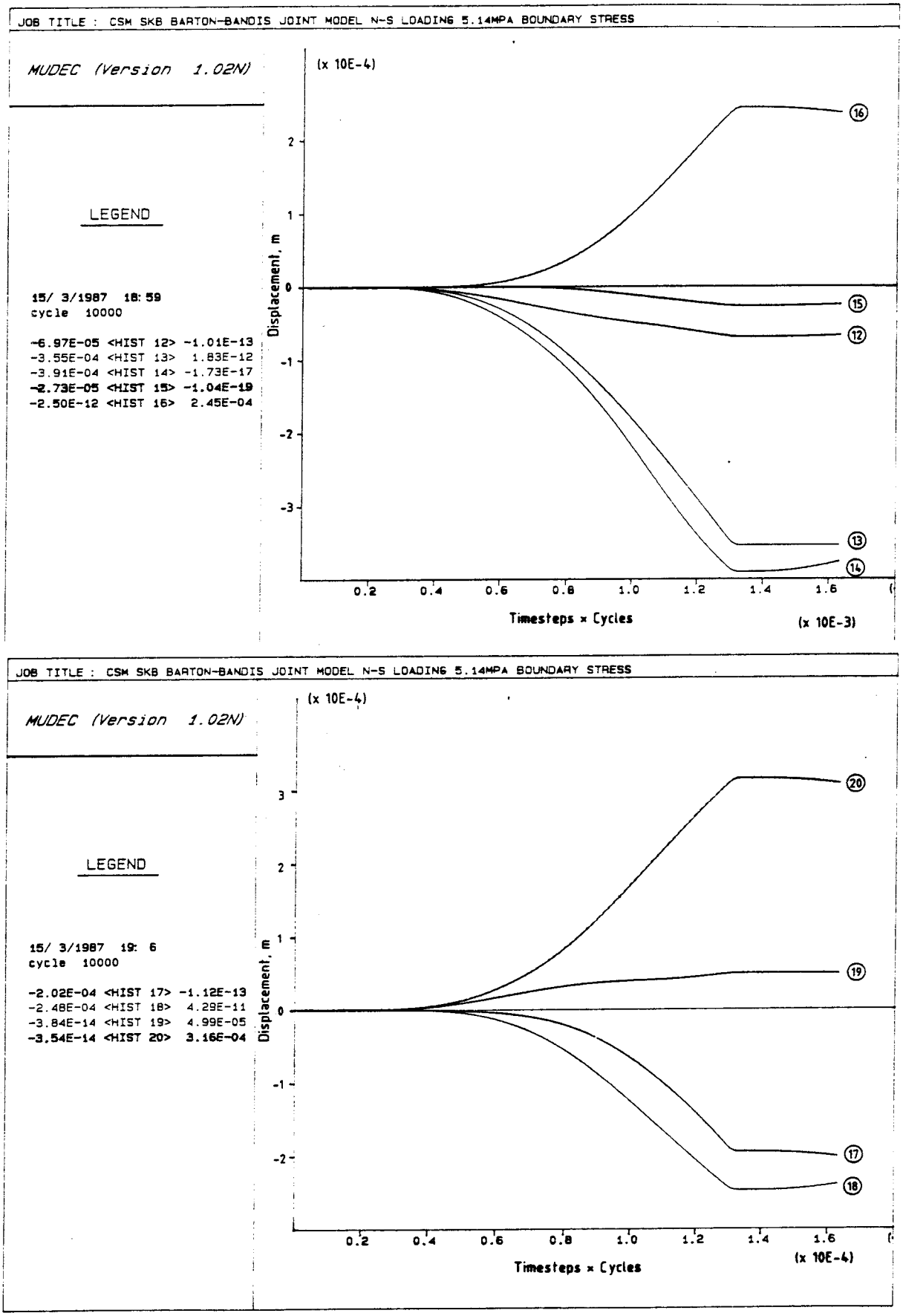

Fig.5.6. N-S Uniaxial Loading. Stress boundaries with Barton-Bandis joint model. History plots of nine instrumented point (y-direction).

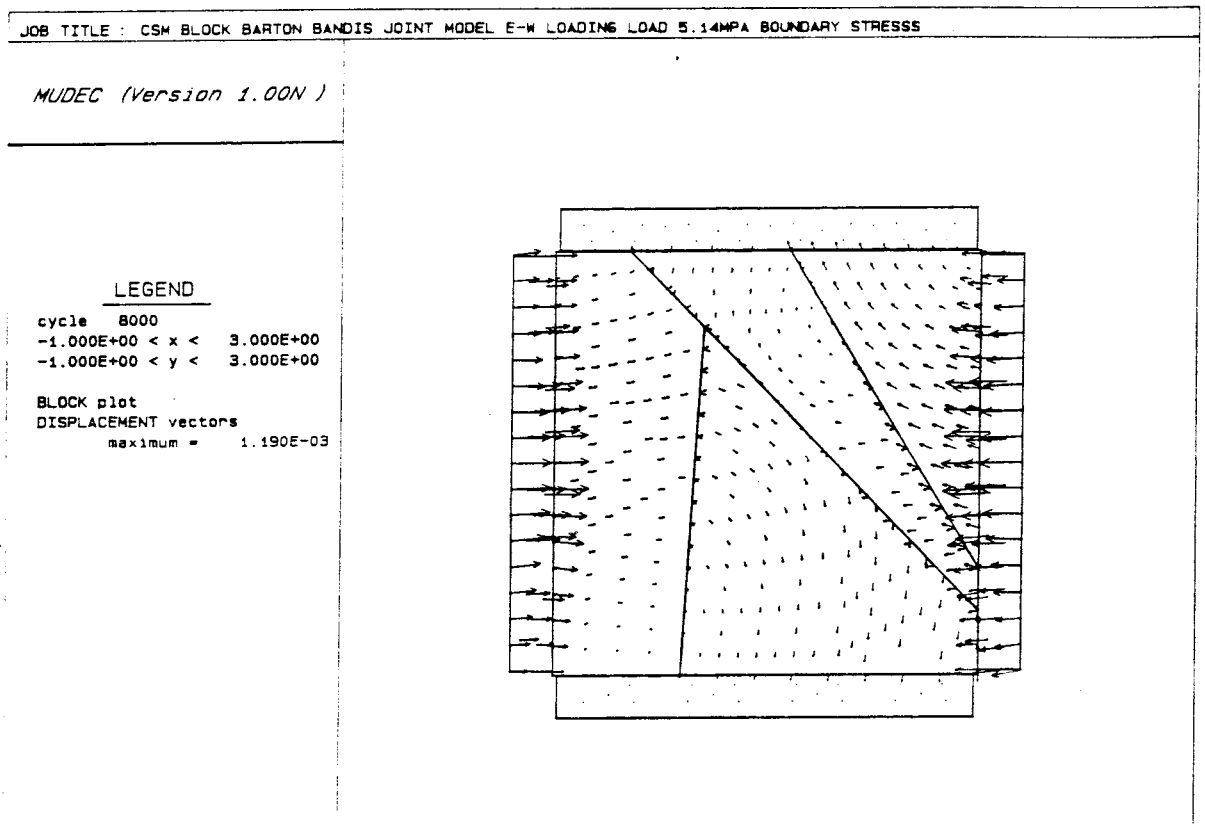

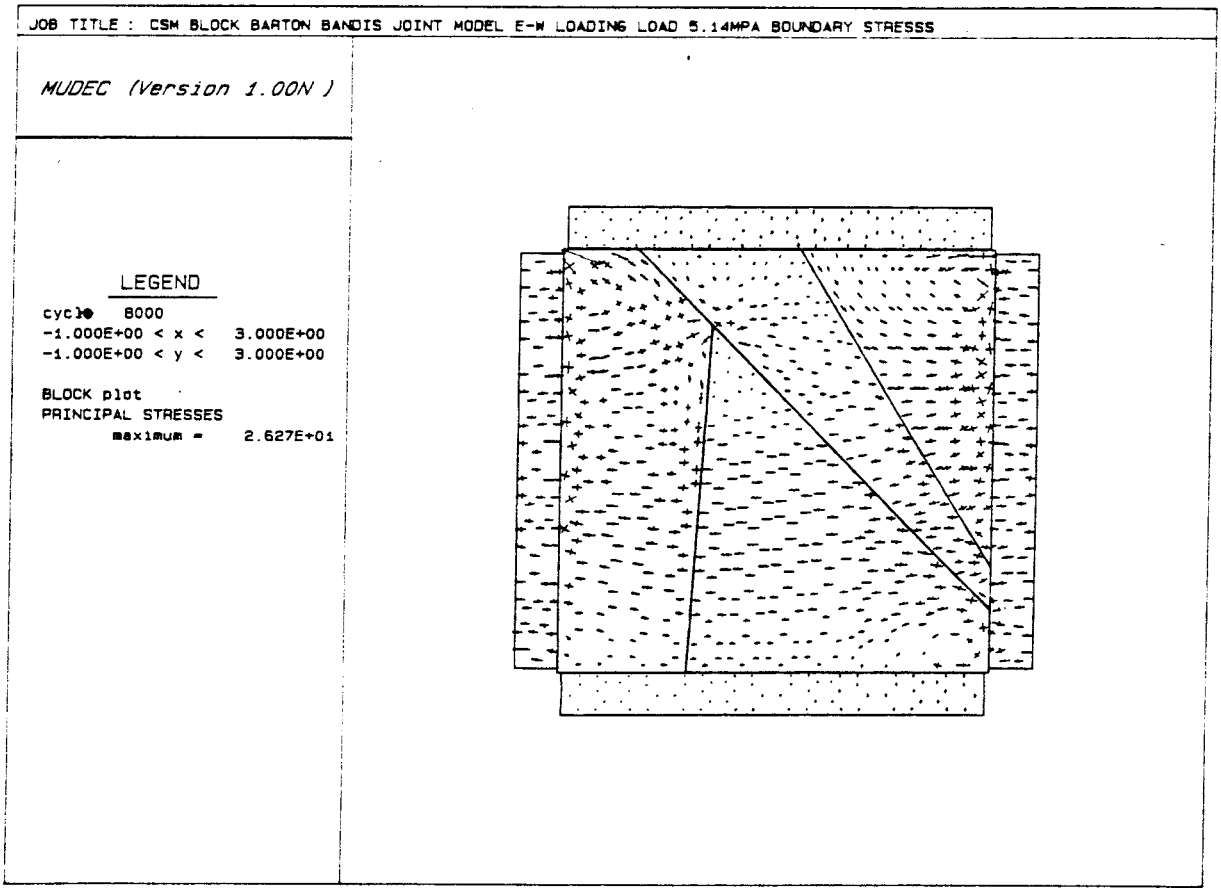

Fig.6.1. E-W Uniaxial Loading. Stress boundaries with Barton-Bandis joint model. Displacement vectors and principial stresses plots.

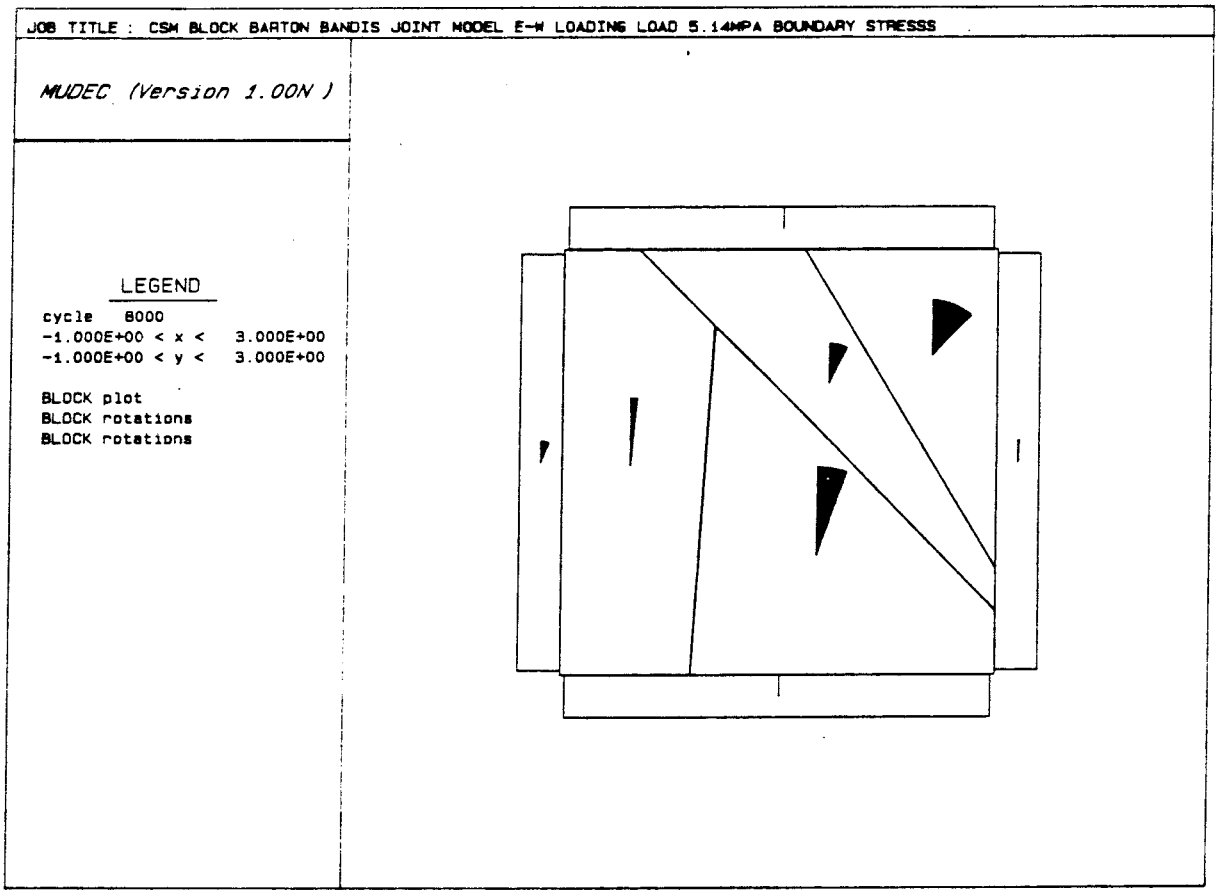

Fig.6.2. E-W Uniaxial Loading. Stress boundaries with Barton-Bandis joint model. Block rotation plot.

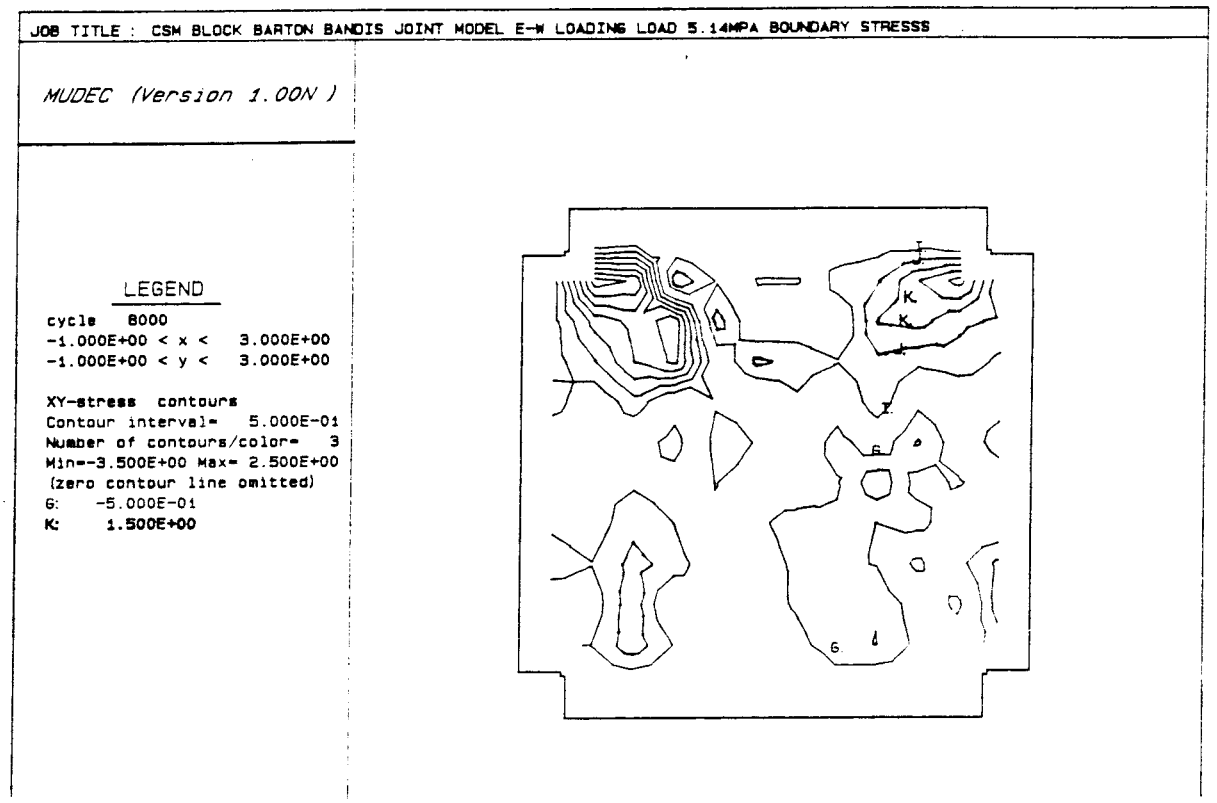

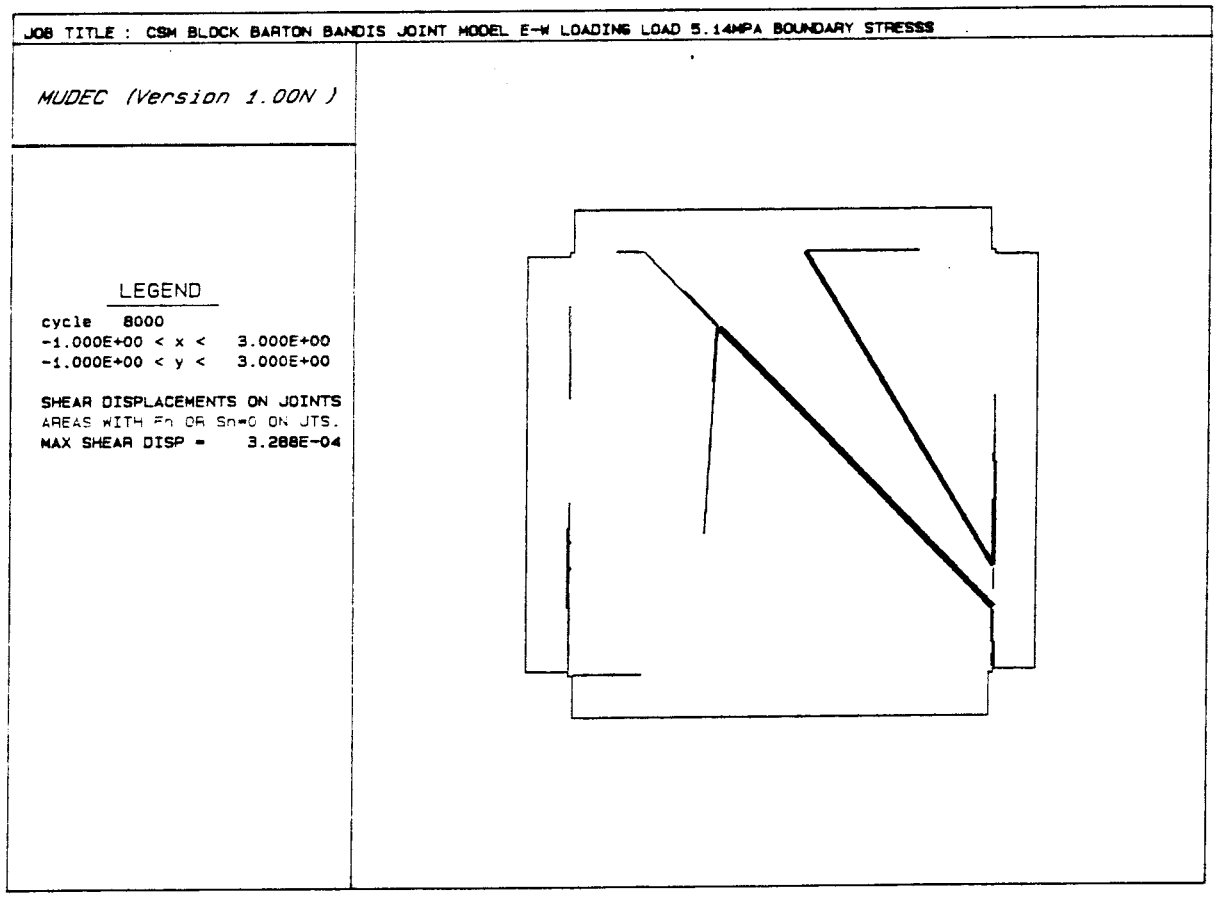

Fig.6.3. E-W Uniaxial Loading. Stress boundaries with Barton-Bandis joint model. Shear stresses and shear displacement plots.

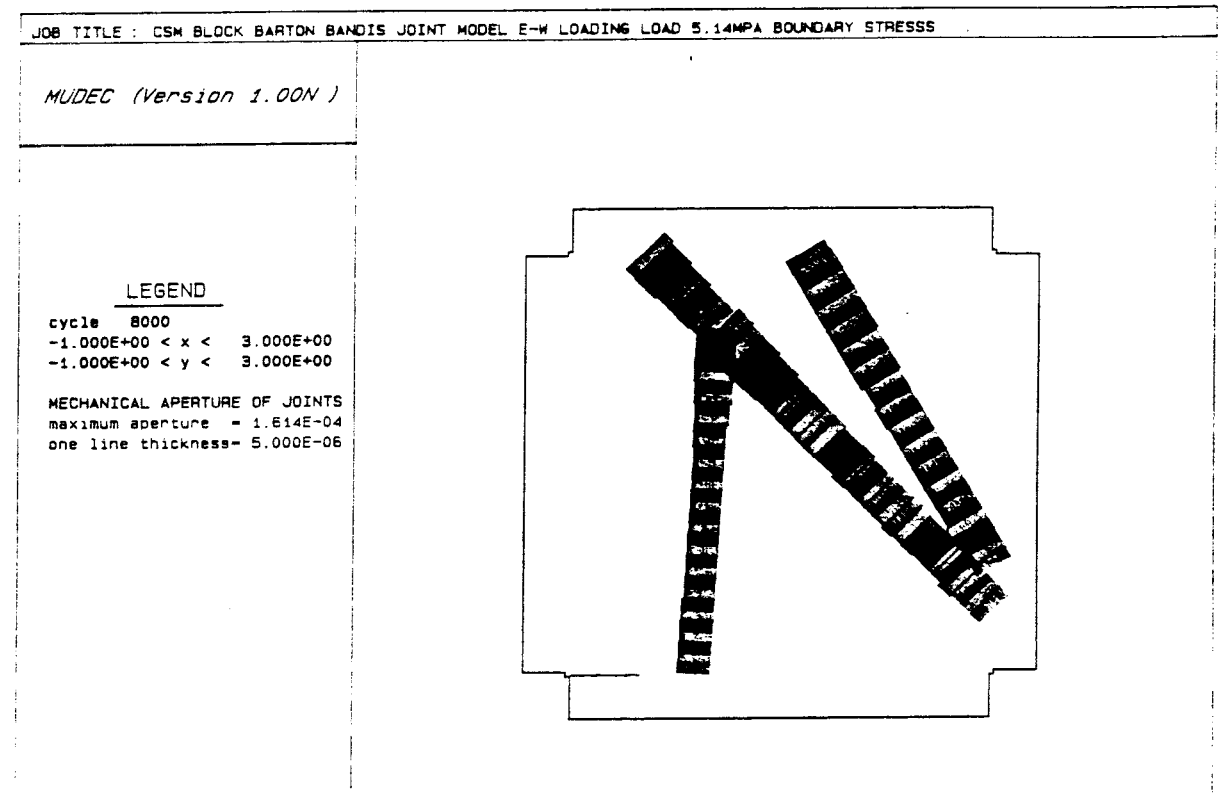

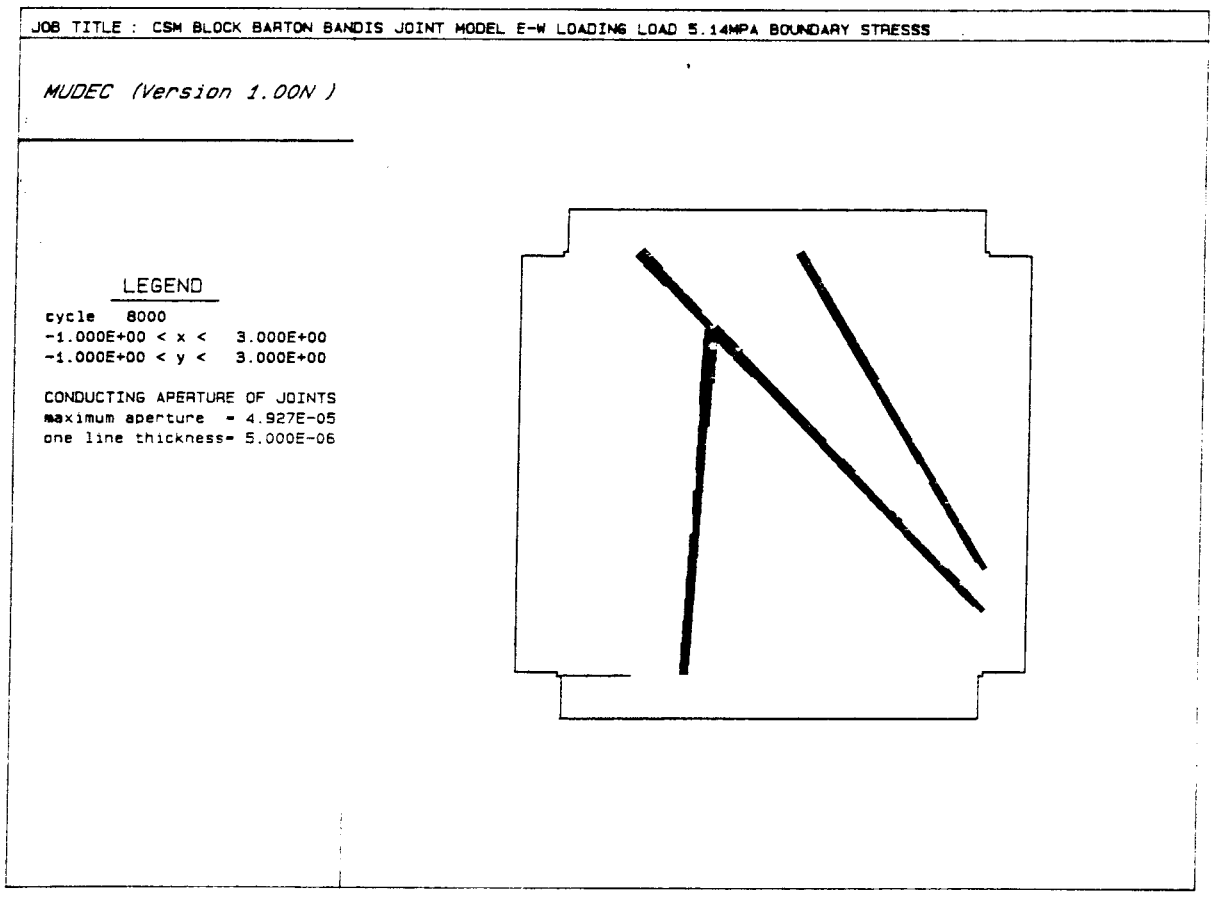

Fig.6.4. E-W Uniaxial Loading. Stress boundaries with Barton-Bandis joint model. Mechanical and conducting aperture of joint sets.

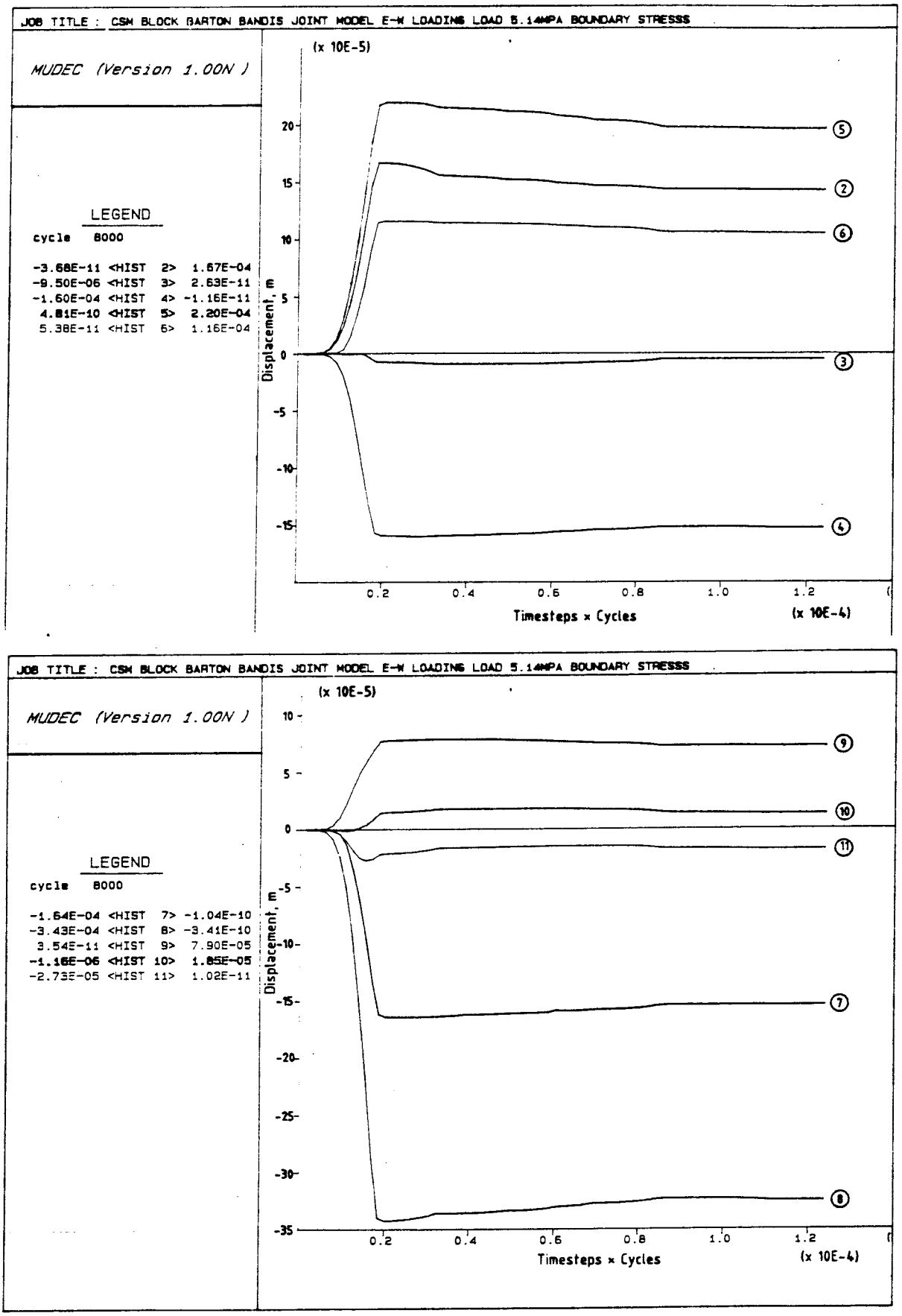

Fig.6.5. E-W Uniaxial Loading. Stress boundaries with Barton-Bandis joint model. History plots of ten instrument points (x-direction).

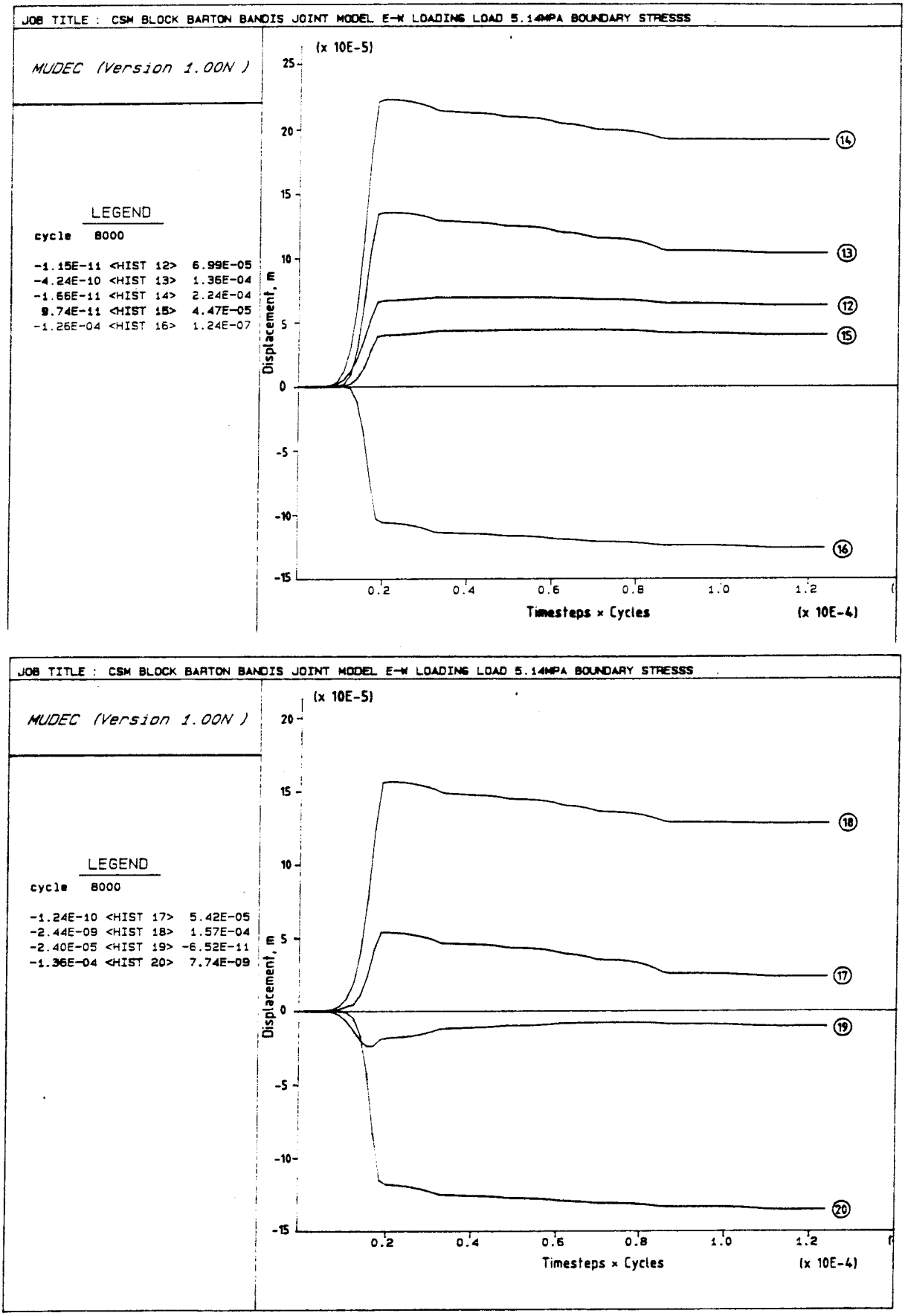

Fig.6.6. E-W Uniaxial Loading. Stress boundaries with Barton-Bandis joint model. History plots of nine instrumented points (y-direction).

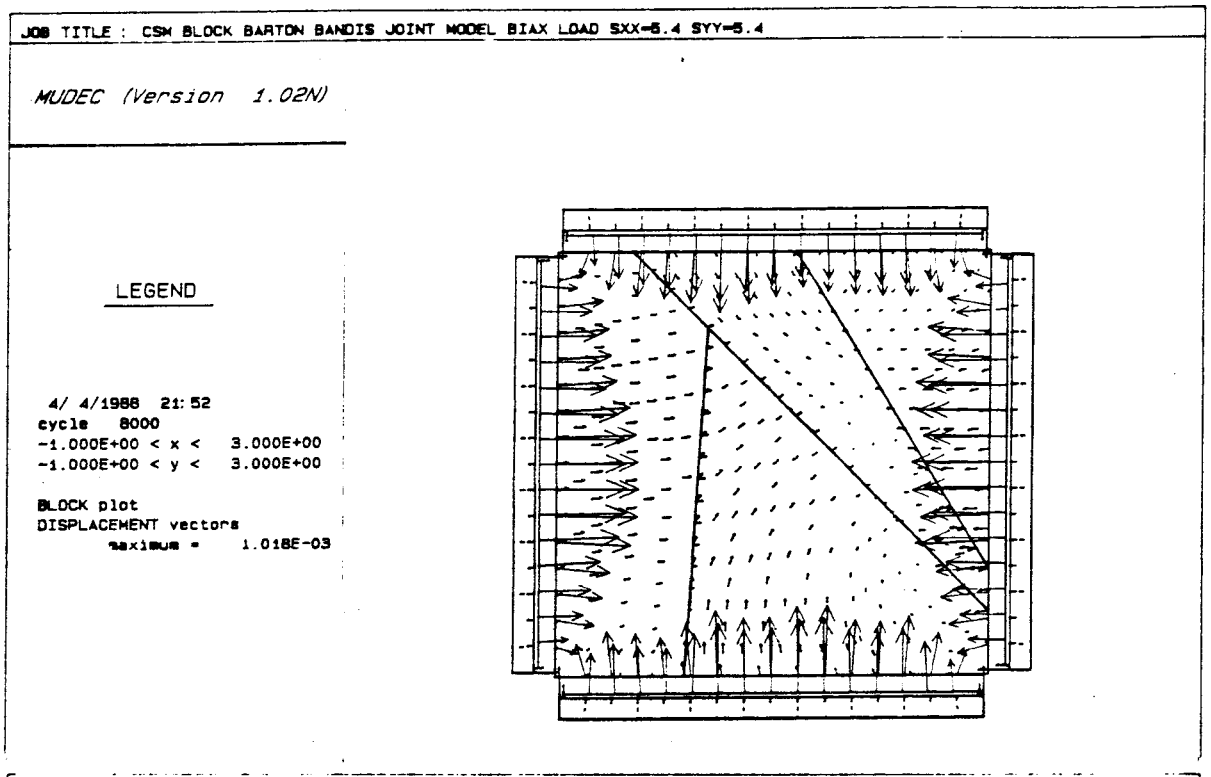

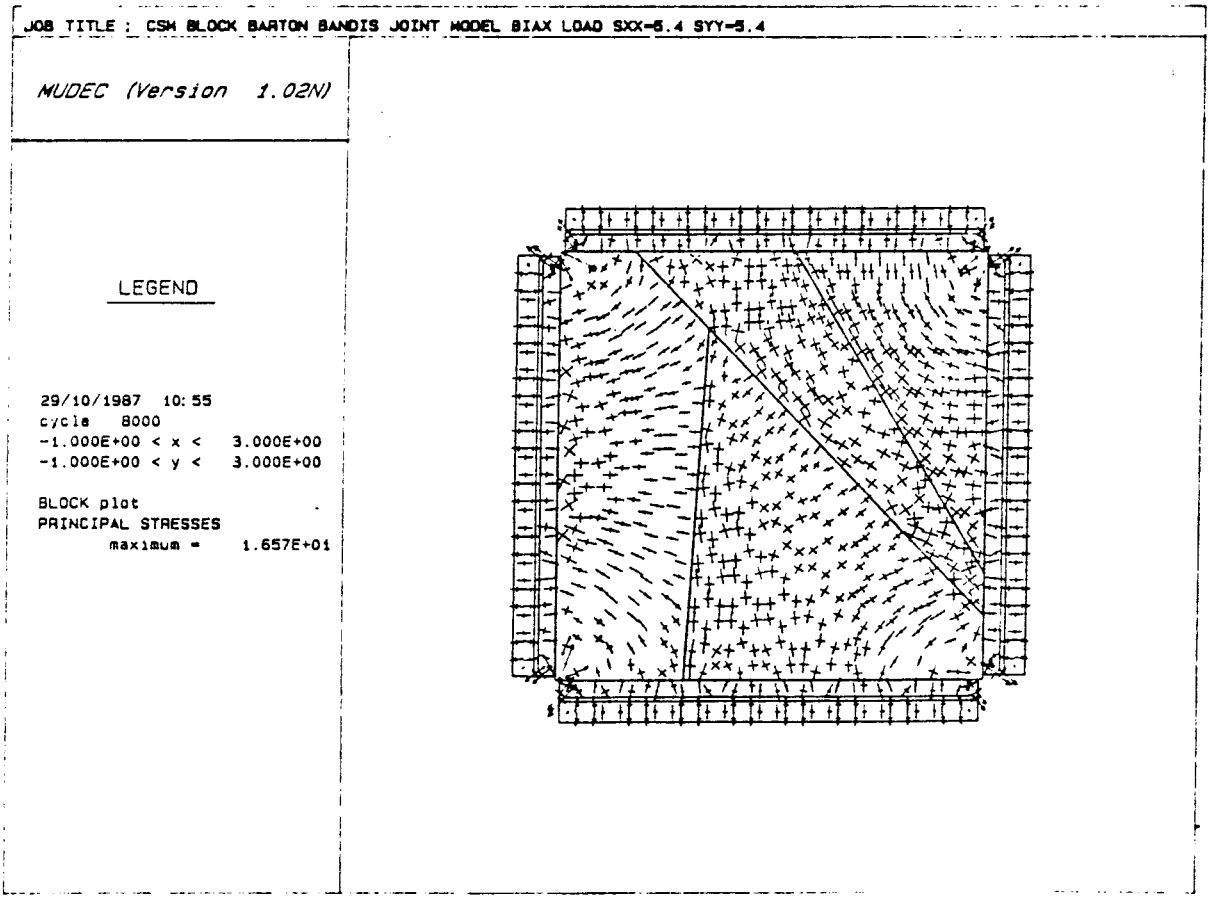

Fig. 7.1 Biaxial loading. Fluid pressure boundaries with Barton Bandis joint model. Displacement vectors and principal stresses plot.

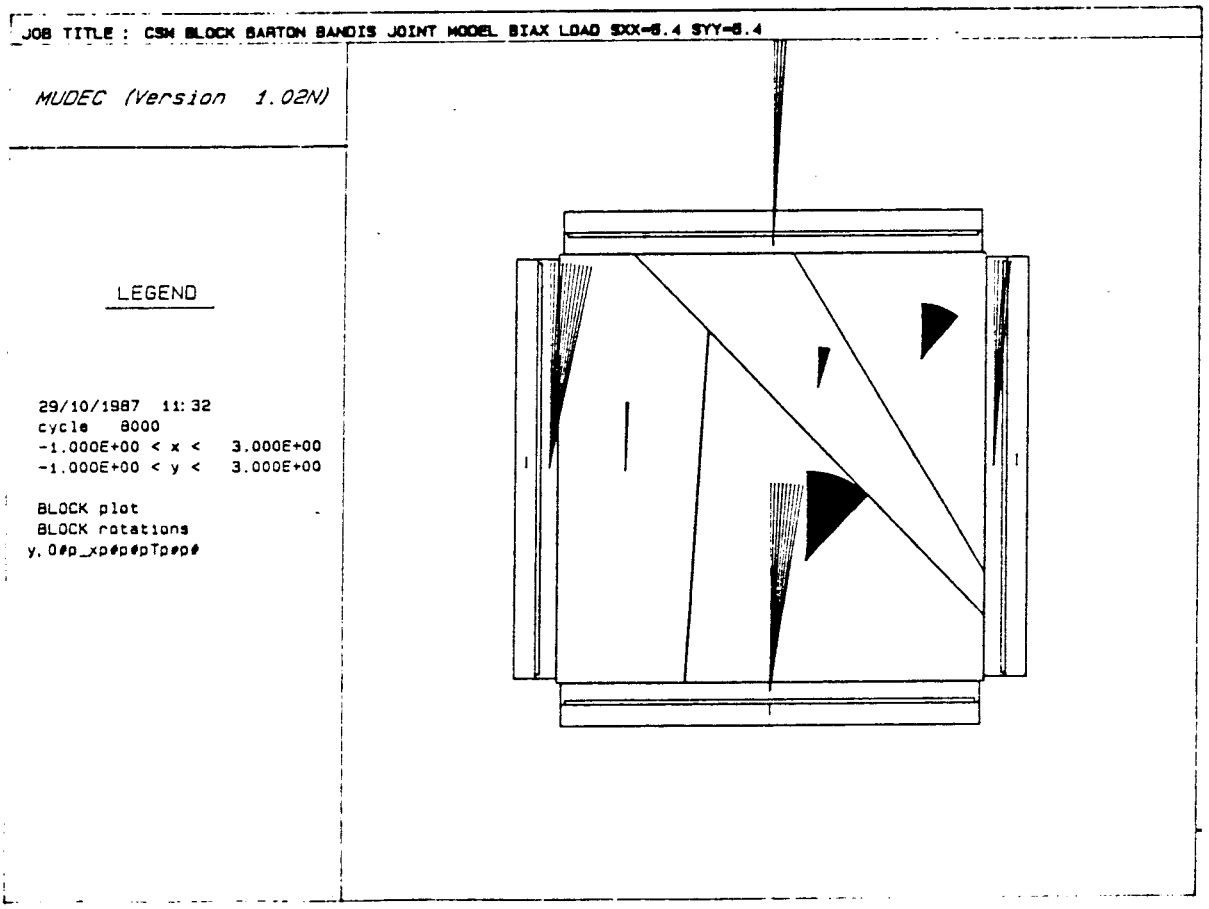

Fig. 7.2 Biaxial loading. Fluid pressure boundaries with Barton Bandis joint model. Block rotation plot.

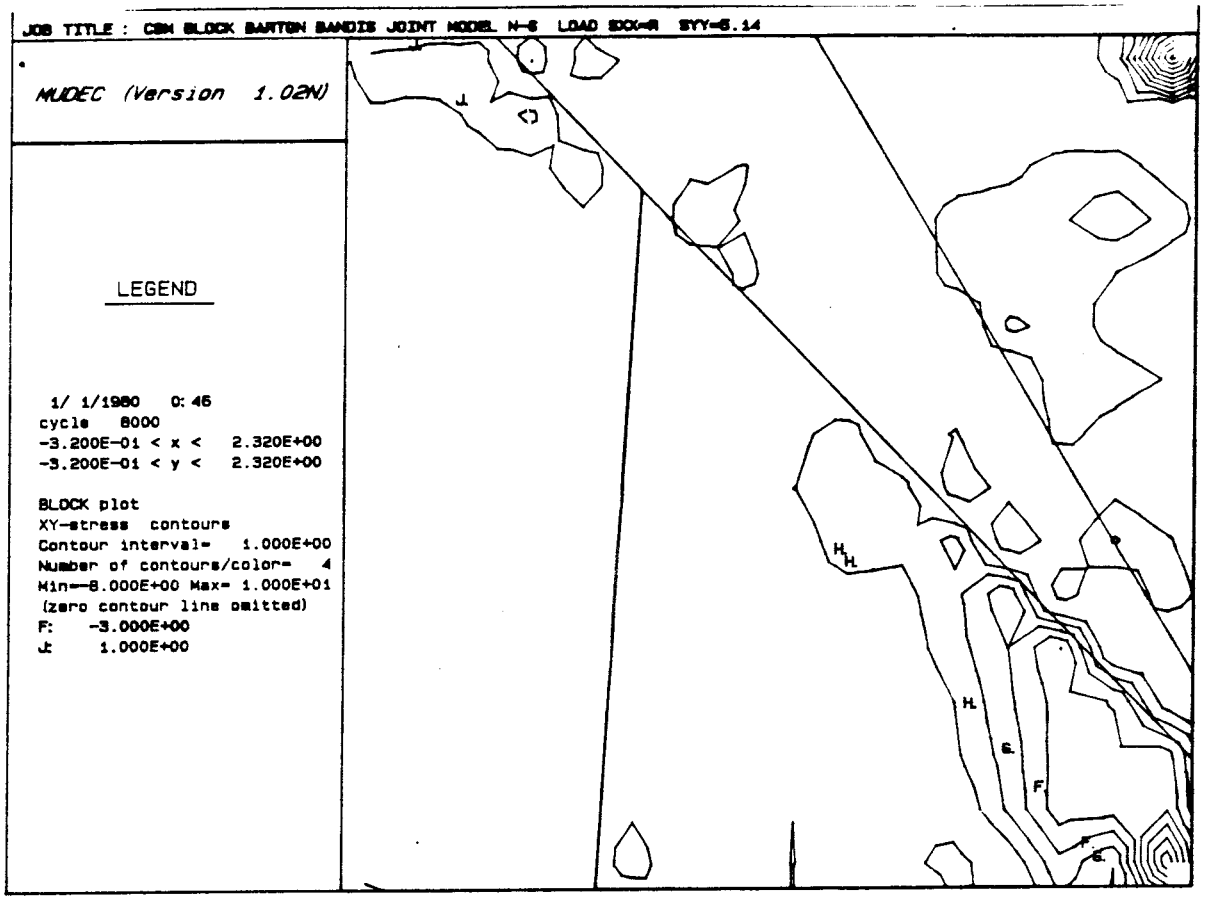

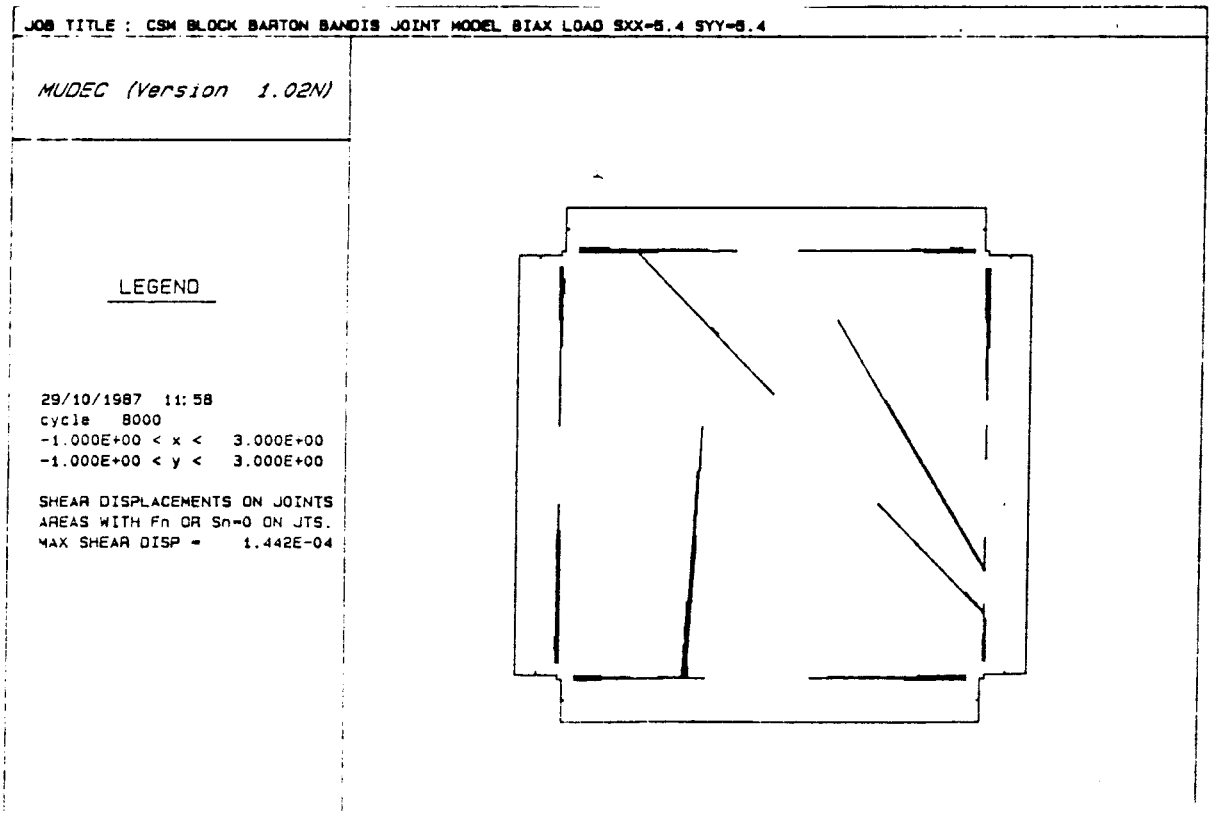

Fig. 7.3 Biaxial loading. Fluid pressure boundaries with Barton Bandis joint model. Shear stresses and shear displacement plots.

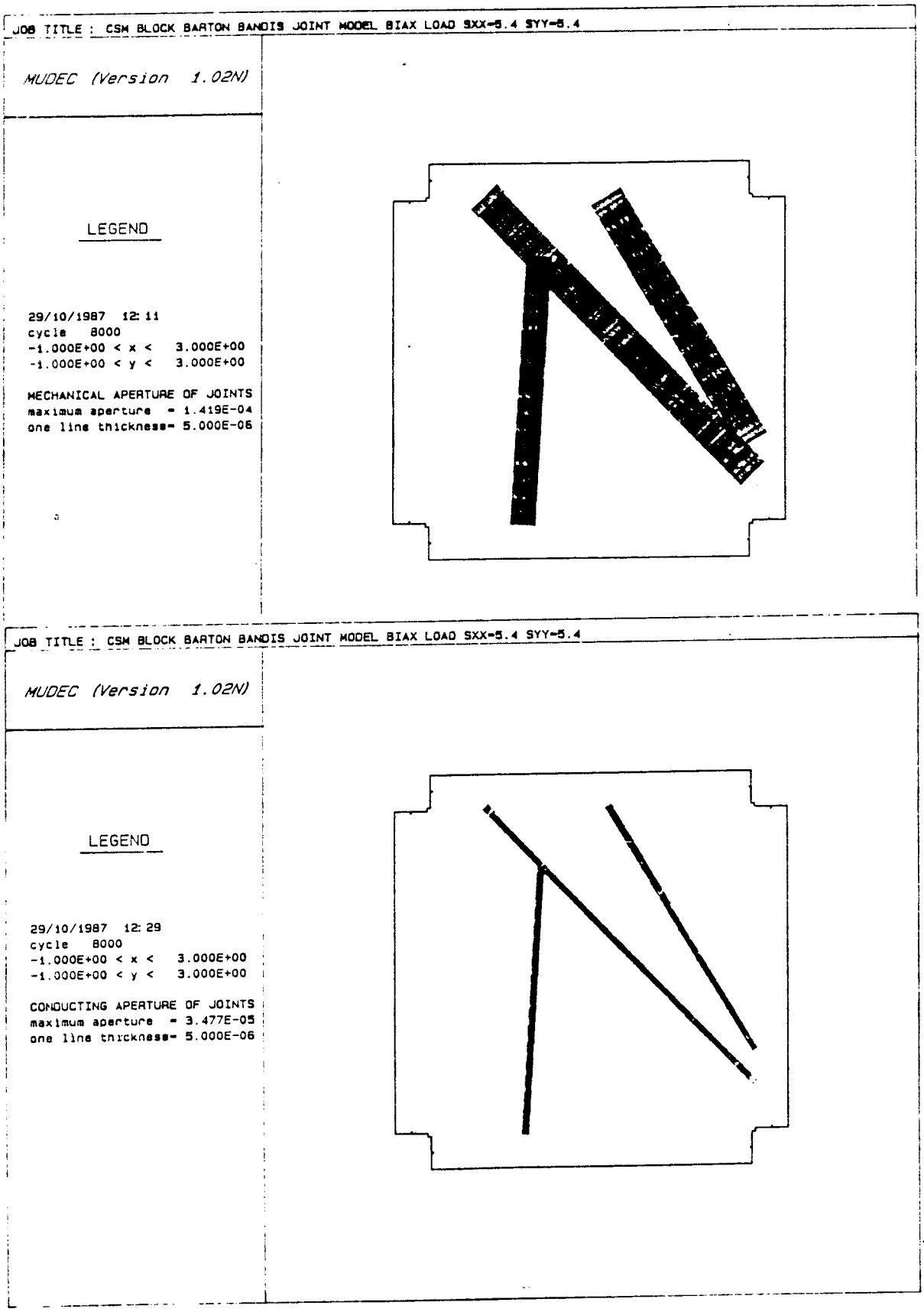

Fig. 7.4 Biaxial loading. Fluid pressure boundaries with Barton Bandis joint model. Mechanical and conducting aperture of joint sets.

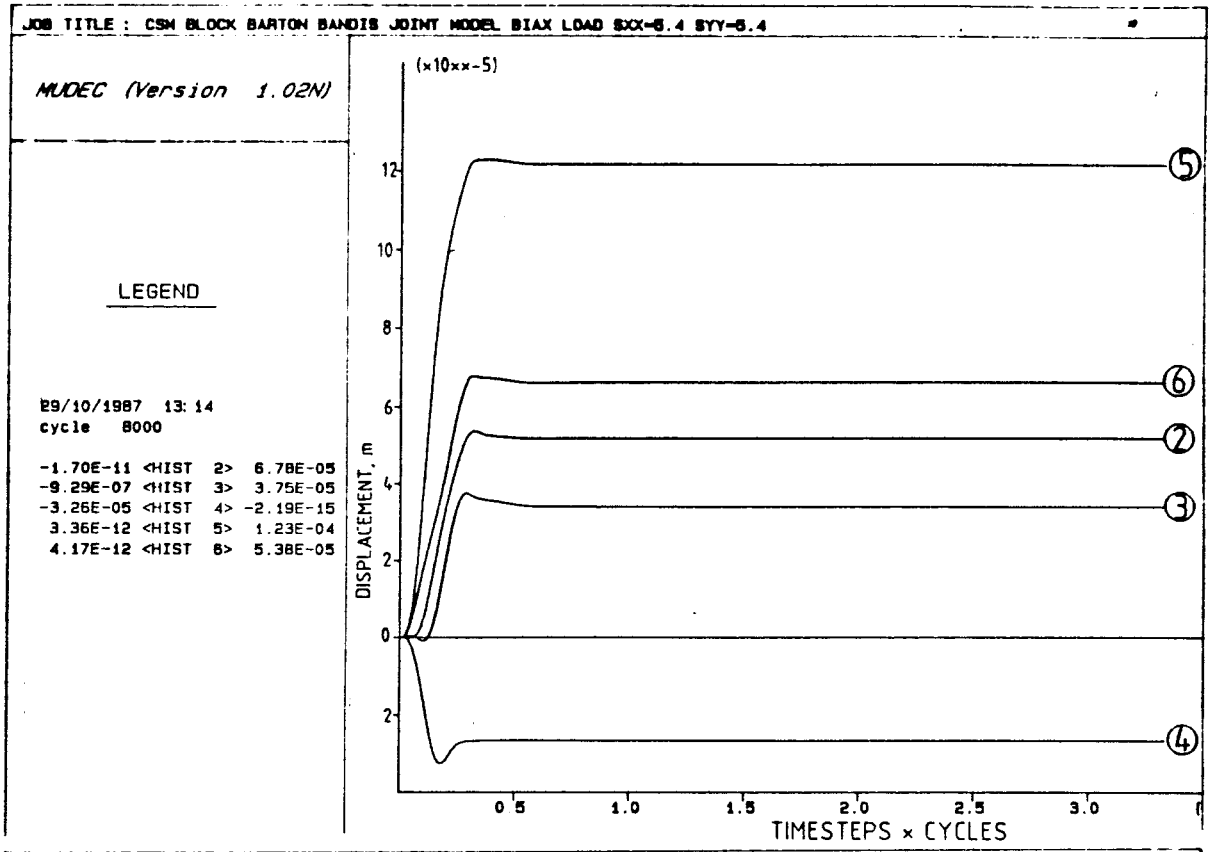

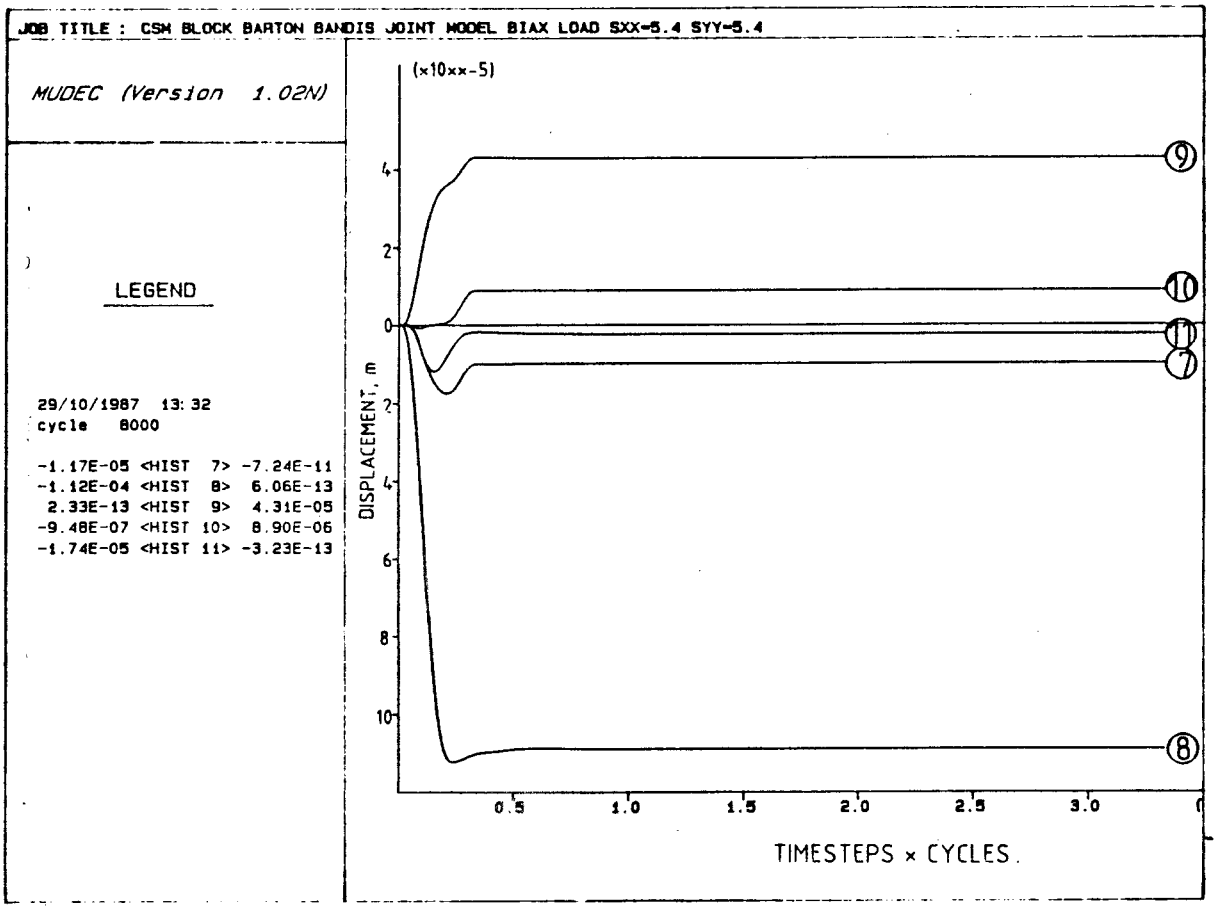

Fig. 7.5 **Biaxial loading. Fluid pressure boundaries with Barton Bandis joint model. History plots of ten instrumented points (X-Direction).**

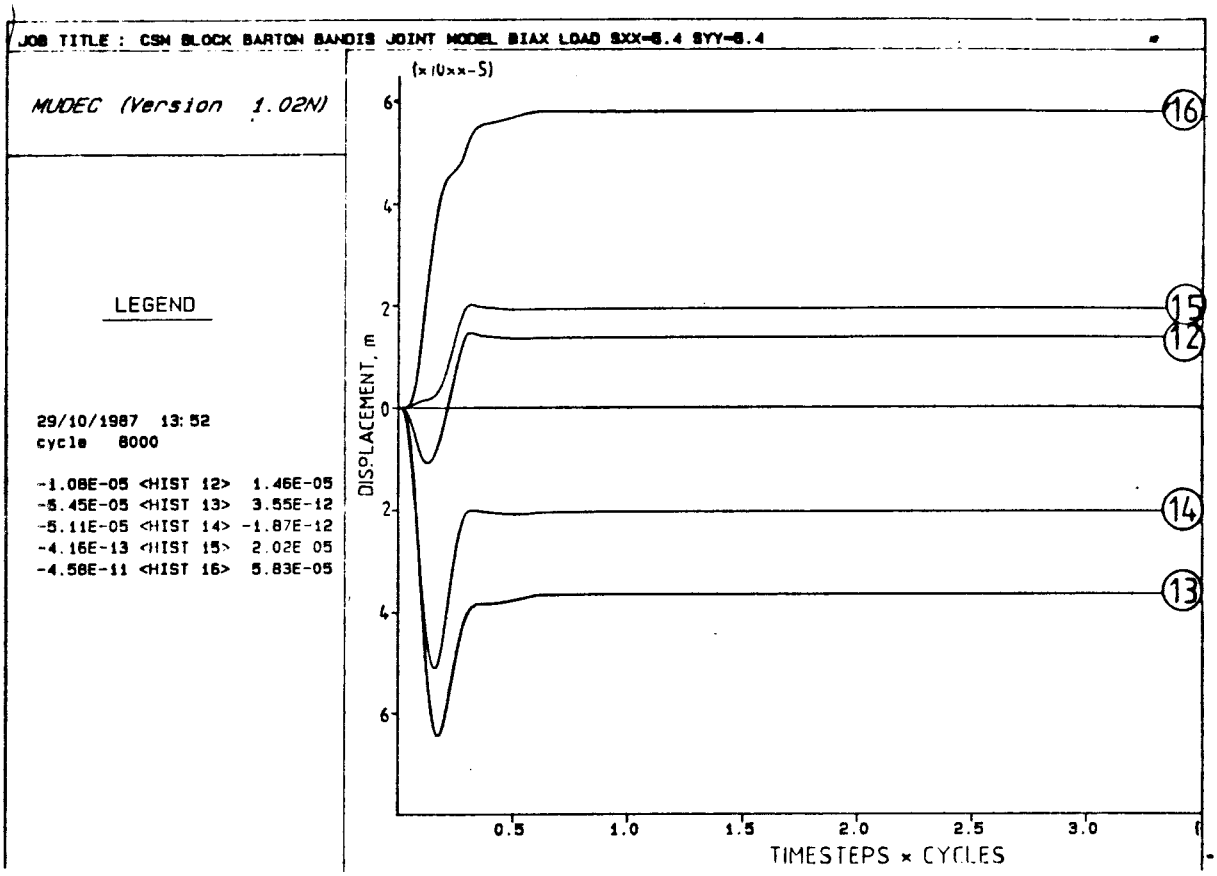

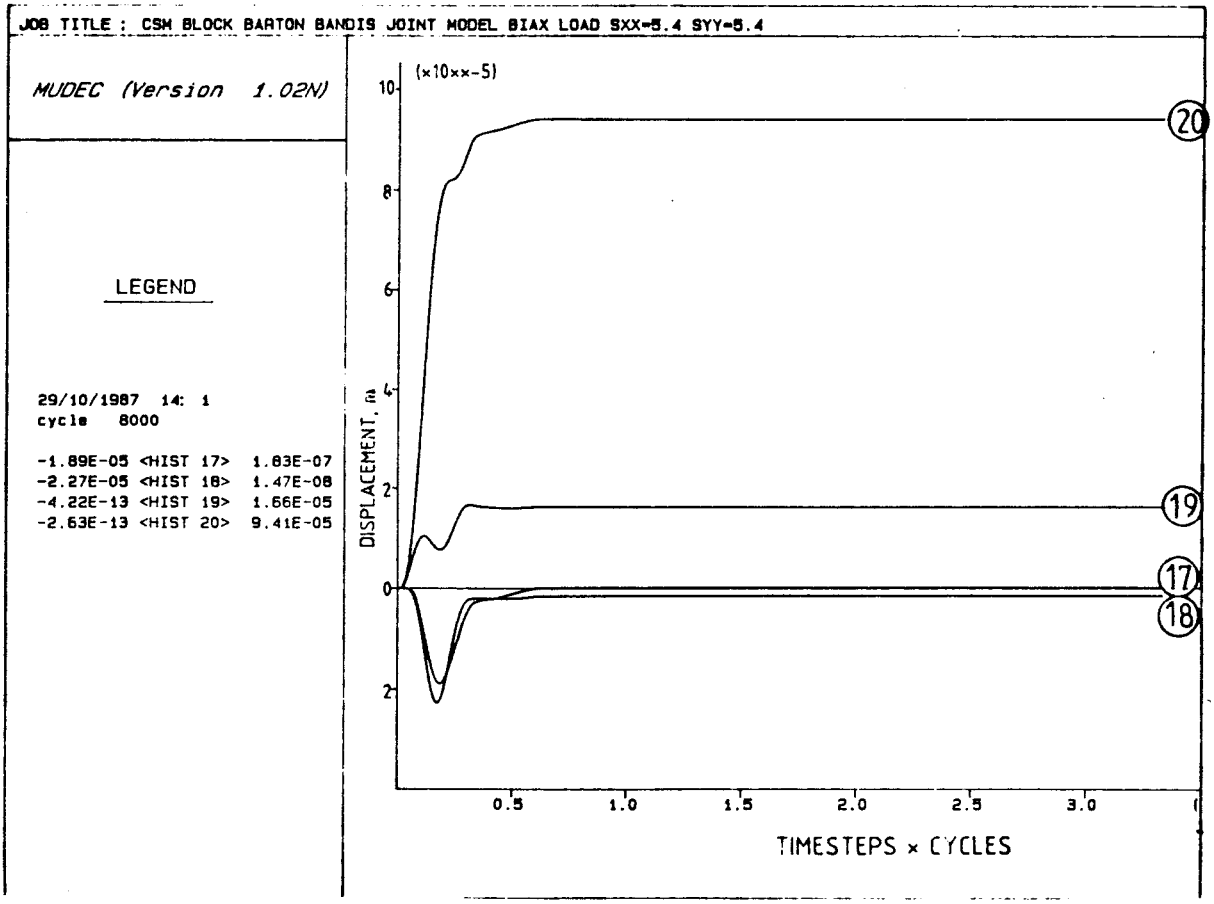

Fig. 7.6 **Biaxial loading. Fluid pressure boundaries with Barton Bandis joint model. History plots of instrumented points (Y-Direction).**

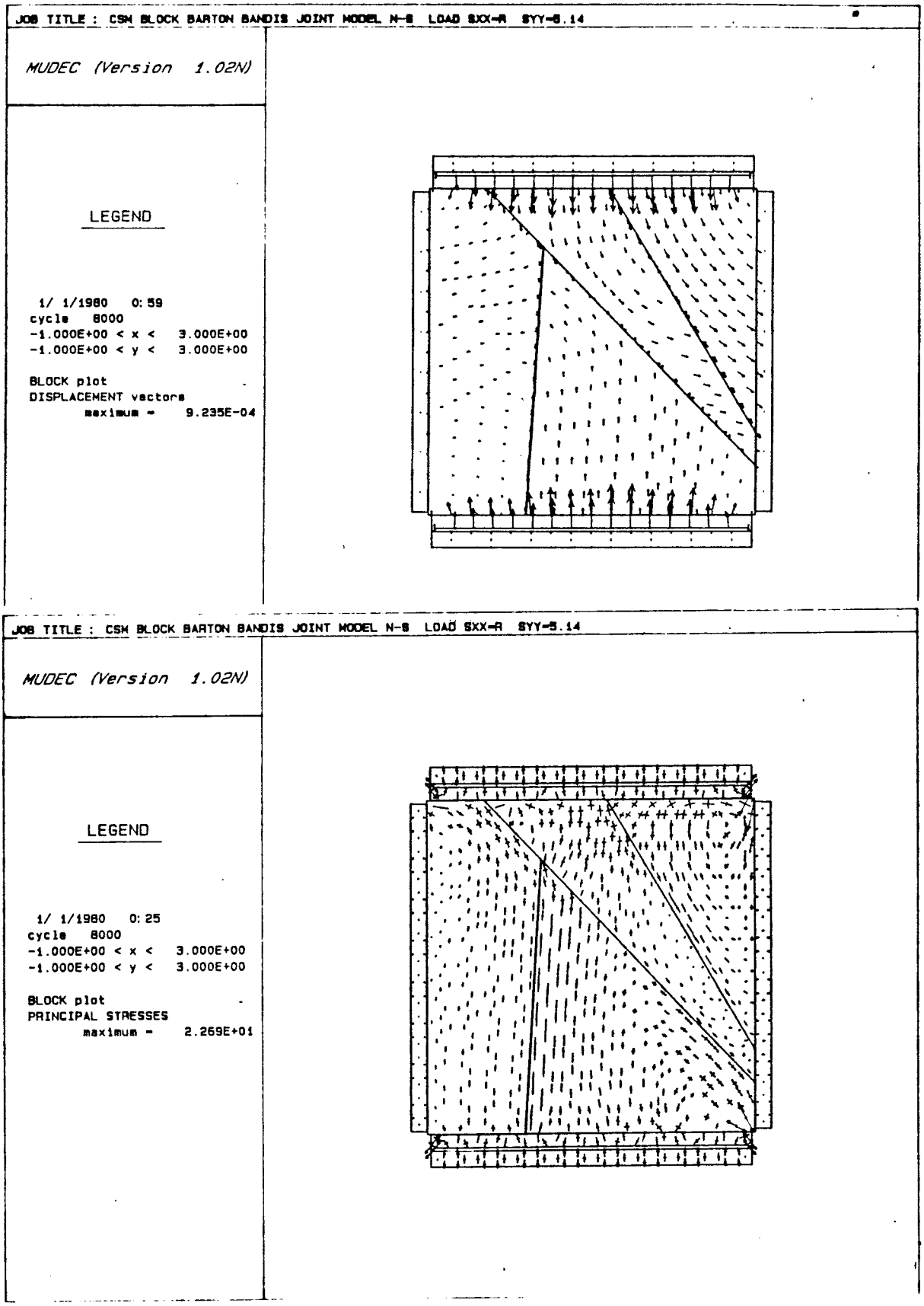

Fig. 8.1 N-S loading. Fluid pressure boundaries with Barton Bandis joint model. Displacement vectors and principal stresses plot.

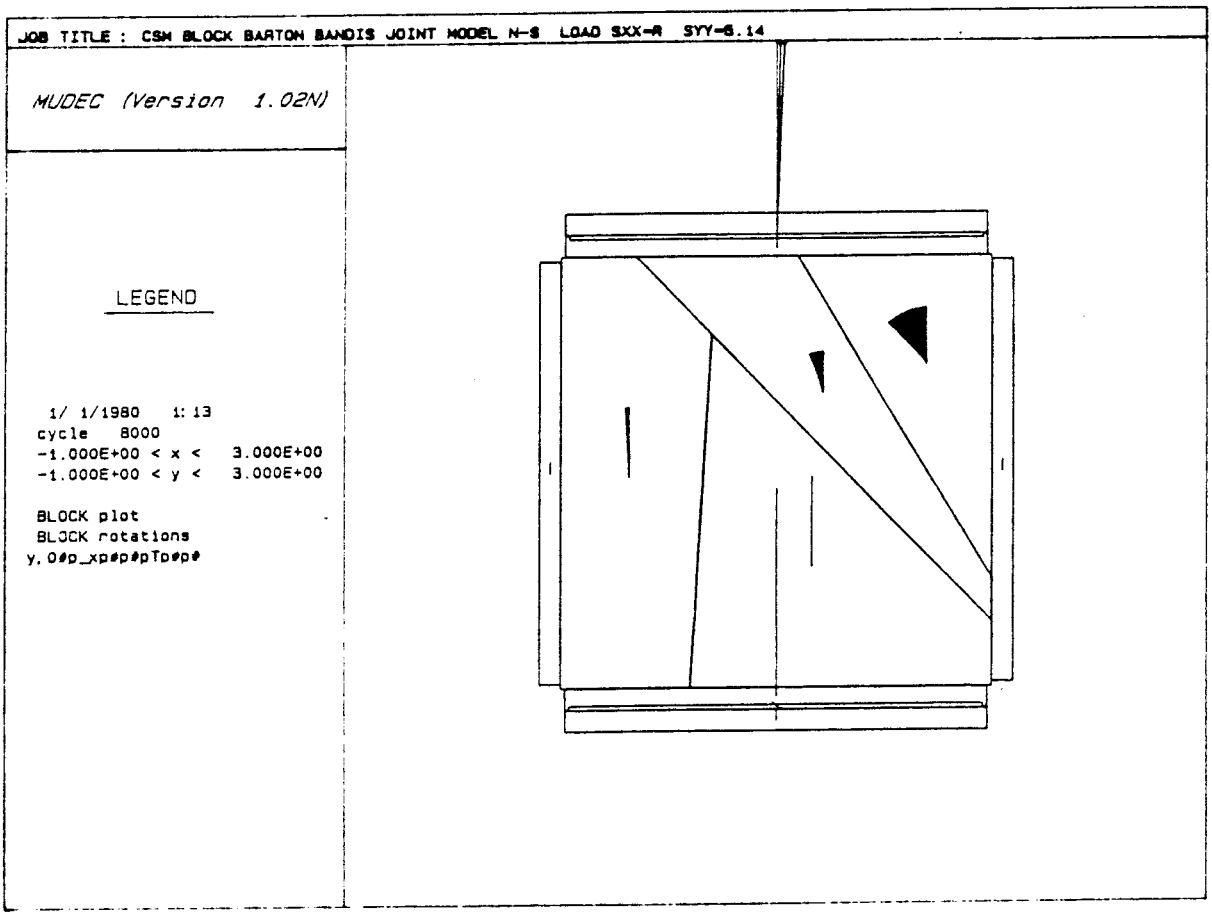

Fig. 8.2 N-S loading. Fluid pressure boundaries with Barton Bandis joint model. Block rotation plot.

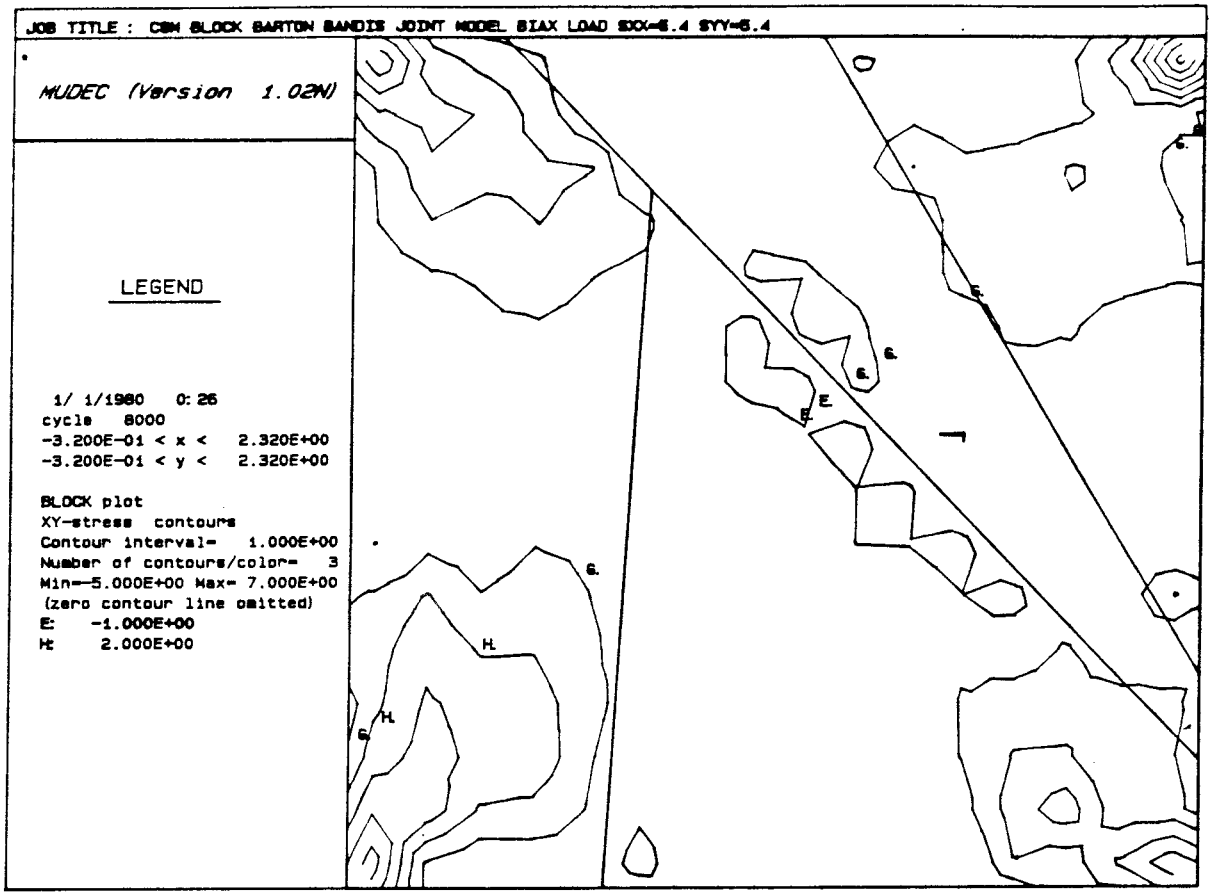

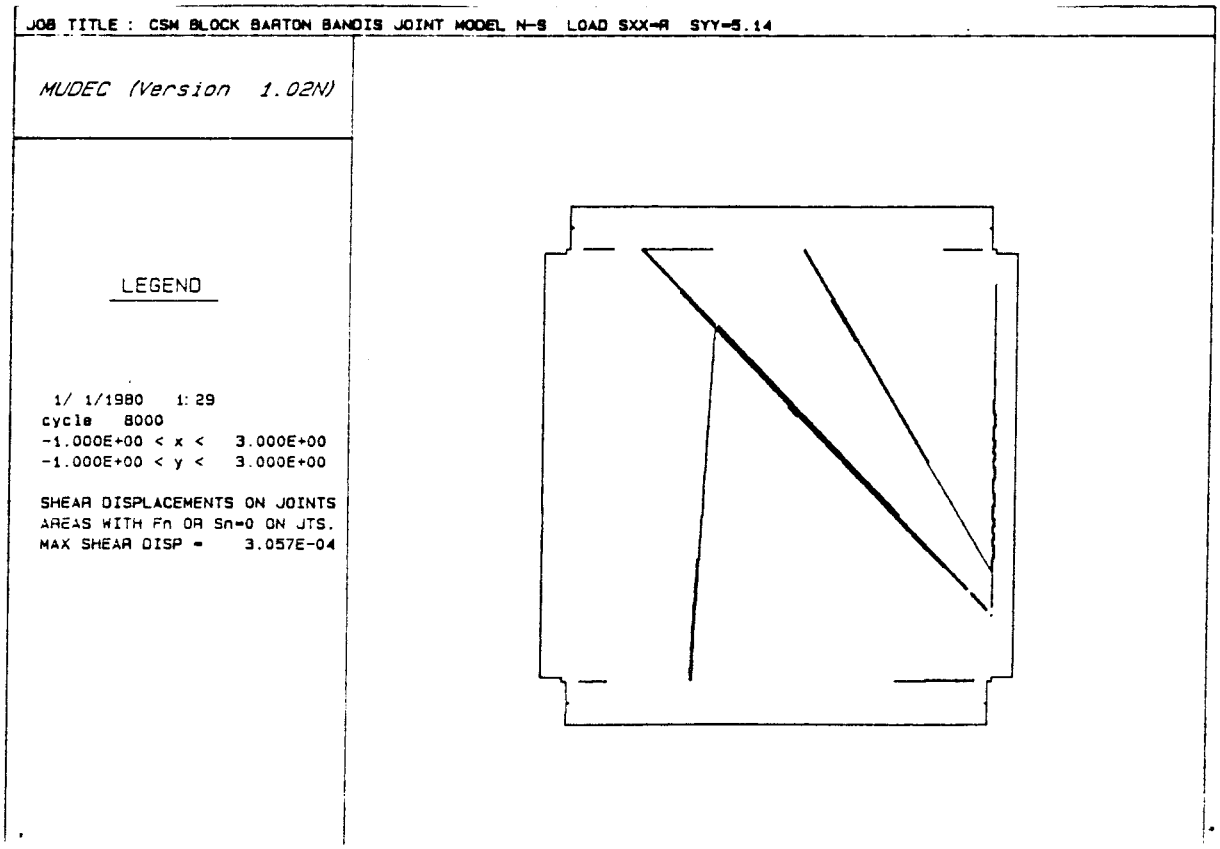

Fig. 8.3 N-S loading. Fluid pressure boundaries with Barton Bandis joint model. Shear stresses and shear displacement plots.

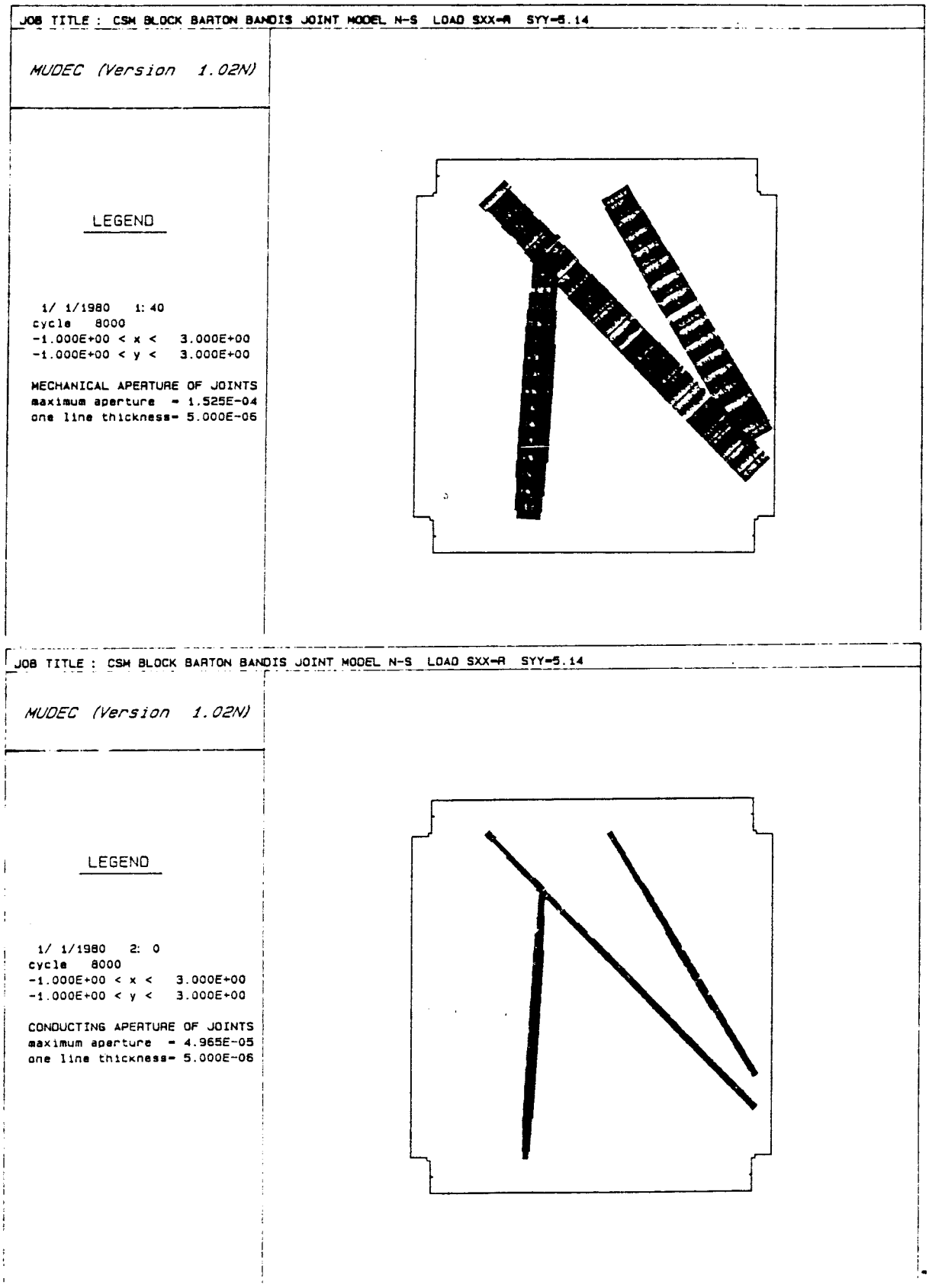

Fig. 8.4 N-S loading. Fluid pressure boundaries with Barton Bandis joint model. Mechanical and conducting aperture of joint sets.

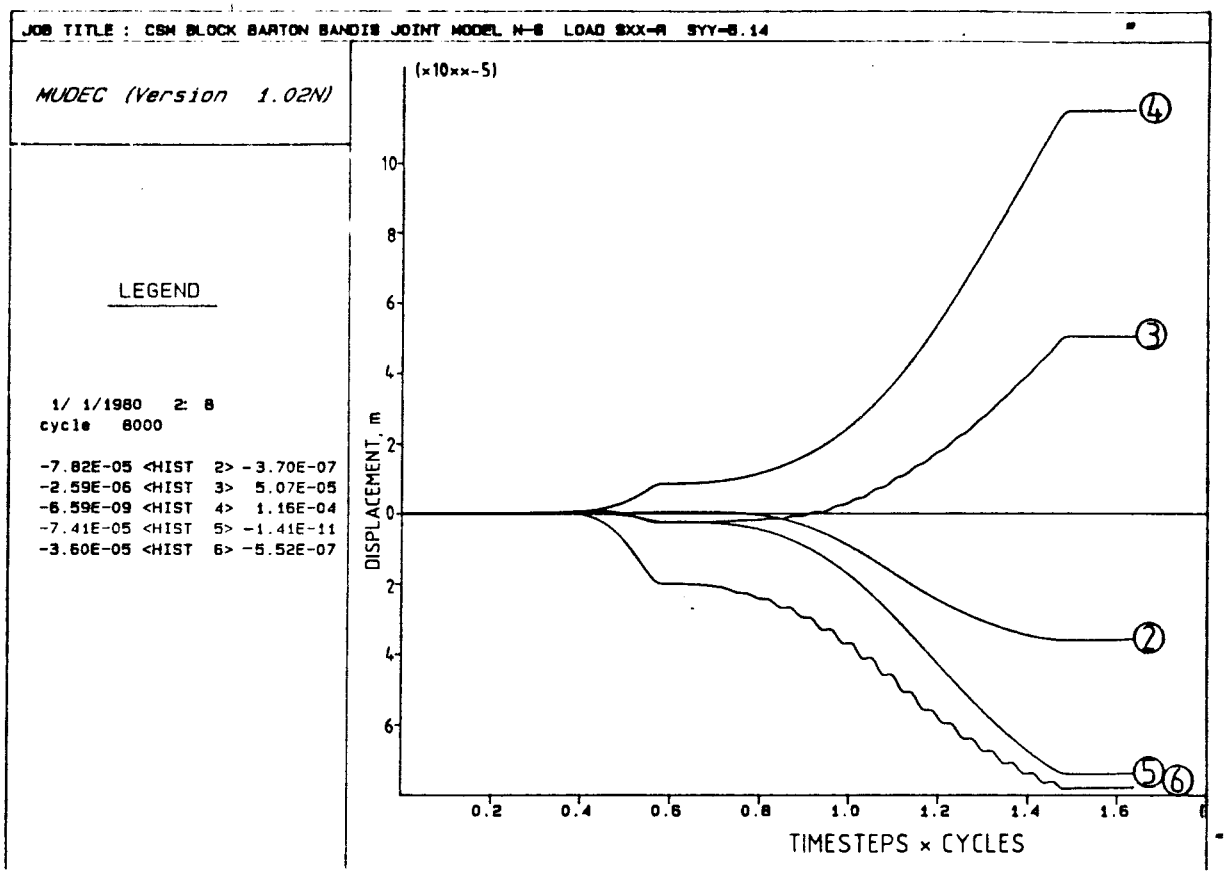

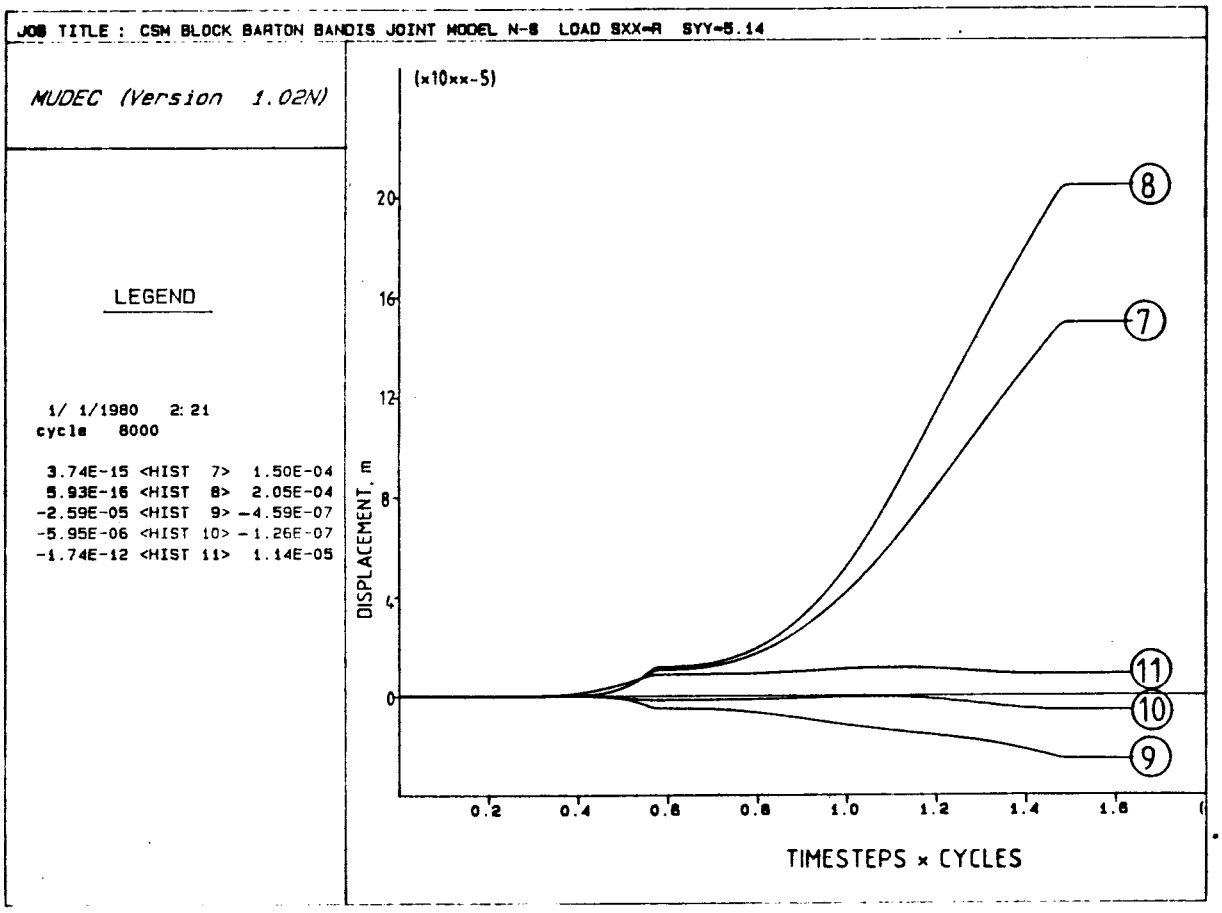

Fig. 8.5 **N-S loading. Fluid pressure boundaries with Barton Bandis joint model. History plots of ten instrumented points (X-Direction).**

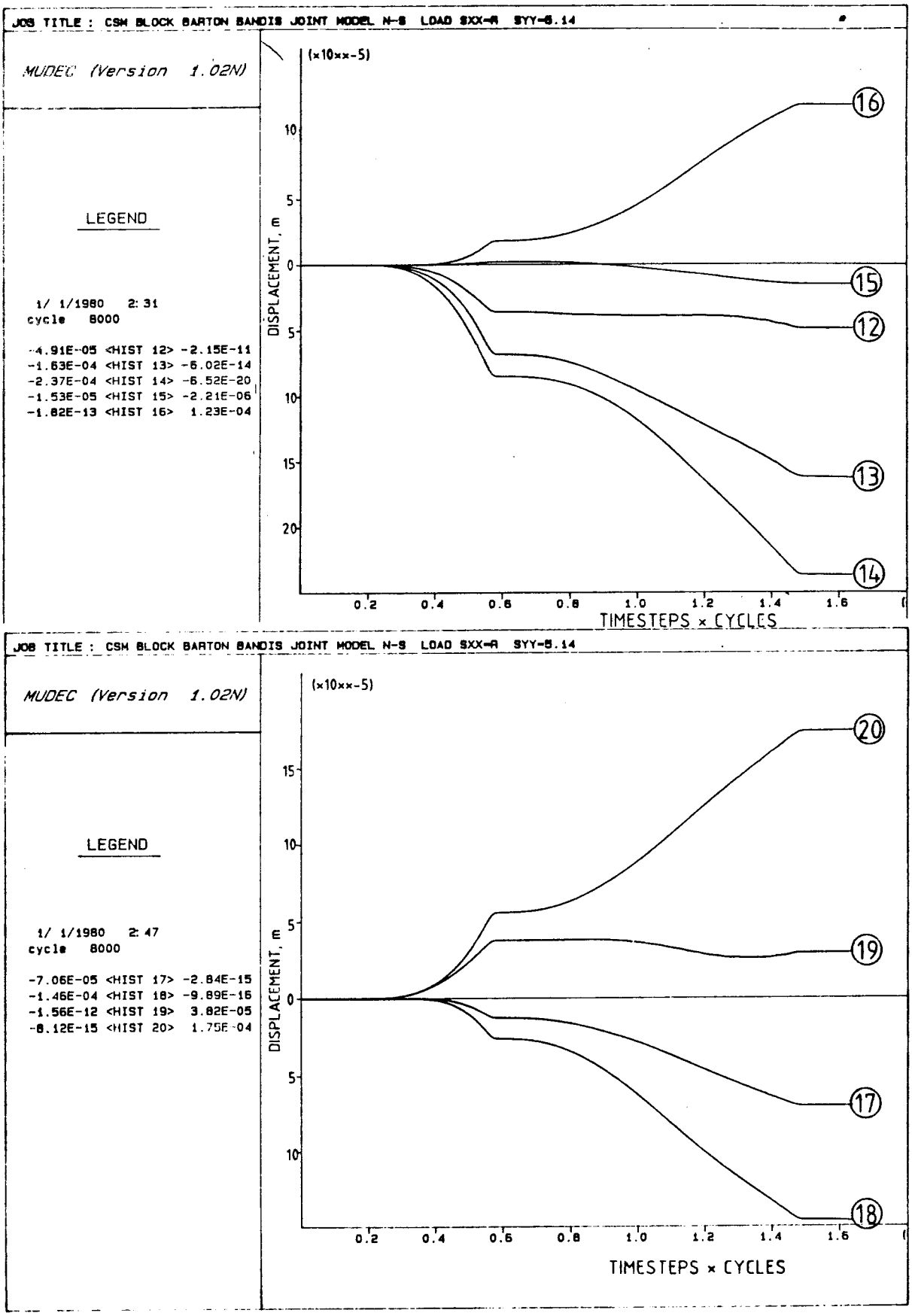

Fig. 8.6 **N-S loading. Fluid pressure boundaries with Barton Bandis joint model. History plots of instrumented points (Y-Direction).**

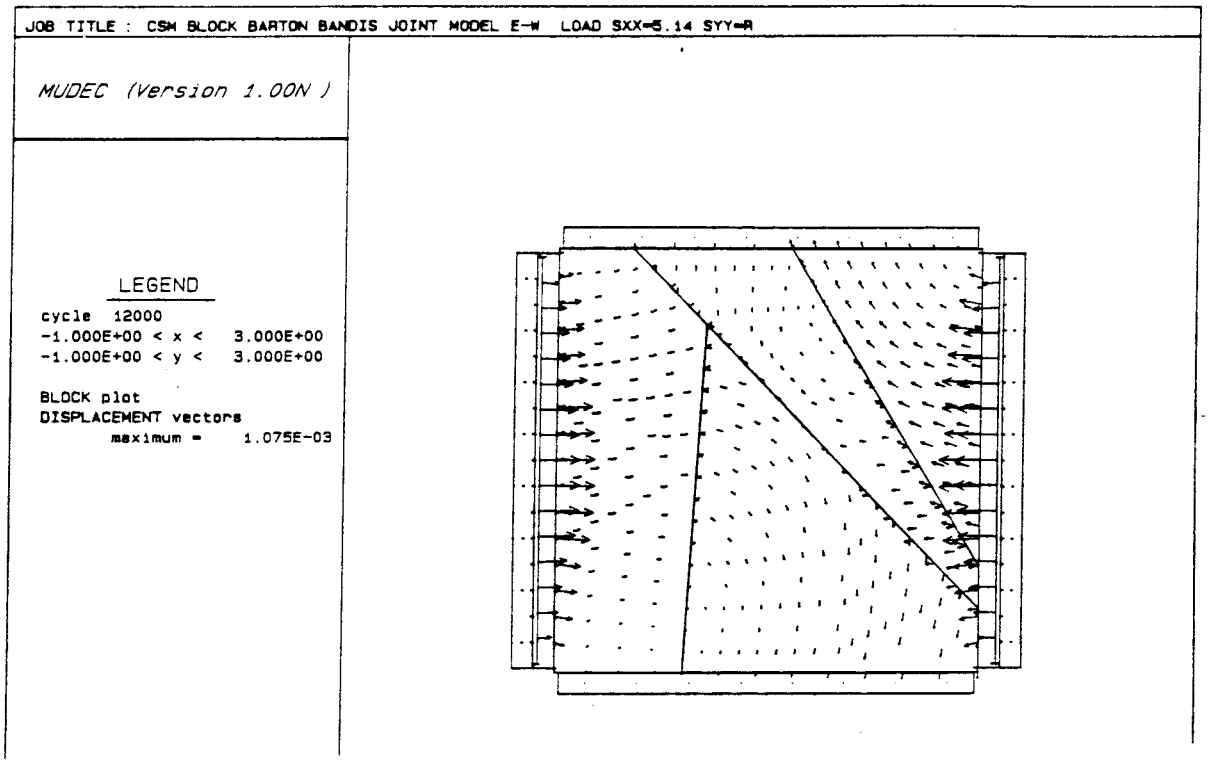

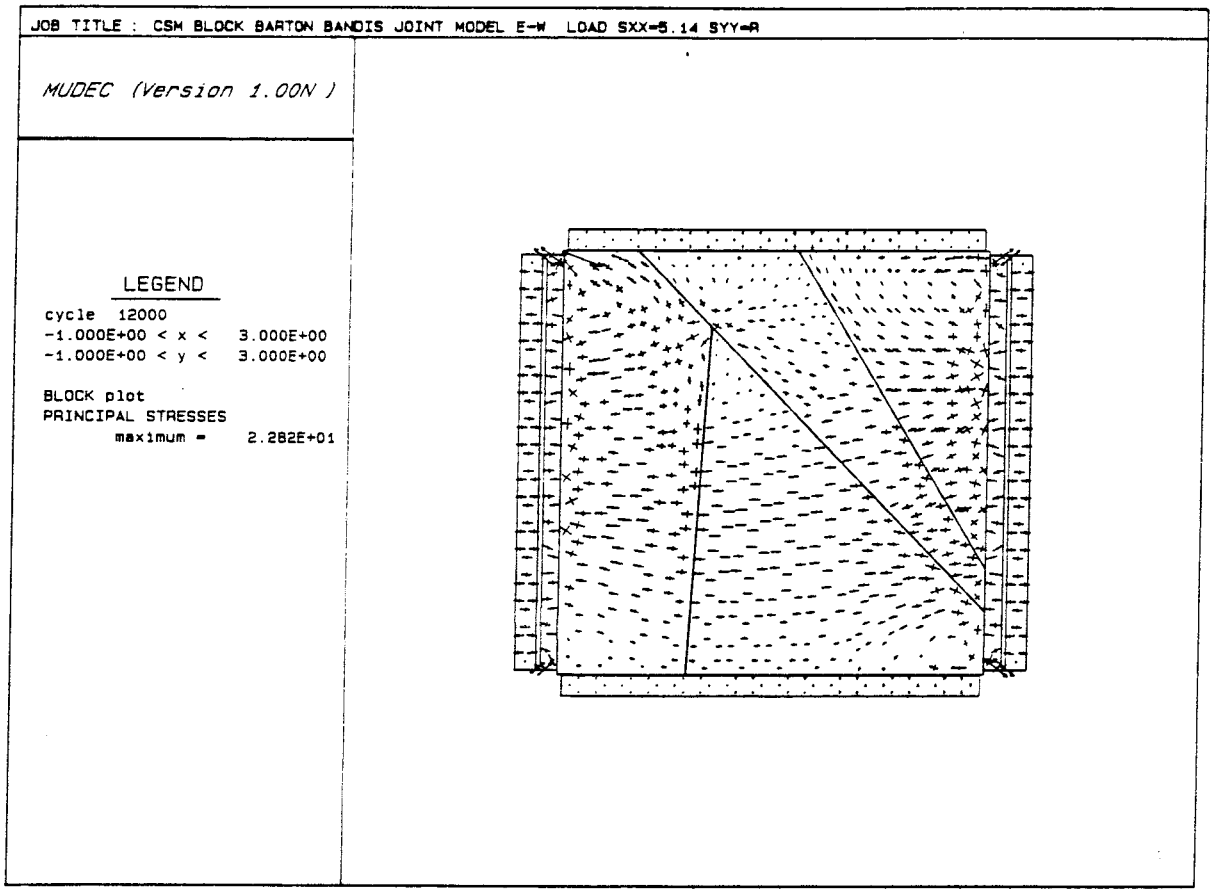

Fig. 9.1 E-W Uniaxial loading.Fluid pressure boundaries with Barton - Bandis joint model.Displacement vectors and principal stresses plots.

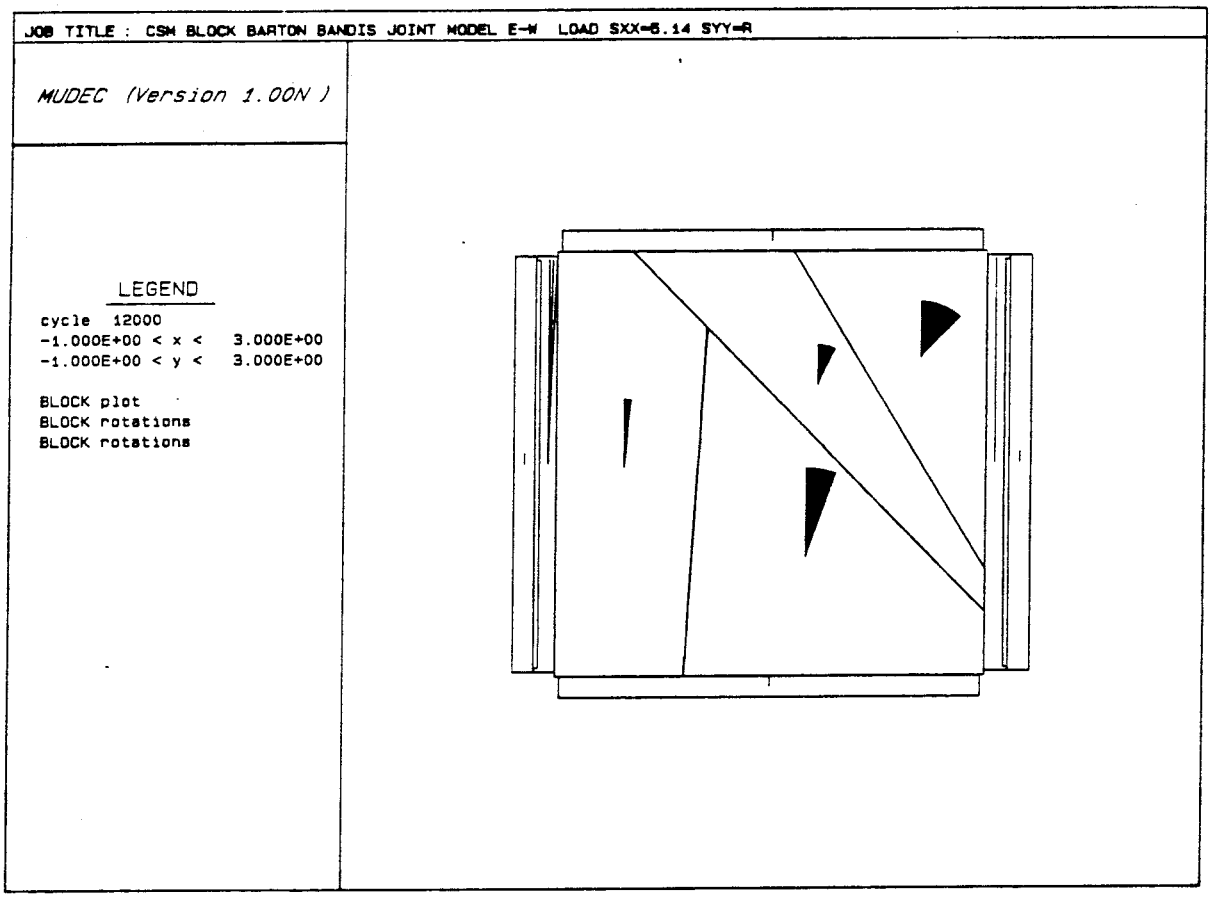

Fig. 9.2 E-W Uniaxial loading.Fluid pressure boundaries with Barton - Bandis joint model. Block rotation plot.

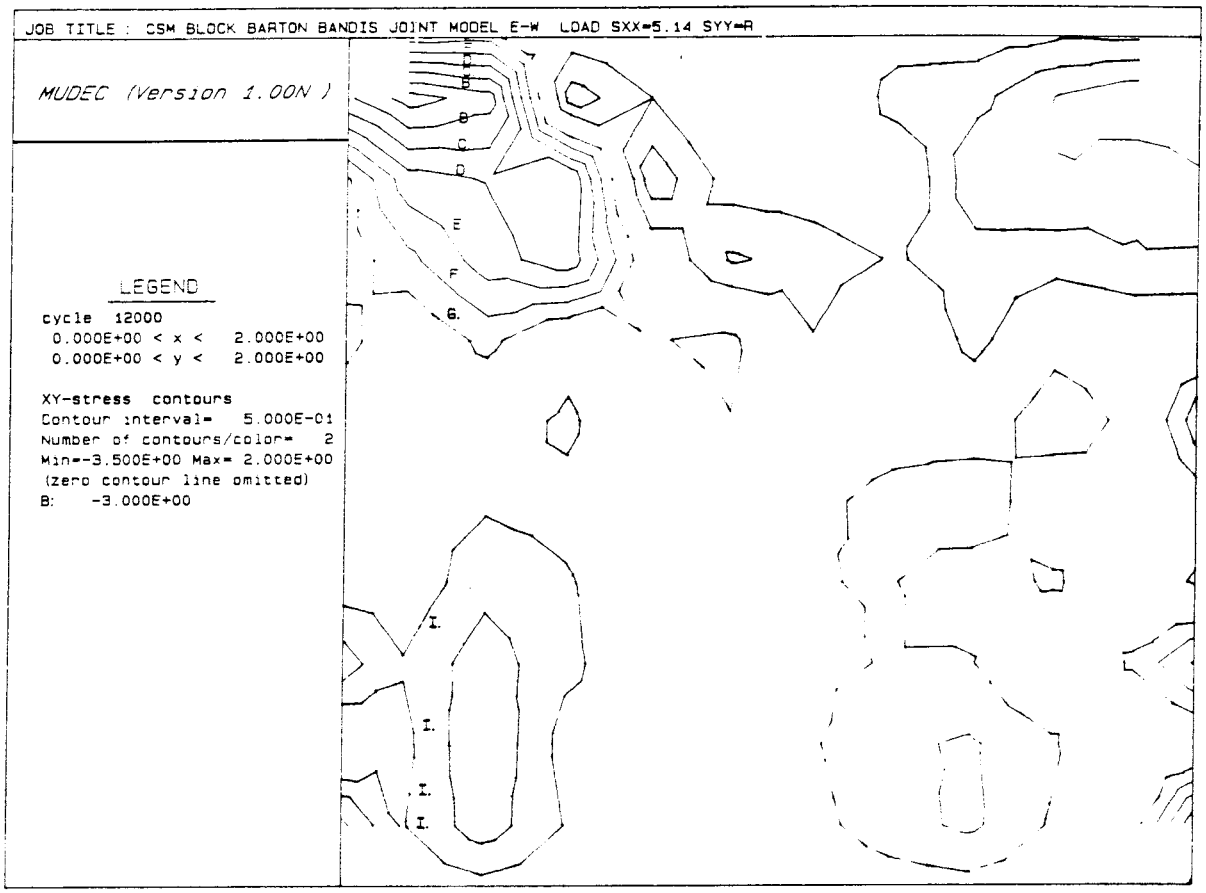

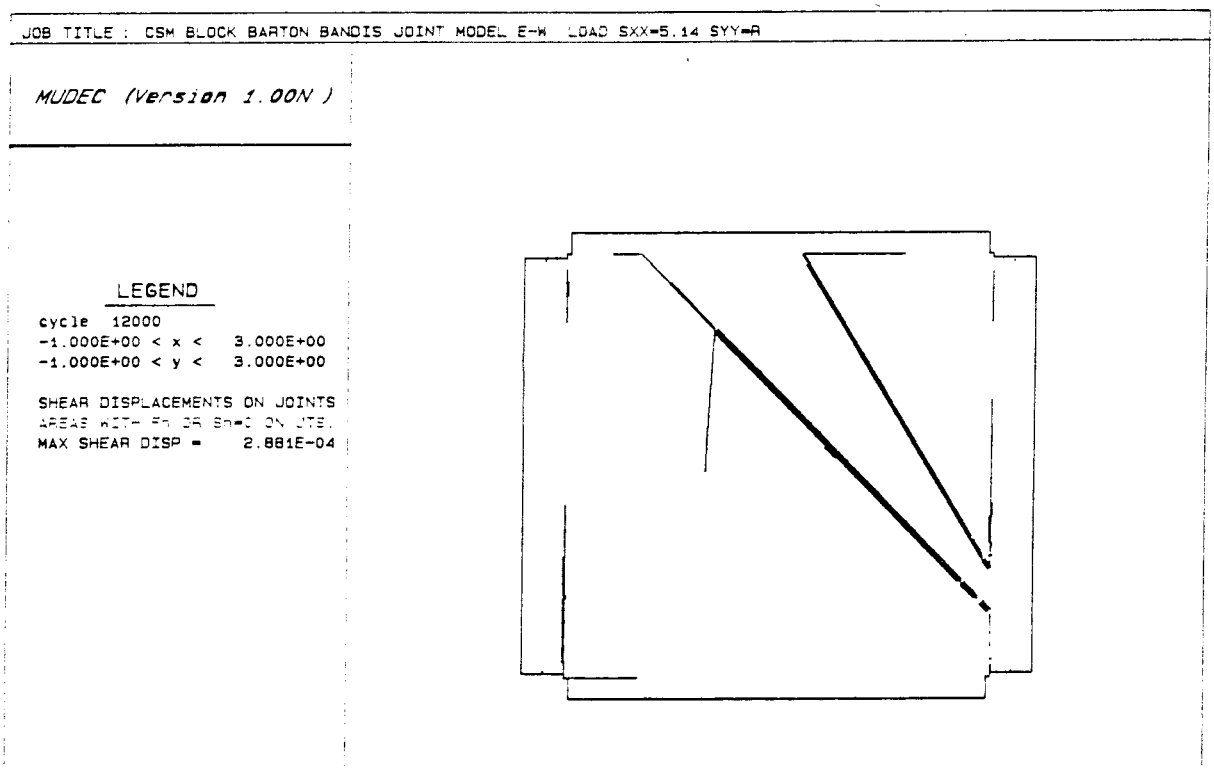

Fig. 9.3 E-W Uniaxial loading.Fluid pressure boundaries with Barton-Bandis joint model.Shear stresses and shear displacement plots.

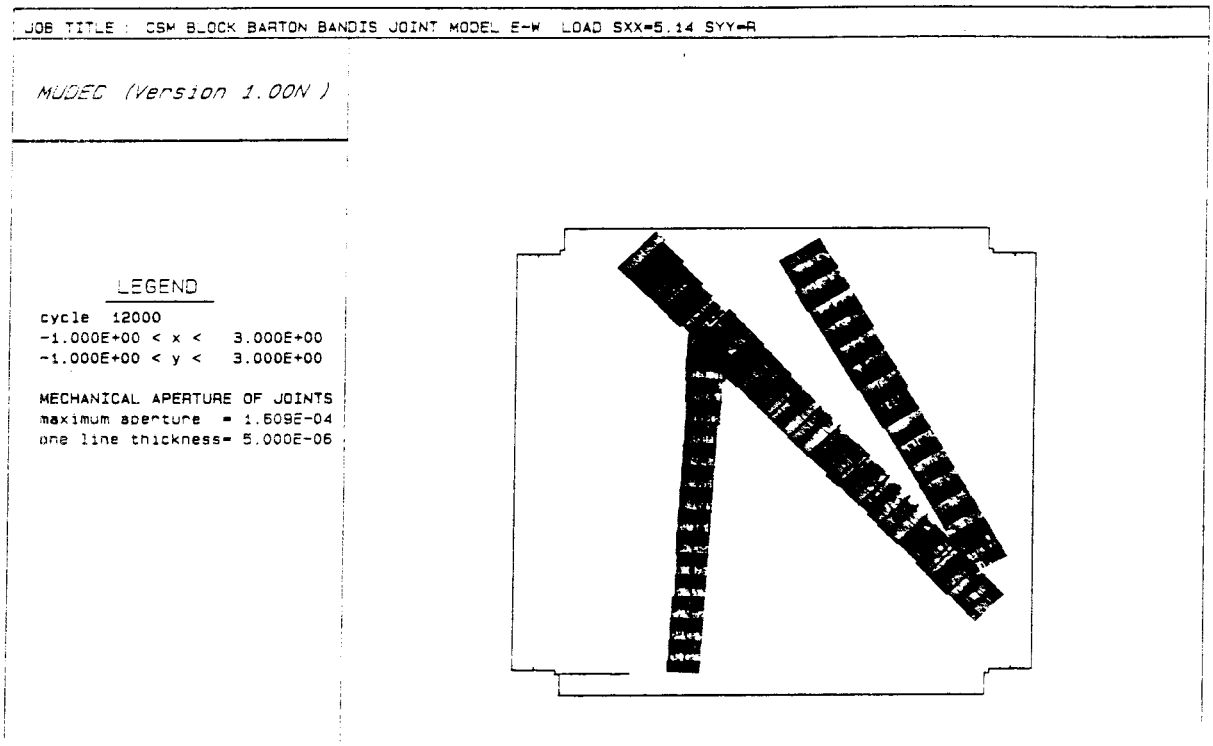

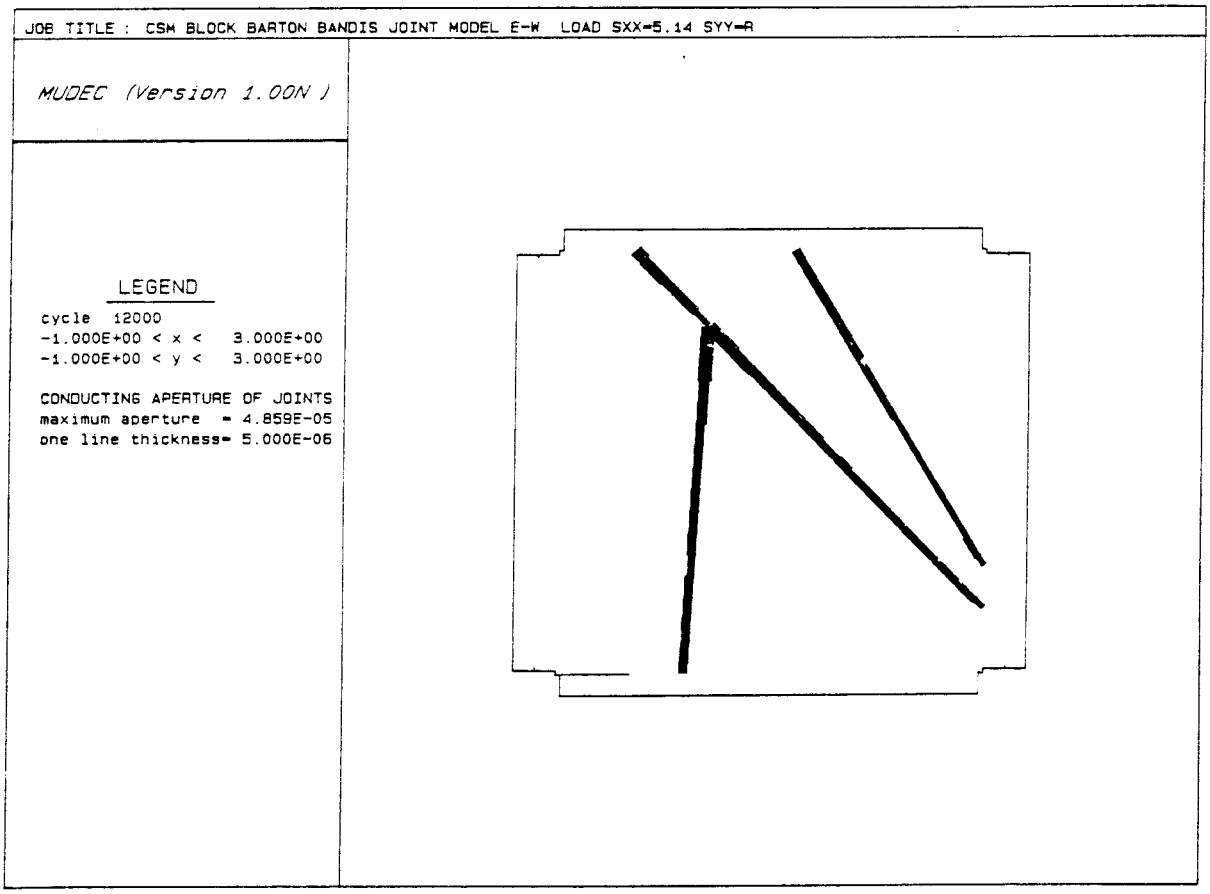

Fig. 9.4 E-W Uniaxial loading.Fluid pressure boundaries with Barton - Bandis joint model. Mechanical and conducting apertures of joint sets.

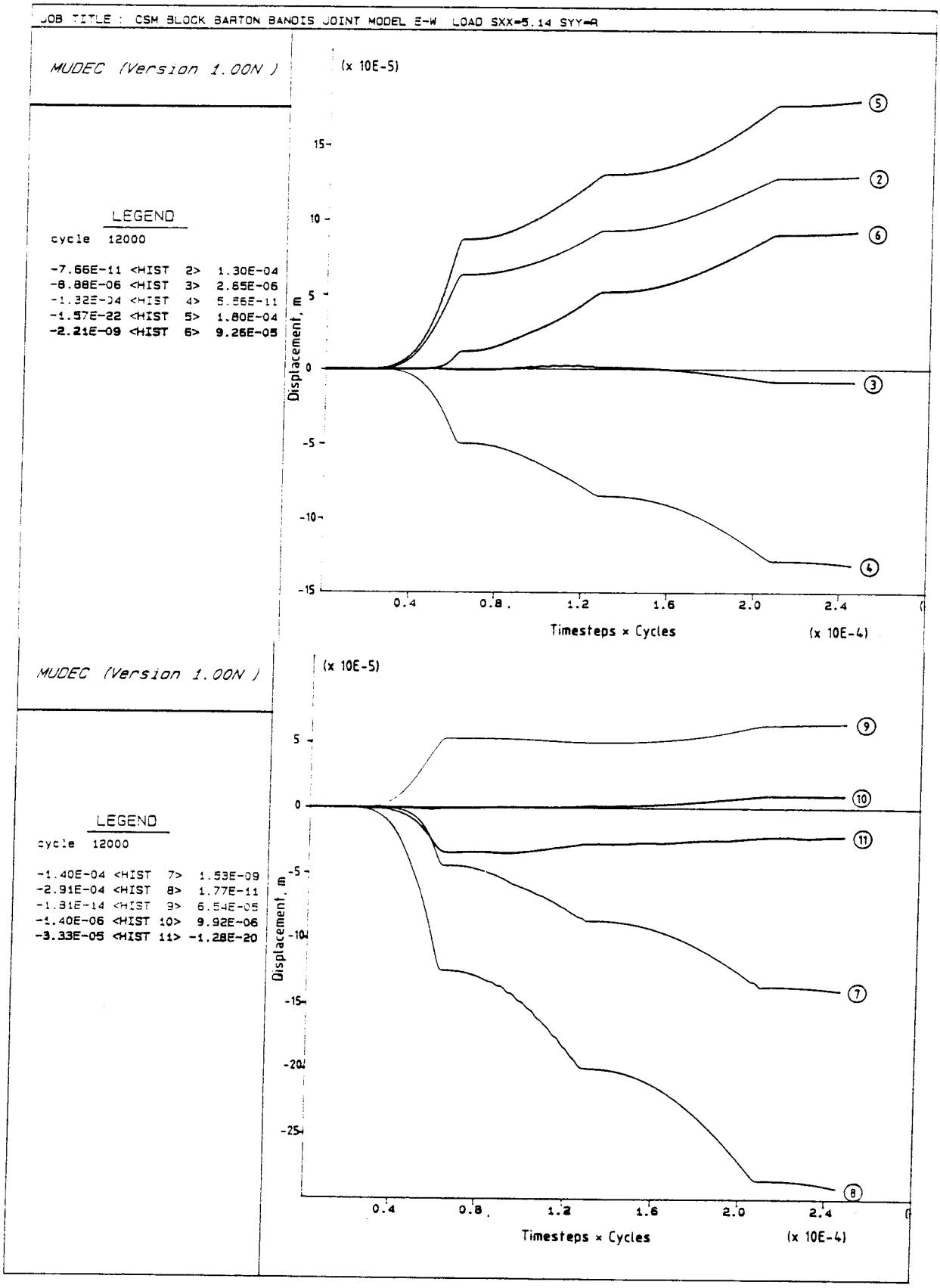

Fig. 9.5 E-W Uniaxial loading.Fluid pressure boundaries with Barton - Bandis joint model. History plots of ten instrumented points (x - direction).

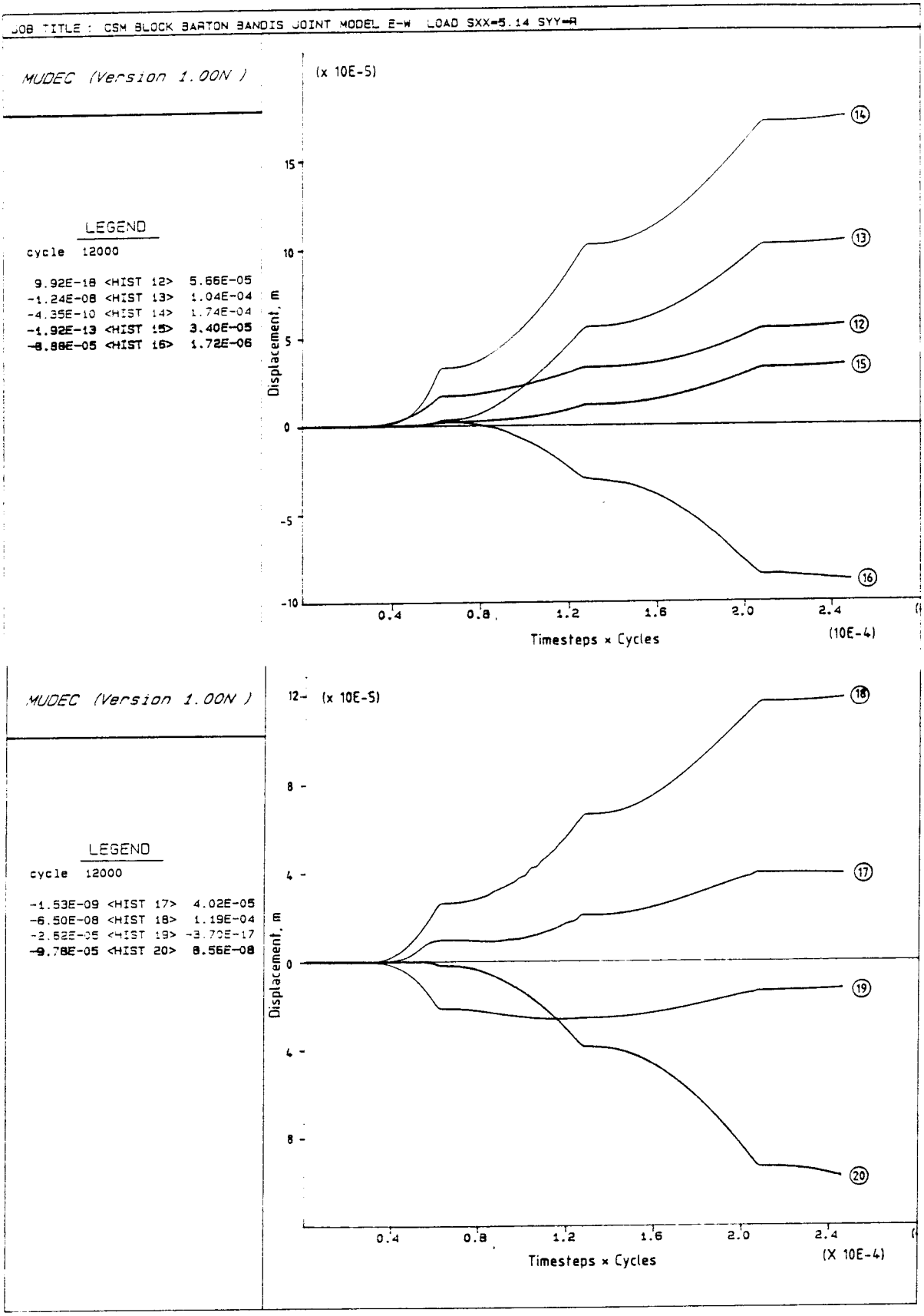

Fig 9.6 E-W Uniaxial loading. Fluid pressure boundaries with Barton - Bandis joint model.History plots of nine instrumented points (y - direction).

List of SKB reports

Annual Reports

1977–78
TR 121
KBS Technical Reports 1 – 120.
Summaries. Stockholm, May 1979.

1979
TR 79–28
The KBS Annual Report 1979.
KBS Technical Reports 79-01 – 79-27.
Summaries. Stockholm, March 1980.

1980
TR 80–26
The KBS Annual Report 1980.
KBS Technical Reports 80-01 – 80-25.
Summaries. Stockholm, March 1981.

1981
TR 81–17
The KBS Annual Report 1981.
KBS Technical Reports 81-01 – 81-16.
Summaries. Stockholm, April 1982.

1982
TR 82–28
The KBS Annual Report 1982.
KBS Technical Reports 82-01 – 82-27.
Summaries. Stockholm, July 1983.

1983
TR 83–77
The KBS Annual Report 1983.
KBS Technical Reports 83-01 – 83-76
Summaries. Stockholm, June 1984.

1984
TR 85–01
Annual Research and Development Report 1984
Including Summaries of Technical Reports Issued during 1984. (Technical Reports 84-01–84-19)
Stockholm June 1985.

1985
TR 85-20
Annual Research and Development Report 1985
Including Summaries of Technical Reports Issued during 1985. (Technical Reports 85-01-85-19)
Stockholm May 1986.

1986
TR 86-31
SKB Annual Report 1986
Including Summaries of Technical Reports Issued during 1986
Stockholm, May 1987

1987
TR 87-33
SKB Annual Report 1987
Including Summaries of Technical Reports Issued during 1987
Stockholm, May 1988

Technical Reports

1988

TR 88-01
Preliminary investigations of deep ground water microbiology in Swedish granitic rocks
Karsten Pedersen
University of Göteborg
December 1987

TR 88-02
Migration of the fission products strontium, technetium, iodine, cesium and the actinides neptunium, plutonium, americium in granitic rock
Thomas Ittner[1], Börje Torstenfelt[1], Bert Allard[2]
[1]Chalmers University of Technology
[2]University of Linköping
January 1988

TR 88-03
Flow and solute transport in a single fracture. A two-dimensional statistical model
Luis Moreno[1], Yvonne Tsang[2], Chin Fu Tsang[2], Ivars Neretnieks[1]
[1]Royal Institute of Technology, Stockholm, Sweden
[2]Lawrence Berkeley Laboratory, Berkeley, CA, USA
January 1988

TR 88-04
Ion binding by humic and fulvic acids: A computational procedure based on functional site heterogeneity and the physical chemistry of polyelectrolyte solutions
J A Marinsky, M M Reddy, J Ephraim, A Mathuthu
US Geological Survey, Lakewood, CA, USA
Linköping University, Linköping
State University of New York at Buffalo, Buffalo, NY, USA
April 1987

TR 88-05
Description of geophysical data on the SKB database GEOTAB
Stefan Sehlstedt
Swedish Geological Co, Luleå
February 1988

TR 88-06
Description of geological data in SKBs database GEOTAB
Tomas Stark
Swedish Geological Co, Luleå
April 1988

TR 88-07
Tectonic studies in the Lansjärv region
Herbert Henkel
Swedish Geological Survey, Uppsala
October 1987

TR 88-08
Diffusion in the matrix of granitic rock. Field test in the Stripa mine. Final report.
Lars Birgersson, Ivars Neretnieks
Royal Institute of Technology, Stockholm
April 1988

TR 88-09
The kinetics of pitting corrosion of carbon steel. Progress report to June 1987
G P Marsh, K J Taylor, Z Sooi
Materials Development Division
Harwell Laboratory
February 1988

TR 88-10
GWHRT – A flow model for coupled groundwater and heat flow
Version 1.0
Roger Thunvik[1], Carol Braester[2]
[1] Royal Institute of Technology, Stockholm
[2] Israel Institute of Technology, Haifa
April 1988

TR 88-11
Groundwater numerical modelling of the Fjällveden study site – Evaluation of parameter variations
A hydrocoin study – Level 3, case 5A
Nils-Åke Larsson[1], Anders Markström[2]
[1] Swedish Geological Company, Uppsala
[2] Kemakta Consultants Co, Stockholm
October 1987

TR 88-12
Near-distance seismological monitoring of the Lansjärv neotectonic fault region
Rutger Wahlström, Sven-Olof Linder,
Conny Holmqvist
Seismological Depertment, Uppsala University,
Uppsala
May 1988

TR 88-13
Validation of the rock mechanics HNFEMP code against Colorado school of mines block test data
Ove Stephansson, Tomas Savilahti
University of Luleå, Luleå
May 1988